SPATIOTEMPORAL regulation of mitotic SPINDLE DYNAMICS and its contribution for CHROMOSOME SEGREGATION



Faculdade
de Medicina
da Universidade
do Porto
2010

REGULAÇÃO ESPÁCIO-TEMPORAL DA DINÂMICA DO FUSO MITÓTICO E O SEU CONTRIBUTO PARA A SEGREGAÇÃO CROMOSSÓMICA

U.PORTO

FMUP FACULDADE DE MEDICINA
UNIVERSIDADE DO PORTO

DISSERTAÇÃO DE CANDIDATURA AO GRAU DE DOUTOR EM BIOMEDICINA APRESENTADA À FACULDADE DE MEDICINA DA UNIVERSIDADE DO PORTO

Artigo, 48º, § 3º - A Faculdade não responde pelas doutrinas expandidas na dissertação. (Regulamento da Faculdade de Medicina do Porto- decreto-Lei Nº 19 337, de 29 de Janeiro de 1931)

NOTA EXPLICATIVA

A presente dissertação foi escrita em Inglês na sua quase totalidade devido ao facto de alguns dos trabalhos terem sido realizados com colaboração internacional.

Dedicada à minha família

Para o Zé Carlos
e para a minha amiga Ana Costa

ACKNOWLEDGEMENTS

This is the moment where the rational side of my brain can rest and the emotional can speak for a while. I would like to share with you my thoughts and sincere acknowledgments.

Firstly I would like to acknowledge my supervisor, Helder Maiato. It was a huge challenge to join Helder´s lab when all he had to offer was a tiny little office full of dreams and amazing ideas. Five years later I am so happy to see that the tiny little office is now a big, healthy, joyful, and competitive lab. With Helder I became a mitotic maniac (as Clare once called me), I learned mitosis and I felt in love for the spindle and its amazing structure. Helder, thank you so much for your permanent enthusiasm, for the challenge, for the awesome discussions, for showing me how fun science can be. It was a privilege to work with you since the very first day and I hope that my eyes will always shine as much as yours every time I speak about science.

Secondly I wish to thank Ted Salmon and his lab. Ted, thank you so much for receiving me in your lab, it was only for a short period but I felt lucky for being there and learning from you.

I also want to express my gratitude to Fundação para a Ciência e a Tecnologia (FCT), for funding my PhD fellowship and to Fundação Calouste Gulbenkian (FCG) for all the financial support essential for allowing me to to attend all the meetings I went to. I would also like to acknowledge Boheringer Inglhem Funds, FCT and FCG for providing me with the opportunity to attend one of the greatest scientific moments of my life, the Physiology Course 2009.

I also want to acknowledge one of my scientific heros, Tozé. I don't have words to tell how much I admire you and how lucky I was to share my work with you. Thank you for making OUR work so beautiful, thank you for all the patience you had trying to explain the physics or the maths behind all the data, thank you for your precious time, thank you for the fun you provide giving me countless Braga-Porto-Braga lifts. I will miss all the fun I had on those brainstorming moments. I just hope to find in my life people as great as you are.

Everyone at the CID lab - Rita, Tozé, Elsa, Jorge, Stef, Mariana, Ana, Sara, Clara, Andrea, Marten - be prepared. I will fight to have enough money to hire you all, so we can work again together one day. I saw every one of you arriving to our lab it will be really difficult to say goodbye.

I also want to thank all the members in the Sunkel lab, specially to Paula Coelho who gave me a huge support, specially when I was filming overnight! Thank you so much for the amazing scientific discussions, for sharing your knowledge with me, for caring, for believing in me. Thank you for your permanent support! To the rest of the Sunkel crew I acknowledge not only your precious reagents, but also your friendship, support and your knowledge.

À Anabela e ao Julio, muito obrigada pela capa fantástica que conseguiram em tão pouco tempo! Foi bom poder contar convosco e com o vosso entusiasmo. Obrigada!

À Rita, à Marisa, à Nuria, ao Gonçalo, à Joana e ao Rachid, quero agradecer a amizade, o carinho, a paciência, os sorrisos e os miminhos. Tudo o que alguém pode desejar quando está longe de casa. Vocês são a minha família da *Invicta*. Graças a vocês apaixonei-me pelo Porto e sinto-me imensamente feliz por viver nesta cidade. As minhas palavras nunca serão suficientes para expressar a minha alegria e felicidade por vos ter como amigos. Sou uma sortuda por vos ter conhecido! Obrigada por encherem a minha vida de doces sorrisos.

À Patricia, à Gabriela, à Marta, à Diana e à Sofia quero agradecer os momentos de pura alegria e resiliência. Obrigada por partilharem comigo a vossa grandeza e generosidade. Obrigada pelo apoio e por manterem o nosso grupo sempre unido e dinâmico.

À minha amiga Cláudia quero agradecer a amizade duradoura que nos aproxima há mais de 20 anos! Obrigada por continuares a existir na minha vida, obrigada pelas constante mensagens de apoio, por acreditares em mim, obrigada pela tua sempre presente generosidade! Obrigada ainda por me teres enviado grande parte dos *papers* que constam na bibliografia desta tese. Foram fundamentais.

Ana, esta tese é também para ti. É infindável a admiração que tenho por ti, pela tua força, por nunca baixares os braços. Guardarei sempre comigo a tua "paz"!

Aos meus pais e ao meu irmão quero agradecer todo o apoio e preocupação. O vosso amor incondicional faz-me seguir sempre em frente, sem nunca pensar em desistir. Obrigada por tudo, vocês são os meus mais importantes pilares!

Por fim quero agradecer ao Zé Carlos todo o amor e dedicação em especial nestes últimos meses. Obrigada por manteres a nossa casa sempre quentinha, pela tua infinita paciência e generosidade. Obrigada pela motivação constante, por seres meu amigo e companheiro, obrigada! Se hoje estou aqui, é também por ti!

ABSTRACT

The synchronous movement of chromosomes during anaphase ensures their correct inheritance in every cell division. This reflects the uniformity of spindle forces acting on chromosomes and their simultaneous entry and progression through anaphase. Although anaphase onset is controlled by the spindle assembly checkpoint, it remains unknown how spindle forces are uniformly distributed among different chromosomes.

Here we show that tension uniformity at metaphase kinetochores and subsequent anaphase synchrony in *Drosophila* S2 cells are promoted by a conspicuous property of metazoan spindles, the microtubule poleward flux. We demonstrate that down-regulation of the molecular *facilitators* of flux, such as CLASP and the kinesin-13 KLP10A, led to a pronounced increase in the variability of inter-kinetochore metaphase tensions coupled to an extended anaphase asynchrony. Moreover, we show that experimental acceleration of mitosis precludes tension equalization and promotes anaphase synchrony. We propose that flux-dependent tension equalization by flux promotes the uniform maturation/correction of microtubule-kinetochore attachments, thereby ensuring the subsequent synchronous segregation of chromosomes during anaphase.

In this study we also took advantage of S2 cells to dissect from a larger perspective the mechanisms and regulation of chromosome segregation. Upon anaphase onset chromosomes move to the spindle poles as the kinetochore microtubules depolymerize (anaphase A), and the spindle elongates (anaphase B). Accordingly, we found that anaphase A and anaphase B onset is simultaneous and the velocities equally contribute for the movement of chromosomes occurring in average at 0.8 and 0.9 μm/min. In this system both movements are still guaranteed by complementary mechanisms. Whereas Pac-Man and poleward flux associated activities are responsible for anaphase A (each contributing with ~50% of the velocity), spindle elongation occurs as a consequence of a synergistic action of poleward sliding (~75%) and cortical driven forces (~25%).

Finally we found that the perturbation of microtubule dynamics by the use of low doses of Taxol or by down-regulation of KLP10A, led to a reduction in the spindle elongation velocity and to the concomitant delay in the nuclear envelope reformation. This suggests the existence of a surveillance mechanism that ultimately guarantees the wrapping of the sister chromatids after proper spatial separation.

Taken together, the results presented in this thesis provide new insights about the mechanisms and regulation of chromosome segregation, while supporting the existence of spatial control mechanisms that ensure mitotic fidelity.

RESUMO

A sincronia do movimento dos cromossomas durante a anafase garante a sua correcta transmissão ao longo de sucessivas gerações. Este movimento síncrono resulta da existência de forças no fuso mitótico que são distribuídas aos cromossomas de uma forma uniforme, e da simultaneidade por eles apresentada no momento inicial da segregação. Embora a transição metafase-anafase seja controlada pelo *checkpoint* do fuso mitótico, permanece desconhecida a forma de como as forças que actuam no fuso são uniformemente distribuídas pelos cinetocoros.

Neste estudo observou-se que a uniformidade de tensão entre pares de cinetocoros durante metafase e a consequente sincronia de movimento durante a anafase em células S2 de *Drosophila* são garantidos por um mecanismo característico dos fusos dos metazoários, o fluxo de microtúbulos. Foi também demonstrado que a redução de expressão de proteínas facilitadoras de fluxo, como a CLASP e a cinesina-13 KLP10A, levam ao consequente aumento na variabilidade de tensões entre pares de cinetocoros durante metafase, e ao movimento assíncrono dos cromossomas durante a anafase. Adicionalmente, foi também observado que a aceleração experimental da duração de mitose leva à perda do equilíbrio de tensões, e a uma consequente segregação desordenada. Neste sentido, é proposto que a uniformização de tensões dependente de fluxo promove a maturação e/ou correcção das ligações dos microtúbulos ao cinetocoro e assegura que os cromossomas executem uma subsequente segregação síncrona.

Neste estudo, as células S2 foram ainda usadas para investigar de forma mais alargada os mecanismos de regulação da segregação de cromossomas. No início de anafase, os cromossomas movem-se em direcção aos pólos como resultado quer da despolimerização dos microtúbulos ligados ao cinetocoro (anafase A), quer da elongação do fuso mitótico (anafase B). Com este trabalho demonstrou-se, que no sistema em estudo, o inicio da anafase A e da anafase B é simultâneo. Demonstrou-se ainda que as velocidades garantidas por cada tipo de segregação contribuem equitativamente para o movimento dos cromossomas alcançando em média os 0.8 e 0.9 μm/min, respectivamente. Neste sistema, ambos os mecanismos são ainda garantidos por processos complementares. Enquanto que mecanismos de despolimerização de Pac-Man, e associados a fluxo, são responsáveis por garantirem o movimento de anafase A (cada um contribuindo com 50% da velocidade), o elongamento do fuso ocorre como consequência de acção sinergística do deslizamento dos microtúbulos interpolares na direcção dos pólos (~75%) e das forças corticais (25%).

Por fim, observou-se ainda que perturbações na dinâmica dos microtúbulos pelo uso de doses baixas de Taxol, ou pela diminuição da expressão de KLP10A, teve como consequência uma redução da velocidade de elongação, bem como a um concomitante atraso na reformação do invólucro nuclear. Estes resultados sugerem a existência de um sistema de controlo que assegura que os cromossomas são envolvidos pelo invólucro nuclear depois de atingirem uma determinada separação espacial.

Em conclusão, os resultados apresentados nesta tese proporcionam um conhecimento detalhado acerca da existência de mecanismos de regulação da segregação de cromossomas, enquanto que suportam a existência de um mecanismo de controlo espacial que assegura a fidelidade mitótica.

TABLE OF CONTENTS

I. GENERAL INTRODUCTION

1. THE CELL CYCLE 1

1.1. Cell Cycle Regulation: A Question of Unidirectionality 1

1.2. Cell Cycle Regulation: A Question of Quality Control 3

2. MITOSIS: A BRIEF PERSPECTIVE 4

2.1. Spatiotemporal Regulation of Mitosis 5

3. SPINDLE STRUCTURE AND ARCHITECTURE 7

3.1. Microtubules 7

3.1.1. Structure 8

3.1.2. Dynamics 8

3.1.3 Microtubule-based forces 9

3.1.4 Spindle microtubules 11

3.2. MAPS and Molecular Motors 11

3.2.1. MAPs 13

3.2.2 Molecular motors 14

3.3. The Kinetochore 16

3.3.1. Structure and composition 16

3.4. The Centrosome 19

3.4.1 Structure and function during mitosis 20

4. SPINDLE DYNAMICS 20

4.1. Spindle Assembly and the Mechanisms of Chromosome Congression 20

4.1.1. The search-and-capture model 21

4.1.2. Kinetochore-mediated k-fiber formation..... 22

4.1.3. Molecular motors and polar ejections forces..... 22

4.2. Kinetochore-Microtubule Attachment..... 23

4.2.1. Biased diffusion mechanism..... 23

4.2.2. Forced-walk mechanism..... 24

4.3. The Spindle Assembly Checkpoint..... 26

4.3.1. The Molecular Machinery..... 26

4.3.2. Tension vs attachment..... 27

4.4 Metaphase: A Dynamic Steady-State..... 29

4.4.1. Turnover..... 29

4.4.2. Poleward microtubule flux..... 29

4.4.3. Error correction-the commitment to anaphase synchrony..... 32

5. CHROMOSOME SEGREGATION..... 33

5.1. Anaphase A..... 34

5.1.1. The traction-fiber model - microtubule minus-end depolymerization. 34

5.1.2. The Pac-Man mechanism - microtubule plus-end polymerization..... 35

5.1.3. Tensile matrix..... 37

5.2. Anaphase B..... 38

6. OBJECTIVES..... 40

II. EXPERIMENTAL WORK

CHAPTER I. Synchronizing chromosome segregation by flux-dependent force equalization at kinetochores..... 43

1. INTRODUCTION..... 43

2. MATERIALS AND METHODS 45

2.1. Cell culture, RNAi treatment and western blot 45

2.2. Drug treatments 45

2.3. Immunofluorescence microscopy 45

2.4. Fluorescent speckle microscopy (FSM) 46

2.5. Time-lapse microscopy 46

2.6. Guided kymography 47

2.7. Collapsed kymography and chromo-kymography 47

2.8. Quantifications 47

2.9. Statistical analyses 48

3. RESULTS 49

3.1. Experimental attenuation of kMT flux in *Drosophila* S2 cells 49

3.2. Flux-associated kMT minus-end depolymerization is down-regulated at anaphase onset and has a minor role in anaphase chromosome-to-pole motility in *Drosophila* S2 cells 52

3.3. KMT flux ensures anaphase synchrony in *Drosophila* S2 cells 54

3.4. Anaphase synchrony reflects the uniformity of forces acting on metaphase kinetochores 57

3.5. Force equalization by flux can be explained by a microtubule-coupling model 62

3.6. The SAC extends the duration of mitosis to allow the uniform distribution of forces acting on metaphase kinetochores 63

4. DISCUSSION 64

CHAPTER II. Chromosome segregation – *How do chromosomes move*? 67

1. INTRODUCTION 67

2. MATERIALS AND METHODS 69

2.1. Cell culture, RNAi treatment and western blot 69

2.2. Drug treatments 69

2.3. FSM, time-lapse microscopy and kymography analyses 69

2.4. Quantifications 69

2.5. Statistical analyses 70

3. RESULTS 71

3.1. Anaphase A and anaphase B onset is simultaneous in *Drosophila* S2 cells 71

3.2. Spindle elongation and kMT shortening equally contribute to chromosome segregation in *Drosophila* S2 cells 72

3.3. Pac-Man mediates kMT-shortening in *Drosophila* S2 cells 79

4. DISCUSSION 80

CHAPTER III. Spatiotemporal analysis of spindle elongation in *Drosophila* S2 cells 83

1. INTRODUCTION 83

2. MATERIALS AND METHODS 85

2.1. Cell culture, RNAi treatment and western blot 85

2.2. Time-lapse microscopy and guided kymography 85

2.3. Quantifications 85

2.4. Statistical analyses 86

3. RESULTS 87

3.1. The spindle elongation depends on the metaphase spindle length and is sensitive to microtubule dynamics, crosslinking activity and centrosome perturbation **87**

3.2. Different patterns of elongation velocities are observed after mitotic spindle perturbations **93**

3.3. Reduction of spindle elongation velocity is balanced by an increase in anaphase duration **98**

4. DISCUSSION **105**

4.1. Regulation of metaphase spindle length **105**

4.2. Spindle elongation capacity: a factor of 2 ..... **106**

4.3. Spindle elongation: a synergistic mechanism **107**

4.4. Anaphase duration: is there a surveillance mechanism **108**

III. CONCLUSIONS

CONCLUSIONS **113**

IV. SUPPLEMENTARY MATERIAL

1. ABBREVIATIONS **117**

2. SUPPLEMENTARY TABLES **118**

3. SUPPLEMENTARY FIGURES **121**

V. REFERENCES

REFERENCES **129**

VI. ORIGINAL ARTICLES

ORIGINAL ARTICLES **153**

ORIGINAL ARTICLE I **154**

I. General Introduction

1. THE CELL CYCLE

The highly coordinated series of events that lead to eukaryotic cell duplication and propagation is called cell cycle. This strictly ordered group of events is characterized by its fidelity and precision that can only be achieved if the unidirectionality and proper regulation are maintained over countless generations.

1.1. Cell Cycle Regulation: A Question of Unidirectionality

The typical cell-cycle-textbook-picture is divided in four well-defined phases, and three switch-like transitions (Fig. 1, a). While discrete stages of the eukaryotic cell cycle are typically defined on the basis of chromosomal events, the switch-like transitions depend on the tight regulation of cyclin-dependent-kinases (CDKs).

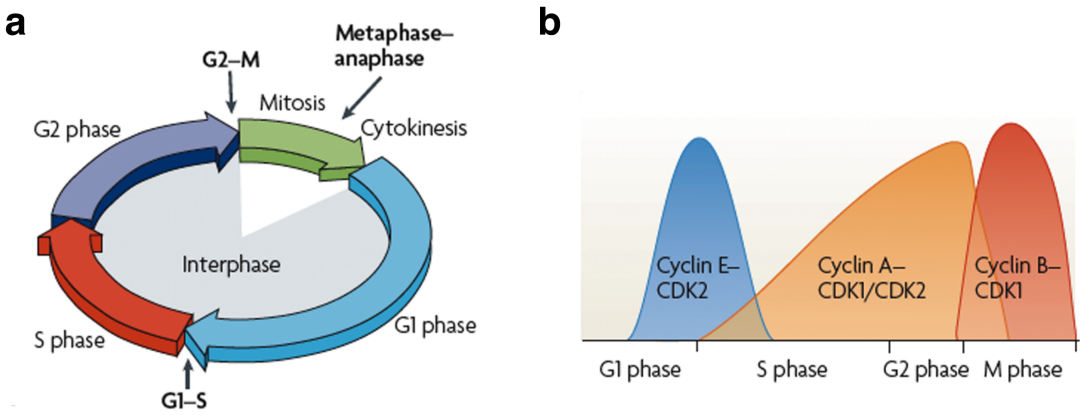


Figure 1 – The classical and minimal models of cell cycle control. a) Cycling cells undergo three major transitions during their cell cycle. The beginning of S phase is marked by the onset of DNA replication. The start of mitosis (M) is accompanied by breakdown of the nuclear envelope and chromosome condensation, whereas segregation of the sister chromatids marks the metaphase-to-anaphase transition. Cyclin-dependent kinases (CDKs) trigger the transition from G1 to S phase and from G2 to M phase by phosphorylating distinct sets of substrates. The metaphase-to-anaphase transition requires the ubiquitylation and proteasome-mediated degradation of mitotic B-type cyclins and various other proteins, and is triggered by the anaphase-promoting complex/cyclosome (APC/C) E3 ubiquitin ligase. **b)** CDK1 and CDK2 can bind cyclins A, B, D and E, whereas CDK4 and CDK6 only partner D-type cyclins. Thick lines represent the preferred pairing for each kinase. Adapted by permission from Macmillan Publishers Ltd: Nature Reviews Molecular Cell Biology (Hochegger *et al.*) © 2008.

During the cell cycle two major events guarantee the maintenance of genetic inheritance: DNA synthesis (S phase) and segregation (M phase). During S phase, the DNA double helix is opened and both strands are faithfully copied. Chromosomes are duplicated and cohesion is established between sister chromatids (Uhlmann and Nasmyth 1998). The M phase (mitosis) is the second major event and the most scenic one. Chromosomes move to the cell's equatorial plane and then, in a choreographic style, sister chromatids are synchronously segregated into the new daughter cells. Most cell cycles contain additional "gap" periods, known as G1 and G2 that separate S and M phases. While G1 precedes S, G2 precedes M phase. Besides separating DNA synthesis from segregation, gap phases also provide additional time for cell growth and serve as important regulatory transitions (Morgan 2007). In the absence of the specific mitogenic signal, cells stop proliferating and exit cycle entering in a non-dividing quiescent state called G0 (Malumbres and Barbacid 2001).

Cell cycle transitions are regulated by CDKs, the so-called cell cycle engines (Nurse 1975; Evans *et al.* 1983; Morgan 1997; reviewed by Nurse 2000). These enzymes are heterodymeric kinases whose catalytic activity depends on an associated cyclin subunit. As cell cycle progresses activity of CDKs will vary due to the oscillations of the interacting cyclin (Fig. 1, b). The unidirectionality of the cycle largely depends on cyclin specificity and on the modulation of its sequential activity. This can be mainly achieved by regulatory mechanisms such as transcriptional activation, inhibitory interactions, ubiquitin mediated-proteolysis and/or phosphorylation (Morgan 1997; Bloom and Cross 2007; Hochegger *et al.* 2008). In metazoans distinct cyclin-CDK holoenzymes assemble at specific cell cycle-stages and are responsible to trigger the events of S and M phases. Although in yeast there is only one CDK, a plethora of cyclins guarantee the sequence of events (Bloom and Cross 2007). By contrast, in mammals there are several CDKs already identified and numerous cyclins but only a subset is involved in cell cycle regulation (Malumbres *et al.* 2009). This includes three interphase CDKs, CDK2, CDK4 and CDK6, a mitotic CDK, CDK1, and ten cyclins that belong to four different classes, the A-, B-, D-, and E-type cyclins (reviewed by Malumbres and Barbacid 2009). Each cyclin-CDK complex promotes the activation of the next in sequence, assuring the ordered transition between cell cycle stages (Morgan 2007).

When a cell "senses" the mitogenic signals, cyclin D binds to CDK4 or CDK6 and prepares the cell for DNA synthesis. Cyclin E becomes activated and binds to CDK2 triggering the process of DNA synthesis. Cyclin A-CDK2 is subsequently activated and responsible for progression and completion of S phase. This complex remains high until the end of G2 and is considered the most potent stimulator of mitosis (Gong *et al.* 2007;

Morgan 2007). Cyclin A is targeted to destruction after nuclear envelope breakdown (NEB) thus facilitating the formation of the cyclin B-CDK1 complex responsible for driving cells through mitosis (Sullivan and Morgan 2007; Malumbres and Barbacid 2009). This complex is also known as the M-phase-promoting factor (MPF; Nurse 1990) and is responsible for the direct regulation of mitosis until the establishment of metaphase (Sullivan and Morgan 2007). Beyond this point mitotic progression depends on another major regulator, the anaphase-promoting complex/cyclosome (APC/C), a multiprotein E3 ubiquitin ligase that ubiquitinylates regulatory proteins, targeting them for degradation by the 26S proteasome (Peters 2006). APC/C is further responsible for targeting Cyclin B to destruction until the beginning of the next cycle (reviewed by Lindqvist *et al.* 2009).

1.2. Cell Cycle Regulation: A Question of Quality Control

The cell cycle progression is monitored by the existence of checkpoints that "guard" critical transitions (Hartwell and Weinert 1989). In order to accurately respond to either internal or external damage conditions a checkpoint should comprise a sensor, that detects the error, a transduction cascade that amplifies the signal and an effector (Wells 1996). Although it has been claimed that checkpoints are not essential in "happy" cells (Khodjakov and Rieder 2009b) it is hard to predict whether a cell will always remain "healthy". During the cell cycle progression there are different checkpoints that allow cell cycle delays when damage or incorrections are "sensed". The DNA damaged checkpoint protects cells against genotoxic agents that may induce mutations within the DNA molecule, delaying the cycle to facilitate the repair and/or damage resolution. If repair is unsuccessful cells may enter senescence, undergo apoptosis, or alternatively the DNA may accumulate alterations that will ultimately lead to genomic instability and/or cell transformation and oncogenesis (Malumbres and Barbacid 2009). Another checkpoint mechanism that guarantees the quality control of the cell cycle is the spindle assembly checkpoint (SAC) that monitors the attachment of chromosomes to the mitotic spindle delaying the metaphase-anaphase transition until all attachments are established (Wells 1996; see section 4.3).

2. MITOSIS: A BRIEF PERSPECTIVE

Walther Flemming firstly described cell division in animal cells in 1870s and mitosis was the name that this process would be given in 1882 (Flemming 1882; Wilson 1925; Flemming 1965; Paweletz 2001). Until the beginning of the 21st century mitosis was seen as a sequence of discrete events. It was mainly divided in five distinct stages: prophase, prometaphase, metaphase, anaphase and telophase (Fig. 2). Because this classification only takes into account the observable alterations in the morphology of the cell (chromosome condensation, nuclear envelope breakdown, congression, segregation, and decondensation) it cannot define mitosis in all eukaryotic systems. In order to overcome this limitation and in an attempt to accurately achieve a *one-fits-all* classification, it was proposed that mitosis should be restaged and subdivided into five transitional phases that molecularly characterize the spatiotemporal regulation of mitosis (Fig. 3, a; Pines and Rieder 2001).

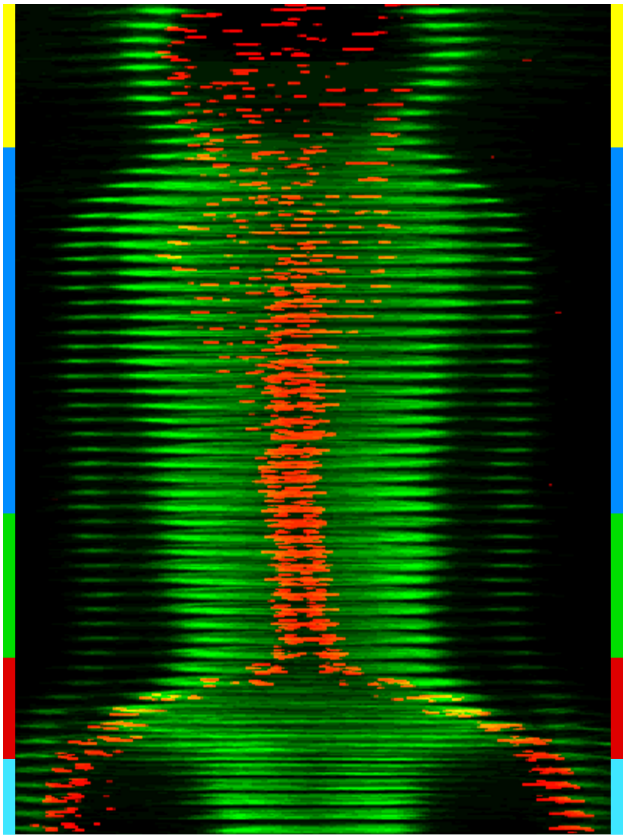


Figure 2 – Live history of a mitotic cell. The kymograph shows the mitosis of a *Drosophila melanogaster* S2 cell in 2D. The horizontal dimension represent space and the vertical, time. In red, it is possible to observe the movement of kinetochores (revealed by the use of CID-mcherry) and in green, spindle microtubules (MTs; revealed by the use of GFP-α-tubulin). Following the time dimension it is possible to observe the nuclear envelope breakdown (revealed by the exclusion of the α-tubulin signal), and the congression of kinetochores to the metaphase plate. After the anaphase onset two main tracks are observed moving towards the poles. Each slice corresponds to a time-lapse frame (30 sec interval). The colored bars on each side of the figure respectively represent: prophase (yellow), prometaphase (blue), metaphase (green), anaphase (red) and telophase (cyan) and are identified in Fig. 3.

2.1. Spatiotemporal Regulation of Mitosis

The first problem when defining mitosis is to establish the time zero, *when does it start*? In the first attempt to clarify mitotic regulation Bullough and Johnson (1951) proposed the existence of an "antephase" that precedes the onset of mitosis and where the commitment to division could be reverted. Some years later, Mazia (1961) envisioned the existence of one *point of no return* that once crossed, cells had to proceed into division without reverting their fate. In fact, Rieder and Cole (1998) described the existence of a G2/M checkpoint from where prophase could not be reverted. During this antephase period Cyclin B-CDK1 is not retained at the nucleus and levels of Cyclin A-CDK are high (Furuno *et al.* 1999). Furthermore, at the end of antephase, polo-like kinases (Plks) and Aurora B also assume an important role. Plk1 is involved in Cyclin B-CDK1 activation (Kumagai and Dunphy 1996; Toyoshima-Morimoto *et al.* 2001) and centrosome maturation (Lane and Nigg 1996), whereas Aurora B is involved in chromosome condensation (Hsu *et al.* 2000).

The second transition proposed by Pines and Rieder 2001, is the commitment to mitosis and is defined as the period where Cyclin B-CDK1 is fully activated. This complex, purified from *Xenopus laevis* and sea urchin egg extracts, was shown to be fundamental for the onset of mitosis and is highly conserved amongst all eukaryotic systems known so far (Lohka *et al.* 1988; Nurse 2000). Its activation starts during G2 due to the action of Cdc25 phosphatases that revert the inhibitory phosphorylations maintained by the Wee and Myt kinases. In vertebrate cells, Cyclin B1-CDK1 activation occurs firstly in the cytoplasm where is mostly localized due to the high shuttling activity that occurs between the nucleus and the cytoplasm (Hagting *et al.* 1998; Yang *et al.* 1998). However, in late G2 it becomes predominantly accumulated at the nucleus and centrosomes. High-levels of Cyclin B-CDK1 activity are still assured by the several Plk1-dependent feedback loops that can amplify the Cyclin B-CDK1 activation signal, assuring the complete commitment to mitosis (Morgan 2007; reviewed by Lindqvist *et al.* 2009).

Once the full commitment is achieved, mitosis proceeds to the third transition, the spindle assembly checkpoint. SAC monitors the attachment of kinetochores to the mitotic spindle delaying mitosis until all kinetochores become stably attached (see section 4.3.1 for details). This signaling pathway involves a highly regulated machinery (reviewed by Musacchio and Salmon 2007) that hampers the mitotic exit by inhibiting the association of the APC/C to its Cdc20 activator. The APC/C^{Cdc20} complex is responsible for targeting to destruction two important regulatory proteins, securin (reviewed by Nasmyth *et al.* 2000), and Cyclin B (Wheatley *et al.* 1997). Before the anaphase onset, the cohesins that hold

sister chromatids together, still need to be cleaved. This function is executed by a specific protease, known as separase, released upon securin degradation (its inhibitory partner) (Fig. 3, b).

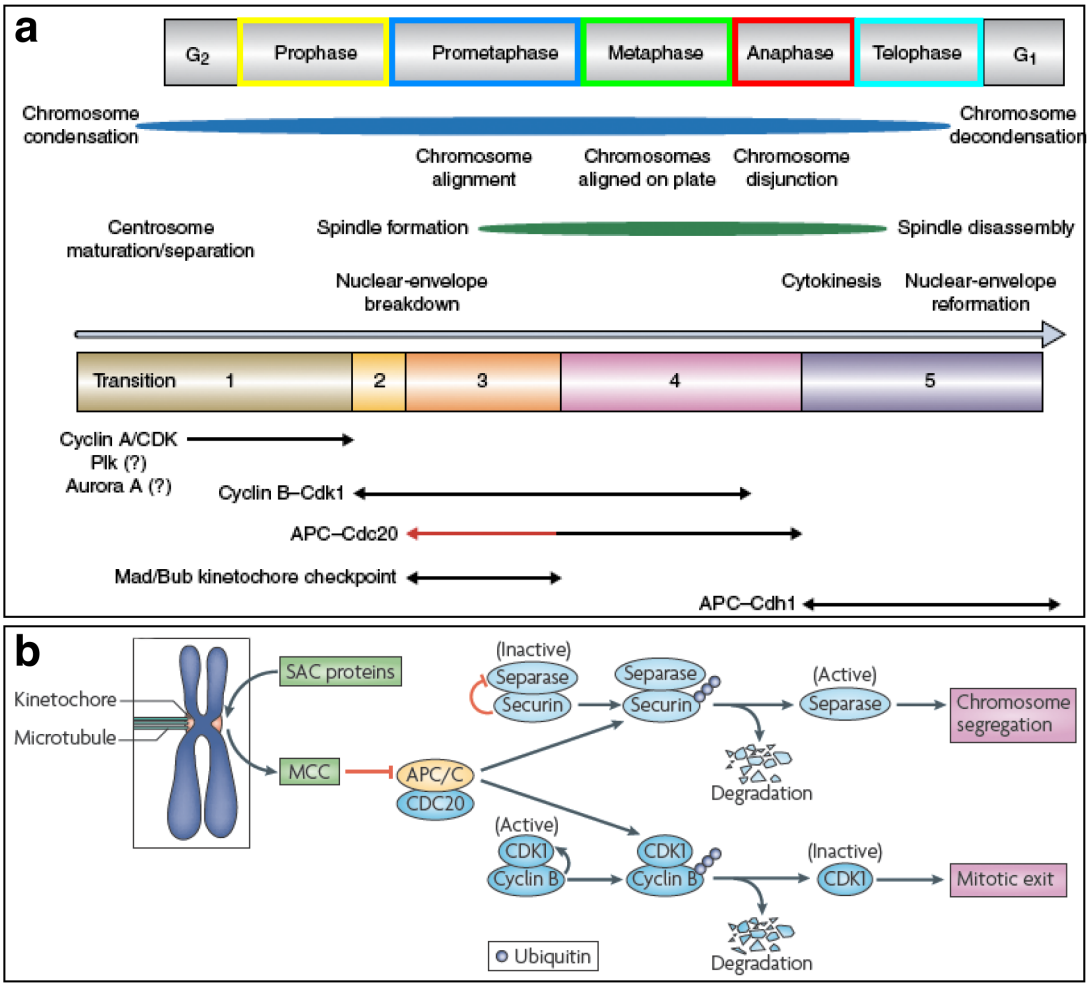


Figure 3 – Biochemical regulation of mitotic transitions. **a)** Comparison of the traditional (top) and transitions (bottom) phases of mitosis. The changes in cell-cycle regulators that were used to define transitions are shown below the timeline. The period during which APC/Cdc20 is active but is modulated by the kinetochore-attachment checkpoint is shown in red. Transition 1: "antephase" and the end of G2; transition 2: the commitment to mitosis; transition 3: satisfying the criteria to exit mitosis; transition 4: escaping from mitosis; transition 5: returning to interphase. Colored boxes are coded according to the legend in Fig. 2. **b)** Chromosome segregation is restrained by the SAC until chromosomes are properly attached. SAC proteins are located at the kinetochores that are unattached to microtubules and form the mitotic checkpoint complex (MCC), which is proposed to inhibit the ability of cell division cycle 20 (cdc20) to activate the APC/C. During the transition from metaphase to anaphase, Cyclin B and securin (the inhibitor of separase) are ubiquitylated by the APC/C and degraded by the 26S proteasome. As a result, separase is activated, sister chromatids move towards the opposite poles of the mitotic spindle, and the mitotic exit is performed. Adapted by permission from Macmillan Publishers Limited: Nature Cell Biology, (Wittmann *et al.*) © 2001; and Nature Reviews Molecular Cell Biology (Yanagida) © 2009.

Recently, it was shown that in budding yeast a positive feedback loop involving the regulatory phosphatase Cdc14 is responsible for the abruptness of the metaphase-anaphase transition (Holt *et al.* 2008). Cdc14 is activated by separase and lacks orthologues in higher eukaryotes. Once activated upon separase release, Cdc14 will actively desphosphorylate securin thus promoting its polyubiquitylation and the consequent destruction (reviewed by Sullivan and Morgan 2007). The increased rates of securin proteolysis will promote the extremely efficient separase release, and in turn more Cdc14 will become active. This positive feedback loop was suggested to act as an abrupt "switch off" that ensures the synchronous entry into anaphase (Holt *et al.* 2008).

The fourth transition state is still characterized by the consequences of CDK1 inactivation due to Cyclin B destruction. Finally, the fifth transition is the return to interphase and is characterized by the destruction of the APC/C cofactor Cdc20, and its consequent replacement by Cdh1 that will help to regulate the late mitotic events.

3. SPINDLE STRUCTURE AND ARCHITECTURE

The mitotic spindle is the key player of mitosis. In order to accurately segregate the genetic material, this high-ordered structure needs to be assembled and disassembled in an extremely precise way within a specific time. The spindle structure was first isolated by Mazia in 1952 from sea urchin eggs (Mazia and Dan 1952) and by that time it was physically demonstrated that the so called mitotic apparatus was composed by the spindle, asters and chromosomes. One year later, Shinya Inoué using polarizing light microscopy confirmed that a fibrous structure composed of continuous fibers, chromosomal fibers and astral rays did exist in living cells and was not an artifact from fixation procedures (Inoue 1953; reviewed in Inoue 1981). A *dynamic mitotic era* had begun.

3.1. Microtubules

It was due to the birefringence property of microtubules (MTs) that it was possible not only to observe the fibers, but also to perturb their stability and interpret the outcome in living cells. In the early 1950's and 1960's it was observed that spindle fibers birefringence was not static and could be reversibly reduced to an equilibrium value by low temperature or colchicine treatment (reviewed in Inoue 2008). With the concomitant

and parallel use of electron microscopy (Harris 1962), and the improved use of glutaraldehyde as a fixative (Sabatini *et al.* 1963) it was possible to confirm that spindle fibers are dynamic labile structures composed of linearly aggregated polymers which constitute the MTs (Harris 1962; Ledbetter and Porter 1963). MTs were thus recognized as the main structural element of the mitotic spindle.

3.1.1. Structure

MTs are stiff, hollow cylindrical polymers assembled from parallel protofilaments each composed of α- and β-tubulin heterodymers. Each heterodymer constitutes a MT subunit and is organized in a head-to-tail fashion within the linear protofilament. As tubulin subunits are oriented in the same direction (αβ-αβ-αβ), MTs have structurally different ends. One end has β-tubulin exposed and is conventionally called the plus-end, whereas the other end has α-tubulin and is called the minus-end. This structural polarity is important for MT function as both ends have different polymerization kinetics. *In vitro* β-tubulin is exposed at the faster polymerizing MT plus-end, while α-tubulin is exposed at the slower polymerizing minus-end (review in Desai and Mitchison 1997; Alberts 2002; Scholey and Mogilner 2003; Morgan 2007).

3.1.2. Dynamics

Tubulin dymers are more than MT building blocks. They work as GTPases: enzymes that bind to GTP and catalyze its hydrolysis to GDP phosphate (Fig. 4). Tubulin uses the energy of GTP binding and hydrolysis to change its conformation, changing the affinity of tubulin for the ends of MTs (Roychowdhury *et al.* 1999). Hydrolysis of the GTP bound β-tubulin occurs during or soon after polymerization. Since GDP is trapped within the tubulin structure it cannot be replaced by GTP. Most β-tubulin therefore exists in the GDP-bound form, although the plus end of the MT is often composed of newly added GTP-tubulin molecules that have not yet hydrolyzed their GTP. This is called a GTP cap (Morgan 2007). It is thought that the GTP cap constrain the rest of the polymer to maintain a straight conformation as opposed to the curved conformation of GDP bound protofilaments (reviewed by Kline-Smith and Walczak 2004).

When growing in buffers, MTs may exhibit two behaviors: treadmiling (Margolis *et al.* 1978) and dynamic instability (Mitchison and Kirschner 1984a).

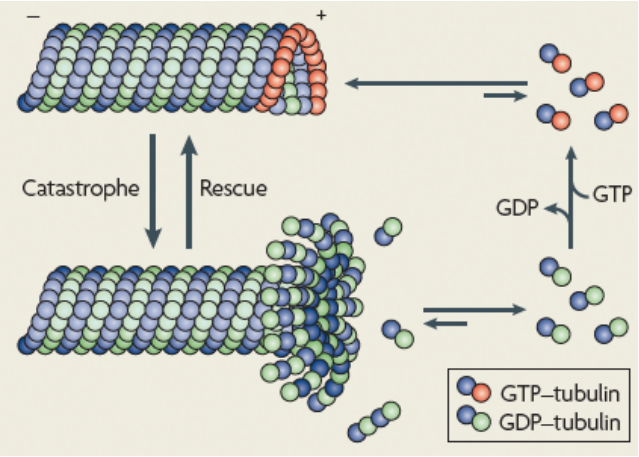


Figure 4 – Microtubule Dynamics. MTs exhibit a specialized non-equilibrium polymerization behavior, termed dynamic instability, in which polymerizing and rapidly depolymerizing polymers coexist at steady state. The transition from polymerization to depolymerization is the catastrophe, and the reverse transition is rescue. Polymerization triggered GTP hydrolysis on β-tubulin provides the energy source for this non-equilibrium behavior; the resulting GDP is locked into the polymer lattice until depolymerization releases the subunit. The energy of GTP hydrolysis is stored as mechanical strain in the GDP–tubulin polymer lattice, resulting in >1,000-fold higher dissociation of GDP–tubulin at a depolymerizing end relative to dissociation of GTP–tubulin at a polymerizing end. Adapted by permission from Macmillan Publishers Limited: Nature Reviews Molecular Cell Biology (Cheeseman and Desai) © 2009.

Dynamic Instability is a process in which the individual MT ends stochastically switch between phases of growth and shortening (Mitchison and Kirschner 1984a). It is dependent on GTP hydrolysis and characterized by four main variables: the rate of MT growth, the rate of MT shortening, the frequency of transition from the growth or pause state to shortening *(catastrophe)*, and the frequency of transition from shortening to growth or pause (*rescue*; Walker *et al.* 1988). *In vivo*, dynamic instability allows MTs to explore the interior of the cell in order to contact with specific structures like kinetochores or cell cortex.

Treadmilling is the second dynamic behavior of MTs that also depends on GTP hydrolysis. It was firstly described as an *in vitro* property (Margolis and Wilson 1978) and 20 years later was also described *in vivo* (Rodionov and Borisy 1997). It refers to the net growth at one MT end, and the balanced shortening at the opposite one. It involves the intrinsic flow of MT subunits, from MT plus-end, down to the minus-end (Margolis and Wilson 1978; Margolis and Wilson 1981).

3.1.3. Microtubule-based Forces

The assembly (Dogterom and Yurke 1997) and disassembly (Koshland *et al.* 1988) of MTs can generate force. While MT polymerization leads to the generation of pushing forces, the disassembly of MTs leads to the generation of pulling forces (Tolic-Norrelykke 2008). MT-coupled pulling and pushing forces play an essential role in organelle and

mitotic spindle positioning as well as chromosome motility (Coue *et al.* 1991; Lombillo *et al.* 1995; Gonczy 2002; Dogterom *et al.* 2005; Tolic-Norrelykke 2008).

MT polymerization generates **pushing** forces. When the plus-end of a growing MT encounters a fixed object, the addition of tubulin subunits will exert a compression force, and displace the MTs in the opposite direction (Dogterom and Yurke 1997; Holy *et al.* 1997). These forces are efficient for movements over short distances. If MTs became too long they will easily buckle, as the force needed to buckle a MT decreases with the square of its length (Janson and Dogterom 2004; Dogterom *et al.* 2005; Tolic-Norrelykke 2008). *In vivo*, pushing forces are known to position the nucleus in the fission yeast *Schizosaccharomyces pombe* (Tran *et al.* 2001), but is still not know if it is important to generate force for chromosome segregation.

Pulling forces are predominantly promoted by MT depolymerization coupled to accessory proteins as motors and/or adaptors. Koshland *et al*. (1988) provided, for the first time, *in vitro* evidences that MT plus-end depolymerization can drive chromosome movement even if ATP was diluted from the experiment. Accordingly, Coue *et al*. 1991 confirmed those studies observing that the depolymerizing ends of MTs could pull particles at rates of almost 30 μm/min against viscous forces of ~10 pN.

At the cortex pulling forces are generated through MTs whose minus-ends are at the spindle poles and the plus-ends are at the cell cortex. Cortical anchors maintain interactions with the plus-ends of MTs, whereas minus-end directed motors concomitantly move in the minus-end direction. Force is driven and tension is generated (Dogterom *et al.* 2005; Tolic-Norrelykke 2008). Evidence for the existence of pulling forces at the cell cortex came from the pioneering experiments of Aist and Bearns (1981) in the fungus *Fusarium solanii*. Using a laser microbeam they cut the central region of the spindle and observed that extranuclear forces pull on the spindle poles and indeed, after severing, the velocity of segregation was accelerated (Aist and Berns 1981). Similar conclusions were obtained by Kronebuschand and Borisy (1982) after cutting the central spindle of the rat-kangaroo kidney epithelium cells PtK1 (*Potorous tridactylus*). Laser severing experiments were also crucial to understand the asymmetrical spindle positioning in the one-cell-stage *Caenorhabditis elegans* embryos. Grill *et al* (2001) demonstrated that pulling forces external to the spindle act on the two spindle poles, but a stronger net force acts on the posterior pole. The asymmetry in the pulling forces results in an asymmetric spindle position, which ultimately translates into an asymmetric cell division.

3.1.4. Spindle microtubules

The mitotic spindle is composed of three different MT-arrays: astral, kinetochore and interpolar MTs (Fig. 5). They may have different kinetic properties depending on the structure or protein, which they interact to.

Astral-microtubules (astral-MTs) are nucleated by the centrosomes in a radial symmetry. Whereas the plus-ends rapidly grow towards the cytoplasm and cell cortex, the slow growing minus-ends are anchored at the centrosome. Depending on the system, astral MTs are important to position the spindle and/or generate the force for chromosome segregation through force generation at the cortex (see section 3.1.2). In plants (Schmit 2002) and most female meiotic systems (Schuh and Ellenberg 2007), aster-like MTs can also be assembled .

Kinetochore-microtubules (kMTs, also known as k-fibers) establish the connection between chromosomes and the poles of the spindle. They are less dynamic than astral MTs and are arranged in an uniform polarity where the plus-ends are end-on attached to the kinetochore and the minus-ends are clustered at the poles. KMTs mediate chromosome movement and are crutial to silence the spindle assembly checkpoint (SAC).

Interpolar-microtubules (ipMTs, also known as non-kinetochore MTs) constitute all the MTs that lie between the two poles, apart from kMTs, and have faster turnover than these ones (Saxton *et al.* 1984). Their minus-ends are either localized at the poles or throughout the spindle (Burbank *et al.* 2006). Plus-ends may extend to the spindle central region where they interact in an antiparallel way with MTs from the opposite pole. IpMTs are the instrumental unit for the establishment of bipolarity, they can assemble into a bipolar structure in the absence of kinetochores and/or centrosomes (Heald *et al.* 1996) and they work as a platform for spindle inward and outward force generation. Furthermore ipMTs are fundamental for spindle elongation mechanism during anaphase and cytokinesis initiation (Glotzer 2009).

3.2. MAPs and Molecular Motors

The dynamic behavior of MTs enables a rapid response of the different MT-arrays to different *stimuli* within the cell. MTs can exert forces, probe cellular space and rapidly reorganize throughout the cell cycle.

In vitro studies from purified tubulin showed that MT dynamics *per se* is not enough to explain its *in vivo* high-performance (Simon *et al.* 1992; Desai and Mitchison 1997). Remarkably, it was described that in the cell environment, MTs could polymerize about fourfold faster than a similar concentration of purified tubulin (Kinoshita *et al.* 2001; reviewed in Gadde and Heald 2004). In physiological conditions MT dynamics is regulated and optimized to accuracy due to the existence of a plethora of MT-associated proteins (MAPs) and motors. These accessory proteins are capable of interacting with MTs in a nucleotide-insensitive manner (reviewed by Brust-Mascher and Scholey 2007), and specifically modify their rates of growth and the frequency of catastrophes.

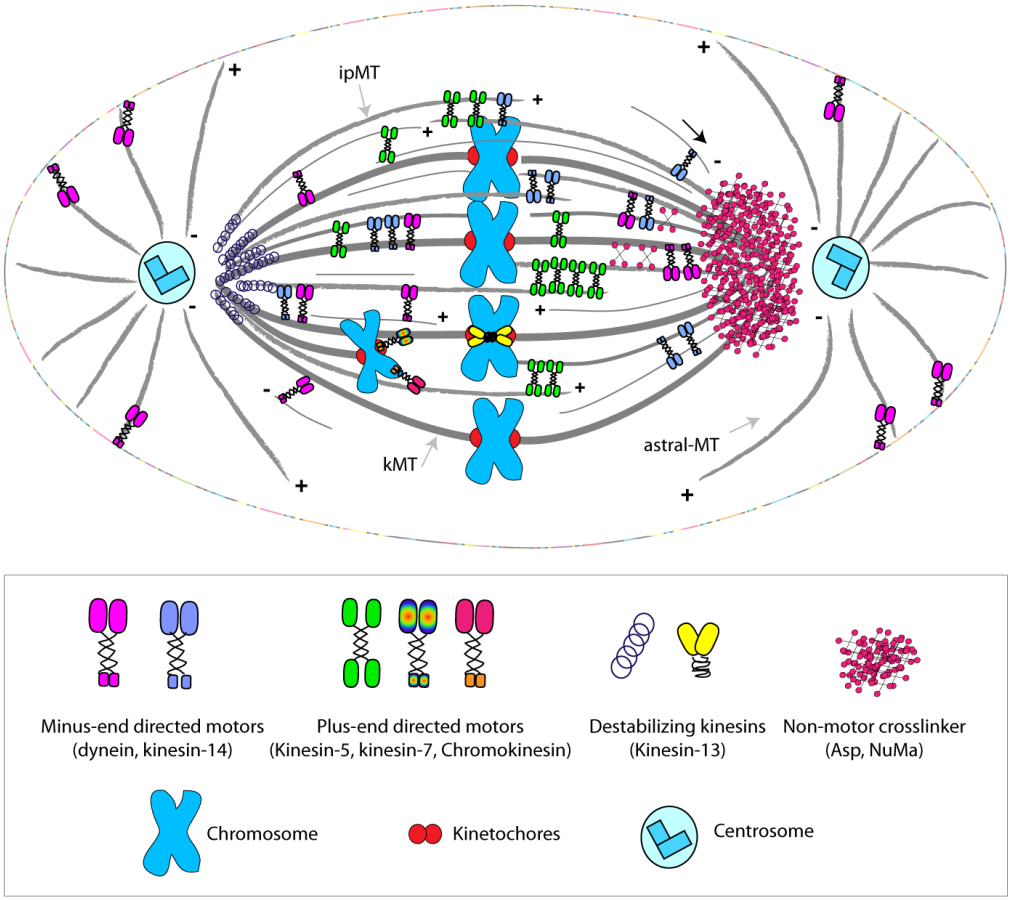


Figure 5- The key components of the spindle apparatus. The mitotic spindle is composed of different sets of MTs: astral-MTs (nucleated away from the centrosome), ipMTs (antiparallel arrays crosslinked by motors or non-motor proteins) and kinetochore-MTs (bundles of MTs attached to kinetochores). The kinetochores are specialized *multitask* structures that couple chromosomes to the rest of the spindle and are responsible for their movement. A plethora of motors and crosslinkers are still involved in the regulation of MT dynamics, movement and spindle architecture maintenance. The black arrow points towards the direction of MT translocation.

3.2.1. MAPs

There are different classes of MAPs within the spindle that can be distinguished either by their effects on MT dynamics (destabilizing and stabilizing factors) or where they bind to MTs (plus-end tracking proteins and crosslinkers).

Destabilizing factors are proteins that increase the frequency of MT catastrophes. One group of the so-called catastrophe factors is composed of kinesin-13 proteins (also known as KinI family) that has been shown to have an important role in spindle function, specially in spindle assembly, dynamics, proper chromosome attachment and segregation (reviewed by Ems-McClung and Walczak 2010). These proteins although structurally related to kinesins, they do not use their motor domain to produce movement. Instead, they use it to bind to MT ends and induce catastrophes by triggering conformational changes that disrupts lateral interactions between protofilaments (Moores and Milligan 2006; Morgan 2007). Members of this group include MCAK that was shown to antagonize the role of the stabilizing factor XMAP215 (reviewed by Kline-Smith and Walczak 2004). Due to its localization at the centromere, MCAK was also suggested to regulate proper kinetochore-MT attachment by promoting kMT turnover (Wordeman *et al.* 2007). In *Drosophila melanogaster*, members of this group include KLP10A, KLP59C and KLP59D that were implicated in MT dynamics regulation and part of the chromosome segregation machinery (Rogers *et al.* 2004; Buster *et al.* 2007; Rath *et al.* 2009). Op18/stathmin is another well conserved destabilizing protein that can promote catastrophes enhancing tubulin dissociation from MT plus-ends (Cassimeris 2002).

Stabilizing factors are proteins that bind along the MTs or at their ends in order to promote growth. The highly conserved polymerase XMAP215/TOG/Stu2p/Dis1 was described to promote MT elongation *in vitro* (Gard and Kirschner 1987) stimulating the growth rate at MT plus-ends (Kinoshita *et al.* 2001; Kinoshita *et al.* 2002). Furthermore, its binding to MTs, blocks the binding of destabilizing proteins such as kinesin-13 proteins.

+TIPs are a specialized group of stabilizing MAPs that are essentially involved in the regulation of MT dynamics (Carvalho *et al.* 2003). A conspicuous property of these factors is their preferential binding to growing MT plus-ends where they accumulate and assemble into clusters that decorate MTs. These clusters have a “comet-like” behavior and can be easily visualized *in vitro* and *in vivo* using widefield microscopy. This specific localization and behavior facilitates their role in the regulation of MT interactions with different cellular structures such as kinetochores, cell cortex, organelles and membranes

(reviewed in Akhmanova and Steinmetz 2008). Members of this group include, CLIPs, CLASPs, EB1, APC and many other proteins primarily involved in the regulation of MT dynamics (reviewed by Maiato *et al.* 2004c) Particularly, CLASPs can be seen in different mitotic structures and in all MT arrays (Inoue *et al.* 2000; Lemos *et al.* 2000). This protein has been implicated in several mitotic functions, particularly those that regulate the dynamics of kinetochore-MT attachment, and the quality control of chromosome segregation (Maiato *et al.* 2003a; Maiato *et al.* 2005; Pereira *et al.* 2006; Maffini *et al.* 2009; Reis *et al.* 2009).

Crosslinking proteins include motors and non-motor MAPs that have the capacity to crosslink adjacent MTs and organize bundles. These proteins assume important roles not only in spindle assembly (Walczak and Heald 2008) and equilibration of spindle inward and outward forces (see next section for details; Peterman and Scholey 2009), but also facilitating the spindle elongation movement by creating a stable central spindle (Glotzer 2009). In vertebrates, NuMA (Merdes *et al.* 1996; Gordon *et al.* 2001; Silk *et al.* 2009) and TPX2 (Wittmann *et al.* 2000; Manning and Compton 2007) have been shown to be fundamental in spindle assembly specially by promoting anchoring and crosslinking of MT minus-ends at the spindle poles. The minus-end directed motor HSET was also implicated in this function (Gordon *et al.* 2001). In *Drosophila,* spindle pole focusing is assured by ASP (do Carmo Avides and Glover 1999; Morales-Mulia and Scholey 2005), Mob4 (Trammell *et al.* 2008) and by the minus-end directed motors Ncd and dynein (Goshima *et al.* 2005a; Morales-Mulia and Scholey 2005).

Finally, crosslinkers can also assume a crucial role in central spindle assembly, mainly by organizing ipMT into bundles where motors can work in order to promote sliding. PRC1/Ase1p is a highly conserved MAP and can be found in metazoans (Jiang *et al.* 1998; Verni *et al.* 2004), plants (Chan *et al.* 1999), and yeast (Pellman *et al.* 1995; Loiodice *et al.* 2005). This crosslinker localizes to the central spindle where it was shown to directly bundle MTs. In yeast, ase1 was recently shown to promote spindle elongation (Fu *et al.* 2009; Khmelinskii *et al.* 2009) and merotelic attachment prevention (Courtheoux *et al.* 2009).

3.2.2. Molecular Motors

The coordinated interaction of different MT-arrays and the establishment of a bipolar spindle depend on the precise action of MT-based motors. These proteins are mechanochemical enzymes that use ATP hydrolysis to generate force and motion (Sharp *et al.* 2000a; Sharp *et al.* 2000c). MT motors are typically dimers of two identical subunits,

each containing a globular head or motor domain that is also ATPase. ATP hydrolysis causes small conformational changes in a globular motor domain that is amplified and translated into movement with the aid of accessory structural motifs. Additional domains outside the motor core are responsible for dimerization, regulation and interaction with other molecules (Schliwa and Woehlke 2003). MT Motors can be divided into two major families (Hirokawa *et al.* 1998), the kinesin or kinesin-related proteins (Vale *et al.* 1985), and dynein (Paschal *et al.* 1987).

Kinesins. There are two different types of kinesins, each characterized by the localization of its motor domain and consequently by its directed movement. Whereas N-terminal kinesins are plus-end directed (KIN N), C-terminal kinesins move towards the MT minus-ends (KIN C). Different KIN N were shown to be important during mitosis including members of the kinesin-5, kinesin-6 and kinesin-7, and the chromokinesins kinesin-4 and kinesin-10. The bipolar kinesin-5 proteins form tetramers with motor domains at both ends of a central rod. Functionally, these motors can crosslink (van den Wildenberg *et al.* 2008) and walk along antiparallel MTs (Kapitein *et al.* 2005). Kinesin-5 proteins (Eg5/KLP61F/Cin8p and Kip1p; vertebrates/*Drosophila*/*Saccharomyces cerevisiae*) are responsible for the generation of poleward forces that can drive MT sliding (Miyamoto *et al.* 2004; Shirasu-Hiza *et al.* 2004; Brust-Mascher *et al.* 2009) and promote pole-to-pole separation (Hoyt *et al.* 1992; Heck *et al.* 1993; Sharp *et al.* 1999). Antagonistic KIN C, kinesin-14 motors (HSET/Ncd/Kar3; vertebrates/*Drosophila*/*S. cerevisiae*) have also the capacity to slide antiparallel MTs (Braun *et al.* 2009; Fink *et al.* 2009), although in the inward direction thus balancing the force promoted by kinesin-5 motors. Furthermore, kinesin-14 proteins are responsible for focusing MTs at the spindle poles (Goshima *et al.* 2005a). Kinesin-6 motors (MKLP1/Pavarotti/Klp9p; vertebrates/Drosophila/*S. pombe*) were known until now, to be mainly involved in central spindle assembly and MT bundling (Glotzer 2009), however, recent studies showed that this protein can form dimers and tetramers important for sliding MTs apart. This kinesin-6 motor was thus implicated as a force-driver for spindle elongation in *S. pombe* (Fu *et al.* 2009). It is still unknown whether this function is conserved amongst other eukaryotes. CENP-E is a kinesin-7 motor, that during mitosis, associates to the outer plate of kinetochores (reviewed by Maiato *et al.* 2004a) and drives chromosome congression (Kapoor *et al.* 2006). Finally, the chromokinesins, kinesin-4 and kinesin-10 are associated with chromosome arms and were shown to be involved in chromosome positioning at the spindle equator (Tokai *et al.* 1996; Antonio *et al.* 2000) and accurate chromosome condensation and segregation (Mazumdar *et al.* 2004).

Cytoplasmic dynein motors are large, multimeric, minus-end directed motors that link microtubules to other proteins in many cellular locations. They were shown lo localize at the kinetochores (Pfarr *et al.* 1990; Whyte *et al.* 2008), cell cortex (Gonczy *et al.* 1999; Fink *et al.* 2006) and along spindle MTs (Varma *et al.* 2008), where they execute a variety of functions that includes centrosome separation (Gonczy *et al.* 1999), chromosome capture and congression (Yang *et al.* 2007), spindle assembly and positioning (Gonczy 2002), spindle pole organization (Goshima *et al.* 2005a) and SAC (Howell *et al.* 2001; Wojcik *et al.* 2001).

3.3. The Kinetochore

Since the first drawings of mitosis it was possible to observe that chromosomes are not static (Flemming 1882; Wilson 1925; Flemming 1965) as they always appear in different positions within the mitotic spindle. Chromosomes align and segregate due to the existence of a large proteinaceous assembly, the kinetochore (from the Greek *kinetos*=movement *chore*=place). This structure connects the chromosomes to the spindle, and besides powering their movement, it also works as a signaling platform during mitosis (Fuller and Stukenberg 2009). The development of cell biological and biochemical super-resolution techniques has been crucial for the mapping and resolution of kinetochore structure and composition. While electron microscopy and tomography studies provide a deeper insight about the structure, proteomics provides a better understanding about its components and interactions (Dong *et al.* 2007; Welburn and Cheeseman 2008; Wan *et al.* 2009). Kinetochores are also very dynamic structures, as they have to assemble and disassemble every cell cycle. In order to interact with MTs, the kinetochore interface should be labile as MT dynamics vary a lot during mitosis (see section 4.2 for kintochore-MT attachment).

3.3.1. Structure and composition

The first electron microscopy studies revealed that vertebrate kinetochores have a trilaminar morphology (Brinkley and Stubblefield 1966; Cleveland *et al.* 2003) composed of electron-opaque outer and inner plates separated by an electron translucent-middle layer (Fig. 6, a and b). The inner plate is composed of proteins that are constitutively located throughout the cell cycle and constitute the interface with centromeric chromatin. The outer plate contains the proteins that will interact with the plus-ends of MTs and are loaded in the beginning of mitosis. Outside the outer plate it is still possible to find the

fibrous corona where motors such as CENP-E, CLASPs or SAC proteins localize (Santaguida and Musacchio 2009).

The simplest kinetochore described is the one from *Saccharomyces cerevisiae* that binds only to one MT. Its core structure is composed of more than 70 proteins clustered in eight multi-component protein complexes that are mostly conserved from yeast to humans where it typically binds to 25-30 MTs (Joglekar *et al.* 2009; Bloom and Joglekar 2010). This structural conservation soon led to the proposal of a repetitive subunit model where kinetochores that bind to multiple MTs are composed of repetitive models of simpler kinetochores (reviewed by Zinkowski *et al.* 1991; Brinkley *et al.* 1992). However, recent high-resolution electron tomography studies found no evidence for the existence of those repetitive units, proposing alternatively, a flexible fibrilar network that interacts with the MTs it encounters (Dong *et al.* 2007).

The inner domain of the kinetochore is assembled from proteins constitutively present at centromeres during all the cell cycle. The first protein to assemble is a conserved hallmark of the centromere-kinetochore interface and the core unit of nucleosomes, CENP-A (Earnshaw and Rothfield 1985; reviewed by Black and Bassett 2008). This protein is an isoform of the histone H3 that in both humans and flies replaces H3 in the nucleosomes of chromatin at the base of kinetochores (Blower *et al.* 2002; Wan *et al.* 2009). Following CENP-A, fourteen proteins compose the constitutive centromere-associated network (CCAN) and include, CENP-C, implicated in loading CENP-A to centromeres, CENP-H/I and CENP-K-U/W. All this CCAN subunits require CENP-A for their localization and are associated to CENP-A throughout the cell cycle (reviewed by Cheeseman and Desai 2008; Welburn and Cheeseman 2008; see also Santaguida and Musacchio 2009). Conversely to the constitutive localization of inner proteins throughout the cell cycle, outer kinetochore complexes are just loaded in the beginning of prophase and leave kinetochores upon anaphase onset or once they disassemble at the end of mitosis. The assembly of the KMN network will provide the core MT-attachment sites. Three highly conserved complexes compose the KMN network: the Mis12 complex (Mis12, Dsn1, Nnf1, and Nsl), Knl1 (Knl1, Zwint), and the Ncd80 complex (composed of Hec1/Ndc80, Nuf2, Spc24 and Spc25) (Fig. 6, c and d). Other regulatory complexes may associate within the outer kinetochore, throughout the fibrous corona, namely the SAC components, MT motor proteins, CENP-F and proteins that regulate MT plus-end dynamics (Maiato *et al.* 2004a; Cheeseman and Desai 2008; see also Santaguida and Musacchio 2009; Wan *et al.* 2009).

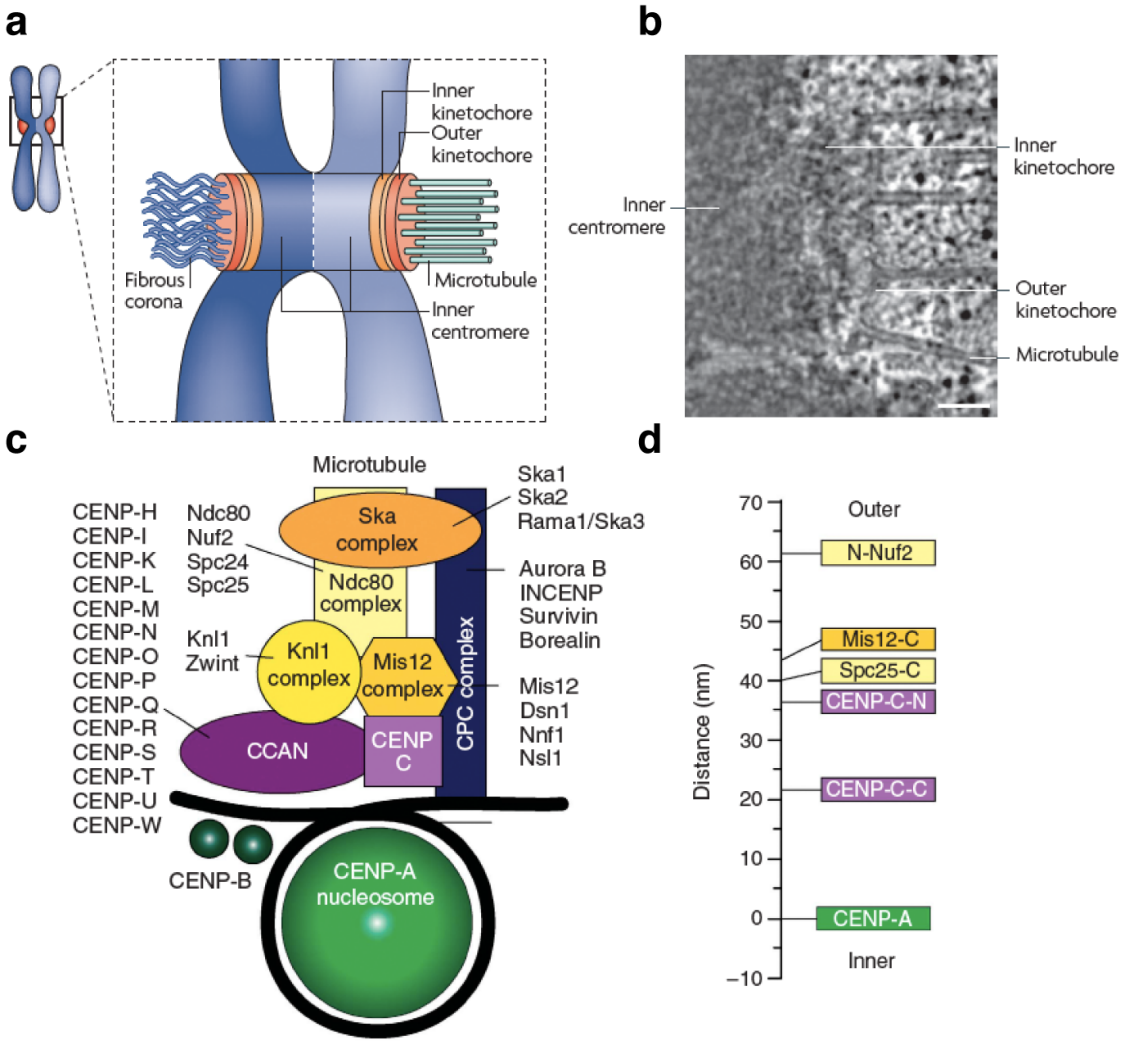


Figure 6 – The kinetochore structure and composition. **a)** A schematic representation of a mitotic chromosome with paired sister chromatids — the chromatid on the right is attached to microtubules and the chromatid on the left is unattached. The inner kinetochore, the outer kinetochore, the inner centromere and the fibrous corona, which is detectable on the unattached kinetochore, are highlighted. **b)** Electron micrograph of a human kinetochore. The micrograph represents a single slice from a tomographic volume of a high-pressure frozen mitotic cell and has been labeled as in "a" to highlight the key structural features of the kinetochore. Scale bar, 100 nm. **c)** Outer kinetochore representation of metazoans where the different component complexes are shown. **d)** Average location of kinetochore proteins along the axis of the kinetochore–microtubule attachment in metaphase in *D. melanogaster*. N- and C- indicates N- and C-termini. Adapted by permission from Macmillan Publishers Limited: Nature Reviews Molecular Cell Biology (Cheeseman and Desai) © 2009, and EMBO Journal (Santaguida and Musacchio) © 2009.

3.4. The Centrosome

Centrosome is the major organizer of MT arrays in metazoans and is fundamental for the cell cycle fidelity in most animal cells. This organelle was firstly identified by Flemming but received its name from Theodor Boveri in the late 19th century due to its localization in the center of the cell (Wilson 1925; Mazia 1984; Urbani and Stearns 1999; Paweletz 2001; Nigg and Raff 2009). Its functions have been studied and dissected for more than 100 years and it was shown that centrosomes are involved in determining the shape, polarity and motility of different cells (reviewed by Nigg and Raff 2009). This complex structure is important during cell division and its duplication is tightly regulated throughout the cell cycle (reviewed by Bettencourt-Dias and Glover 2007). Despite its importance, this structure was described to be absent in higher plants and in some female meiotic systems. In fact, acentrosomal cells and female meiotic systems are able to organize the cytoskeleton and a functional spindle (Heald *et al.* 1996; Murata *et al.* 2005; Schuh and Ellenberg 2007). Recent experiments in cells devoid of functional centrosomes led to the discovery and characterization of alternative non-centrosomal MT-organizing centers (aMTOC) capable of nucleating MTs and important to MT cytoskeleton remodeling (Moutinho-Pereira *et al.* 2009). Moreover it is described that even in cells that have centrosomes, secondary MTOCs may co-exist and contribute to spindle assembly and MT-cytoskeleton organization (Miller *et al.* 2009).

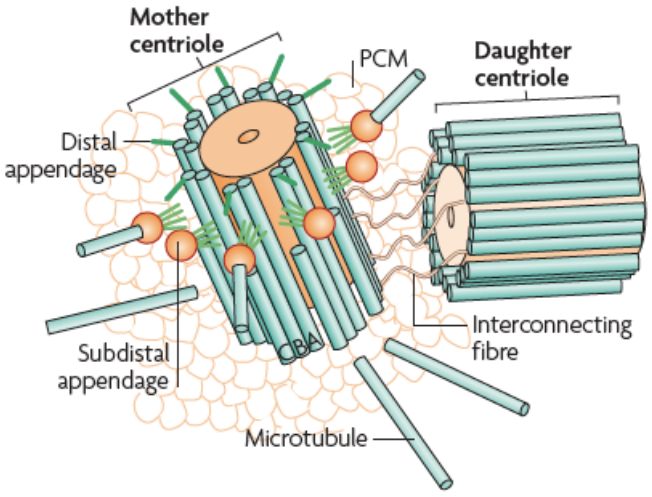


Figure 7 – Centrosome structure. The centrosome is composed of a pair of centrioles each with nine-fold symmetry due to the nine triplet MTs and with ~0.5 μm in length. Pericentriolar material surrounds centrioles and allocate MT nucleation. Adapted by permission from Macmillan Publishers Limited: Nature Reviews Molecular Cell Biology (Bettencourt-Dias and Glover) © 2007

3.4.1. Structure and function during mitosis

Centrosomes are complex structures composed of two centrioles surrounded by an electrondense matrix, the pericentriolar material (PCM). Centrioles are MT-based short cylinders that are oriented perpendicularly to each other (Fig. 7). The lattice of the cylinders is composed of nine triplets of MTs, which confers to centrioles a symmetric organization (for reviews see Doxsey 2001; Bettencourt-Dias and Glover 2007). The PCM usually surrounds the centrioles and is responsible to anchor and nucleate MTs. This meshwork contains a fibrous scaffold decorated with several MT nucleating γ-tubulin ring complex (γ-TuRC). From electron-microscopy studies it was possible to unveil that γ-TuRCs cap MT's minus-ends, while working as templates for new MTs, which grow by addition of tubulin subunits at the plus-end (Erickson 2000; Moritz *et al.* 2000).

Although not essential for the mechanics of chromosome segregation, it is not evident that the high fidelity of chromosome segregation and progression throughout cell cycle is maintained after centrosome depletion and/or ablation (Hinchcliffe *et al.* 2001). During mitosis, centrosomes are important to center the mitotic spindle within the cell through their astral-MTs (Gonczy 2002). Also, it was shown that if centrosomes were not present or if they were ablated in vertebrate cells, cytokinesis abscission and exit from mitosis would be delayed or even impaired (Khodjakov and Rieder 2001; Piel *et al.* 2001).

4. SPINDLE DYNAMICS

The mitotic spindle is the most complex structure that a cell can build during its cell cycle. Although this structure and its functions have been dissected for over a century, it still hides mysteries that will feed the curiosity and knowledge of future scientific generations.

4.1. Spindle Assembly and the Mechanisms of Chromosome Congression

In order to maximize the probability of a faithful and equitable segregation, the cell must assemble a bipolar spindle where sister-chromatids bi-orient and start to segregate from the same division plane (Fig. 8). During evolution the establishment of a metaphase plate in the spindle equatorial region has been conserved amongst metazoans and higher plants. In order to congress, kinetochores need first to attach to MTs and then move in the

direction of the spindle equator. Congression will thus determine the duration of prometaphase and it may last until the spindle is completely assembled (reviewed by Rieder and Salmon 1994). The two main pathways currently debated to explain spindle assembly in eukaryotic systems also suggest mechanisms for chromosome congression. Besides the search-and-capture model and the chromatin mediated spindle assembly, chromosome congression can also be explained by motors and by a polar ejection force (also known as *polar wind*).

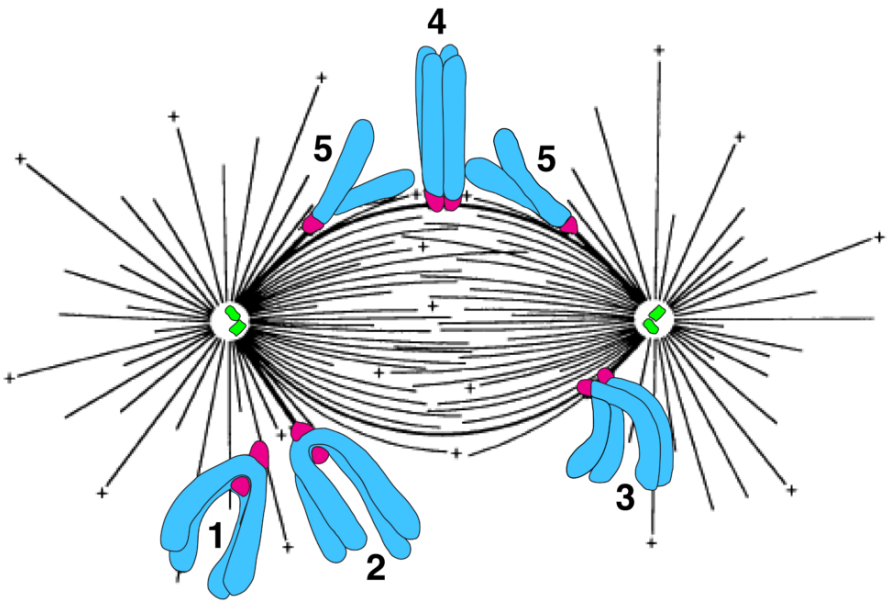


Figure 8 – Chromosome movements during mitosis. Throughout mitosis chromosomes show different kinds of movement: 1 and 2) monooriented chromosomes 1) glide and 2) depolymerize MTs towards the poles; 3) bioriented chromosomes start to congress and 4) align at the metaphase plate; 5) segregating towards the poles occurs after the anaphase onset. Adapted from Rieder and Salmon (1994).

4.1.1. Search-and-capture model

It was in the beginning of the last century that the centrosomes were first proposed by Boveri as the centers of cell division (reviewed by Karsenti and Vernos 2001) and until recently, they were considered the principal centers for MT nucleation and spindle assembly in animal cells (Wittmann *et al.* 2001). The combination of *in vitro* studies describing the dynamic instability property of MTs (Mitchison and Kirschner 1984a) with the demonstration that isolated centrosomes could nucleate and assemble MTs (Mitchison and Kirschner 1984b) led to the proposal of the "search-and-capture" model. This model states that highly dynamic MTs nucleated by the centrosome randomly probe the three-dimensional space, until they are captured and stabilized by kinetochores (Kirschner and

Mitchison 1986). Accordingly, monooriented chromosomes are expected to stay near the pole until the unattached sister kinetochore establishes the attachment to the opposite pole. Bi-oriented chromosomes are thus expected to congress by the depolymerization of the leading kMT (reviewed by Rieder and Salmon 1994; Walczak *et al.* 2010). This model although very intuitive seems unlikely. Wollman *et al* (2005) using mathematical modeling verified that without any bias toward chromosomes, the search-and-capture model would not be fast enough to account for the typical duration of spindle assembly, requiring several hours until all the chromosomes of a human cell could congress to the metaphase plate .

4.1.2. Kinetochore-mediated k-fiber formation

The spindle assembly can also be explained by a second model that attributes to chromatin the capacity of generating a gradient of Ran-GTP that promotes MT nucleation and stabilization in the vicinity of chromosomes (reviewed by Karsenti and Vernos 2001; Kalab *et al.* 2002). The acentrosomal pathway exists not only in plants and animal oocytes (McKim and Hawley 1995) but also in systems where centrosomes are normally present (Khodjakov *et al.* 2000; Maiato *et al.* 2004b; Basto *et al.* 2006; Tulu *et al.* 2006).

Experiments where the spindle was pharmacologically destabilized (Khodjakov *et al.* 2003) or kMTs were thermally perturbed by laser ablation, have demonstrated that kinetochores have the capacity to reform kMTs that are subsequently incorporated within the spindle (Maiato *et al.* 2004b; Pereira *et al.* 2009). Accordingly, kMT formation can thus be initiated when a kinetochore captures short, non-centrosomal MTs that are nucleated near the chromosome primary constriction (Snyder and McIntosh 1975; Tulu *et al.* 2003). After being captured by the kinetochore, plus-end polymerization will be promoted and the fiber will grow outwards until it encounters a centrosomal MT. This will eventually reposition the chromosome at the spindle equatorial region.

4.1.3. Molecular motors and the polar ejection forces

Motors localized at kinetochores can also contribute to the movement of monooriented chromosomes towards the spindle equator. In fact, it was recently shown that kinetochores do not need to establish end-on attachments to kMTs to congress to the metaphase plate (Cai *et al.* 2009). Particularly, Kapoor and co-workers have shown that kinetochores could slide on mature kMTs of bi-oriented chromosomes through the action of the plus-end directed motor CENP-E (Kapoor *et al.* 2006). Chromosome congression can still be facilitated by the *polar wind* (reviewed by Fuller 1995). The model for this mechanism suggests that chromosomes, as a whole, can be pushed away from their

associated pole, by growing astral MTs without an apparent intervention from the kinetochores (Rieder and Salmon 1994). Furthermore, different molecular motors localized in the chromosomes arms were suggested to be involved in this movement, specially the kinesin-10 KID, and KLP1 (reviewed by Walczak *et al.* 2010).

4.2. Kinetochore-Microtubule Attachment

The flawless execution of mitosis requires the proper bipolar attachment of chromosomes to the mitotic spindle (Fig. 10, a-d). This function is executed by kinetochores that assume a central role in the quality control of mitosis. Kinetochore-MT attachments have to be stable, yet dynamic, in order to correct and establish proper attachments, transduce force, and above all, couple MT dynamics to chromosome movement. In recent years two different models have been debated in order to explain the simultaneity of kMT attachment and movement: the *biased diffusion mechanism* and the *forced walk mechanism*.

4.2.1. Biased diffusion mechanism

The biased diffusion model was the first mechanism to be proposed in order to explain kinetochore-MT interaction, specifically depolymerization-coupled movement. Terrell Hill (1985) modeled the kinetochore as a "sleeve" (or channel) with sets of MT binding-sites. At the kinetochore, sleeves encircle the plus-ends of MTs promoting multiple weak/dynamic linkages between the kinetochore and the MT. Thermal fluctuations allow sliding of the kinetochore sleeve relative to MTs. Maximal insertion of MT plus-ends into the sleeve is thus energetically favorable promoting an increase in the number of kinetochore-to-MT interactions. Conversely, if the plus-end of MT starts to lose subunits the sleeve would follow the depolymerizing MT plus-end (Desai and Mitchison 1997; Joglekar and Hunt 2002; Miranda *et al.* 2005; Westermann *et al.* 2005; Gardner and Odde 2006; McIntosh *et al.* 2008; Bloom and Joglekar 2010).

Recent experimental work supports the Hill sleeve model, bringing it again to discussion. The tomography reconstruction of the mammalian kinetochores proposes the existence of a fibrilar mesh that permits multiple kinetochore-MT interactions either at the tips of MTs or at their lattice (Fig. 9, a-c; Dong *et al.* 2007). It also suggests that the KNL1 and Ndc80/Hec1 are part of the long fibrous elements hypothesizing that is the Ndc80/Hec1 complex that extends out to attach to kMT walls. Two seminal works have identified this complex has the coupler between kinetochore and MTs. The characterization of the Ndc80/Hec1 complex showed that it has both kinetochore and MT

binding sites (Cheeseman *et al.* 2006) being also capable of regulating kinetochore-MT dynamics and MT attachment (DeLuca *et al.* 2006). Finally, the "*pie in the sky*" for the Ncd80/Hec1 as the kinetochore-MT coupler, resulted from three important works. Whereas Guimaraes *et al* (2008) and Miller *et al* (2008) showed that in vertebrate cells Ncd80/Hec1 performed weak/electrostatic MT-interactions, Powers *et al* (2009) showed *in vitro* that the bias diffusion of this complex was sufficient to track depolymerizing MTs (Fig. 10, a). Understanding the existence of a stable yet dynamic kinetochore-MT interaction, promotes a strong bias to accept this model in light of the kinetochore multitasking activity. Overall, the Ncd80/Hec1 complex should definitely be part of the textbook model for the kinetochore-MT attachment in vertebrate cells.

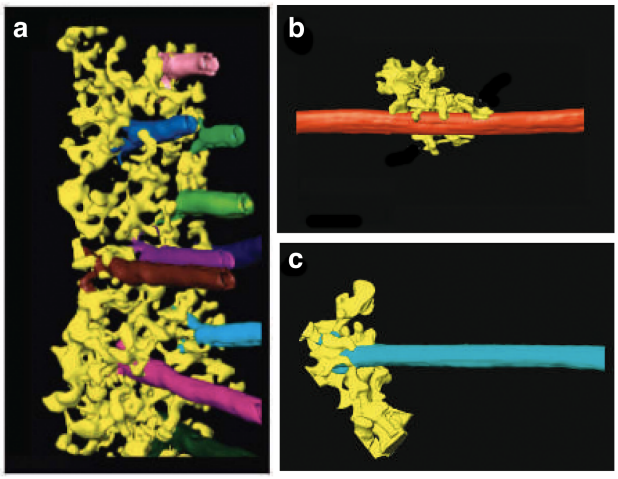


Figure 9 – Flexible network model. a) Electron tomography of PtK1 kinetochores reveals a fibrous structure of the outer plate that rearranges upon MT attachment. **b)** Short fibers can laterally interact with MTs or **c)** end-on attachment can be performed. Adapted by permission from Macmillan Publishers Limited: Nature Cell Biology (Dong *et al.*) © 2007.

4.2.2. Forced-walk mechanism

An alternative model for the kinetochore-MT interaction is the forced-walk mechanism (Fig. 10, b and c), which explains the kinetochore-coupled movement with the energy stored in the lattice of MTs. When GTP hydrolysis occurs in the plus-ends of kMTs, depolymerizing MTs will bent their tubulin protofilaments. The existence of a kinetochore coupler that resists to the free bending can use this energy to drive chromosome segregation. The discovery that the *Saccharomyces cerevisiae* DASH (Dam1) complex oligomerizes *in vitro* to form rings around the lattice of MTs (Miranda *et al.* 2005; Westermann *et al.* 2005) brought a strong input for this model as it was shown that those rings could stay associated to MTs, working as a processive coupler (Westermann *et al.* 2006; Grishchuk *et al.* 2008a). The lack of evidence for the existence of such rings, even in the budding yeast, led to the investigation whether non-circling couplers could also be processive (Grishchuk *et al.* 2008b). McIntosh *et al* (2008) using PtK1 cells suggested the existence of a new fibrilar coupler that can couple MT-attachment to the generation of

movement. Accordingly, they found 2-4 nm filaments that connect to the bent tips of curved MTs, proposing that the end-on attachment could, indeed, do mechanical work (Bloom 2008).

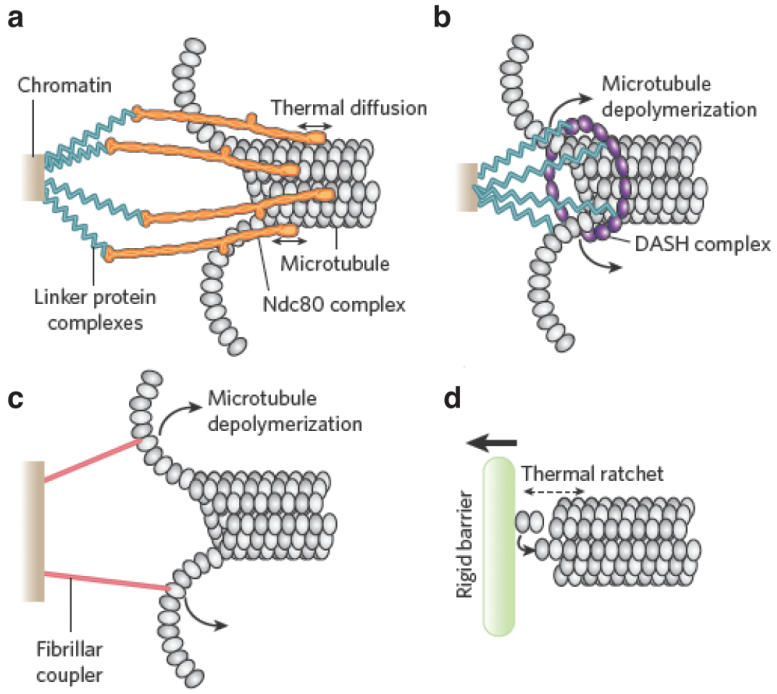


Figure 10- Proposed mechanisms for microtubule-depolymerization-coupled force generation at the kinetochore. Two types of mechanism have been proposed: biased diffusion (a) and forced walk (b, c). **a)** Microtubules can be persistently attached to lattice-binding proteins such as the Ndc80 complex through many diffusive couplers (for example, flexible, positively charged amino acids at the amino terminus of the Ndc80 subunit of the Ndc80 complex) attached at different distances from the plus end. Thermal diffusion is depicted as random fluctuations of the microtubule lattice (double-headed arrows). Depolymerization at the microtubule plus-end provides a bias to the diffusive movements while attachment can be maintained. **b)** The discovery of DASH rings and subsequent *in vitro* studies led to the idea that ring couplers (such as the DASH complex) are involved in force generation. Energy from microtubule depolymerization drives the rings towards the microtubule minus end (curved arrows). **c)** Ultrastructural study of the vertebrate kinetochore uncovered the presence of fibrilar couplers (pink) that attach to peeling microtubule protofilaments at specific locations. This discovery led to the idea that fibrillar couplers can themselves be force generators. **d)** Ratchet model, when the plus end of a microtubule polymerizes against a rigid barrier, such as the cell wall, this can also generate forces, albeit smaller ones, but these forces are not thought to have a significant role in kinetochore motility. Adapted by permission from Macmillan Publishers Limited: Nature (Bloom and Joglekar) © 2010.

4.3. The Spindle Assembly Checkpoint

The spindle assembly checkpoint prevents the onset of anaphase until all chromosomes are stably attached to the mitotic spindle. Kinetochores are the sensors for this signal-transduction network that will generate the wait-anaphase signal until a proper and stable attachment is maintained.

4.3.1. Molecular machinery

Almost 20 years ago two genetic screens using the budding yeast, led to the discovery of genes responsible for the SAC signaling pathway: the mitotic arrested-deficient *mad1*, *mad2* and *mad3* (this later being BUBR1 in metazoans; Li and Murray 1991), and the budding uninhibited benzimidazol *bub1*, *bub2* and *bub3* genes (Hoyt *et al.* 1991). These genes are conserved from yeast to humans. Mad and Bub proteins accumulate at kinetochores early in mitosis and both can be found associated with the KMN network where they become ideally positioned to monitor the establishment of a proper attachment (Cheeseman and Desai 2008). In the absence of kMTs, the kinetochore serves as a platform for the assembly of the major anaphase onset inhibitor, the mitotic checkpoint complex (MCC). MCC is composed by the checkpoint proteins Mad2, BubR1, Bub3, and also by the APC/C cofactor Cdc20. As it was briefly discussed in the section 2.1, the downstream target of the SAC is the APC/C (Peters 2006). In order to promote the anaphase onset, APC/C needs to bind to its cofactor Cdc20. One of the functions of Mad2 is to entrap Cdc20 before MT attachment can silence the wait anaphase signal. Upon SAC satisfaction, Mad2 will no longer sequester Cdc20 and this protein will bind to its APC/C partner, promoting the exit from mitosis. Besides MCC other core components of SAC include Mad1 and Mps1. These proteins are important to amplify the SAC signal and the rate of MCC formation (reviewed by Musacchio and Salmon 2007). Finally, after attachment is established the checkpoint must be switched off. In order to execute a progressive down-regulation of SAC, Mad1, Mad2, RZZ complex, Mps1 and other proteins are transported away from the kinetochore along MTs. In metazoans this “stripping” is mostly mediated by dynein (Howell *et al.* 2001; Wojcik *et al.* 2001; reviewed by Musacchio and Salmon 2007).

4.3.2. Tension *vs* attachment

A long-standing question in the field is what generates the wait-anaphase signal that ultimately controls mitotic progression. Two general hypotheses have been debated for the last two decades in order to identify the inputs that "signal" the checkpoint response: one is the kinetochore-MT attachment and the other, the tension generated across sister kinetochores upon chromosome's bipolar attachment. The first evidence for the existence and importance of tension for the stability of bipolar attachment came from a set of elegant micromanipulation experiments performed by Nicklas and co-workers using grasshopper spermatocytes (Nicklas and Koch 1969; Li and Nicklas 1995). Accordingly, they observed that the lack of tension due to syntelic attachments (both chromosomes attached to MTs from the same pole; see Fig. 11, a-d) led to a meiotic arrest that could be overcome if mechanical tension was applied in the opposite direction of chromosome attachment. Conversely, a classical experiment done by Rieder *et al* (1995) using laser ablation in PtK1 cells, showed that if the last unattached kinetochore was ablated from the spindle, the cell would rapidly release the wait-anaphase signal entering anaphase with a mono-oriented kinetochore. This experiment pointed towards an explanation that is MT attachment, and not tension, that elicits the wait anaphase signal in vertebrate cells. Furthermore, recent experiments using cells with unreplicated genomes have strongly supported this hypothesis. O'Connell *et al* (2008) demonstrated that cells could progress through mitosis independently on the attachment performed by single kinetochores (mono- or merotelic). Furthermore, they showed that although Mad2 was absent from kinetochores upon anaphase transition, BubR1 was still present at higher levels.

Another difference between the two-debated hypotheses is the differential recruitment of SAC proteins to kinetochores. Whereas Mad1 and Mad2 localize to unattached kinetochores, they are absent from kinetochores that although attached are not under tension (Waters *et al.* 1998). Conversely, BubR1 and Bub1 localize to kinetochores of both attached and unattached kinetochores when the centromere is relaxed. BubR1 levels are reduced once sister kinetochores are pushed in opposite directions (Hoffman *et al.* 2001; Skoufias *et al.* 2001). Moreover, the phosphorylation state of the 3F3/2 phosphoepitope is also recognized as a marker for tension (Gorbsky and Ricketts 1993; Nicklas *et al.* 1995), as it is highly phosphorylated in low-tension conditions. Recently it was proposed that the state of phosphorylation of 3F3/2 works as a readout for the intra- rather than inter-kinetochore tension (Maresca and Salmon 2009). In yeast, the lack of tension is still sensed by the Aurora B orthologue Ilp1 that ultimately potentiates the checkpoint by creating unattached kinetochores (Biggins and Murray 2001; Pinsky and Biggins 2005; Pinsky *et al.* 2006).

The tension *vs* attachment question remains unsolved, and although it is clear that what is being "sensed" are unattached kinetochores (Khodjakov and Rieder 2009b), a unifying hypothesis is being defended by the proponents of the "one pathway hypothesis" that gather SAC and error correction in the same checkpoint pathway (Maresca and Salmon 2010).

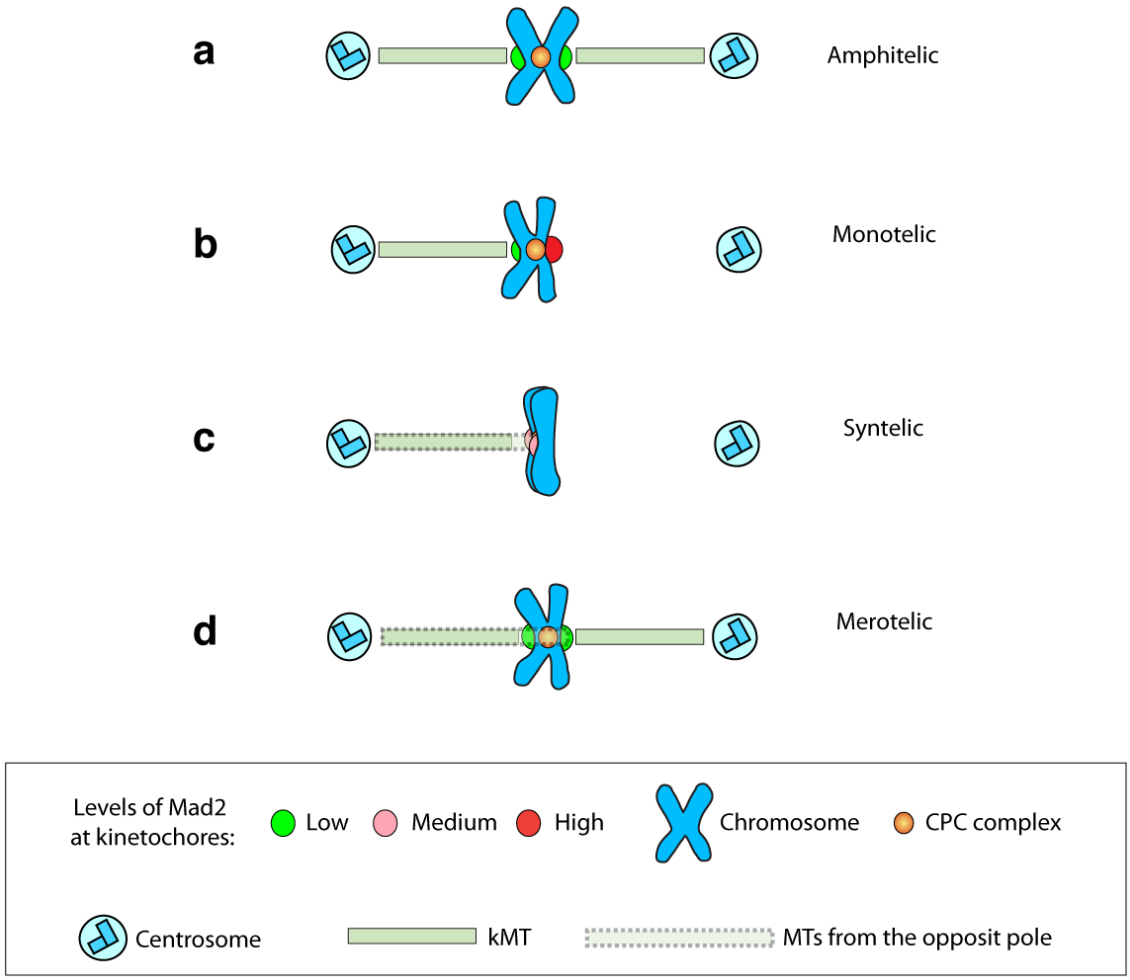


Figure 11 – Correct and incorrect kinetochore-to-microtubule attachment. **a)** Amphitelic attachment is performed when sister-kinetochores facing opposite poles, attach MTs from the nearest one. **b)** Monotelic attachment is a normal prometaphase condition where one sister kinetochore is attached to one pole but not yet to the other. High levels of Mad2 signal the unattached kinetochore. **c)** Syntelic attachment is an incorrect condition achieved when both kinetochores are attached to MTs from the same pole. As the inter-kinetochore tension is reduced, these attachments become more prone to destabilization regulated by the chromosome passenger complex (CPC), and Mad2 may transiently accumulate to kinetochores. **d)** Merotelic attachment is performed when one kinetochore attaches to MTs from both poles. If sister-chromati is correctly attached and a threshold of inter-kinetochore tension is achieved, the wrong attachment may not be destabilized and the checkpoint satisfied.

4.4. Metaphase: a Dynamic Steady-State

The static spindle-textbook-pictures can strongly hinder the dynamic activity that characterizes a metaphase spindle. Although the conspicuous steady-state metaphase spindle is characterized by a constant length and shape, MTs are still dynamic and can be recycled due to the activity of MT turnover and poleward flux.

4.4.1. Turnover

One of the properties that characterize the dynamic state of mitotic spindle is the capacity it has to rapidly renew its MTs. Different subpopulations of MTs constitute mitotic and meiotic spindles, and their turnover rates can vary throughout the different stages of mitosis. Classical studies have shown that MTs half-life can vary from ~3 min in interphase to ~10-80 sec in metaphase (Saxton *et al.* 1984). These fast rates of metaphase are conserved amongst different systems (Salmon *et al.* 1984; Hamaguchi *et al.* 1987; Cassimeris *et al.* 1988; Gorbsky *et al.* 1990; Buster *et al.* 2007; Cheerambathur *et al.* 2007) and are attributed to MT dynamic instability of non-kinetochore MTs. Zhai *et al* (1995), showed in a quantitative study that during metaphase kMTs could also turnover, albeit slower ($t_{1/2}$=4.7min). This observation recalls the importance of the liability of kinetochore-MT attachment that if in one hand has to be strong to guarantee chromosome motility, on the other has to be labile enough to permit the disassembly of incorrect kinetochore-MT attachments. Zhai *et al* still showed that kMT turnover is reduced upon the metaphase-anaphase transition ($t_{1/2}$=22.4 min), suggesting an active regulation of kMT release upon anaphase onset (Gorbsky and Borisy 1989; Zhai *et al.* 1995).

4.4.2. Poleward microtubule flux

The mechanism of poleward flux is conserved among high eukaryotes (Rogers *et al.* 2005) and is currently considered a hallmark of metazoan spindles (Kwok and Kapoor 2007). Within the spindle, poleward translocation of MTs occurs with the consequent incorporation of MT subunits at the plus-ends and disassembly at the poles (Mitchison *et al.* 1986; Mitchison 1989). This mechanism is distinct from the simple treadmilling model (Fig. 12, a) proposed by Margolis (1978), as the rates of poleward flux cannot be explained simply by the intrinsic properties of MTs. It relies on the activity of motors and thus on ATP consumption (Sawin and Mitchison 1991). Several players have been involved in the regulation of this mechanism, however its importance depends on the system studied.

The existence of poleward flux was firstly inferred by Inoue (1964) and Forer (1965) by the observation of the movement of Areas of Reduced Birefringence (ARBs),

and since then different lines of investigation have been conduced to describe and unveil its importance in the context of cell division.

Four main mechanisms are currently debated concerning the origin of the flux-driving force. The first, assumes that force is generated at the kinetochore-MT interface by pushing forces triggered by MT polymerization. However if this was true, how could we explain the simultaneous incorporation of MT subunits while kinetochores are still under tension? Incorporation of MT subunits would lead to centromere compression instead of stretching. The second model states that MTs are "reeled in" at the poles due to MT disassembly by kinesin-13 motors (Fig. 12, b). In fact, it was recently observed that depletion of KLP10A in *Drosophila* embryos (Rogers *et al.* 2004) and RNAi knock-down in S2 cells lead to reduction of poleward flux (Rogers *et al.* 2004; Buster *et al.* 2007). Nevertheless, this mechanism does not explain why kMTs that are severed away from the pole and have a stable minus-end, re-grow at flux rates (Maiato *et al.* 2004b; Pereira *et al.* 2009). In order to promote force and thus MT translocation, kinesin-13 motors need to be mechanically anchored while they disassemble MTs. Electron microscopy studies have shown that kinesin-13 proteins are able to form spirals and rings around the MTs (Tan *et al.* 2006; Mulder *et al.* 2009; Pereira *et al.* 2009), however these reconstitutions did not combine the simultaneous interactions of kinesin-13 with MTs and a fixed structure. Moreover, it was observed that after kMT ablation, the generated plus-end was rapidly depolymerized while the remaining kMT visually lost its anchorage to the poles before growing again (Maiato *et al.* 2004b; Pereira *et al.* 2009). This re-growth can be explained by a third mechanism that assumes that poleward flux depends on the outward sliding promoted by plus-end-directed motors (Fig. 12, c and d). Force could be exerted by motors attached to a "structural" matrix, or it could be exerted by sliding of interpolar MTs and further transmitted to the kMTs through crosslinkers or by other couplers (Mitchison 2005). In this model, minus-end depolymerization at the poles is thus a downstream event that occurs in order to maintain the steady length of the metaphase spindle. Finally, kMT re-growth after laser ablation can also be explained by another model where matrix associated proteins, such as myosin, interact with the spindle-associated actin that can propel them poleward thus driving MT flux (see Fig. 12, e; Forer *et al.* 2007; Forer *et al.* 2008).

Although the mechanism of poleward flux has been intensively studied, its function still remains obscure. In systems such as crane fly spermatocytes flux was suggested to be the main segregation mechanism as its velocity during anaphase is greater than the chromosome poleward movement (LaFountain *et al.* 2004). In other systems it was also invoked as a crucial mechanism for the dynamic organization of bipolar spindle assembly

(Mitchison 2005), and more recently it was suggested as part of the error correction mechanism (Ganem and Compton 2006).

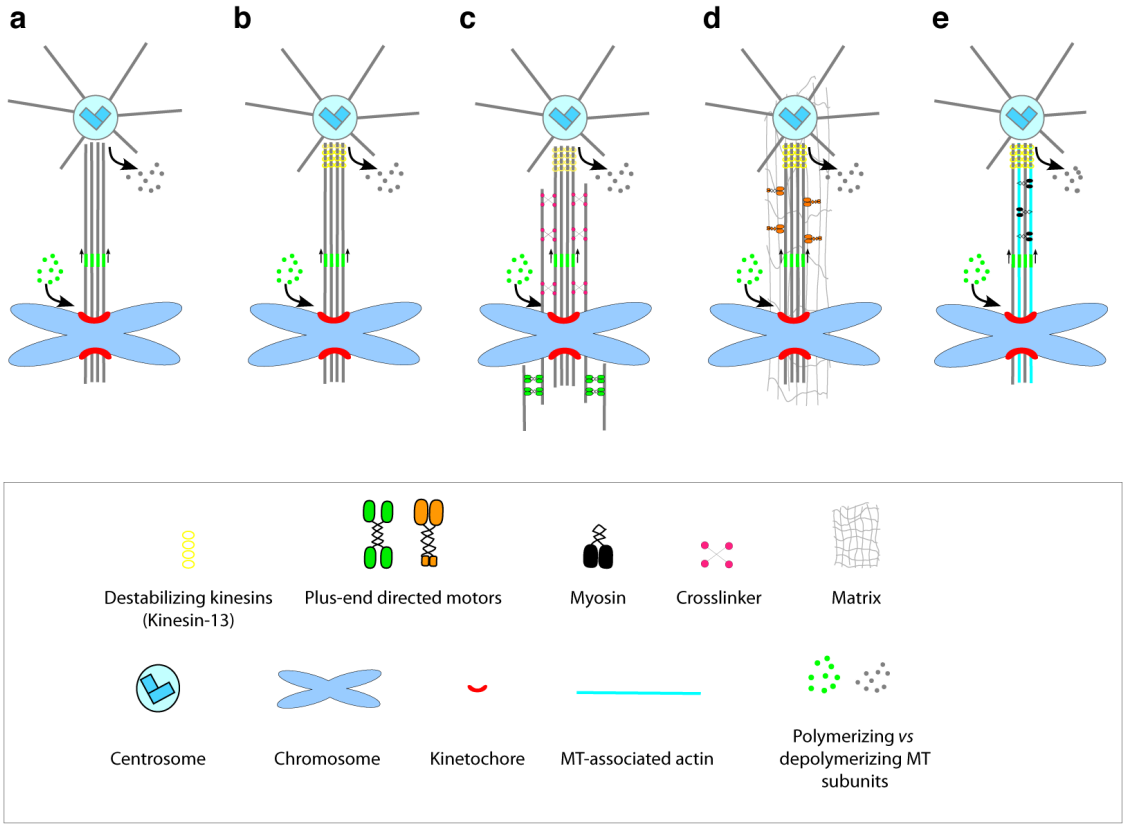


Figure 12 - Models for the microtubule poleward flux and force generation. a) Poleward movement of microtubule subunits was theoretically described by Margolis (1978) as a consequence of intrinsic properties of MTs. Three assumptions were established: the plus- and the minus-ends of MTs should be free to exchange tubulin subunits, minus-ends of kMTs should be anchored at the poles and the plus-ends of MTs should perform lateral interactions to MTs so they can exchange subunits at their tips. The next four models assume that MTs have a passive role in force generation. **b)** A putative mark on the lattice of kMT (shown in green) will move poleward as a consequence of MT depolymerization at the poles executed by kinesin-13 proteins (represented by rings around minus-ens of MTs as described by Tan *et al.* 2006). As a consequence MT-subunits will be incorporated at the kinetochores (Maiato *et al.* 2005). **(c-d)** KMT flux results from the force generated by plus-end directed motors that can either **c)** slide poleward antiparallele MTs (the force is further transmitted by crosslinker interaction between those MTs and the kMTs) or **d)** being attach to a matrix can exert plus-end directed movement on kMT, thus generating poleward translocation. In order to prevent detachment of MTs in c and d models, MT subunits will be incorporated at the kinetochores, and depolymerization at the poles occurs as a downstream event that guarantees a steady spindle length. **e)** The matrix model postulates that the myosin that interacts with MT-associated actin will generate poleward forces that pull MTs. As a consequence MT subunits will be incorporated at the plus-ends and will be lost at the minus-ends.

4.4.3. Error correction - the commitment to anaphase synchrony

It was recently shown that when flux is perturbed the incidence of errors is markedly increased (Ganem *et al.* 2005; Ganem and Compton 2006). The concomitant occurrence of poleward flux and tension generation at the kinetochores, predicts an interdependency of both mechanisms.

Although tension might not be required to signal checkpoint it is critical for error correction. A key regulator of this mechanism is Aurora B kinase that belongs to the chromosome passenger complex, and is responsible for the regulation of MCAK, a kinesin-13 protein involved in kMT turnover (Lan *et al.* 2004; Cimini *et al.* 2006; Knowlton *et al.* 2006; Famulski and Chan 2007; Zhang *et al.* 2007). Error correction through Aurora B depends on tension and consequently on the accessibility of this kinase to its kinetochore substrates. In the absence of inter-kinetochore tension, Aurora B substrates become spatially closer to the inner centromeric region, phosphorylation occurs, and the affinity of these substrates to MTs is destabilized. Conversely, upon bi-orientation tension is promoted, Aurora B will no longer access to its substrates, and kinetochore-MT attachments become more stable (Liu *et al.* 2009). Efforts have been made to understand the relationship between MT dynamics/stability and error correction, and a consensus is being achieved concerning a gradual threshold of tension that must be accomplished. Whereas a weak kinetochore-MT interaction will lead to low tension and destabilization of MTs, high kinetochore-MT affinity will impair the correction of any error that may occur (Bakhoum *et al.* 2009b; Khodjakov and Rieder 2009a). Recently, it was observed that an exaggerated stability of kinetochore-MT attachment is, by itself, sufficient to induce chromosome instability in chromosomally stable diploid cells (Bakhoum *et al.* 2009a).

Taken together this is suggestive that whereas the turnover of MTs is important for error correction, poleward MT flux is somehow involved in error prevention. By promoting the "constitutive" dynamics and equilibrium of the metaphase spindle the probability of errors events might be reduced and the synchrony of segregation assured.

5. CHROMOSOME SEGREGATION

Chromosome segregation has attracted the attention of cell biologists throughout generations and although it has been studied for more than one century now (Wilson 1925; Ostergren *et al.* 1960; Mazia 1961; Flemming 1965; Inoue and Sato 1967; Forer and Wilson 1994; Maiato and Lince-Faria 2010), the mechanisms that drive and guarantee chromosome segregation are not completely understood. Work in different biological systems, such as budding (Kahana *et al.* 1995; Saunders *et al.* 1995) and fission yeast (reviewd by Piel and Tran 2009), plants (Inoue and Bajer 1961; Inoue 1964; Dhonukshe *et al.* 2006), insects (LaFountain *et al.* 2004; reviewed by Brust-Mascher and Scholey 2007) and vertebrates (Gorbsky *et al.* 1987; Mitchison and Salmon 1992; Waters *et al.* 1996) has contributed to the knowledge of this mechanism and, whereas particular details may be observed in some biological systems, they may remain obscure in others.

To understand anaphase one must not ignore the previous mitotic stages as Ostergren *et al*. (1960) defended: *"During the course of mitosis there are found a number of different movement phenomena and, although the anaphase movements of the chromosomes may appear as the most striking and spectacular event of mitosis, it must be born in mind that anaphase is a continuation of the previous mitotic stages and that these previous stages also imply important phenomena of chromosomal movements and equilibria, which to a large extent might be due to the same or related mechanisms as also work during mitosis"*.

After SAC satisfaction, cohesins are targeted to destruction and sister-chromatids are moved apart. Segregation occurs through two complementary mechanisms, one is the movement of chromosomes towards the poles, the anaphase A (also known as kMT shortening), and the other is the elongation of the spindle that moves chromosomes by sliding the two half spindles apart, the anaphase B.

5.1. Anaphase A

Models to explain anaphase A have been addressing the molecular basis of force production to move chromosomes towards the poles (Fig. 13, a-c). Inoue and Sato (1967) soon proposed that the anaphase movement of chromosomes was due to the "*slow removal of the material from the chromosomal spindle fibers particularly towards the spindle pole region*". During anaphase A chromosome motion is thus coupled to kMT-shortening and it may occur through MT depolymerization at the kinetochores-MT interface, or at the pole region. Accordingly, three hypotheses are currently debated.

5.1.1. The *traction fiber* model - microtubule minus-end depolymerization

The *traction fiber model* was first proposed by Van Beneden (1883) who defended that chromosomes in anaphase are pulled to the poles by traction fibers capable of contraction and elongation (see also Schrader 1944). Later, Oestergren (1951) re-established this hypothesis defending that anaphase chromosomes are dragged poleward by forces generated along the length of kinetochore fibers (see also Ostergren *et al.* 1960; Mazia 1961). The first live evidence for a traction fiber mechanism resulted from the observation that ARBs generated in crane fly (*Nephrotoma suturalis*) spermatocytes spindles move poleward on average with the same velocities as the chromosomes during anaphase (Forer 1965). Photoactivation experiments revealed later that MT-minus end depolymerization could indeed generate force to move chromosome poleward (Waters *et al.* 1996). Although this mechanism has been shown to drive chromosome segregation in plants (Dhonukshe *et al.* 2006) and insect spermatocytes (LaFountain *et al.* 2004), it is not sufficient to explain anaphase A in others (reviewed by Maiato and Lince-Faria 2010). In fact, in *Xenopus laevis* extracts force is generated along the kMT through the action of the bipolar motor Eg5. This results in movement of kinetochores by a passive attachment to moving MTs, and depolymerization at the poles (Maddox *et al.* 2003; Mitchison 2005). MT disassembly at the poles is thus considered a passive mechanism and a consequence of the MT steady state that regulates the spindle length in metaphase (Margolis and Wilson 1978; Matos *et al.* 2009). In recent years, kinesin-13 molecules implicated in regulation of poleward flux during metaphase have been considered the depolymerizers in anaphase, particularly Kif2A in vertebrates (Ganem *et al.* 2005), and KLP10A in *Drosophila* cells (Rogers *et al.* 2004; Buster *et al.* 2007).

5.1.2. The Pac-Man mechanism - microtubule plus-end depolymerization

In marked contrast to the traction fiber model, the *Pac-Man* model proposes that kinetochores have an active role in force generation of motile chromosomes (Cassimeris *et al.* 1987; Gorbsky *et al.* 1987; Forer 1988; Gorbsky *et al.* 1988; Nicklas 1988; Nicklas 1989). The idea that the kinetochore is an active participant and not an anchorage for a chromosomal fiber dates from 1929, when Belar proposed that kinetochores "glide" (i.e. slide) along chromosome fibers (Belar 1929; see also Schrader 1944). 30 years later Mota proposed that "*the chromosome has in itself the energy for the anaphase movement and that the centromere (i.e. the kinetochore) is not only the point through which the chromosome is moved, but also its own engine"* opening the way to the currently debated model (Mota 1957; see also Maiato and Lince-Faria 2010). The first *in vivo* observations that recognized the kinetochores as the main driver for anaphase A resulted from photobleaching experiments where the bleached marks generated in the anaphase spindle remained relatively stationary with respect to the pole, while chromosomes were observed to move along that generated mark (Gorbsky *et al.* 1987; Gorbsky *et al.* 1988). Later, photoactivation studies corroborated these results, attributing a minor role for kMT depolymerization at the poles as the force driver during anaphase A (Mitchison and Salmon 1992). Different lines of investigation followed these observations and tried to unveil how was force generated at kinetochores. *In vitro* experiments have shown that MTs can generate enough force to drive chromosome segregation (Koshland *et al.* 1988; Coue *et al.* 1991; Grishchuk *et al.* 2005), however mechanochemical evidences soon pointed towards the existence of motors involved in chromosome-to-pole movement (Nicklas 1988).

Due to its localization at the kinetochores, cytoplasmic dynein was the first molecular motor to be assigned as part of the Pac-Man motor (Pfarr *et al.* 1990; Steuer *et al.* 1990). Accordingly, it was shown that inhibition of this minus-end directed motor led to a delay in kMT shortening (Sharp *et al.* 2000b). Further investigations added to this motor other functions during mitosis and spindle assembly (Goshima *et al.* 2005a; Yang *et al.* 2007; Varma *et al.* 2008; Reis *et al.* 2009) that question the direct involvement of dynein in chromosome motion during Anaphase A. Other proteins were implicated in force generation as the kinesin-7 motor CENP-E (Lombillo *et al.* 1995). More recently, two kinesin-13 motors were shown to be important in the *Drosophila* Pac-Man activity. Whereas impairment of KLP59C function reduces kMT shortening velocity in *Drosophila* embryos, no effect was observed in *Drosophila* S2 cells where KLP59D was alternatively found to regulate kMT depolymerization (Rath *et al.* 2009).

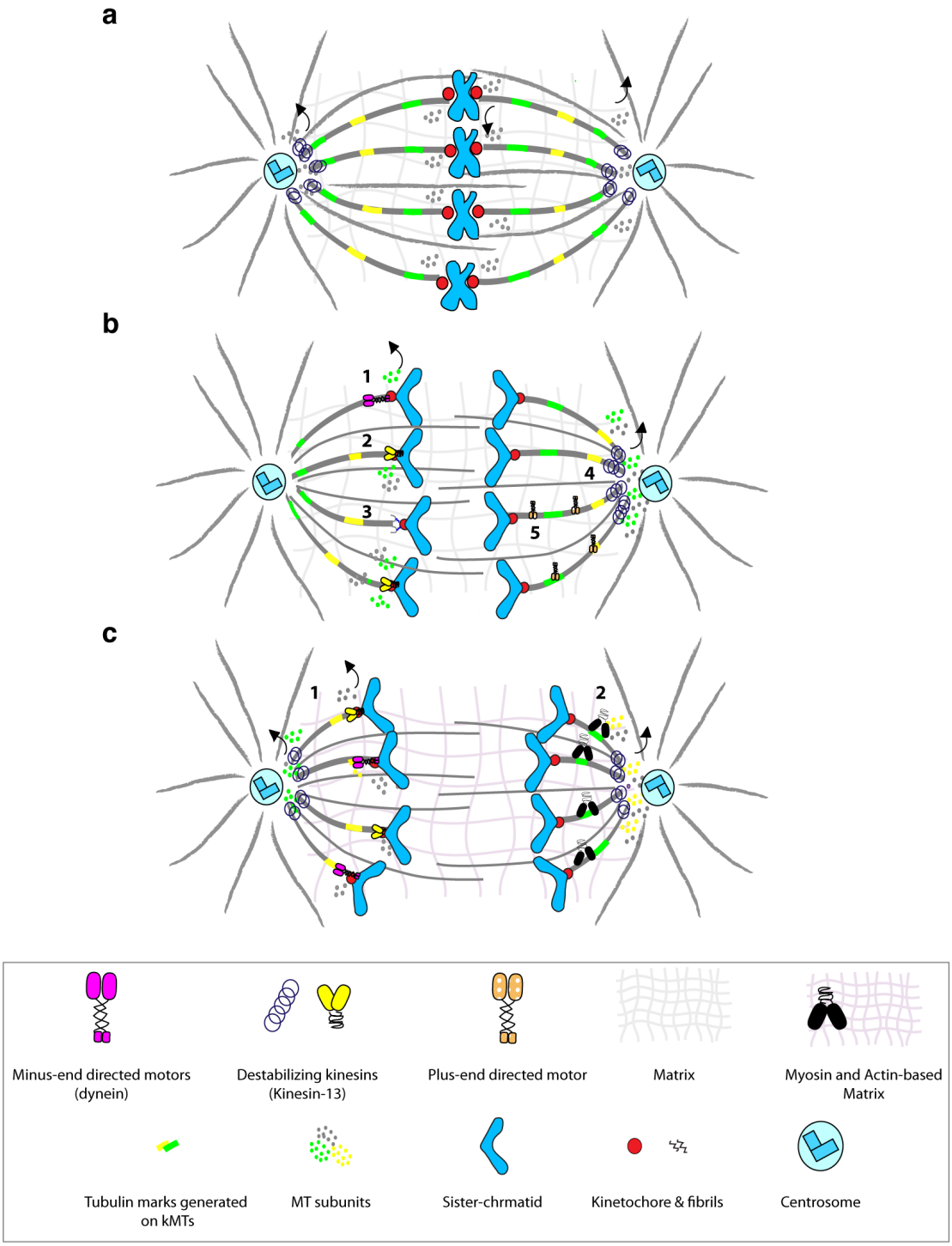


Figure 13 – Schematic representation of anaphase A models. a) During metaphase labeled tubulin move poleward due to the property of MT flux. After anaphase onset tubulin fiduciary marks can be used as references to follow the movement of chromosomes. Chromosome-to-pole movement can be explained by **b1-2)** Pac-Man, **b3)** MT plus-end depolymeryzation, **b 4-5)** traction fiber and **c-2)** tensile matrix models. **b1)** Kinesin-13 depolymerizers and **b2)** dynein, were the proteins invoked to be part of the Pac-Man mechanism. **b3)** Conformational wave model where the bending of protofilaments at microtubule plus-ends coupled to kinetochore fibrils, drive chromosome movement independently on ATP hydrolysis.

5.1.3. Tensile matrix

A matrix model has been invoked as a model to explain the movement of chromosomes towards the poles as a *contemporary* version of the traction fiber model proposed by Oestergren (Forer and Wilson 1994; Pickett-Heaps *et al.* 1996; Pickett-Heaps *et al.* 1997; Pickett-Heaps and Forer 2001; Pickett-Heaps and Forer 2009). The *tensegral* hypothesis suggests that anaphase poleward force is generated by a component separated from the spindle MTs, the matrix, that exerts force along the length of the fiber. The MTs of the fiber both give force and direction to the force-producing matrix and resist the force it generates (Pickett-Heaps *et al.* 1997). Accordingly, Pickett-Heaps and Forer have been proposing actin as one of the matrix components because its inhibition, achieved by the use of drugs as cytochalasin D and latrunculin, often led to the impairment of chromosome motion during meiosis in crane fly spermatocytes (Forer 1988; Forer and Pickett-Heaps 1998). These authors also suggested that myosin is part of the matrix and in combination with actin, may support MT motors that act on kMTs (Forer *et al.* 2007). Furthermore, they argued that the celular mechanisms that have been selected throughout evolution are those that share functions during all the organism cell cycle, such as MTs and actin motors (Forer *et al.* 2003), and not those proposed by other anaphase A models (Pac-Man, treadmiling and MT-fluxing) that participate exclusively during a specific moment of mitosis (Pickett-Heaps and Forer 2009). Although this model has been observed in *Haemantus* system (Schmit and Lambert 1990), in other models such as LLC-PK cells no similarity was observed (Maiato and Lince-Faria 2010). This is suggestive that for different eukaryotic systems, different mechanisms assure the same important functions.

b 4-5) Traction fiber based mechanism where the force generated by **b4)** kinesin-13 depolymerization or **b5**) motors attached to a matrix drive poleward flux. Depolymerization at the poles works as a downstream event. **c1**) Combination of Pac-Man and flux-based depolymerization at the poles is most polpular mechanism in animal cells. **c2**) Tensile matrix mechanism where myosin interacting with actin will generate compression forces that are applied to kMT generating the force that drives flux and the movement of chromosomes towards the poles. Depolymerization at the poles will also work as a downstream event. Anaphase A can be explained by different combinations of mechanisms depending on the system studied.

5.2. Anaphase B

Anaphase B refers to the spindle elongation movement that happens upon anaphase onset and is characterized by the expansion of the two half-spindles in opposite directions (Fig. 14) In metazoans, separation of the two half-spindles leads to a reduction in the density of MTs in the central region of the spindle thus facilitating furrow ingression and further cytokinesis. Anaphase B contribution to chromosome segregation may vary amongst different organisms and even amongst cells of one organism. Whereas in one extreme as giant amoeba, yeasts and worms, anaphase B is predominant (Mazia 1961; Oegema and Hyman 2006; Piel and Tran 2009), in the other extreme, such as higher plants, this movement may be slight (Mazia 1961; Hayashi *et al.* 2007).

Mechanistically, the separation of the two half-spindles can be driven by pulling forces exerted on astral MTs or by ipMT outward sliding. Although centrosomes and astral MTs were first proposed as the main drivers of spindle elongation (Boveri 1888; Mazia 1961), shared attention was given to ipMTs due to the discovery of interdigitating/overlapping MT in the central region of the anaphase spindle (reviewed by McIntosh et al. 1975).

Since one important question about anaphase is how forces are generated, experimental work soon proposed putative drivers. Micromanipulation studies where the spindle central region was either laser ablated (Aist and Berns 1981) or cut with a microneedle (Kronebusch and Borisy 1982) recognize the astral forces as drivers of the movement, further suggesting that the central spindle works as a governor that limits the rate of anaphase B movement. Accordingly, dynein was suggested to be involved in astral pulling by promoting the sliding of astral MTs against the cell cortex (Sharp *et al.* 2000a; Fink *et al.* 2006). On the other hand, Leslie and Picket-Heaps (1983) using diatoms as a model, proposed that the spindle elongation driving force was localized in the central region of the spindle where MTs overlap. With the development of fluorescent marking tools and photobleaching approaches this hypothesis gained further support as it was possible to observe through live imaging antiparallel sliding of interzonal MTs coupled to a consequent MT polymerization in the overlapping region (Saxton and McIntosh 1987; Shelden and Wadsworth 1990).

The fast development of cell biology tools has improved our knowledge about the mechanisms that promote chromosome motility during anaphase. The present challenge will drive our understanding towards the molecular regulators of each mechanism and to the identification of any putative crosstalk that may combine and/or compensate both mechanisms.

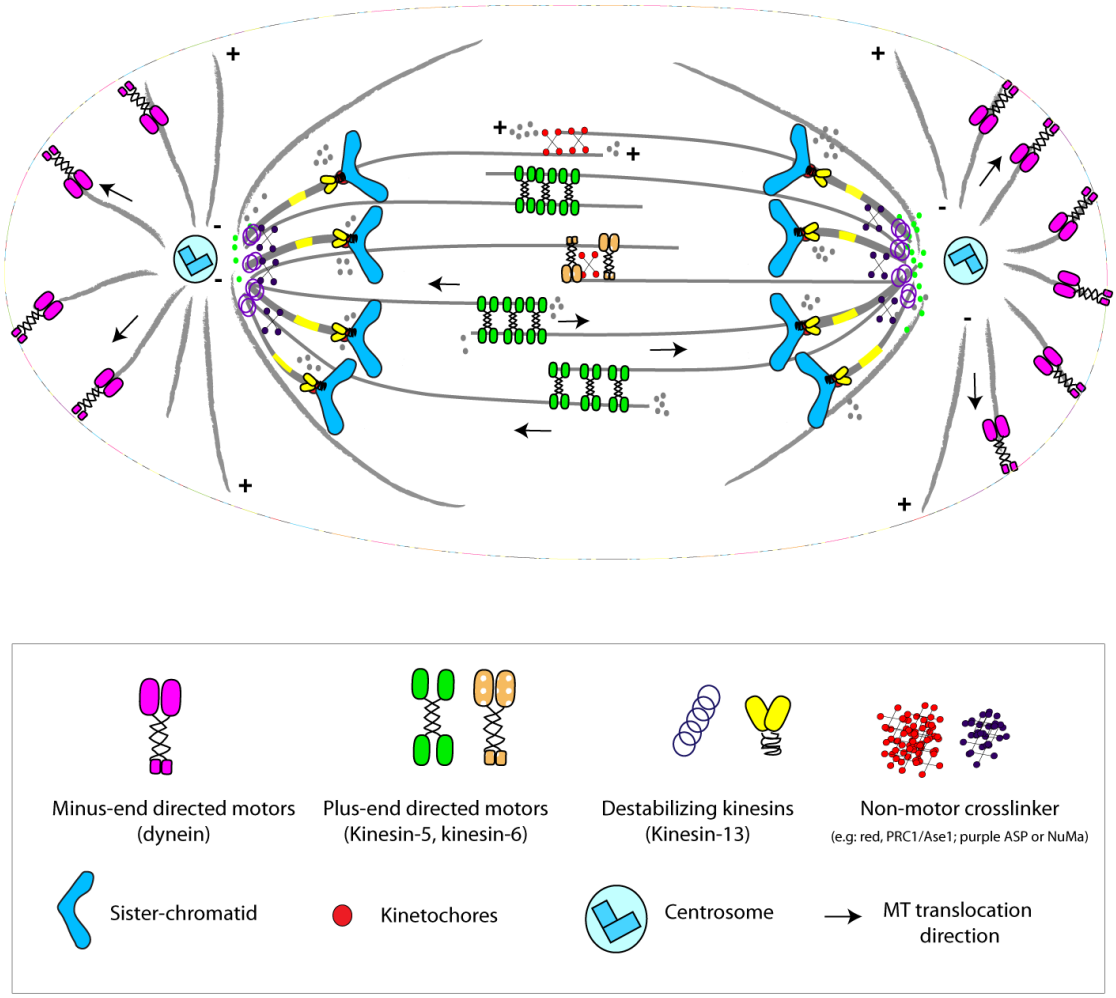


Figure 14 – Anaphase B model. Spindle elongation can be driven by antiparallel MT sliding at the central region of the spindle, or as a consequence of pulling cortical forces exerted by dynein coupled to astral-MTs. Crosslinkers are need to bundle non-kinetochore microtubules so motors can slide them apart. As a consequence MT subunits are incorporated at the plus-ends of ipMT. Froce generated by ipMT sliding can be transmitted through crosslinkers to kMTs contributing to anaphase A.

6. OBJECTIVES

Due to the existence of redundant mechanisms among different organisms it is difficult to establish a common model that explains the movement of chromosomes in all eukaryotic systems. The aim of this work was to understand the spatiotemporal regulation of spindle-MT dynamics and its contribution for chromosome segregation in animal cells. Accordingly, in the first chapter of this thesis I present the work developed towards the explanation of the poleward mechanism of flux and its contribution to the equilibrated forces of metaphase and the quality control of anaphase. Using high-resolution spinning disk microscopy combined with different fluorescently labeled cell lines, and with the use of recently developed tools for kymograph analysis (Pereira and Maiato 2010), we quantitatively characterize mitotic flux and its implications for the steady-state of metaphase and mitotic progression. In Chapter II and Chapter III, we focus our attention on the anaphase movement of chromosomes in *Drosophila melanogaster* S2 cells. Accordingly, in Chapter II we quantitatively characterize chromosome-to-pole movement in this system showing the simultaneity of anaphase A and anaphase B onset and clarifying the contribution of Pac-Man to kMT shortening. In Chapter III we extensively quantify spindle elongation during anaphase B and we identify key regulators that may work in a synergistic way to guarantee the accurate movement. Finally, we propose the existence of a surveillance mechanism that regulates the timely reformation of nuclear envelope after chromosome segregation.

II. EXPERIMENTAL WORK

CHAPTER I.

Synchronizing chromosome segregation by flux-dependent force equalization at kinetochores

1. INTRODUCTION

The sense and purpose of mitosis is revealed in its climax during anaphase (Mazia 1961) when sister-chromatids migrate synchronously towards opposite poles. This critical task is accomplished by a highly dynamic microtubule (MT)-based apparatus - the *mitotic spindle*, which interacts with specialized structures at the centromere of each chromosome termed *kinetochores* (Maiato *et al*. 2004a). Anaphase synchrony prevents the occurrence of lagging chromosomes that could lead to the formation of micronuclei after nuclear envelope restoration or reversion of cleavage-furrow ingression during cytokinesis. These cytological features may lead to aneuploidy or polyploidy and have been associated with elevated risk of cancer in mammalian models and humans (Tucker and Preston 1996; Ganem *et al*. 2007). In higher eukaryotic cells, anaphase synchrony is ensured by the strategic positioning of all chromosomes at the cell equator during metaphase and the strict coordination of sister-chromatid separation. While anaphase onset is regulated by the spindle assembly checkpoint (SAC), which ensures that all kinetochores are properly attached to the spindle before loss of sister-chromatid cohesion (Musacchio and Salmon 2007), the mechanism responsible for the uniform action of spindle forces at kinetochores remains to be elucidated.

During metaphase, many animal and plant spindles are characterized by a conspicuous "flux" activity due to continuous MT poleward translocation, while maintaining steady-state length (Mitchison 1989; Rogers *et al*. 2005). Spatiotemporal scales of flux dictate that spindle MTs are fully recycled prior to anaphase, which results from continuous incorporation of tubulin subunits at kinetochores (Maiato *et al*. 2005) balanced by MT depolymerization at the poles (Rogers *et al*. 2004). In addition, sister kinetochores on metaphase chromosomes are pulled toward opposite poles by spindle forces that stretch the inter-connecting centromeric chromatin. This tension is thought to control the maturation (King and Nicklas 2000) and correction (Nicklas and Ward 1994) of kinetochore-MT attachments before cells enter anaphase.

Simultaneity of tension and MT translocation/flux relative to the kinetochore suggests that the flux-driving force is not generated at the kinetochore-MT interface. Indeed, any mechanical event at this interface that hypothetically pushes kinetochore MTs (kMTs) poleward (e.g. a kinesin power stroke) would react against the kinetochore structure, leading to centromere compression, not stretching. MT poleward flux may be driven by active MT minus-end depolymerisation at the poles (Waters *et al*. 1996; Rogers *et al*. 2004; Ganem *et al*. 2005) or by motors acting along the length of kMTs (Mitchison 2005; Forer *et al*. 2008). Growing emphasis in several cell types is being given to kinesin-5 motors, which slide apart anti-parallel interpolar MTs (ipMTs), as the main flux-driving force (Miyamoto *et al.* 2004; Goshima *et al.* 2005b; Brust-Mascher *et al.* 2009). Polymerization and depolymerization at MT plus- and minus-ends, respectively, are viewed as downstream responses to MT poleward translocation that regulate spindle length (Gaetz and Kapoor 2004; Maiato *et al*. 2005). In this framework, kinesin-5 motors may drive kMT flux by directly cross-linking kMTs to ipMTs of opposite polarity (Mitchison 2005) or, indirectly, by laterally transmitting the force generated by sliding ipMTs to kMTs within the same half-spindle. The key ingredient in both models is that ipMT sliding may prompt kMT poleward translocation through force transmission via a mechanical coupler, which in a more general view may consist of proteins with MT cross-linking activity (Manning and Compton 2007) or a viscoelastic network (Brangwynne *et al*. 2006). The existence of such mechanical coupler may be heuristically inferred by the fact that spindles rotate and translate as a unified structure, which ultimately means that all chromosomes are mechanically connected.

The conservation and energetic cost of flux during metaphase, together with its dispensability for chromosome segregation in systems where it is normally present (Ganem *et al*. 2005; Buster *et al*. 2007) poses obvious questions regarding its functional roles. Besides, MT poleward translocation relative to the kinetochore (i.e. kMT flux) reflects the relaxation of the kinetochore-MT interface (implying a certain loss of tension), which may be seen as an apparent disadvantage to the cell. Here we used *Drosophila* S2 cells to test whether the existence of flux represents a way to redistribute excess tensions on metaphase chromosomes, thereby contributing to the equalization of forces acting at kinetochores and anaphase "quality".

2. MATERIALS AND METHODS

2.1. Cell culture, RNAi treatment and western blot

Drosophila S2 cells were cultured as previously described (Maiato *et al*. 2003; Pereira *et al*. 2009). Briefly, these cells were grown in plastic culture flasks at 25ºC supplemented with 10% fetal bovine serum (FBS). RNAi of CLASP, KLP10A, CLASP/KLP10A and Mad2 in S2 cells was performed as described using published targeting sequences (Rogers *et al*. 2004; Maiato *et al*. 2005; Orr *et al*. 2007; Pereira *et al*. 2009; see Table S1). KLP10A knock-down was better achieved after 2 pulses of dsRNA. The first at t0 and the second after 48 hours (h). Phenotypes were quantified by light microscopy every 24h over 7 days. Protein extracts were quantified by the Bradford assay, boiled for 5 minutes in SDS sample buffer and subjected to SDS-PAGE, followed by transferring to nitrocellulose membranes and immunodetected with the appropriate antibodies. Protein knock-down was monitored using the following antibodies (see supplemental Table I for dilutions): rabbit anti-CLASP and anti-Mad2 (gift from Cláudio Sunkel, IBMC, University of Porto, Portugal), rabbit anti-KLP10A (gift from Jonathan Scholey, University of California at Davis, CA), mouse anti-α-tubulin clone B512 (Sigma). Secondary antibodies were visualized using the ECL system (Amersham). Knock-down levels were quantified using the QuantityOne® software from BioRad.

2.2. Drug treatments

To suppress MT dynamics in S2 cells we used 10 nM Taxol for 10 min before time-lapse recording or immunofluorescence processing. Whenever indicated, the proteasome inhibitor MG132 was used at 20 μM for 2h. To determine the inter-kinetochore rest length, we treated S2 cells with 30 μM colchicine for 2h to induce MT depolymerization.

2.3. Immunofluorescence microscopy

S2 cells were grown on 0.5 mg/ml concanavalin A (Sigma) coated coverslips and processed for immunofluorescence as described (Maiato *et al*. 2004b). Primary antibodies used were rabbit anti-γ-tubulin (gift from Alain Debec, Institut Jacques Monod, Paris,

France); mouse anti-α-tubulin clone B512 (Sigma); rabbit anti-BubR1 and anti-Scc1 (gifts from Cláudio Sunkel); chicken anti-CID (gift from Gary Karpen, University of California at Berkeley, CA); rabbit anti-Aurora B (gift from Mar Carmena and Bill Earnshaw, University of Edinburgh, UK).

Quantitative three-dimensional data sets were collected using Zeiss Imager. Z1 microscope equipped with an Axiocam MRm CCD and using a 100x, 1.4 NA oil immersion objective at 0.25 μm z-steps, using Axiovision software. Images were subsequently blind-deconvolved with AutoDeblur X2 software (Media Cybernetics) and processed for publication using Photoshop CS3 (Adobe).

2.4. Fluorescent speckle microscopy (FSM)

To measure flux rates we used S2 cells stably expressing GFP-α-tubulin under the control of a leaky inducible metallothionein promoter and CID-mCherry (Coelho *et al*. 2008). Without induction, low levels of GFP-α-tubulin are expressed. Cells were grown in concanavalin A-coated coverslips (0.25mg/ml) and mounted in modified Rose chambers with Schneider´s medium (Sigma-Aldrich) containing 10% of FBS (Pereira *et al*. 2009). Time-lapse images were collected every 5 sec at 25ºC with a Nikon TE2000U inverted microscope equipped with a Coolsnap HQ2 CCD camera (Photometrics, Tucson, AZ) using a 100x 1.4 NA plan-Apochromatic objective, and driven by NIS-elements (Nikon, Japan). Images were subsequently blind-deconvolved with AutoDeblur X2 (Media Cybernetics).

2.5. Time-lapse microscopy

S2 cells stably expressing GFP-α-tubulin and CID-mCherry or mRFP-BubR1 (mRFP-BubR1 construct was modified from a vector kindly provided by Roger Karess, Institut Jacques Monod, Paris, France) were grown on concanavalin A coated coverslips (0.25 mg/ml) and mounted in modified Rose chambers with Schneider´s medium (Sigma) containing 10% FBS. Four-dimensional data sets covering the entire cell volume were collected every 30 sec with 1 μm z-steps with a 100x 1.4 NA plan-Apochromatic objective at 25ºC with an Andor Revolution Spinning Disc confocal system (Andor) equipped with an Electron Multiplying CCD (EMCCD) iXon^{EM}+ camera, two laser lines (488 and 561 nm) and a Yokogawa CSU-22 unit based on an Olympus IX81 inverted microscope and driven by Andor IQ.

2.6. Guided kymography

Either to kymograph the entire spindle or to prepare the data for local kymograph analysis we used a custom routine written in Matlab (Mathworks, Natick, MA) to compensate for spindle rotation and translation described by the following steps: 1) 2D tracking of spindle poles; 2) Region-of-interest (ROI) dimensions definition; 3) thick-kymograph generation with the ROI being automatically translated and rotated every frame according to the 2D coordinates of the two reference objects in step 1. The direct output is a whole-spindle kymograph that can be used to generate a set of aligned images which are the basis for all subsequent analysis (Pereira and Maiato 2010).

2.7. Collapsed kymography and chromo-kymography

Raw kymographs are composed of an image stack at different time points, each with dimensions *n* x *m*. Collapsed kymographs are projections of the raw kymograph that result from conversion of each time point image matrix into a vector, according to some weighed combination (e.g., average or maximum) of the pixels along each column of the ROI. Chromo-kymographs are a generalization of collapsed kymographs on which 3 different weight functions are applied, each one generating an RGB channel of the output chromo-kymograph (Pereira and Maiato 2010) .

2.8. Quantifications

Spindle length from fixed material was measured for each bipolar spindle as the distance between opposite poles revealed by γ-tubulin immunostaining.

Flux velocities were measured by kymograph analysis in which a long thin rectangular region covering the entire spindle length is extracted from each image in the time-lapse series and sequentially aligned with reference to the poles. The position of the rectangular region was chosen by the presence of a kinetochore pair and correspondent kMTs. On these collapsed kymographs, slopes corresponding to the movement of bright or dark speckles over time (equivalent to the flux velocity) were directly measured. Results obtained by this method revealed slightly faster kinetochore MT flux velocities than those obtained by other techniques such as photobleaching or photoactivation of spindle MTs (Maiato *et al*. 2005; Rogers *et al*. 2005; Buster *et al*. 2007).

MT minus-end depolymerization rates in anaphase were quantified by subtracting the MT minus-end slope to the speckle slope. MT minus-ends were determined using collapsed kymographs, which gather all MT minus-ends converging to a common focus.

Inter-kinetochore distances measured from fixed samples were obtained after immunofluorescence as the distance between centroids of CID-labeled kinetochore pairs through metaphase z-stacks using ImageJ 1.30 software (National Institutes of Health, Bethesda, MD). Inter-kinetochore distances measured from living cells represent the distance between centroids of opposite CID-mCherry pairs through metaphase z-stacks 2 min before anaphase onset. Anaphase onset was inferred as the moment where at least two kinetochore pairs were at a distance higher than 1.2 μm. Intra-cellular tension variability was quantified upon calculation of the coefficient of variation, $\delta_T/\langle T\rangle$,which for a linear spring is equal to $\delta_d/(\langle d\rangle - d_0)$, where d is the inter-kinetochore distance in metaphase and d_0 is the inter-kinetochore distance in prophase (rest length).

Quantification of BubR1 fluorescence at kinetochores was performed relative to CID fluorescence as previously described (Hoffman *et al*. 2001) using ImageJ 1.30 software. Aurora B and CID signals were measured in the entire metaphase plate for a fixed ROI.

Cold stable kMTs were quantified by immunofluorescence after 10 minutes at 4 °C.

Metaphase duration was defined from the moment of alignment of the last chromosome at the metaphase plate until anaphase onset.

Quantifications of anaphase parameters are explained in the Materials and Methods section in Chapter II.

2.9. Statistical analyses

A statistical analysis was performed using either parametric one-way (ANOVA) or non-parametric analysis of variance (Kruskal-Wallis) for multiple group comparisons according to the normality of the distribution as determined by Kolmogorov-Smirnov test. All pair-wise multiple comparisons were subsequently analyzed using either *post hoc* Student-Newman-Keuls (parametric) or Dunn's (non-parametric) tests. Parametric t-test or non-parametric Mann-Whitney was used for two group comparisons. We used both standard-deviation and inter-quartile range as measures of the distribution spread. All statistical analysis was performed using SigmaStat 3.5 (Systat software, IL).

3. RESULTS

3.1. Experimental attenuation of kMT flux in *Drosophila* S2 cells

To test whether flux-associated slippage at the kinetochore-MT interface contributes to a uniform distribution of forces acting on kinetochores we started by experimentally reducing kMT flux on bipolar spindles. In *Drosophila* S2 cells kMT flux requires CLASP-mediated incorporation of tubulin subunits at kinetochores (Maiato *et al*. 2005), which is balanced by KLP10A-dependent microtubule depolymerization at the poles (Rogers *et al*. 2004; Buster *et al*. 2007). Whereas CLASP knock-down by RNAi causes a strong accumulation of prometaphase cells with monopolar or short spindles (Fig. 1, a-g; see also Maiato *et al*., 2005), KLP10A RNAi does not preclude bipolar spindle formation and function, despite increased spindle length (Fig. 1, a-e, i and j; see also Rogers *et al*., 2004). As an experimental hypothesis we reasoned that simultaneous depletion of CLASP and KLP10A by RNAi in S2 cells would rescue normal spindle bipolarity and cease flux. Accordingly, the phenotypes resulting from CLASP, KLP10A and CLASP/KLP10A RNAi treated cells were analyzed and quantified at different time points (Fig. S1). A clear phenotype could be observed 48h after RNAi treatment, becoming firmly established at 72-120h, consistent with a crescent reduction of protein levels (Fig. 1, a). Therefore subsequent studies were performed between 72 and 120h. As already described by Layocock *et al.* (2006), we also observed that after CLASP RNAi knock-down almost all mitotic cells arrested in prometaphase (97%; *n*= 416; Fig. 1, b), usually with short (32.6%; Fig. 1, c and f) and monopolar (58.2%; Fig. 1, c) spindles, as a consequence of spindle collapse (Fig. 1, g). The spindle length of CLASP RNAi bipolar spindles was significantly reduced in relation to control prometaphase spindles (6.7±1.8 μm and 11.9±2.3, μm respectively; Fig. 1, d). Down-regulation of KLP10A led also to an increase of 20% in the accumulation of prometaphase cells (60%; *n*=150; Fig. 1, b). The main phenotypes observed during prometaphase and metaphase for KLP10A depleted cells, were monopolar (35.9%; Fig. 1, c and j), long bipolar (17.1%; Fig. 1, c and i) and monoastral bipolar (19.3%; Fig. 1, c) spindles. KLP10A RNAi bipolar spindles were often longer than their control counterparts (15.1 ± 4 μm and 11.3 ± 1.9 μm, respectively; Fig. 1, d). When CLASP and KLP10A were simultaneously knock-down, normal bipolarity was restored (5.65% in CLASP and 44.8% in CLASP/KLP10A RNAi treated cells; Fig. 1, c) and the latter were allowed to proceed into metaphase and anaphase (Fig. 1, b). Spindle length was also significantly recovered (11.3 ± 1.9 μm in control and 10.6 ± 1.9 μm in CLASP/KLP10A RNAi treated spindles; Fig. 1, d and h).

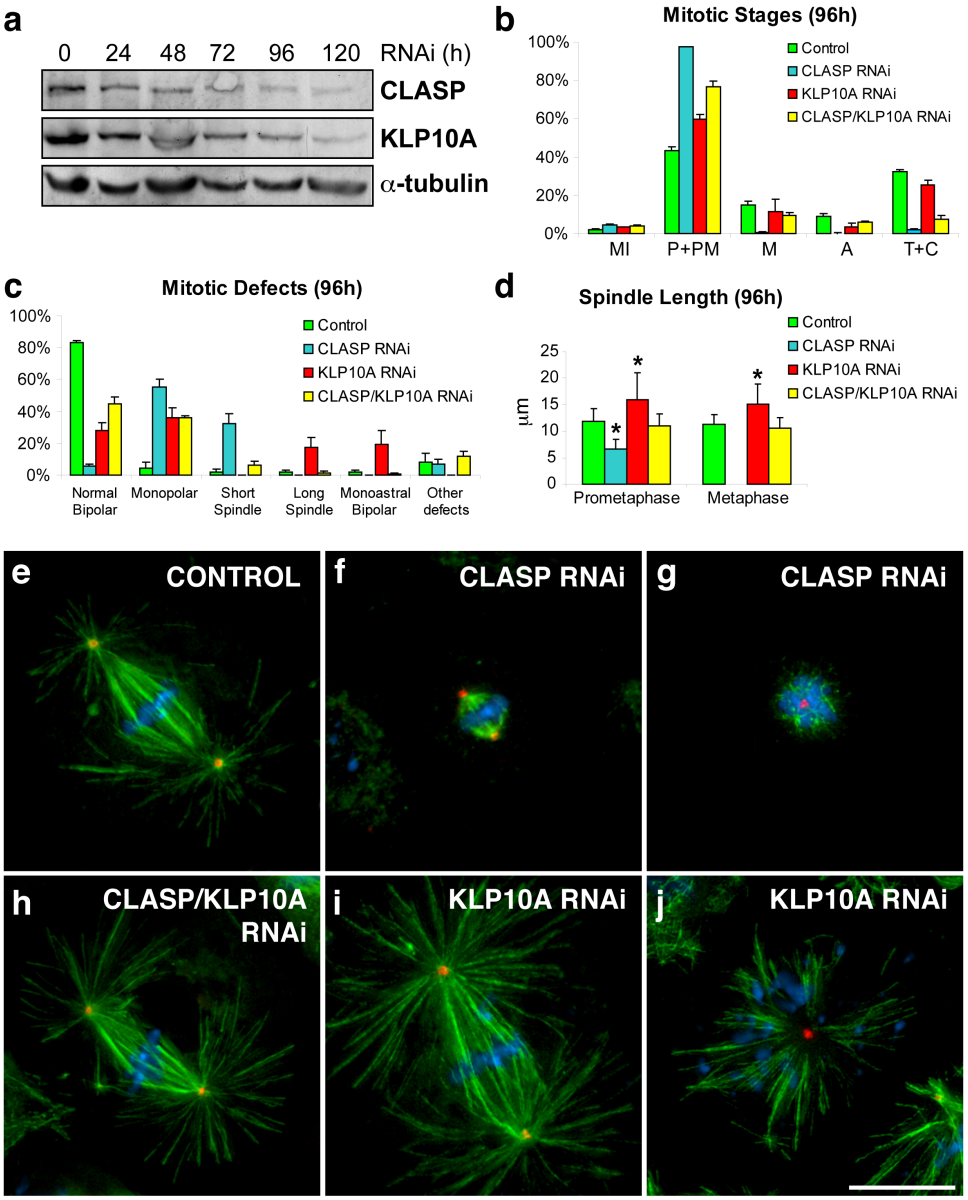


Figure 1. Phenotypic analyses of CLASP, KLP10A and CLASP/KLP10A RNAi in Drosophila S2 cells. **(a)** Western blot analysis after CLASP and KLP10A RNAi at different time-points revealed a 70-90% reduction in protein levels 96h after RNAi treatment. α-tubulin was used as loading control. **(b)** Quantification of mitotic parameters reveals a significant rescue of CLASP phenotype by simultaneous depletion of KLP10A. Note that metaphases and anaphases were restored in the double RNAi experiments. **(c** and **d)** Quantification of mitotic defects in controls and after CLASP, KLP10A and CLASP/KLP10A RNAi show that simultaneous depletion of CLASP and KLP10A significantly restored spindle bipolarity and length. Plotted values represent the mean from at least 3 experiments and error bars represent the respective standard deviations. Asterisks in **(d)** indicate statistically significant differences when compared with controls ($p<0.001$; unpaired t-test). **(e-j)** Immunofluorescence analysis of mitotic spindles from control, CLASP, KLP10A, and CLASP/KLP10A RNAi. MTs (green) and centrosomes (red) were respectively revealed with anti-α and γ-tubulin antibodies, while DNA (blue) was counterstained with DAPI. Bar, 5 μm.

With this first experimental procedure we achieved an apparently normal bipolar spindle where we could test the impact of flux impairment. To verify whether bipolar spindles after KLP10A or CLASP/KLP10A RNAi undergo slower kMT flux, we used time-lapse fluorescent speckle microscopy (FSM; Fig. 2, a-d'). With this high-resolution system, poleward movement of microtubules in metaphase spindles can be readily visualized as small amounts of fluorescently labeled, and unlabeled, tubulin are randomly incorporated into polymerizing microtubules (Waterman-Storer *et al*. 1998; Danuser and Waterman-Storer 2006). For this reason, we took advantage of a *Drosophila* S2 cell line stably expressing GFP-α-tubulin under the control of an inducible metallothionein promoter. In the absence of induction, leaky basal levels of GFP-α-tubulin are expressed (Goshima *et al.* 2005b). To accurately measure flux within distinct kMTs, this cell line was co-transfected with a vector expressing an inner kinetochore protein, CID, tagged to mCherry (Coelho *et al*. 2008).

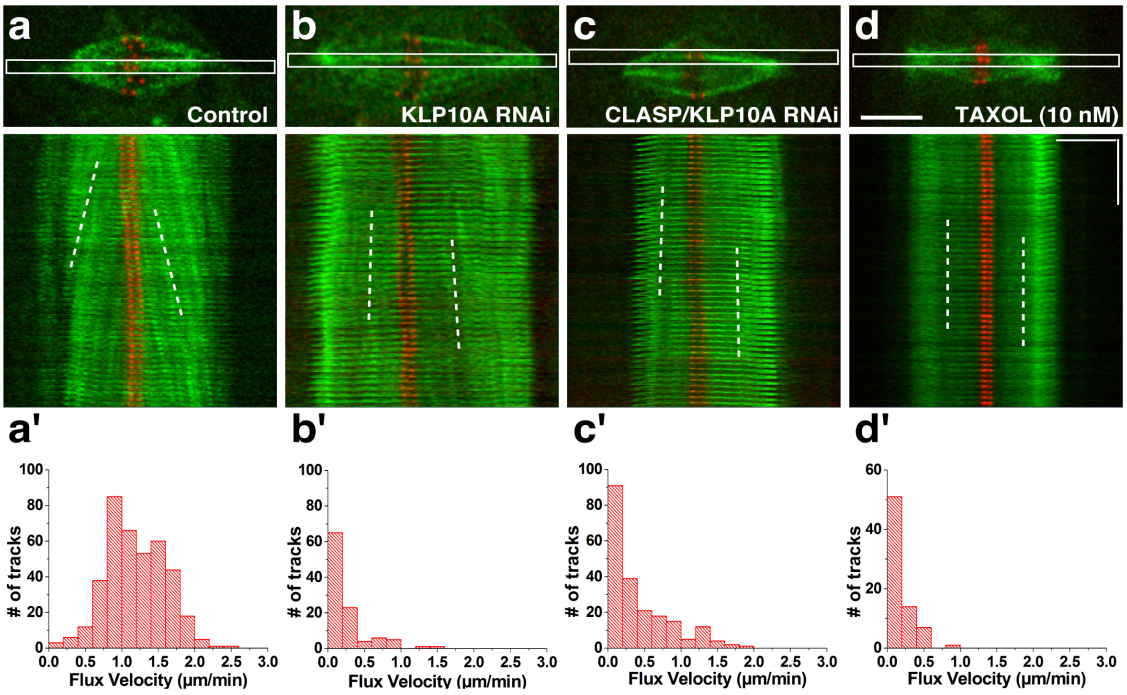


Figure 2 - Quantitative analysis of kinetochore microtubule poleward flux by fluorescent speckle microscopy (FSM). S2 cells stably expressing low levels of GFP-α-tubulin (green) and CID-mCherry (red) were used to analyze kMT poleward flux by FSM. **(a)** Control, **(b)** KLP10A RNAi, **(c)** CLASP/KLP10A RNAi and **(d)** Taxol-treated cells. Speckle poleward velocity was determined by measuring the slopes obtained from the kymographs (white broken lines). **(a'-d')** Distribution of flux velocity in control, KLP10A RNAi, CLASP/KLP10A RNAi and Taxol-treated cells, respectively. Horizontal bar, 5 µm; vertical bar, 1 min. All treatments are statistically different from controls ($p<0.05$; Dunn's test).

Flux velocities were measured by kymograph analysis, in which a long thin rectangular region aligned along the axis of speckle movement within a k-fiber is extracted from each image in the time-lapse series and paste sequentially side-by-side to make a montage of the region over time (Fig. 2, a-d). In these 2D kymographs, oblique lines corresponding to the movement of bright microtubule speckles are drawn over time. The slopes of those lines reveal the velocity of speckle movement (Waterman-Storer *et al*. 1998). KMT flux in control metaphase cells is 1.2 μm/min (median) at 25°C, with only 2% of the speckles moving slower than 0.2 μm/min relative to kinetochores (Fig. 2, a and a'; Table I). After KLP10A or CLASP/KLP10A RNAi kMT flux drops to 0.2 μm/min (Fig. 2, b-c'; Table I), which is comparable to the velocity of kMT flux observed after microtubule stabilization with 10 nM taxol (Fig. 2, d and d'; Table 1). Although flux velocity is slow, these slowly fluxing spindles satisfy the SAC, enter anaphase, and segregate chromosomes. We conclude that KLP10A or CLASP/KLP10A RNAi represent valid strategies to reduce kMT flux, while allowing the formation of functional bipolar spindles in S2 cells (Fig. 3 a-c').

3.2. Flux-associated kMT minus-end depolymerization is down-regulated at anaphase onset and has a minor role in anaphase chromosome-to-pole motility in *Drosophila* S2 cells

We next used dual-wavelength spinning-disk confocal microscopy to investigate the impact of reduced kMT flux on chromosome segregation (Fig. 3, a-f; see Chapter II for a detailed analysis). Anaphase poleward velocity of sister chromatids after KLP10A or CLASP/KLP10A RNAi was reduced by ~0.5 μm/min relative to controls (Fig. 3, d; see Chapter II for details). This reduction was essentially due to a KLP10A-dependent decrease in the velocity of spindle elongation (Fig. 3, e) and not due to reduced kMT shortening velocity (Fig. 3, f). Because KLP10A is apparently not required for the formation of the spindle mid-zone or recruitment of kinesin-5 motors to this location (Fig. S2), we reasoned that the slower spindle elongation could be caused by increased resistance due to cortical interactions with the abnormally long astral MTs observed after perturbation of KLP10A (Fig. 1, h and j). Indeed, co-depletion of KLP10A with Sas4, a protein required for the formation of functional centrosomes and astral MTs (Basto *et al*. 2006), restores Sas4 spindle elongation velocity (see Chapter II).

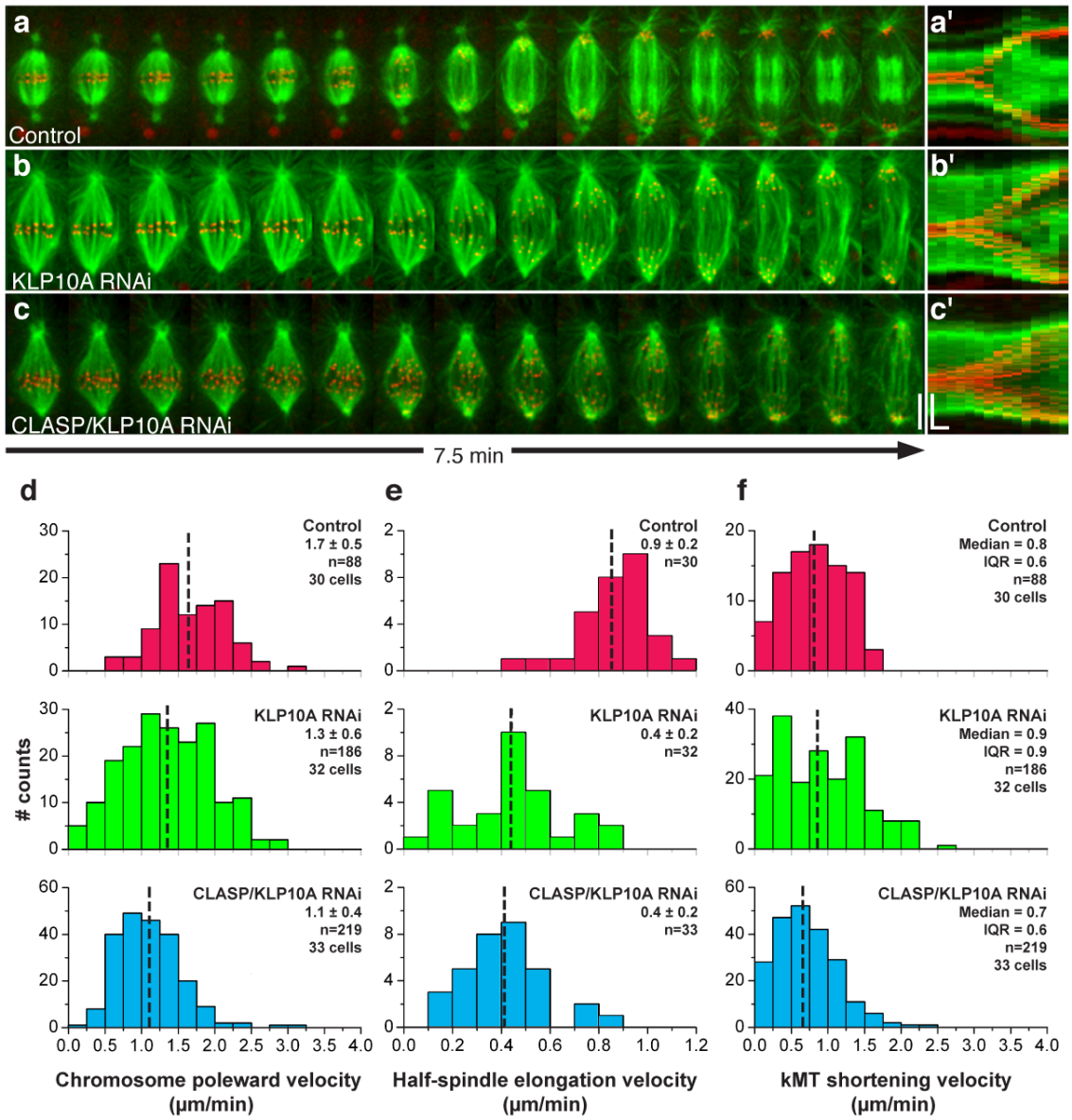


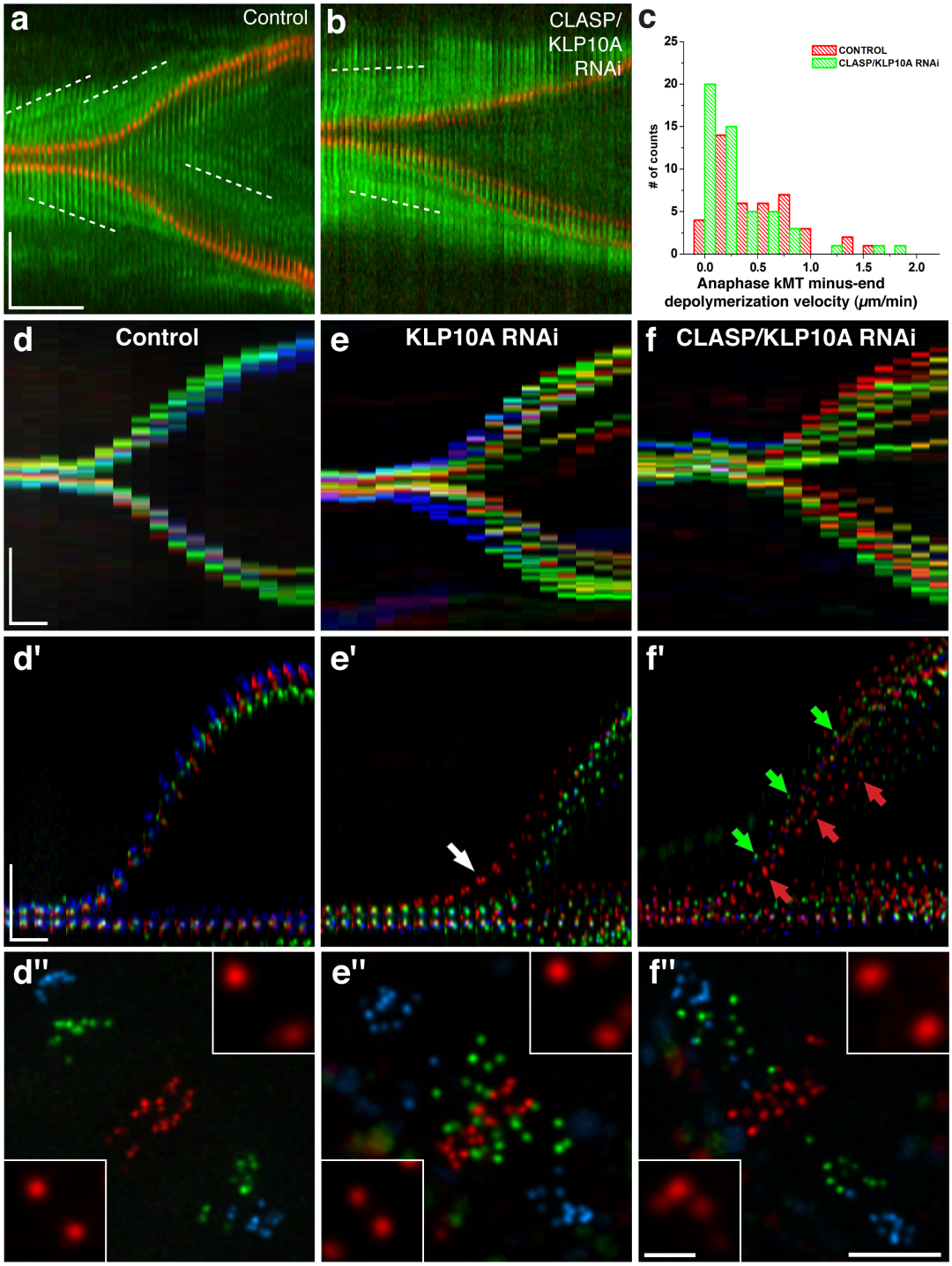
Figure 3. Analysis of chromosome and spindle dynamics during anaphase. (a–c) S2 cells stably expressing GFP– α-tubulin (green) and CID-mCherry (red) were used to track kinetochore movement and spindle elongation during anaphase. **(a)** Control **(b)**, KLP10A RNAi and **(c)** CLASP/KLP10A RNAi cells. Bar, 5 μm. **(a'–c')** Corresponding collapsed kymograph analysis. Horizontal bar, 60 s; vertical bar, 5 μm. **(d)** Distribution of chromosome poleward velocity in control, KLP10A, and CLASP/KLP10A RNAi. All RNAi treatments are statistically different from control ($P < 0.05$; Dunn's test). **(e)** Distribution of spindle elongation velocity. All RNAi treatments were statistically different from controls ($P < 0.001$; Student-Newman-Keuls test). **(f)** Distribution of kMT shortening velocity in control, KLP10A, and CLASP/KLP10A RNAi. The differences were not statistically significant. The mean ± SD or median and interquartile range are indicated for each distribution. The mean or median values are marked with a broken vertical line.

Our results show that a substantial decrease in metaphase flux velocity does not significantly affect the average velocity of kMT shortening in anaphase. To investigate this further, we performed FSM in control anaphase cells and found that kMT translocation velocity is equivalent to that observed in metaphase, as revealed by the constant slope of speckle tracks on kMTs (Fig. 4, a; Table 1). Because in S2 cells spindles elongate immediately after anaphase onset at ~0.9 μm/min (see Chapter II), this indicates that MT minus-end depolymerization must be attenuated by an equivalent rate. Indeed, we found that more than 50% of the speckles move slower than 0.4 μm/min relative to spindle MT minus-ends (Fig. 4, a and c; Table 1), which is consistent with a model where the extent of down-regulation of MT minus-end depolymerization governs the rate of spindle elongation during anaphase (Brust-Mascher *et al*. 2004). Finally, the rate of speckle movement relative to kMT minus-ends in anaphase is only marginally affected after RNAi depletion of CLASP/KLP10A, suggesting that their flux-associated activities during metaphase in untreated cells are significantly down-regulated at anaphase onset (Fig. 4, b and c; Table 1).

3.3. KMT flux ensures anaphase synchrony in *Drosophila* S2 cells

Although experimental attenuation of flux has only a minor effect on average kinetochore-to-pole velocity, we discovered that it significantly impaired anaphase synchrony (Fig. 4, d-f''; see also Fig S3). To measure the uniformity of chromosome segregation after attenuation of flux we developed a chromo-kymograph algorithm to show the movements of multiple kinetochores as a function of time through the metaphase-anaphase transition. In control cells, we generally observed two main kinetochore tracks during anaphase indicating synchronous segregation of chromosomes (Fig. 4, d and d'; n=30 cells).

Figure 4 - Quantitative analysis of kinetochore microtubule minus-end depolymerising activity and chromosome segregation during anaphase. (a and b) *Drosophila* S2 cells stably expressing low levels of GFP-α-tubulin (green) and CID-mCherry (red) were used to track tubulin speckle movement (white broken lines) relative to spindle MT minus ends by FSM. **(a)** Control cell. **(b)** CLASP/KLP10A RNAi cell. Note that in both cases, kinetochores approach the speckles. **(c)** Distribution of kMT minus end depolymerization in Control and CLASP/KLP10A RNAi cells. The differences are statistically significant ($p<0.05$; Mann-Whitney test). **(d-f)** Chromo-kymograph analysis of kinetochores in Control, KLP10A RNAi and CLASP/KLP10A RNAi cells at the metaphase-anaphase transition.



(d'-f') Overlay of guided kymographs showing three kinetochore pairs colour coded red/green/blue. Arrows indicate precocious entry of anaphase (white) or differential poleward migration (green/red). **(d''-f'')** Respective projections of three different time frames. Red/green/ blue, correspond to 1, 3.5 and 7 min after anaphase onset. Insets highlight the kinetochore pairs where inter-kinetochore distances were maximum and minimum. Bars: horizontal (space) 5 μm; vertical (time) 1 min; (inset) 1 μm.

After KLP10A or CLASP/KLP10A RNAi, we typically found 3-12 kinetochore tracks per cell (Fig. 4, e, e', f and f'; Fig. S3; n=31 cells for each RNAi), despite the formation of normal metaphase plates. Closer inspection of the chromo-kymographs revealed marked asynchrony in the entry and/or poleward migration during anaphase (Fig. 4, d-f'').

One plausible explanation for the observed asynchrony during anaphase could be the presence of kinetochores with merotelic attachments (Cimini *et al*. 2004). Indeed, members of the kinesin-13 family were implicated in correcting kinetochore-MT attachments in human cells (Ganem *et al.* 2005; Bakhoum *et al.* 2009b). Therefore it is possible that KLP10A, which localizes to centromeres in addition to spindle poles (Rogers *et al*. 2004), is also involved in this process. Analysis of KLP10A RNAi spindles revealed the persistence of cold-resistant kMTs that were indistinguishable from controls, suggesting normal kinetochore function (Fig. 5, a-c). Because the correction of merotelic attachments involves mechanisms acting before and during anaphase (Cimini *et al*. 2003), we quantified merotelic attachments after KLP10A RNAi using two criteria - accumulation of Aurora B at the inner centromere during metaphase (Knowlton *et al*. 2006) and stretching of the merotelic kinetochore during anaphase (Cimini *et al*. 2004). We were unable to detect a significant enrichment of Aurora B on metaphase plates after knocking-down KLP10A (Fig. 5, d-f). In contrast, our live-cell analysis of anaphase did reveal a 2-3 fold increase in the percentage of KLP10A (n=31) and CLASP/KLP10A (n=29) depleted cells with merotelic attachments in anaphase (13% and 10% respectively, as opposed to 4% of control cells, n= 25). However, we never found more than one chromosome or chromatid with merotelic-attached kinetochores per depleted cell, which is too infrequent to account for the observed level of asynchrony in anaphase cells depleted of KLP10A or CLASP/KLP10A. Still, it remains possible that these numbers represent an underestimate of the full complement of merotelic attachments, especially more subtle cases, which cannot be resolved by the abovementioned methods. We conclude that molecular players involved in kMT flux may be implicated in correcting erroneous kinetochore-MT attachments invisible to the SAC and somehow help ensuring the coordinated movement of chromosomes during anaphase.

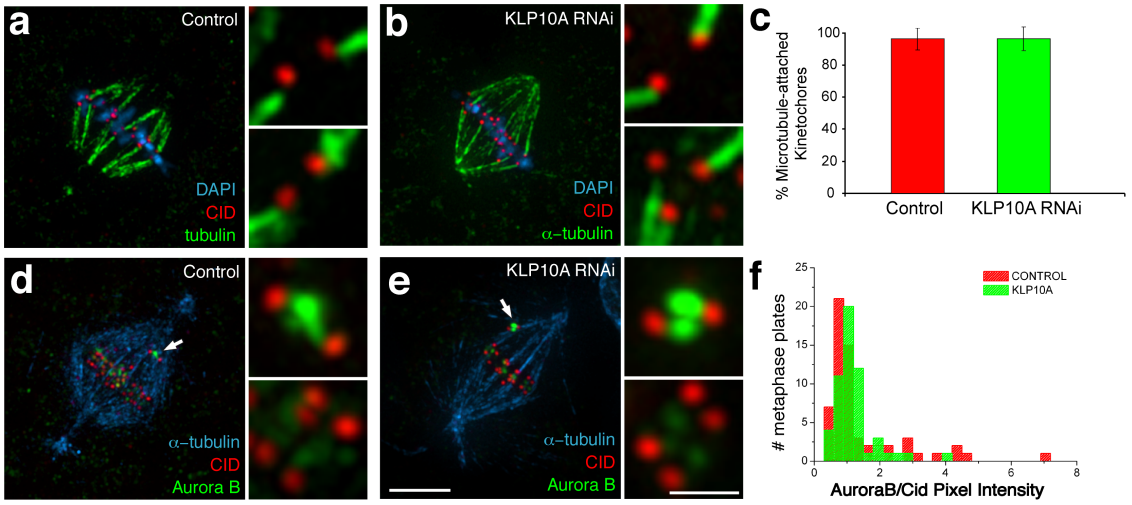


Figure 5. Analysis kinetochore–MT attachments after KLP10A RNAi. (a and b) Formation of stable kMTs after cold treatment in control and KLP10A RNAi cells, respectively. MTs (green) and kinetochores (red) were, respectively, revealed with anti–α-tubulin and anti-CID antibodies, whereas DNA (blue) was counterstained with DAPI. Bars, 5 µm. (insets) Highlight of the kinetochore–MT interactions after cold treatment. Bars, 1 µm. **(c)** The formation of cold-resistant kMTs after KLP10A RNAi (96.4%, n = 25 cells) was not statistically different from control cells (96.2%, n = 25 cells; P = 0.733, Mann-Whitney test). Median and interquartile range, are indicated in the graph. **(d–f)** Aurora B accumulation (green) during metaphase in control and KLP10A-depleted cells was not statistically different (P = 0.322; Mann-Whitney test). MTs (blue), kinetochores (red), and Aurora B (green) were respectively revealed with anti–α-tubulin, anti-CID, and anti–Aurora B antibodies. Insets highlight the higher levels of Aurora B on misaligned chromosomes (arrows) and the lower levels on metaphase chromosomes. Bars, 5 µm; inset bars, 1 µm.

3.4. Anaphase synchrony reflects the uniformity of forces acting on metaphase kinetochores

Flux players may promote anaphase synchrony by mediating the equalization of forces acting at kinetochores of metaphase chromosomes. Indeed, measurement of inter-kinetochore distances as a readout of centromere tension in living metaphase cells revealed that tension was highly variable between sister kinetochore pairs after KLP10A or CLASP/KLP10A RNAi (Fig. 6, a). In agreement, live-cell imaging of the tension-sensitive protein BubR1 in KLP10A or CLASP/KLP10A-depleted cells revealed that several kinetochores retain abnormal high levels of BubR1, which correlated with a delayed initiation of poleward migration and local degradation of the cohesin subunit Scc1 (Fig. 7,

a-e''). Quantitatively, we confirmed that flux reduction by these methods causes an increase in the variability of BubR1 at metaphase kinetochores, which is attenuated if cells are allowed to stay in metaphase for 2 h by incubation with the proteasome inhibitor MG132 (Fig. 5, b-h').

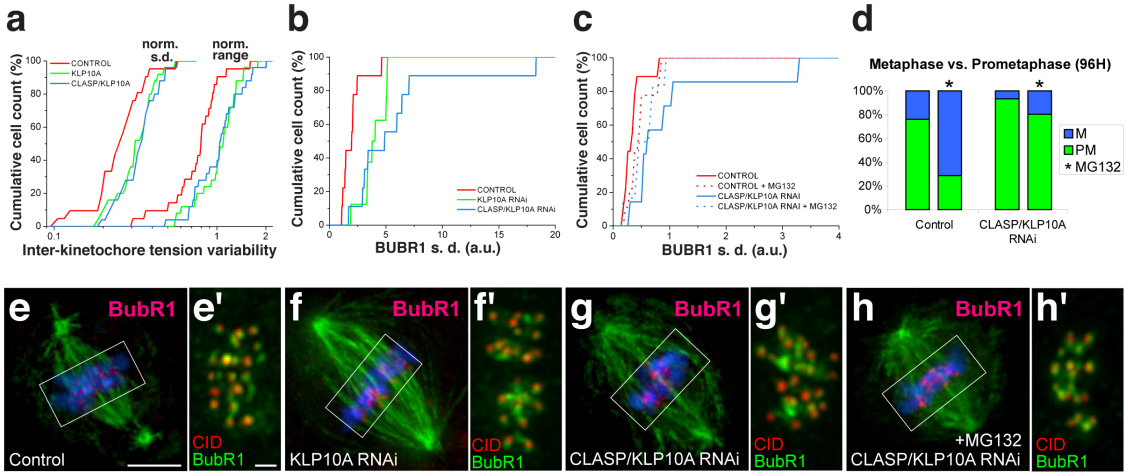


Figure 6. Experimental analysis of tension uniformity during metaphase. (a) Cumulative histogram for the normalized standard deviation (left) and range (right) of intracellular inter-kinetochore distances along a metaphase plate for control (n=21), KLP10A RNAi (n=25) and CLASP/KLP10A RNAi (n=25), where n is the number of cells. CLASP/KLP10A RNAi is statistically different from control but not KLP10A RNAi ($p<0.05$; Dunn's test). **(b)** Cumulative histograms for the standard deviation of BubR1 fluorescence intensity for control (n=10), KLP10A RNAi (n=7) and CLASP/KLP10A RNAi (n=7) cells. Both treatments cause a statistically significant variability relative to controls ($p<0.05$; Dunn's test). **(c)** Cumulative histograms for the standard deviation of BubR1 fluorescence intensity on metaphase kinetochores in control and CLASP/KLP10A RNAi before and after incubation with MG132 for 2 h. Note the approximation of the Control and CLASP/KLP10A RNAi distributions after MG132 treatment. Only CLASP/KLP10A RNAi is statistically different from controls ($p<0.05$; Dunn´s test). **(d)** Quantification of prometaphase and metaphase figures in fixed cells before and after MG132 treatment. Note that CLASP/KLP10A RNAi treated cells have problems aligning chromosomes at the metaphase plate, which is slightly attenuated if additional time is provided by incubation with MG132. (e-h) Mitotic spindles from control, KLP10A RNAi, CLASP/KLP10A RNAi and CLASP/KLP10A RNAi after MG132 treatment, respectively. α-tubulin is in green, BubR1 is in red and DNA is in blue. Bar, 5 μm. (e'-h') Insets of the respective metaphase plates shown in **(e-h)**, where CID is shown in red, and BubR1 in green. Only cells with aligned chromosomes after CLASP/KLP10A RNAi were used for all quantitative analyses of metaphase. Bar, 1 μm.

Table 1 Summary of measured mitotic parameters

Experiment	Metaphase flux velocity	Anaphase kMT minus-end depolymerization velocity	Inter-KT distance measured from fixed cells	Pixel Intensity BubR1/CID	Inter-KT distance measured from live imaging
	μm/min	*μm/min*	*μm*		*μm*
Control					
M	1.2[a]	0.4[a]	1.0[a]	1.1	0.9[a]
SD	0.4	0.4	0.2	0.6	0.1
IQR	0.6	0.5	0.2	0.8	0.2
n	392 tracks; 23 cells	43 tracks; 8 cells	207 tracks; 34 cells	59 tracks; 9 cells	198 tracks; 21 cells
Control + colchicine					
M			0.7		
SD			0.1		
IQR			0.2		
n			56 tracks; 8 cells		
Control + MG132					
M			1.1[a]	1.2	
SD			0.2	0.6	
IQR			0.4	0.7	
n			125 tracks; 20 cells	57 tracks; 9 cells	
Control (Prophase)					
M					0.4[a]
SD					0.1
IQR					0.2
n					n=102; 3 cells
KLP10A RNAi					
M	0.2[a]		0.9[a]	1.6	0.8[a]
SD	0.3		0.2	0.9	0.1
IQR	0.2		0.2	1.2	0.2
n	105 tracks; 6 cells		137 tracks; 16 cells	50 tracks; 8 cells	267 tracks; 25 cells
KLP10A RNAi + MG132					
M			0.9		
SD			0.2		
IQR			0.2		
n			50 tracks; 7 cells		
KLP10A RNAi (Prophase)					
M					0.4[a]
SD					0.1
IQR					0.1
n					79 tracks; 3 cells
CLASP/KLP10A RNAi					
M	0.2[a]	0.2[a]	1.0	1.7[a]	0.8[a]
SD	0.4	0.4	0.2	1.7	0.2
IQR	0.6	0.4	0.2	1.5	0.2
n	208 tracks; 13 cells	51 tracks; 10 cells	159 tracks; 23 cells	51 tracks; 9 cells	241 tracks; 25 cells

Table 1. Summary of measured mitotic parameters *(continued)*

Experiment	Metaphase flux velocity	Anaphase kMT minus-end depolymerization velocity	Inter-KT distance measured from fixed cells	Pixel Intensity BubR1/CID	Inter-KT distance measured from live imaging
CLASP/KLP10A RNAi + MG132					
M			1.1[a]	1.4[a]	
SD			0.2	0.7	
IQR			0.2	1.0	
n			129 tracks 20 cells	44 tracks 8 cells	
CLASP/KLP10A RNAi (Prophase)					
M					0.4 [a]
SD					0.1
IQR					0.1
n					22 tracks 2 cells
MAD2 RNAi					
M					0.8 [a]
SD					0.2
IQR					0.2
n					122 tracks 12 cells
MAD2 RNAi (Prophase)					
M					0.4 [a]
SD					0.1
IQR					0.1
n					54 tracks 3 cells
Taxol 10 nM					
M	0.1[a]		0.7	3.3[a]	
SD	0.2		0.1	2.0	
IQR	0.2		0.1	3.4	
n	73tracks; 5 cells		44 tracks; 7 cells	42 tracks; 7 cells	

Blank cells indicate that the value was not determined. KT, kinetochore; M represents the mean, except for the distributions that do not follow a Gaussian distribution; IQR, interquartile range*; n*, number of measurements (in the prophase situation n represents the number of inter-kinetochore distances measured before nuclear envelope breakdown). [a] Distributions that do not follow a Gaussian distribution, where median is represented.

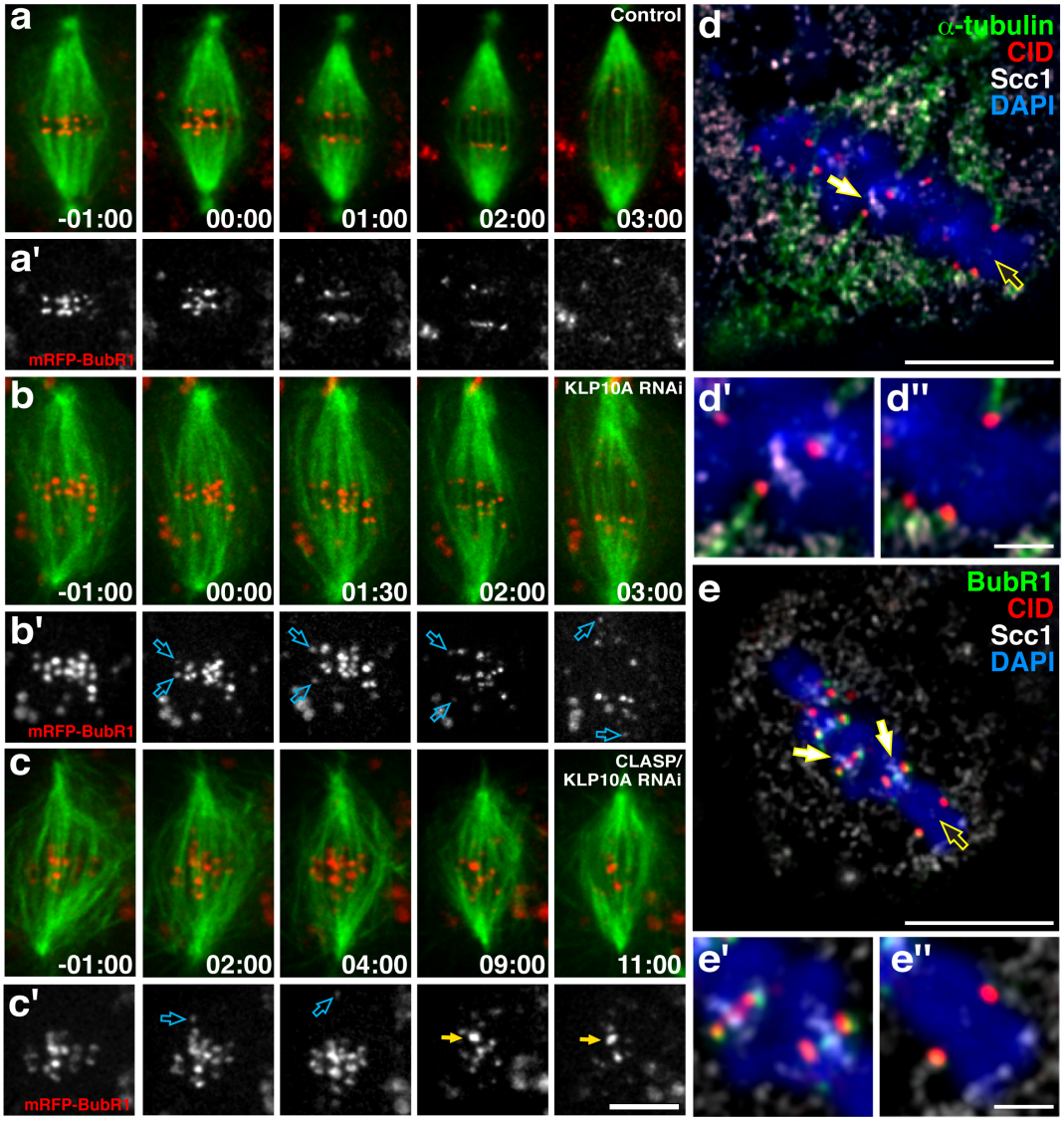


Figure 7. The timing of sister-chromatid separation in anaphase correlates with BubR1 levels at kinetochores. (a and **a')** Control S2 cell stably expressing mRFP-BubR1 (red) and GFP–α-tubulin (green). Note that mRFP-BubR1 levels at kinetochores homogenously decrease in all chromosomes at anaphase onset. **(b–b'** and **c–c')** A KLP10A- and CLASP/KLP10A-depleted cell showing marked asynchronous sister–chromatid separation with the first kinetochore pair that separated (blue arrows) associated with lower mRFP-BubR1 levels when compared with those that separated last (yellow arrows). **(d)** Differential degradation of Scc1 (white) at the metaphase–anaphase transition in a KLP10A-depleted cell. MTs are shown in green, the kinetochore marker CID is shown in red, and DNA was counterstained with DAPI (blue). **(d'–d'')** Higher magnification views of the chromosomes indicated with arrows in d. **(e)** A KLP10A-depleted cell showing differential degradation of Scc1 (white), where undetectable Scc1 correlates with lower BubR1 (green) levels at kinetochores. The kinetochore marker CID is shown in red and DNA was counterstained with DAPI (blue). Bars, 5 μm. **(e'–e'')** Higher magnification views of the chromosomes indicated with arrows in e. Open and closed arrows in d and e represent undetectable and detectable Scc1, respectively. Bars in d'' and e'', 1 μm.

3.5. Force equalization by flux can be explained by a microtubule-coupling model

In an attempt to explain how kMT flux contributes to the uniformity of forces on metaphase kinetochores we developed a minimal mathematical model for the metaphase spindle[1]. In this model we assume that the flux driving force is not generated at the kMT but is laterally transmitted to it through the action of a viscoelastic coupler that acts as a mechanical mediator. In this context, it is assumed that force is generated on ipMT through anti-parallel sliding driven either by plus end-directed bipolar motors (Goshima *et al.* 2005b; Brust-Mascher *et al.* 2009) or by active depolymerases at ipMT minus-ends (Rogers *et al*. 2004). We support that forces are laterally transmitted to kMTs based on the poleward translocation at near flux rates of laser-severed kMTs (Pereira *et al*. 2009), which don't reach near the poles and whose minus ends are not depolymerising (Maiato *et al*. 2004b), suggesting that kMT minus-end depolymerization *per se* is not a major flux-driving force but a length control mechanism. The poleward force generated is still resisted by the affinity of kinetochore-MT interface that depending on its strength modulates flux velocity. Whereas weak affinity leads to a high flux velocity, a strong affinity will slow it down. The model still assumes that centromere is elastic and responds to tension exerted on/through kMTs. Analytical solutions from the model suggest that microtubule slippage in response to poleward force transmission will redistribute tension among kMT within a characteristic time that converges to an equilibrium. The modulation of kinetochore-MT affinity will determine the flux velocity as well as the uniformization time.

[1] As the development of the work described in this chapter was done in co-authorship, the model will be described and explained in A. J. Pereira thesis. For the understanding of our conclusions I briefly describe the parameters and some results from the model, although it is important to emphasize that the original idea and the development of the analytical model was done by A. J. Pereira. For details please see Matos *et al.* (2009).

3.6. The SAC extends the duration of mitosis to allow the uniform distribution of forces acting on metaphase kinetochores

If cells require time for a uniform distribution of tension on metaphase chromosomes, one would predict that acceleration of mitosis prevents this equalization. Mad2 is a key-signaling component of the SAC that extends the duration of mitosis until all kinetochores are attached to the spindle (Meraldi *et al*. 2004). Indeed, RNAi depletion of Mad2 in S2 cells (Fig. 8, a) significantly accelerated mitosis so that cells entered anaphase prematurely (Fig. 8, b; see also Orr *et al*. 2007). Additionally, Mad2-depleted cells that were able to form a metaphase plate showed increased inter-kinetochore tension variability (Fig. 8, c) and underwent asynchronous chromosome segregation during anaphase (8, d). These results support our theoretical prediction that cells require time for a uniform distribution of forces acting on kinetochores.

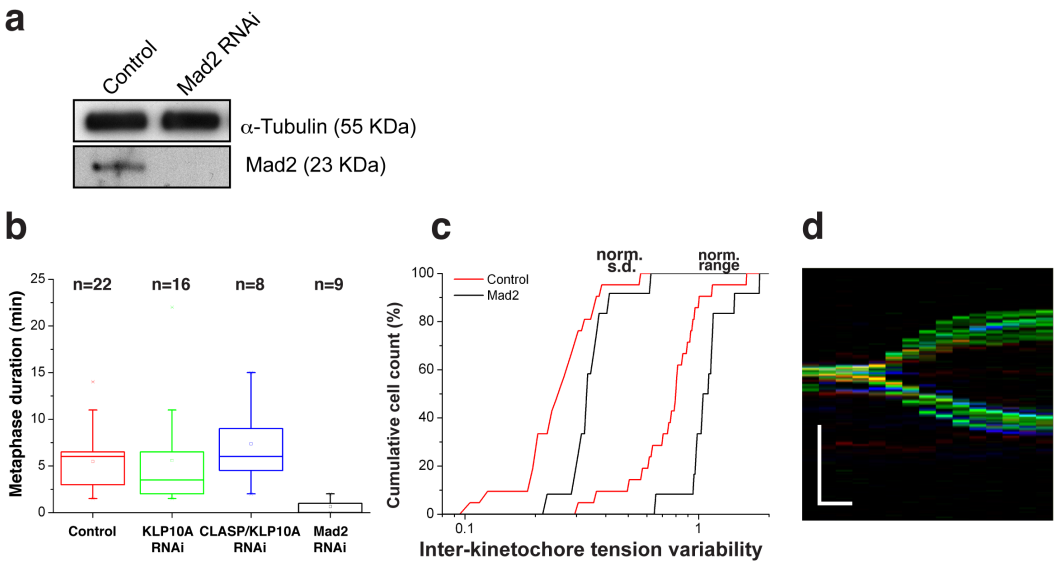


Figure 8. Tension uniformity and synchrony analysis after acceleration of mitosis. (a) Western blot showing Mad2 depletion 96h after RNAi. α-tubulin was used as loading control. **(b)** Metaphase duration in Control, KLP10A RNAi, CLASP/KLP10A RNAi and Mad2 RNAi cells where *n* represents the number of cells capable of forming a metaphase plate. The box plot determines the interquartile range, the line inside the box represents the median, the point inside the box represents the mean, and the whiskers determine the limits of the distribution disregarding outliers. Mad2 RNAi is the only treatment that is statistically different from controls ($p<0.001$, Mann-Whitney test). **(c)** Cumulative histogram for the normalized standard deviation (left) and range (right) of intracellular inter-kinetochore distances along a metaphase plate for control (n=21) and Mad2 RNAi (n=12), where n is the number of cells. Mad2 RNAi is statistically different from controls ($p<0.05$, Student t-test). **(d)** Chromo-kymograph analysis of a representative Mad2-depleted cell. Bar, 10 μm.

4. DISCUSSION

In this work we propose that flux-associated slippage of MTs at kinetochores allows spindle forces to become evenly distributed along the metaphase plate. The rationale behind this model is that MT slippage at a given kinetochore interface reflects a mechanical relaxation event which allows ipMT sliding motors to do further work, thus providing extra tension to other chromosomes. Sustained slippage events occurring along the metaphase plate eventually drive the spindle to an equilibrium state characterized by homogeneous tension. Tension equalization during metaphase ensures that any mechanism relying on tension, such as the maturation and correction of kinetochore-MT attachments (Nicklas and Ward 1994; King and Nicklas 2000; Liu *et al*. 2009), recruitment of SAC proteins (Pinsky and Biggins 2005; Musacchio and Salmon 2007) or even the coordination of cohesin degradation between sister chromatids (this study), operates uniformly along the metaphase plate.

The close match found between equalization time and metaphase duration is, in our opinion, the strongest support for a flux-dependent mechanism for tension equalization. However, such correlation poses a delicate question regarding the relationship between equalization time and the SAC. One possibility is that SAC-silencing requires that all chromosomes overcome a given tension threshold. In fact, a uniform distribution of tension maximizes the probability of globally surpassing *any* threshold. Alternatively, SAC satisfaction may rely only on MT occupancy at kinetochores. A cell with a satisfied SAC in the absence of such tension equalization mechanism would be expected to segregate its chromosomes at distinct times and/or with distinct velocities. Because metaphase duration is not significantly affected after experimental perturbation of flux and acceleration of mitosis precludes tension equalization, a plausible explanation for the observed asynchronous chromosome segregation is the reduced capacity to evenly mature and correct kinetochore-MT attachments that nevertheless satisfy the SAC. Recent works support that inter-kinetochore tension is dispensable to satisfy the SAC (O'Connell *et al*. 2008; Maresca and Salmon 2009; Uchida *et al*. 2009). However, tension may provide an important readout to allow the detection and correction of potential errors prior to anaphase onset (Pinsky and Biggins 2005). Indeed, application of tension to kinetochores is known to promote its saturation with MTs (King and Nicklas 2000), possibly by increasing MT stability due to spatial separation of kinetochore substrates from Aurora B at centromeres (Liu *et al*. 2009). However, maximizing tension by firmly grabbing MTs at their kinetochore-attachment sites would not only prevent the release of erroneous

attachments, but also hinder kMT flux/slippage, which could lead to chromosome segregation defects (Ganem and Compton 2006; Bakhoum *et al.* 2009b). Therefore, at the expense of some local loss of tension, MT affinity at kinetochores must be regulated to allow MTs to slip and possibly detach. According to our MT-coupling model, the system will respond globally to equilibrate tensions and consequently all tension-dependent processes, precluding the need for tight spatial regulation of force distribution.

Our experimental perturbation of kMT flux involved down-regulation of CLASP and KLP10A, which appeared not to be implicated in force production but rather on how the spindle responds to it. Localization of CLASP at the kinetochore and its requirement for kMT flux away from the kinetochore (Maiato *et al*. 2005) suggest that its main function is to regulate the affinity of kMT attachments by decreasing the frictional drag. In support of this conclusion, preventing Hec1 phosphorylation by Aurora B increases the affinity of the Ndc80 complex to MTs, which impairs kMT flux and turnover, while causing a 50% reduction of CLASP levels at kinetochores in Ptk1 cells (DeLuca *et al*. 2006). It is interesting to note that, while in this cell type the described perturbation leads to hyper-stretching of the centromere without affecting spindle bipolarity, CLASP RNAi in S2 cells leads to spindle collapse without any obvious increase in inter-kinetochore tension (Maiato *et al*. 2005). These different responses might reflect mechanical peculiarities associated with each cell type. On the other hand, KLP10A depletion likely prevents MT depolymerization at the poles, leading to increased resistance to kMT poleward translocation and consequent flux reduction (see Materials and Methods). Similar to polymerization at the kinetochore, depolymerization at the pole seems essentially a reactive mechanism that regulates kMT length upon translocation. Additionally, localization of KLP10A at the centromeres may account for the observed role in the correction of erroneous attachments described in this paper, which may be intrinsically coupled to its role in flux.

One important outcome of asynchronous chromosome segregation is the increased risk of aneuploidy. Recent work in budding yeast, which lack any detectable flux (Maddox *et al*. 2000), provided a molecular explanation for the abrupt degradation of cohesins at anaphase onset (Holt *et al*. 2008). Noteworthy, budding yeast do not align their chromosomes at the cell equator and rely heavily on spindle elongation for accurate chromosome segregation (Straight *et al*. 1997). In contrast, animal and plant cells establish a metaphase plate, a high-order state that is only justified if the subsequent synchronous migration of sister chromatids is ensured, where a mechanism involved in force equalization may be essential. The emergence of flux in higher eukaryotes and its contribution to anaphase "quality" may play particularly important roles in the prevention

of chromosomal abnormalities observed in cancers or in several human syndromes, many of which result from defects in chromosome segregation during meiosis, where flux is indeed maintained at high rates.

CHAPTER II.

Chromosome segregation – *How do chromosomes move*?

1. INTRODUCTION

How do chromosomes move? What are the forces involved in chromosome segregation? How are these forces molecularly regulated? These are some of the long-standing questions that have attracted scientists since the end of the 19th century. Until today it has been difficult to achieve common answers as different organisms and species may segregate their chromosomes in distinct ways.

The physical segregation of sister chromatids is mediated by the spindle apparatus and can occur either as a consequence of kMT-shortening (anaphase A), or spindle elongation (anaphase B). Different models have been developed to explain each mechanism and depending on the organism one may be more important than the other. Anaphase A can be explained by two main models, the most popular is the "Pac-Man" model which postulates that kinetochores pull chromosomes poleward while they disassemble kMT at the plus-ends (Cassimeris *et al.* 1987; Gorbsky *et al.* 1987). The other model postulates that chromosomes move towards the poles due to the flux associated kMT disassembly near the poles (Inoue and Sato 1967; LaFountain *et al.* 2004). Anaphase B, on the other hand, may occur either as a consequence of astral pulling forces (Kronebusch and Borisy 1982; Waters *et al.* 1993) or outward sliding, mediated by MT crosslinkers and motors (Brust-Mascher *et al.* 2004; see also Peterman and Scholey 2009). Understanding the segregation mechanism of each eukaryotic system permits the accurate investigation on the respective molecular regulation of force generation.

In higher plants and meiotic cells such as grasshopper (*Melanoplus femurrubrum*) spermatocytes, chromosome segregation is mainly guaranteed by anaphase A, being anaphase B largely reduced (LaFountain *et al.* 2004; Hayashi *et al.* 2007). In these systems, flux associated MT minus-end depolymerization accounts with the great majority of force that assures chromosome movement (LaFountain *et al.* 2004; Dhonukshe *et al.* 2006). Conversely, it has been shown that in vertebrate mitotic systems such as newt lung cells, the force generated at kinetochores is the main driver of anaphase A, while kMT disassembly at the poles only accounts for ~1/3 of this movement (Mitchison and Salmon 1992).

In *Drosophila* embryos, it was proposed that flux associated MT depolymerization at the poles is the main driver of anaphase A, contributing to ~90% of the movement (Maddox *et al.* 2002). However, these results are controversial as Brust-Mascher *et al*. 2002, invokes that flux only accounts for ~30-45% of the anaphase A movement in this organism (Brust-Mascher and Scholey 2002; Brust-Mascher *et al.* 2009). In *Drosophila* cells different studies have been made to understand the forces involved in chromosome segregation. Although a Pac-Man-flux mechanism has been suggested as the main driver, a consensus was still not achieved and a plethora of molecular players were suggested to be involved in force production (Buster *et al.* 2007; Zhang *et al.* 2007; Rath *et al.* 2009).

In this chapter we aimed to integrate, in one single system, the molecular understanding of anaphase A and anaphase B, and test different models already proposed to explain chromosome segregation. In order to achieve this goal and to perform a quantitative analysis we took advantage of *Drosophila* S2 cells. This system provides a plus over many cell types to study chromosome segregation as it offers a powerful set of experimental solutions that allows high-resolution spatiotemporal observations (Bettencourt-Dias and Goshima 2009; Moutinho-Pereira *et al.* 2010). Among these, it is important to highlight the availability of a fully sequenced and well-annotated genome and the conservation of more than 60% of the genes with humans (Adams *et al.* 2000). Additionally, specific gene silencing is easily achieved by RNA interference (RNAi) and a strong effect can be observed simply by adding dsRNA to culture cells (Maiato *et al.* 2003b; Bettencourt-Dias and Goshima 2009; Pereira *et al.* 2009). Also, *Drosophila* culture cells have a low chromosome number (typically between 4-12) and details can be easily observed by high-resolution microscopy by the use of available stable cell lines expressing fluorescent components of the mitotic apparatus.

2. MATERIAL AND METHODS

2.1. Cell culture, RNAi treatment and western blot

Drosophila S2 cells were cultured as described in Chapter I. RNAi depletion of *Drosophila* KLP10A, CLASP/KLP10A, Sas4, Sas4/KLP10A and Mad2 was performed as described and using the published targeting sequences (Rogers *et al.* 2004; Maiato *et al.* 2005; Morales-Mulia and Scholey 2005; Goshima *et al.* 2007; Orr *et al.* 2007; Rodrigues-Martins *et al.* 2007; Pereira *et al.* 2009; see Table S1). Sas4 depletion was achieved after 16 days of treatment (four transfection cycles with 4-days interval). KLP10A depletion was achieved after 4 days of treatment (two transfection cycles with 2-days interval); KLP10A RNAi within Sas4/KLP10A co-depletion was started at the time of the last cycle of Sas4 RNAi. The other knock-downs were achieved after 4-days of single treatment. Depletions were monitored by western blot as described in Chapter I (data shown in Chapters I and III; for antibodies and dilutions see Table S2). Because Sas-4 is not an abundant protein in *Drosophila* cells, we were not able to monitor the efficiency of its depletion by western blot (Basto *et al*. 2006; Rodrigues-Martins *et al*. 2007).

2.2. Drug treatments

Taxol 10 nM was used to suppress microtubule dynamics as described in Chapter I.

2.3. FSM, time-lapse microscopy and kymography analysis

FSM, time-lapse microscopy and kymography analysis were performed as described in Chapter I.

2.4. Quantifications

Chromosome segregation parameters were measured and evaluated from kymograph analyses. *Chromosome poleward velocity* relative to the equator was measured following each CID-mCherry track obtained from kymographs covering the entire cell volume. Velocity was determined measuring the slope of the fastest linear movement after

anaphase onset within each half-spindle. The distribution shown in the histogram represents each track measured in the total number of cells.

Spindle elongation velocity was measured by following spindle MT minus-ends. Slopes were determined for the same period of time when chromosome poleward velocity was measured. Each value shown in the histogram is the average from the slopes of both half-spindles per cell.

KMT shortening velocity was quantified as the difference between each measurement of poleward chromosome velocity and the corresponding half-spindle elongation velocity.

2.5. Statistical analyses

Statistical analysis was performed using either parametric or non-parametric tests depending on the normality of the distributions tested using Kolmogorov-Smirnov test. A parametric *t test* or non-parametric Mann-Whitney was used for two-group comparison. P value was considered extremely significant if $P<0.001$, very significant if $0.001<P<0.01$, significant if $0.01<P<0.05$ and not significant (ns) if $P>0.05$. All the analysis was done using GraphPad Prism, version 5.00 for Macintosh, GraphPad Software, San Diego California USA, www.graphpad.com.

3. RESULTS

3.1 Anaphase A and anaphase B onset is simultaneous in *Drosophila* S2 cells

To characterize chromosome segregation in *Drosophila* S2 cells we quantitatively analyzed mitotic progression using dual-wavelength spinning disk confocal microscopy. Although it is well established that anaphase A and anaphase B onsets are uncoupled in *Drosophila* embryos (Brust-Mascher and Scholey 2002; Brust-Mascher *et al.* 2004; Cheerambathur *et al.* 2007), this has never been properly addressed in S2 cells.

To clarify this issue and observe the metaphase-anaphase transition, we started by using a cell line stably expressing mRFP-BubR1 and GFP-α-tubulin. BubR1 is a tension-sensitive kinase that is enriched at kinetochores when they are not under-tension, and reduced once tension is achieved. Accordingly, we observed that BubR1 signal decreases throughout metaphase being almost absent when cells enter anaphase (Fig. 1, a).

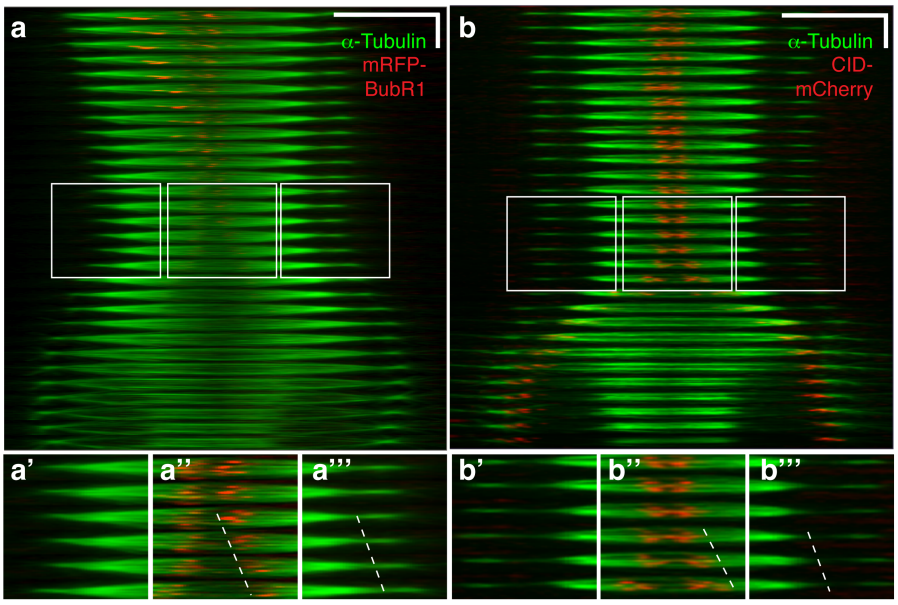


Figure 1 – Concomitant anaphase A and anaphase B onset. S2 cells stably expressing GFP-α-tubulin and **(a-a''')** mRFP-BubR1 or **(b-b''')** CID-mCherry were used to analyze the timing of anaphase A and anaphase B onset. **(a'' and b'')** Dashed lines are guided-lines that track the movement of kinetochores and **(a''' and b''')** the poles. Insets are 2x magnifications of the selected regions. Horizontal bar, 5 μm; vertical bar, 60 sec.

If the signal intensity is enhanced it is still possible to observe that the initiation of kinetochore migration is concomitant with the movement of the poles (Fig. 1. a', a'' and a'''; time-lapse= 30 sec). This cell line offers a good solution to monitor the time of metaphase-anaphase transition. Anaphase A and anaphase B onset was also simultaneous for the cell line subsequently used, stably expressing CID-mCherry and GFP-α-tubulin (Fig. 1. b', b'' and b''').

3.2. Spindle elongation and kMT shortening equally contribute to chromosome segregation in *Drosophila* S2 cells

In an attempt to evaluate the contribution of different mechanisms to chromosome segregation we analyzed anaphase in the absence of flux related mechanisms. This was achieved by depleting KLP10A and CLASP/KLP10A (Buster *et al.* 2007), and by treating cells with 10nM Taxol (Fig. 2, a-d; see Chapter I for details). Furthermore, we tested the contribution of centrosomes and the impact of an accelerated mitosis by respectively depleting Sas4 and the SAC protein Mad2 (Fig. 2, e-g).

To quantitatively perform this analysis we defined and measured three parameters: chromosome poleward velocity (Table 1), spindle elongation velocity (Table 2) and kMT shortening velocity (Table 3). These parameters were quantified from collapsed kymographs (Fig. 2. a'-g') as described in Figure 3 (see Materials and Methods for details). Our first interesting observation was that in control cells, anaphase A and anaphase B equally contribute to chromosome poleward velocity. Whereas spindles elongated at an average velocity of 0.9±0.2 μm/min (mean±SD; Table 2), the average kMT-shortening velocity was 0.8±0.4 μm/min (mean±SD; Table 3).

Next we hypothesized that if minus-end depolymerization is the main driver of anaphase A, its down-regulation would significantly impair kMT-shortening and reduce chromosome poleward velocity. Accordingly, we observed that the knock-down of the microtubule-destabilizing kinesin-13, KLP10A (Rogers *et al.* 2004) led to a reduction of 20% in the chromosome poleward velocity (Table 1). However, the slow movement observed after this depletion was a consequence of reduction in the spindle elongation velocity (0.5±0.2μm/min; mean±SD), and not on the kMT-shortening velocity (0.9±0.6μm/min; mean±SD). Interestingly, when centrosomes were co-depleted with KLP10A, spindle elongation velocity was recovered to the same extent as when centrosomes were depleted alone (0.7±0.2 μm/min; mean±SD). The reduction in the spindle elongation velocity after KLP10A depletion may be explained by the existence of

long asters (Fig 2. c, see also Chapter I for phenotypic details) that may exert pushing forces that will hamper the elongation of the two half-spindles. This reduced chromosome poleward velocity was also observed after CLASP/KLP10A RNAi (Tables 1 and 2).

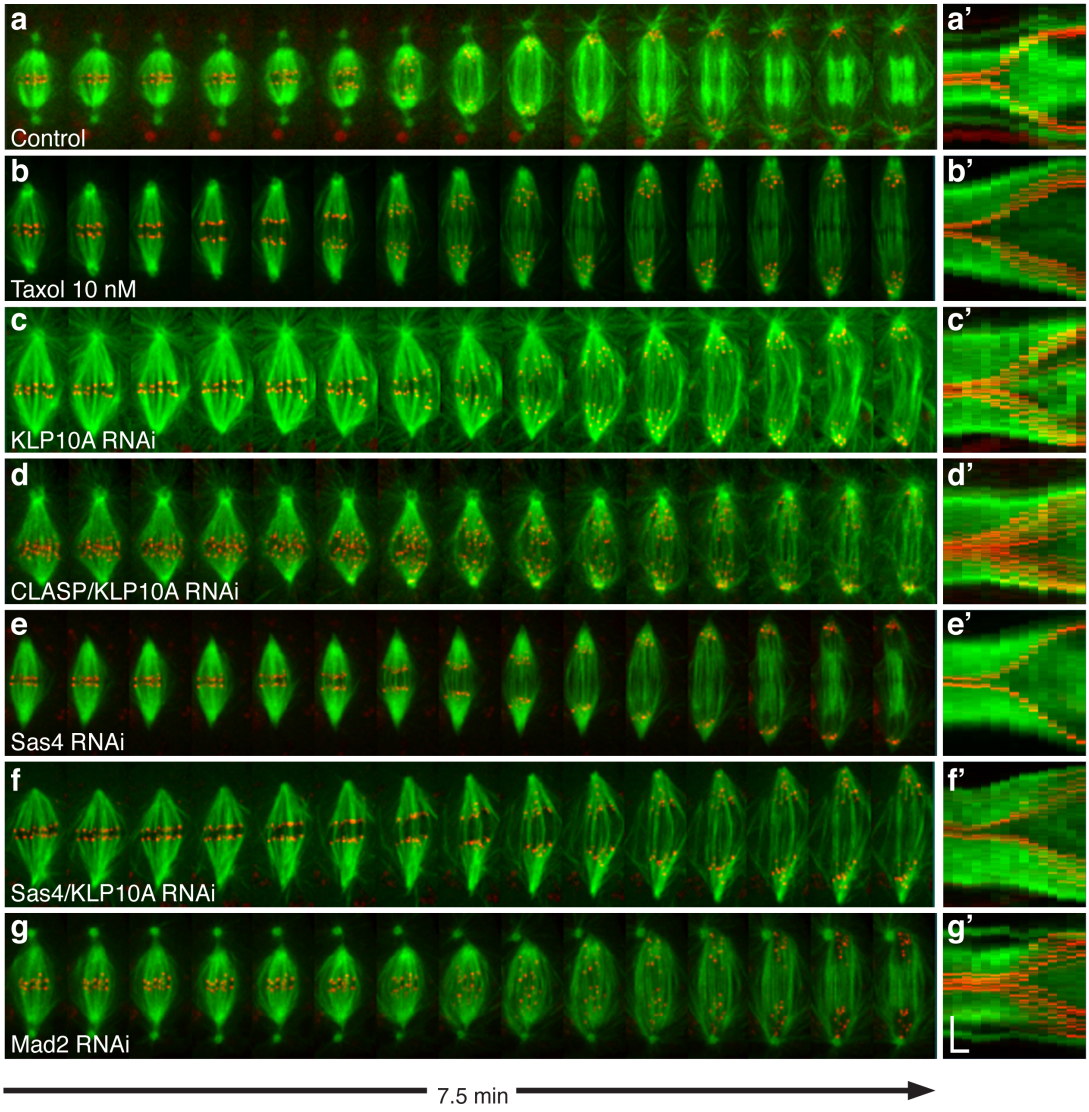


Figure 2 – Phenotypic analysis of the metaphase-anaphase transition. (a-g) S2 cells stably expressing GFP-α-tubulin and CID-mCherry were used for the analyses of chromosome movement under the conditions depicted. **(a'-g')** The Collapsed kymographs were used to track the movement of kinetochores and the coupled MT minus-ends, at the spindle pole region. Vertical bar, 5 μm; Horizontal bar 60sec. Time-lapse, 30 sec.

The most significant reduction in the chromosome poleward velocity was observed after 10 nM Taxol treatment. *In vitro* at nanomolar concentrations (<100 nM), substoichiometric binding of Taxol molecules to tubulin in MTs selectively suppresses shortening rates at MT plus-ends (Derry *et al.* 1995; Jordan and Wilson 1998). Moreover, as reported in the previous chapter, cell treatment with 10 nM Taxol reduces flux to low levels. Here we observed a reduction of ~40% in the chromosome poleward velocity (Table 1). This was due to a decrease in the spindle elongation velocity (0.60±0.1μm/min; mean±SD; Table 2, Fig. 5, a) and in the kMT-shortening velocity (0.5, 0.5; median, IQR; Table 3, Fig. 6, a). If under Taxol treatment flux associated activities are not contributing to kMT-shortening, all the chromosomes-to-pole movement observed is due to depolymerization driven at kinetochores. Taking this, it is possible to infer that in *Drosophila* S2 cells the Pac-Man mechanism accounts with ~50% to the Anaphase A movement. This is in accordance with the anaphase kMT minus-end depolymerization velocity measured from the movement of tubulin speckles (see Chapter I), where the median velocity observed was 0.4 μm/min. If the kMT shortening velocity is ~0.8 μm/min and the minus-end depolymerization is accounting to 50% of the movement, the Pac-Man will account for the remaining 50%.

Next we observed that after Sas4 and Sas4/KLP10A RNAi although the chromosome poleward velocity was on average unaffected (Table 1, Fig. 4 d and e), spindle elongation velocity was slightly reduced (Table 2, Fig. 5 d and e). This is an indication that the astral forces are important to drive spindle elongation. Moreover, we noticed that in the absence of centrosomes the average kMT-shortening velocity was faster than the control (Table 3; Fig. 6, d). This can either be a consequence of an unspecific role of Sas4 during anaphase A, or a consequence of a putative mechanism that can compensate the down-regulation observed for spindle elongation.

Finally, although acceleration of mitosis by Mad2 depletion did not delayed chromosome poleward movement (Table 1, Fig. 4, f), spindle elongation velocity was reduced by 40% (Table 2, Fig. 5, f). This means that kMT-shortening was in fact accelerated after Mad2 depletion (Table 3, Fig. 6, f). The rapid movement of anaphase A (1.1 μm/min) may be a consequence of kMT minus-end depolymerization that might be taking place at metaphase rates. The abnormal metaphase and the fastest anaphase transition could possibly prevent the suppression of MT flux that is required to subsequently couple spindle elongation as predicted by Brust-Mascher *et al* (2004).

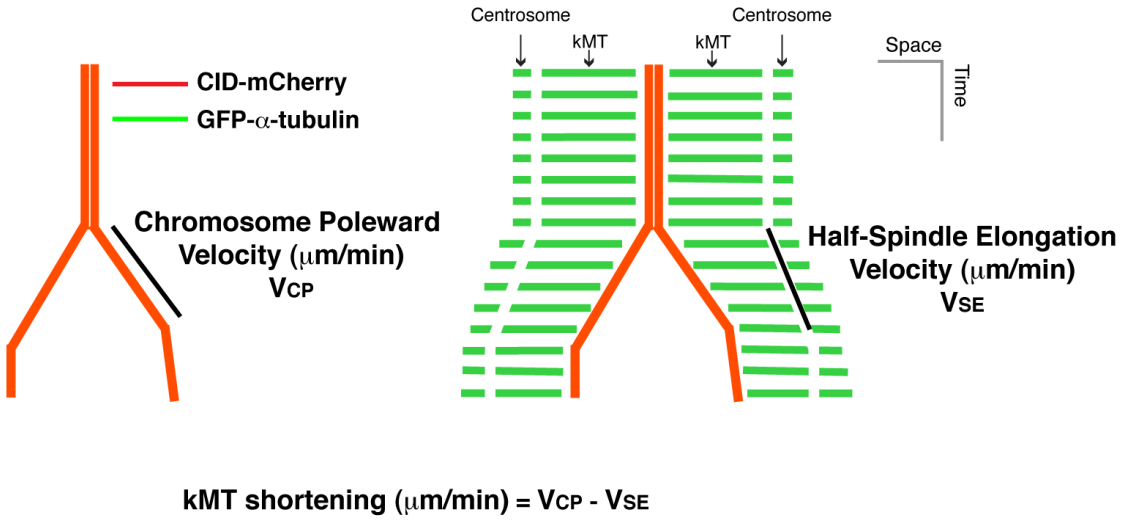


Figure 3 – Schematic representation of anaphase parameters. Kymograph projections were obtained from spinning-disk confocal time-lapse movies using S2 cells stably expressing CID-mCherry and GFP-α-tubulin. Quantifications were performed tracking the movement of kinetochores (chromosome poleward velocity), and the poles (Half-spindle elongation velocity). KMT shortening velocity was inferred by subtracting half-spindle elongation velocity to the chromosome poleward velocity.

Table 1 – Chromosome poleward velocity

Treatment	K-S	N	Mean	SD	SEM	Median	25th Q	75th Q	P
Control	Y	88	1.65	0.48	0.05	1.65	1.31	2	
Taxol10nM	Y	112	1.05	0.43	0.04	1.01	0.74	1.35	< 0.0001
KLP10A RNAi	Y	186	1.34	0.60	0.04	1.32	0.88	1.77	< 0.0001
CLASP/KLP10A RNAi	Y	219	1.11	0.43	0.03	1.06	0.78	1.38	< 0.0001
Sas4 RNAi	N	124	1.66	0.45	0.04	1.74	1.41	1.94	ns
Sas4/KLP10A RNAi	Y	84	1.62	0.56	0.06	1.59	1.27	1.95	ns
Mad2 RNAi	Y	153	1.55	0.64	0.05	1.56	1.05	2.07	ns

Detailed analysis of independent experiments in which cells were treated either with Taxol or with the different dsRNA depicted. The results are compared with Control untreated cells. All units are μm/min except No that refers to the number of CID tracks analyzed from the number of cells in Table 2. P value is represented for either unpaired t test or Mann-Whitney test depending if the population follows (Y), or not (N), a Gaussian distribution. K-S refers to normality tested using the Kolmogorov-Smirnov test. Ns refers to not significant.

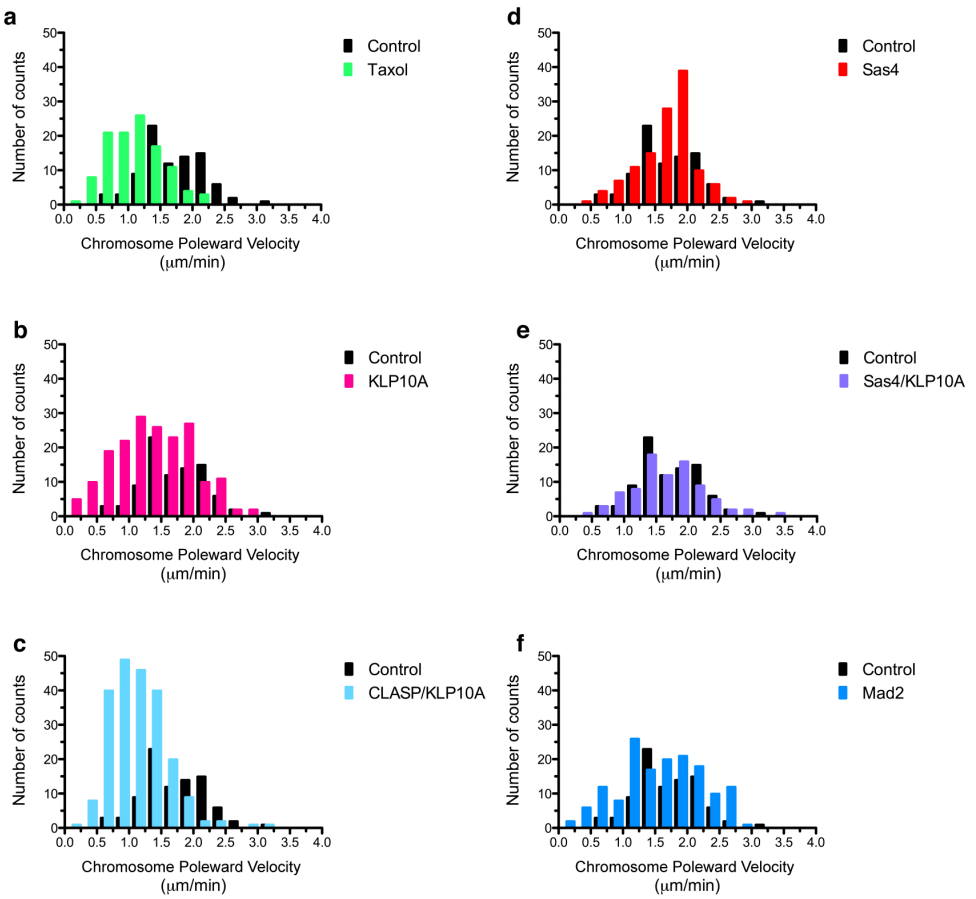


Figure 4 – Quantification of anaphase parameters – Chromosome poleward velocity. (a-f) Distribution of chromosome poleward velocity. To prevent overlap, the represented colored data was moved 0.06 μm/min within the x-axis.

Table 2 – Spindle elongation velocity

Treatment	K-S	N	Mean	SD	SEM	Median	25th Q	75th Q	P
Control	Y	30	0.86	0.16	0.03	0.86	0.80	0.96	
Taxol 10nM	Y	18	0.55	0.11	0.03	0.55	0.49	0.63	< 0.0001
KLP10A RNAi	Y	32	0.45	0.22	0.04	0.45	0.30	0.56	< 0.0001
CLASP/KLP10A RNAi	Y	33	0.42	0.17	0.03	0.40	0.31	0.51	< 0.0001
Sas4 RNAi	N	29	0.74	0.19	0.03	0.72	0.68	0.87	0.0043
Sas4/KLP10A RNAi	Y	14	0.74	0.16	0.04	0.74	0.63	0.85	0.0270
Mad2 RNAi	Y	19	0.54	0.23	0.05	0.47	0.33	0.7	< 0.0001

Detailed analysis of independent experiments in which cells were treated either with Taxol or with the different dsRNA depicted. The results are compared with Control untreated cells. All units are μm/min except No that refers to the number of spindles analyzed. P value is represented for either unpaired t test or Mann-Whitney test depending if the population follows (Y), or not (N), a Gaussian distribution. K-S refers to normality that was tested using the Kolmogorov-Smirnov test. Ns refers to not significant.

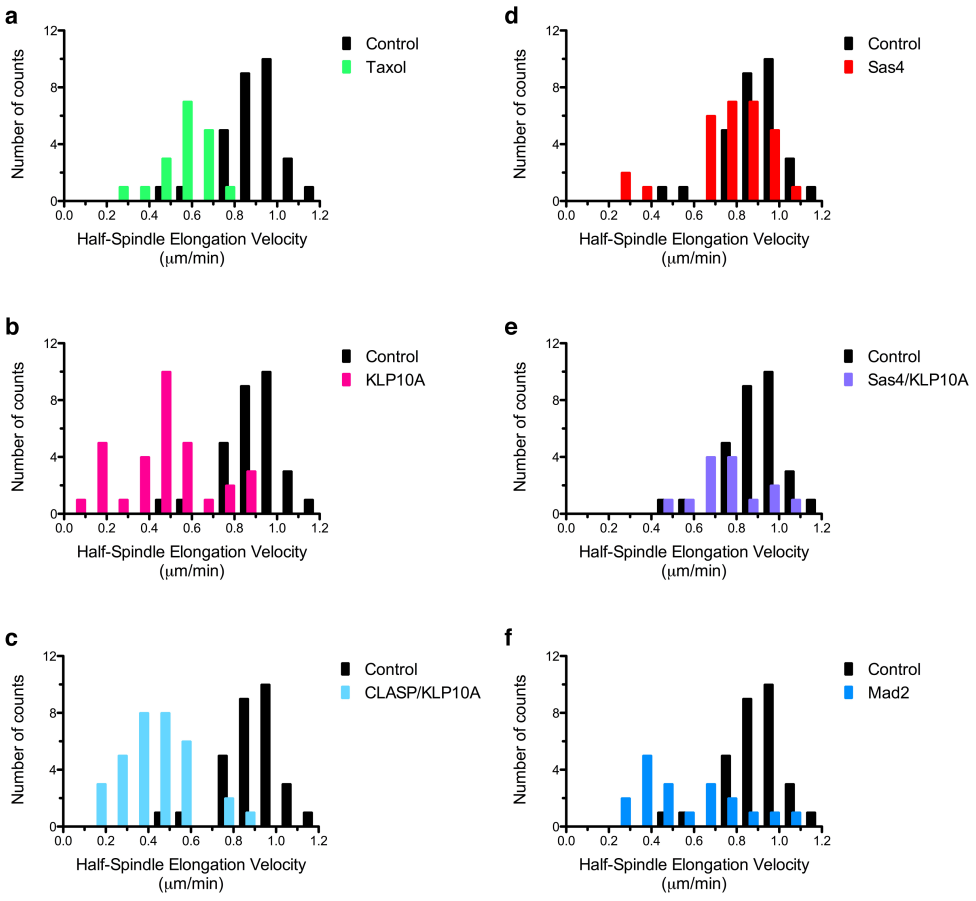


Figure 5 – Quantification of anaphase parameters - Half-spindle elongation (a-f) Distribution of half-spindle elongation velocity. To prevent overlap, the represented colored data was moved 0.03 μm/min within the x-axis.

Table 3 – kMT shortening velocity

Treatment	K-S	N	Mean	SD	SEM	Median	25th Q	75th Q	P
Control	Y	88	0.81	0.40	0.04	0.82	0.5	1.11	
Taxol10nM	N	112	0.51	0.38	0.04	0.45	0.23	0.72	< 0.0001
KLP10A RNAi	N	186	0.92	0.58	0.04	0.88	0.41	1.35	ns
CLASP/KLP10A RNAi	N	219	0.71	0.42	0.03	0.66	0.4	0.96	0.0205
Sas4 RNAi	N	124	0.98	0.41	0.04	0.99	0.79	1.21	0.0055
Sas4/KLP10A RNAi	Y	84	0.90	0.52	0.06	0.88	0.51	1.23	ns
Mad2 RNAi	Y	153	1.07	0.56	0.05	1.09	0.69	1.51	0.0002

Detailed analysis of independent experiments in which cells were treated either with Taxol or with different the dsRNA depicted. The results are compared with Control untreated cells. All units are μm/min except No that refers to the number of CID tracks analyzed from the number of cells on table 2. P value is represented for either unpaired t test or Mann-Whitney test depending if the population follows (Y), or not (N), a Gaussian distribution. K-S refers to normality that was tested using the Kolmogorov-Smirnov test. Ns refers to not significant.

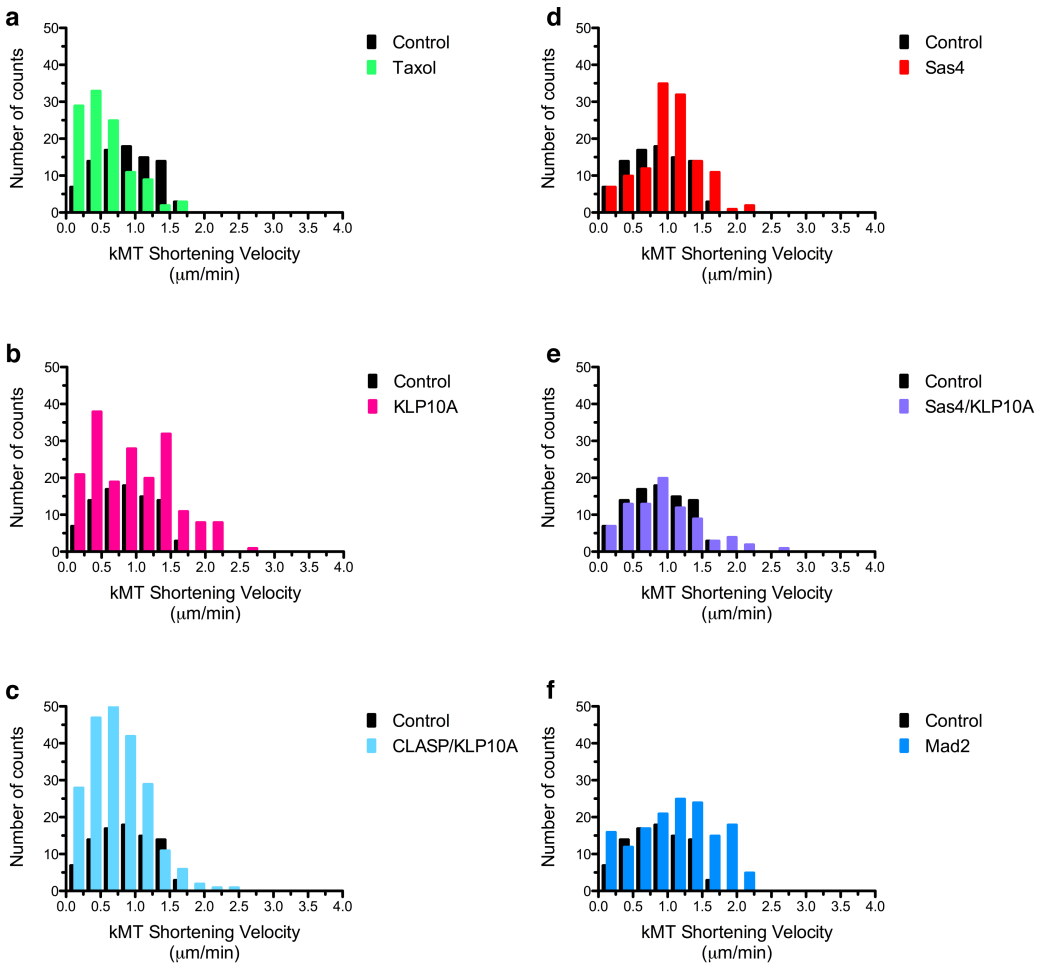


Figure 6 – Quantification of anaphase parameters – KMT shortening. (a-f) Distribution of kMT shortening velocity. To prevent overlap, the represented colored data was moved 0.03 μm/min within the x-axis.

3.3. Pac-Man mediates kMT-shortening in *Drosophila* S2 cells

S2 cells expressing low levels of GFP- α-tubulin were used to accurately observe the movement of tubulin speckles during metaphase-anaphase transition (Fig. 7, a-c). From the data described in the previous chapter we now know that minus-end depolymerization rate is reduced by ~70%, upon anaphase onset. This change in the speckle velocity can be easily observed after re-alignment of the mitotic spindle having the left kinetochore as a fixed reference (Fig 7, b; Pereira and Maiato, 2010). If minus-end depolymerization is faster, one should observe in the left side of the kymographs (Fig. 7, b and c) that the speckle and kinetochore movements diverge. On the other hand, if depolymerization at kinetochores is faster, we should observe that speckle and kinetochore movements converge. In fact, from the chromo-kymograph analysis is possible to observe that although speckle movement diverges from kinetochore in metaphase, both converge during anaphase (Fig 7, b and c). Furthermore, if the speckle movement is driven by spindle translocation, the track of the pole movement (guided by the blue dashed lines) should be parallel to the one followed by the speckle. In fact, we observed that once the speckle movement changes direction (white *vs.* red dashed lines), the pole track follows nearly parallel. The fact that both lines are not perfectly parallel, suggests that depolymerization at the poles is still occurring, although, for this kMT, slower than the Pac-Man velocity.

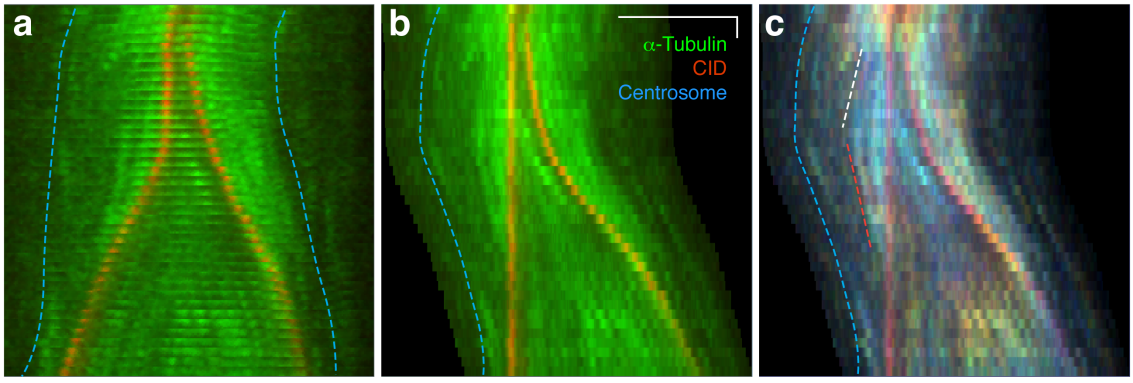


Figure 7 – Pac-Man evidence during anaphase. (a-c) S2 cells stably expressing low levels of GFP-α-tubulin and CID-mCherry were used to track tubulin speckle movement relative to MT minus-end by FSM. **(a)** Kymographs were aligned either having the equatorial region as the reference point or **(b-c)** the left kinetochore. Note the change in the direction of the speckle after anaphase onset. **(c)** Dashed white line represents the movement of speckle toward the pole during metaphase, whereas red dashed line represents its movement after the anaphase onset. Blue dashed lines are guiding centrosomes through time. Horizontal bar, 5 μm; Vertical bar 10 sec.

DISCUSSION

Progressive understanding of microtubule dynamics and chromosome segregation has improved in the last three decades due to the development of imaging techniques combined with the use of fluorescently tagged proteins and generation of fiduciary marks along the spindle (reviewed by Mitchison and Salmon 2001; Civelekoglu-Scholey and Scholey 2010). Accordingly, in this study we have used S2 cells stably expressing GFP-α-tubulin (at low and high levels), in combination with either the kinetochore marker CID-mCherry, or the tension sensitive protein mRFP-BubR1, to characterize chromosome movement during anaphase in the *Drosophila* S2 cells.

Our first important observation shows that anaphase A and anaphase B onset is simultaneous and that both mechanisms equally contribute to chromosome segregation in S2 cells. This is surprising as in *Drosophila* embryos it is reported that the anaphase A and B onsets are uncoupled (Maddox *et al.* 2002; Brust-Mascher *et al.* 2004). Also, different studies in S2 cells have neglected the importance of anaphase B to guarantee chromosome segregation. In fact, if we look more carefully to the results here presented we should consider anaphase B as the main driving mechanism of chromosome segregation. Although both mechanisms start at the same time and have similar velocities, anaphase B is longer (~5 min) than anaphase A (~2-3 min; see Fig. 2). Therefore it is important to consider and take into account anaphase B, when anaphase A mechanisms are being quantified.

When testing the hypothesis that anaphase A is mainly driven by flux associated mechanisms we observed that the Pac-Man activity can equally contribute to the mechanism of anaphase A. To test whether depolymerization at the minus-ends contributes to kMT-shortening, we perturbed proteins that are involved in flux regulation during metaphase. Accordingly, we depleted KLP10A and CLASP/KLP10A and we observed that average velocity was unaffected. This suggests that KLP10A mediated minus-ends destabilization is normally down-regulated upon anaphase onset. In fact, Brust-Mascher *et al.* 2004, proposed that in *Drosophila* embryos, KLP10A needs to be down-regulated in order to anaphase B proceed. As in our system anaphase A and B are concomitant, this may be an explanation for the unperturbed average velocity of kMT shortening observed. Our experimental results are different from those described by Buster *et al* (2007), which obtained more than 50% reduction in kMT-shortening velocity after KLP10A and CLASP/KLP10A RNAi. One important difference between this previous report and our study was our inclusion of a kinetochore marker and collection of z-stacks

through the entire volume of the cell which allowed us to directly measure kMT shortening velocities for the full chromosome set.

Anaphase A down-regulation was only observed after 10nM Taxol treatment. At this concentration metaphase MT flux is impaired and the microtubule dynamics is perturbed. As shown in Chapter I, depolymerization at the poles can contribute up to 50% of the anaphase A movement in a control situation. As so, we can atribute the kMT-shortening velocity observed after Taxol treatment to the Pac-Man activity and to some residual depolymerization at minus-ends that may still occur. Conversely, anaphase A upregulation was observed for those situations where anaphase B was down-regulated, namely Sas4 and Mad2 depletion. These observations suggest the existance of a compensation mechanism between anaphase A and anaphase B raising the question of why does the cell preserve two mechanisms that guarantee chromosome segregation. Functional redundancy seems to be stable throughout evolution and even if anaphase B is not the main driver of chromosome segregation (LaFountain *et al.* 2004; Hayashi *et al.* 2007), there are no reports of systems where this mechanism is completely abolished.

The acceleration of kMT-shortening velocity observed after Mad2 depletion may still be a consequence of a defective metaphase and unregulated anaphase transition. In fact, it was recently proposed that a competent spindle requires the appropriate time to achieve its full maturation that guarantees proper kinetochore MT-attachments and anaphase spindle elongation (Lince-Faria *et al.* 2009). Furthermore we suggest that the rapid kMT depolymerization is a consequence of the lack of down-regulation of microtubule flux that should be reduced in 70% upon anaphase transition. A detailed FSM analysis should be performed to study this mechanism further.

In conclusion we observed that *Drosophila* S2 cells are a suitable model to sudy the mechanisms that drive and gurarantee chromosome segregation. In accordance, it was observed that in this system chromosome poleward movement is equally driven by anaphase A and anaphase B. The existence of a coupled mechanism of segregation confers to this cells an advantage as it is possible to integrate and chalange in one single system, the knowledge learned from other different models. Furthermore, we observed that minus-end depolymerization and Pac-Man, evenly coutribute to promote anaphase A movement. Nevertheless, further work will be necessary to characterize and understand the mechanisms that drive anapahse B in *Drosophila* S2 cells.

CHAPTER III.

Spatiotemporal analysis of spindle elongation in *Drosophila* S2 cells

1. INTRODUCTION

After anaphase onset the mitotic spindle undergoes a major reorganization that occurs as a consequence of multiple biochemical signals and switches (Sullivan and Morgan 2007). Cyclin B is degraded, CDK1 activity drops, and MTs become more stable. Consequently, kMTs shorten (anaphase A) and the two half-spindles are slid apart (anaphase B). While mechanisms of chromosome segregation during anaphase A are an intensively studied topic, the mechanisms that mediate and guarantee anaphase B are less understood and the focus of this chapter.

In many eukaryotic systems anaphase A starts before anaphase B, however temporal resolution cannot be used as a rule as in some systems such as *Drosophila* S2 cells, both movements are coordinated and start at the same time. Anaphase B (hereafter referred to as spindle elongation) may occur either as a consequence of cortical pulling forces exerted on astral-MTs (Aist and Berns 1981; Kronebusch and Borisy 1982; Waters *et al.* 1993; Sharp *et al.* 2000a) or ipMTs sliding coupled to the polymerization of overlapping microtubules at their plus-ends (Saxton and McIntosh 1987; Shelden and Wadsworth 1990; Brust-Mascher *et al.* 2004; Fu *et al.* 2009; Khmelinskii *et al.* 2009). Depending on the system some mechanisms may prevail or work in a redundant/synergistic way. In the budding yeast *Saccharomyces cerevisiae*, spindle elongation is guaranteed by sliding forces generated at the spindle midzone by the kinesin-5 motors, Cin8 and Kip1 (Saunders *et al.* 1995; Straight *et al.* 1998; Khmelinskii *et al.* 2009), whereas in fission yeast *Schizosaccharomyces pombe* spindle elongation is mainly driven by kip9p-ase1, a kinesin-6 protein associated with a crosslinking protein (Fu *et al.* 2009). In fact, ase1 plays an essential role targeting the kinesin-6 motor to the spindle central region that will slide apart both half-spindles. In budding and fission yeast, chromosome segregation depends on spindle elongation that, in turn, depends on the existence of a midzone region where ipMTs interdigitate, overlap and can be slid apart. In *Caenorhabditis elegans*, although chromosome segregation is driven by spindle elongation, kinesin-5 is not an essential protein (Saunders *et al.* 2007). In this system, outward pulling

forces acting on astral-MTs are prominent and drive spindle positioning and chromosome segregation (Grill *et al.* 2001; Labbe *et al.* 2004; Civelekoglu-Scholey and Scholey 2007; Kozlowski *et al.* 2007; Saunders *et al.* 2007). Differently from *C. elegans,* anaphase in *Drosophila* does not rely only on spindle elongation, and this movement can be driven and guarantee by different factors. Studies in *Drosophila* embryos reported that spindle elongation efficiency requires dynein-mediated cortical pulling forces (Sharp *et al.* 2000a), outward sliding driven by KLP61F (Brust-Mascher and Scholey 2002; Brust-Mascher *et al.* 2004) and ipMT coupling facilitated by KLP3A (Kwon *et al.* 2004). Although these depletions have significantly reduced spindle elongation, other players may still be important.

In the present study we asked whether proteins and structures that were previously implicated in spindle architecture and dynamics maintenance are also important to regulate spindle elongation. We addressed this question in *Drosophila* S2 cells because spindle elongation is concomitant with the anaphase onset, and the time window where both occur is long enough to allow a systematic and standardized characterization (see Chapter II). Accordingly, we defined and measured different parameters that characterize the spindle elongation movement (elongated spindle length, extent of spindle elongation, average spindle elongation velocity, instant spindle elongation velocity and anaphase duration - see Materials and Methods for details) after perturbing mitotic structures, MT dynamics, crosslinkers and motors.

To understand the contribution of centrosomes and astral-MT forces we knock-down the centriolar protein Sas4. This protein is involved in centriole duplication and when down-regulated, functional centrosomes are no longer assembled (Basto *et al.* 2006). MT dynamics was challenged by the perturbation of proteins required to modulate this property, such as CLASP, involved in MT plus-end polymerization (Maiato *et al.* 2002; Maiato *et al.* 2005), and KLP10A (kinesin-13) involved in MT minus-end depolymerization (Rogers *et al.* 2004). In addition, we examined cells treated with 10nM Taxol that at low levels stabilizes MTs without precluding mitotic progression (Logarinho *et al.* 2004; Maresca and Salmon 2009; Moutinho-Pereira *et al.* 2010). To explore the importance of MT coupling at minus-ends and pole focusing, we respectively perturbed the crosslinling protein Asp (do Carmo Avides and Glover 1999; Brust-Mascher and Scholey 2007) and Ncd (Goshima *et al.* 2005a). This kinesin-14 motor is known to promote not only kMTs focusing but also inward MT sliding (Fink *et al.* 2009). Antagonizing outward forces were addressed by depleting either the kinesin 5, KLP61F, (Kapitein *et al.* 2005), or the kinesin-6 protein Pavarotti (Pav). Finally we accelerate the anaphase onset by down-regulating Mad2 (Orr *et al.* 2007). In the absence of this SAC protein, cyclin B is prematurely

degraded (Buffin *et al.* 2007) and mitosis proceeds without a mature spindle (Lince-Faria *et al.* 2009).

2. MATERIAL AND METHODS

2.1. Cell culture, RNAi treatment and western blot

Drosophila S2 cells were cultured as described in Chapter I. RNAi of *Drosophila* Sas4, KLP10A, Sas4/KLP10A, Asp, Ncd, Pav, Pav/Ncd and Mad2 was performed as described and using the published targeting sequences (Rogers *et al.* 2004; Maiato *et al.* 2005; Morales-Mulia and Scholey 2005; Goshima *et al.* 2007; Orr *et al.* 2007; Rodrigues-Martins *et al.* 2007; Pereira *et al.* 2009; see Table S1). KLP10A, Sas4 and KLP10A/Sas4 depletion was done as described in Chapter II. To prevent monopolarity and to obtain CLASP and KLP61F intermediate phenotypes, cells were treated for 2-days using the published targeting sequences (Maiato *et al.* 2005; Goshima *et al.* 2007; see Table S2). Protein knock-down was monitored by western blot as described in Chapter I and using the following antibodies (see also Table S2): rabbit anti-Mad2 (gift from Cláudio Sunkel, IBMC, University of Porto, Portugal) rabbit anti-KLP10A and anti-Ncd (gift from Jonathan Scholey, University of California at Davis, CA), rabbit anti-Pav (gift from David Glover, University of Cambridge, UK), rabbit anti-Asp (gift from Cayatano Gonzalez, ICREA, Barcelona, Spain), mouse anti-α-tubulin clone DM1A (Abcam). Because Sas-4 is not an abundant protein in *Drosophila*, we were not able to monitor the efficiency of its depletion by western blot (Basto *et al.* 2006; Rodrigues-Martins *et al.* 2007). ECL system (Amersham) was used for the detection of HRP conjugated secondary antibodies.

2.2. Time-lapse microscopy and guided kymography

Time-lapse microscopy was performed as described in Chapter I.

2.3. Quantifications

Spindle length refers to the distance between two poles (centrosomes excluded) and was measured every 30 seconds from 2 minutes before the anaphase onset, until 10 min after that moment. All measurements were done from live imaging data.

Metaphase spindle length refers to the pole-to-pole distance one minute before the anaphase onset.

Elongated spindle length refers to the pole-to-pole distance in the first frame where GFP-α-tubulin signal was excluded from the newborn nuclei.

Normalized elongated spindle length was calculated dividing elongated spindle length by the metaphase spindle length.

Cell length was measured in metaphase, as the distance between cell boundaries in the direction of spindle axis.

Average spindle elongation velocity refers to the half-spindle elongation velocity measured between 2 and 4.5 minutes after the anaphase onset, $(d_{4.5}-d_2)/2/t$ where d is the pole-to-pole distance and t the time period. Whereas in Chapter II average spindle elongation (or half-spindle elongation velocity) was measured directly from the chromo-kymograph fastest slops disregarding the timing of the anaphase onset (see Materials and Methods from Chapter II for details), in this chapter average spindle elongation velocity was measured for a specific 2.5 min time window.

Spindle elongation instant velocity refers to the half-spindle elongation velocity measured for each 30 secs from the anaphase onset on.

Anaphase duration was measured as the time between anaphase onset (see Materials and Methods Chapter I) and the first frame where GFP-α-tubulin signal was excluded from the newborn nuclei.

Extent of spindle elongation was measured as the difference between elongated spindle length and metaphase length.

2.4. Statistical analyses

Statistical analysis was performed using either parametric or non-parametric tests depending on the normality of the distributions tested using Kolmogorov-Smirnov test. A parametric *t test* or non-parametric Mann-Whitney was used for two-group comparison. P value was considered extremely significant if $P<0.001$ (***), very significant if $0.001<P<0.01$ (**), significant if $0.01<P<0.05$ (*) and not significant (ns) if $P>0.05$. Correlation analysis was performed using either Pearson correlation (if the sample follows a normal distribution) or Spearman (makes no assumption about the distribution of values). The correlation coefficient, r or rs (Spearman), ranges from -1 to + 1 and the interpretation works as follows: $r=1$ perfect correlation, $0<r<1$ the two variables tend to increase or decrease together, $r=0$ the two variables do not vary together at all, $-1<r<0$ one variable increases as the other decreases and $r=-1$ perfect negative or inverse correlation.

All the analysis was done using GraphPad Prism, version 5.00 for Macintosh, GraphPad Software, San Diego California USA, www.graphpad.com.

3. RESULTS

3.1. The elongated spindle length depends on the metaphase spindle length and is sensitive to microtubule dynamics, crosslinking activity and centrosome perturbation

In order to dissect the regulation of spindle elongation in *Drosophila* S2 cells we started by asking whether the mechanisms that regulate spindle length and stability during metaphase will influence spindle elongation during anaphase. The strategy used to address this question relied on the measurement of pole-to-pole distance from metaphase until the end of anaphase after the depletion of target proteins or structures involved in spindle assembly and architecture maintenance (Fig. 1, a and b). Because complete knock-down of CLASP and KLP61F results in monopolar spindles (Heck *et al.* 1993; Maiato *et al.* 2002) we analyzed their intermediate phenotype obtained after 48h of partial RNAi treatment. In this situation although phenotypes were readily observed (shorter spindles and bipolar monoastral, respectively – see Fig. 1, a), spindle bipolarity could still be achieved and maintained through periods long enough to surpass the metaphase-anaphase transition. Changes in spindle length throughout mitosis were monitored using live cell imaging, and comparisons between different phenotypes were only possible after the alignment of movies to the same time zero. This was established as the first frame of anaphase, and metaphase length was thus measured as the pole-to-pole distance (excluding centrosomes) 1 minute before anaphase (Fig. 2, a). To allow the comparison between spindles with and without centrosomes, poles were defined as the point where MTs terminate. Accordingly, we observed that the average distribution of the metaphase spindle length in control was 10.3±2.2 μm (mean±sd; see Table 1), and after Sas4 depletion, spindles expanded more 35%, reaching the steady-state length with an average of 13.9±3.6 μm (mean±sd; $p \leq 0.0001$, see Table 1). This indicates that centrosomes and/or astral-MT are important for the regulation of spindle length. A statistically significant expansion was also observed after disruption of pole organization through Asp depletion (20%; $p \leq 0.0001$, see Table 1), and after the perturbation of MT dynamics through KLP10A RNAi and Taxol treatment (65% and 25% respectively; $p \leq 0.0005$, see Table 1). A reduction in the spindle length was only observed after CLASP partial depletion (reduction

of 25%; p≤0.005; Table 1). These results are in agreement with the phenotypes previously described (Rogers *et al.* 2004; Goshima *et al.* 2005b; Maiato *et al.* 2005; Morales-Mulia and Scholey 2005).

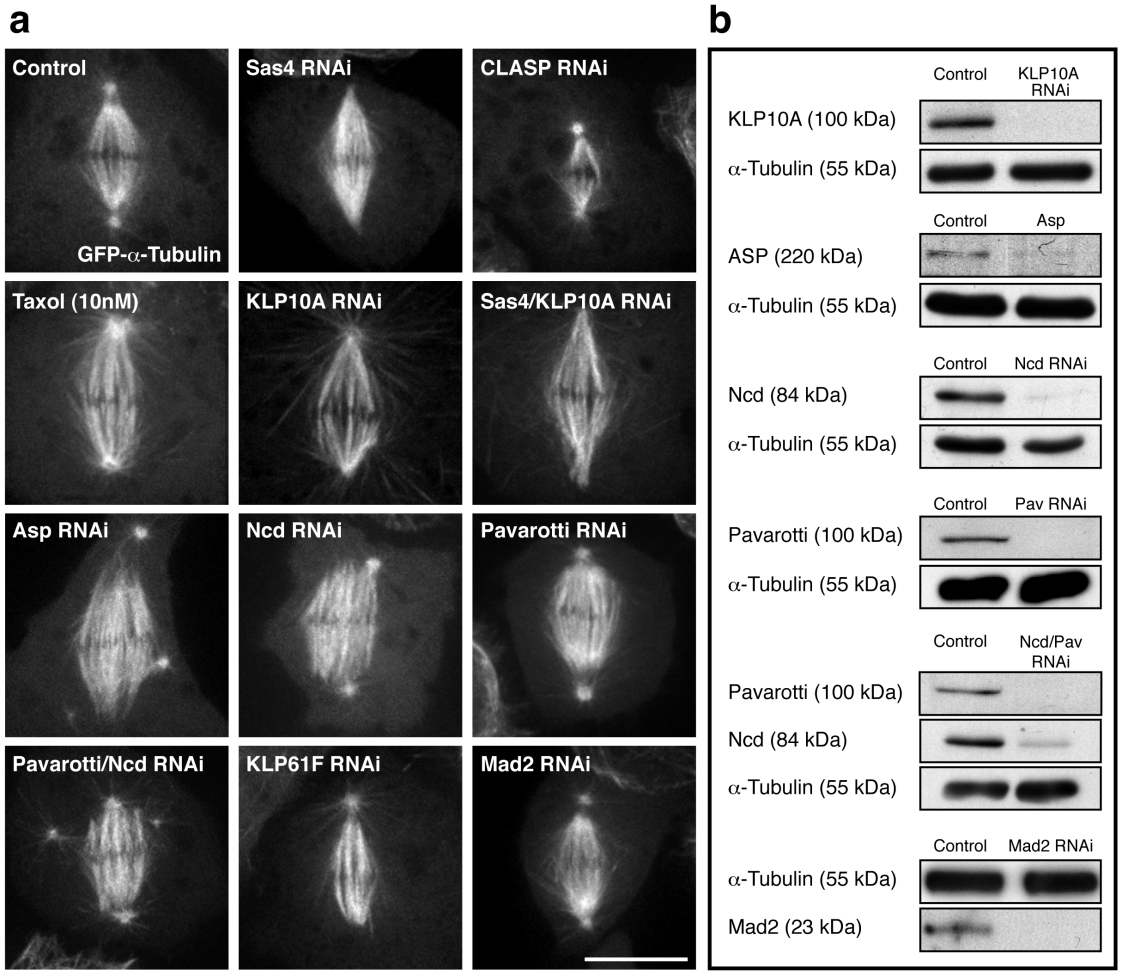


Figure 1 - Metaphase spindles after RNAi and Taxol treatment in *Drosophila* S2 Cells. (a) Phenotypical analysis of cells treated with 10 nM Taxol or with the depicted dsRNA, was preformed from live imaging data using *Drosophila melanogaster* S2 cells stably expressing GFP-α-tubulin. Note the absence of centrosomes after Sas4 and Sas4/KLP10A knockdown, the splayed poles and centrosome displacement after Asp, Ncd and Pav/Ncd knock-down, the bipolar monoastral phenotype after KLP61F partial depletion and the reduced size of CLASP partially depleted spindles. Bar, 10 μm. **(b)** Western blot analysis reveals a depletion of: near 100% of Mad2 and Pavarotti (either single- or co-depleted), 98,2% of KLP10A (co-depleated with Sas4), 97.5% of Asp, 95% of Ncd single-depleted and 90% of Ncd co-depleted. Because Sas-4 is not an abundant protein in *Drosophila*, we were not able to monitor the efficiency of its depletion by western blot.

Table 1 - Metaphase spindle length

Treatment	Normality	No	Mean	SD	SEM	Median	25th Q	75th Q	P
Control	Y	27	10.33	2.17	0.42	10.12	9.16	11.39	
Sas4 RNAi	Y	29	13.92	3.62	0.68	13.37	11.28	16.58	<0.0001
CLASP RNAi	Y	8	7.63	1.59	0.56	7.14	6.38	9.03	0.0026
Taxol10nM	Y	19	12.93	2.49	0.57	11.88	11.12	14.62	0.0005
KLP10A RNAi	Y	22	17.03	3.17	0.68	16.74	14.52	20.02	<0.0001
Sas4/KLP10A RNAi	Y	13	17.42	3.18	0.88	17.02	14.13	20.61	<0.0001
Asp RNAi	N	32	12.86	2.68	0.47	12.17	10.98	15.11	<0.0001
Ncd RNAi	Y	15	11.25	1.97	0.51	10.99	9.66	12.58	ns
Pav RNAi	N	27	10.71	1.65	0.32	10.67	9.75	11.35	ns
Pav/Ncd RNAi	Y	10	11.83	2.17	0.69	11.09	10.09	13.89	ns
KLP61F RNAi	Y	15	10.43	2.55	0.66	9.62	9.21	13.04	ns
Mad2 RNAi	Y	17	10.86	1.80	0.44	10.87	9.22	12.2	ns

Detailed analysis of independent experiments where cells were treated with Taxol, or with the different dsRNA depicted. The results are compared with Control untreated cells. All units are μm/min except No that refers to the number of spindles analyzed. P value is represented for either unpaired t test or Mann-Whitney test depending if the population follows (Y), or not (N), a Gaussian distribution. Normality was tested using the Kolmogorov-Smirnov. Ns refers to not significant.

Although previous work in *C. elegans* embryos showed that spindle elongation depends on the cell size (Hara and Kimura 2009), little is known whether factors external to the spindle will influence anaphase B in *Drosophila* S2 cells. To understand if there is any dependency between the final anaphase spindle length (Fig. 2, b and d; Table 2) and either metaphase (Table 1; Fig. 2, a and c) or cell length (Table S3), we firstly quantified these parameters and then tested the existence of any putative correlation between them (see Materials and Methods for details). Our first results showed that apart from Asp RNAi, all the other perturbations that either led to an expansion (10nM Taxol, Sas4, KLP10A and Sas4/KLP10A RNAi) or reduction (CLASP RNAi) in the metaphase spindle length (Table 1), led also to the corresponding alteration in the elongated spindle length (Fig. 2, c and d; Table 2). This parameter was then plotted against metaphase spindle length (Fig. 2, e) and cell size (Fig. 2, f; see also Table S3), and for both cases all the individual results obtained were pooled together to investigate if the spindles can "adapt" and maintain a characteristic steady-state even if structural perturbations are performed. In fact, a significant correlation was observed between elongated spindle length and metaphase length (Fig. 2, e) and this correlation reflected the behavior of individual treatments (see Fig. S4). However the same did not happen when elongated spindle length was plotted against cell size (Fig. 2, f). The sublinear correlation observed did not correspond to the correlations observed for individual perturbations (Fig. S5). Together these results suggest that the spindle length achieved in the end of anaphase depends on the properties

that define the metaphase spindle length but not on those that determine the characteristic cell size.

Table 2 - Elongated spindle length

Treatment	Normality	No	Mean	SD	SEM	Median	25th Q	75th Q	P
Control	N	27	18.24	3.32	0.64	17.83	16.12	19.14	
Sas4 RNAi	Y	29	20.91	4.14	0.77	20.66	18.38	24	0.0052
CLASP RNAi	N	8	15.93	2.90	1.02	15.34	14.01	16.47	0.0265
Taxol10nM	Y	19	21.03	3.51	0.81	20.15	17.99	25.01	0.0046
KLP10A RNAi	Y	22	22.74	4.01	0.86	23.13	19.05	25.62	0.0002
Sas4/KLP10A RNAi	Y	13	25.51	4.16	1.15	25.92	21.62	29.59	<0.0001
Asp RNAi	Y	32	17.72	3.14	0.55	17.87	15.33	19.12	ns
Ncd RNAi	N	15	17.97	2.12	0.55	17.86	16.53	18.59	ns
Pav RNAi	Y	27	17.66	2.02	0.39	17.53	16.59	19.19	ns
Pav/Ncd RNAi	N	10	19.38	2.65	0.84	18.04	17.44	21.49	ns
KLP61F RNAi	Y	15	21.1	3.34	0.86	20.5	18.04	23.98	0.0101
Mad2 RNAi	Y	17	16.66	2.79	0.68	16.37	15.33	17.9	ns

Detailed analysis of independent experiments where cells were treated with Taxol, or with the different dsRNA depicted. The results are compared with Control untreated cells. All units are μm/min except No that refers to the number of spindles analyzed. P value is represented for either unpaired t test or Mann-Whitney test depending if the population follows (Y), or not (N), a Gaussian distribution. Normality was tested using the Kolmogorov-Smirnov. Ns refers to not significant.

To accurately compare the capacity that the spindles have to elongate during anaphase, elongated spindle length was normalized against metaphase spindle length (Table 3). Apart from Pav/Ncd double depletion, all other treatments affected the capacity that spindles have to elongate. Whereas in control cells spindles nearly duplicate its size during their characteristic anaphase duration, after Mad2, Pav, Sas4, Sas4/KLP10A, Asp and Ncd knock-down, spindles were unable to equalize the control capacity. Conversely, KLP61F and CLASP partial inhibition led to a slight, although statistically significant, increase in this capacity. This indicates that MT polymerization is occurring during spindle elongation in accordance to what was previously predicted (Cheerambathur *et al.* 2007). Curiously, when normalized elongated spindle length was plotted against metaphase spindle length a negative correlation was observed. This suggests that those spindles that are shorter are the ones that have the increased capacity of elongation (Fig. 2, g-h; Fig. S6; Table 4).

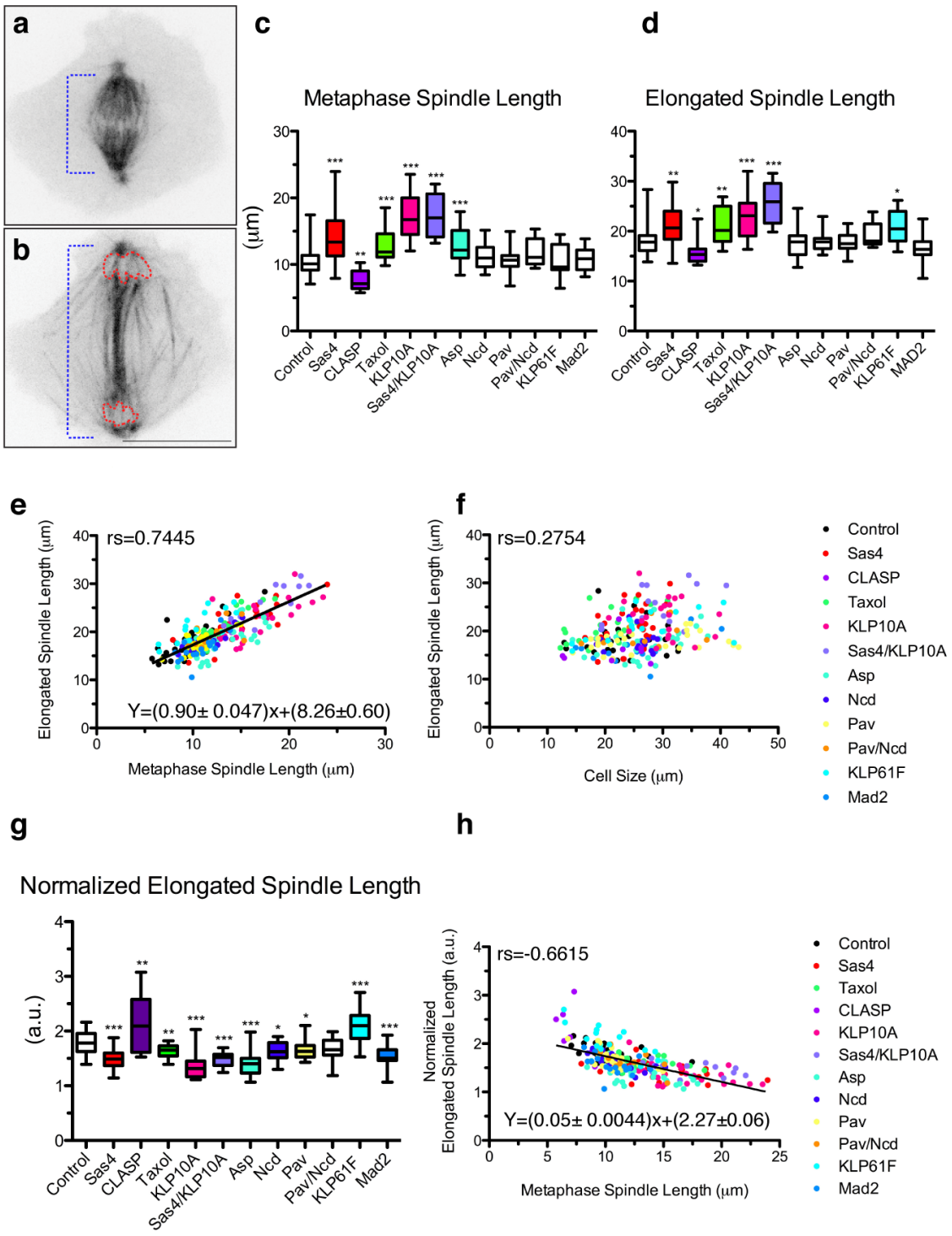


Figure 2 - Elongated spindle length correlates with metaphase spindle length in *Drosophila* S2 Cells. (a) Metaphase and **(b)** telophase figures from a control cell. Elongated spindle length was measured as the pole-to-pole distance in the end of anaphase (dashed blue lines) established from the GFP-α-tubulin signal exclusion in the nuclear region (region delimited by a dashed red line). Bar, 10 μm.

Table 3 - Normalized elongated spindle length

Treatment	Normality	No	Mean	SD	SEM	Median	25th Q	75th Q	P
Control	Y	27	1.78	0.20	0.04	1.78	1.62	1.95	
Sas4 RNAi	Y	29	1.49	0.18	0.03	1.49	1.37	1.60	<0.0001
CLASP RNAi	Y	8	2.16	0.54	0.19	2.10	1.61	2.58	0.0045
Taxol10nM	Y	19	1.64	0.13	0.03	1.66	1.54	1.73	0.0058
KLP10A RNAi	Y	22	1.35	0.21	0.05	1.32	1.17	1.45	<0.0001
Sas4/KLP10A RNAi	Y	13	1.48	0.13	0.04	1.52	1.37	1.58	<0.0001
Asp RNAi	Y	32	1.4	0.21	0.04	1.40	1.23	1.50	<0.0001
Ncd RNAi	Y	15	1.62	0.17	0.04	1.62	1.51	1.79	0.0100
Pav RNAi	Y	27	1.66	0.19	0.04	1.63	1.53	1.73	0.021
Pav/Ncd RNAi	Y	10	1.66	0.22	0.07	1.66	1.56	1.82	ns
KLP61F RNAi	Y	15	2.08	0.31	0.08	2.10	1.87	2.29	0.0005
Mad2 RNAi	Y	17	1.54	0.20	0.05	1.51	1.46	1.66	0.0003

Detailed analysis of independent experiments where cells were treated with Taxol, or with the different dsRNA depicted. The results are compared with Control untreated cells. All units are μm/min except No that refers to the number of spindles analyzed. P value is represented for either unpaired t test or Mann-Whitney test depending if the population follows (Y), or not (N), a Gaussian distribution. Normality was tested using the Kolmogorov-Smirnov. Ns refers to not significant.

(c) Metaphase and **(d)** elongated spindle length distributions where the box plot defines the interquartile range and the line inside the box represents the median value of the distribution. The whiskers determine de maximum and minimum value. Significant differences are depicted as colored plots. Asterisks refer to the statistic difference as described in the materials and methods section (*** $p<0.001$; ** $0.001<p<0.001$; *$0.01<p<0.05$; ns $p>0.05$). Elongated spindle length was plotted against **(e)** metaphase spindle length and **(f)** cell size. In **e** linear regression line includes the control and all treatments depicted (±standart errors of the mean, SEM), $p<0.0001$; **(e and f)** r_s refers to the nonparametric Spearmen correlation coefficient where **(e)** $p<0.0001$ and **(f)** $p=0.0002$. **(g)** Normalized spindle length was determined normalizing elongation spindle length against metaphase spindle length. The box plot is defined as in c and d. **(h)** Normalized elongated spindle length was plotted against metaphase spindle length. Note the negative correlation where shorter spindles elongate more. Linear regression line includes control and all treatments depicted (±standart errors of the mean, SEM), $p<0.0001$; r_s refers to the nonparametric Spearmen correlation coefficient, $p<0.0001$.

3.2. Different patterns of elongation velocities are observed after mitotic spindle perturbations

Next we plotted the normalized pole-to-pole distances as a function of time for all the conditions tested (Fig. 3). From these curves it was possible to characterize the elongation velocity pattern and identified 3 distinct moments: the first is slow, the second is fast and the time of rapid segregation, and finally segregation velocity reaches a plateau, where chromosomes decondense and nuclear envelope reforms.

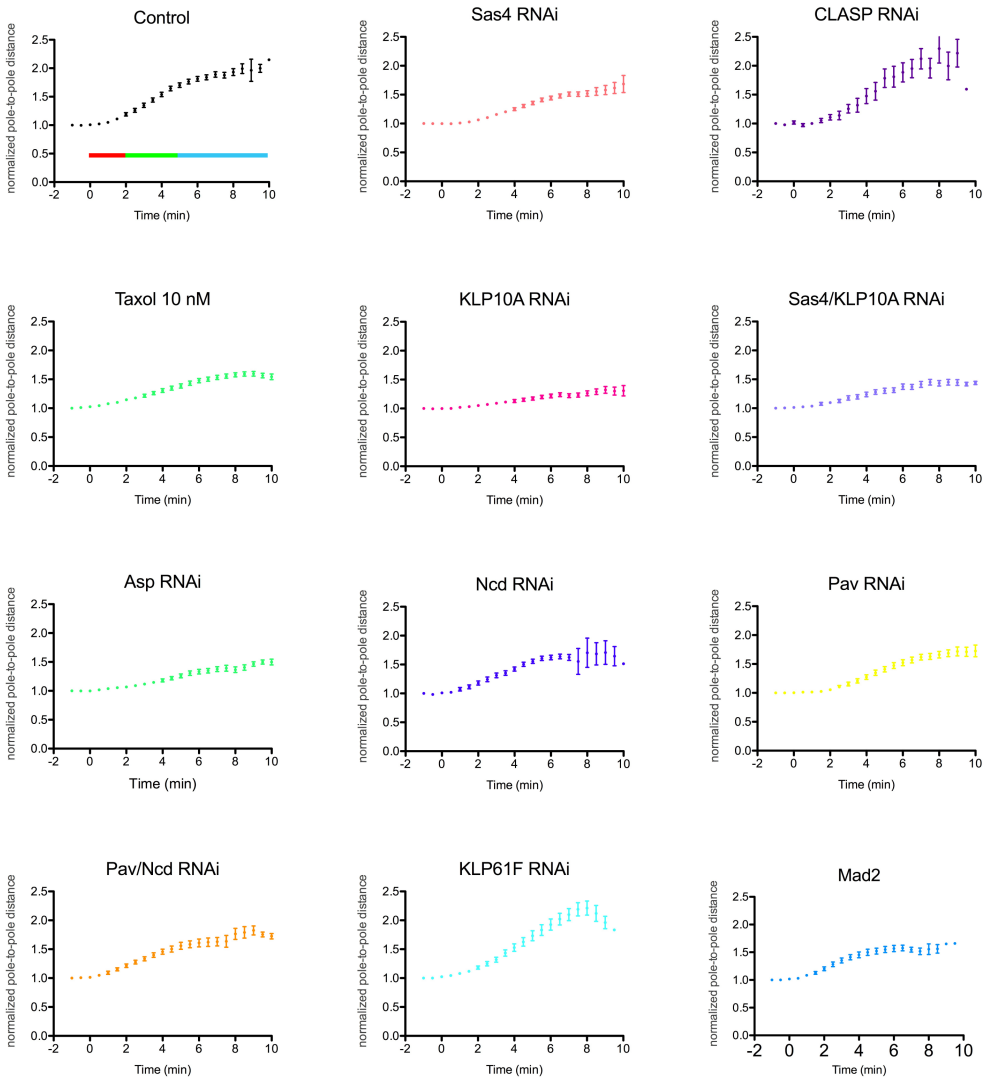
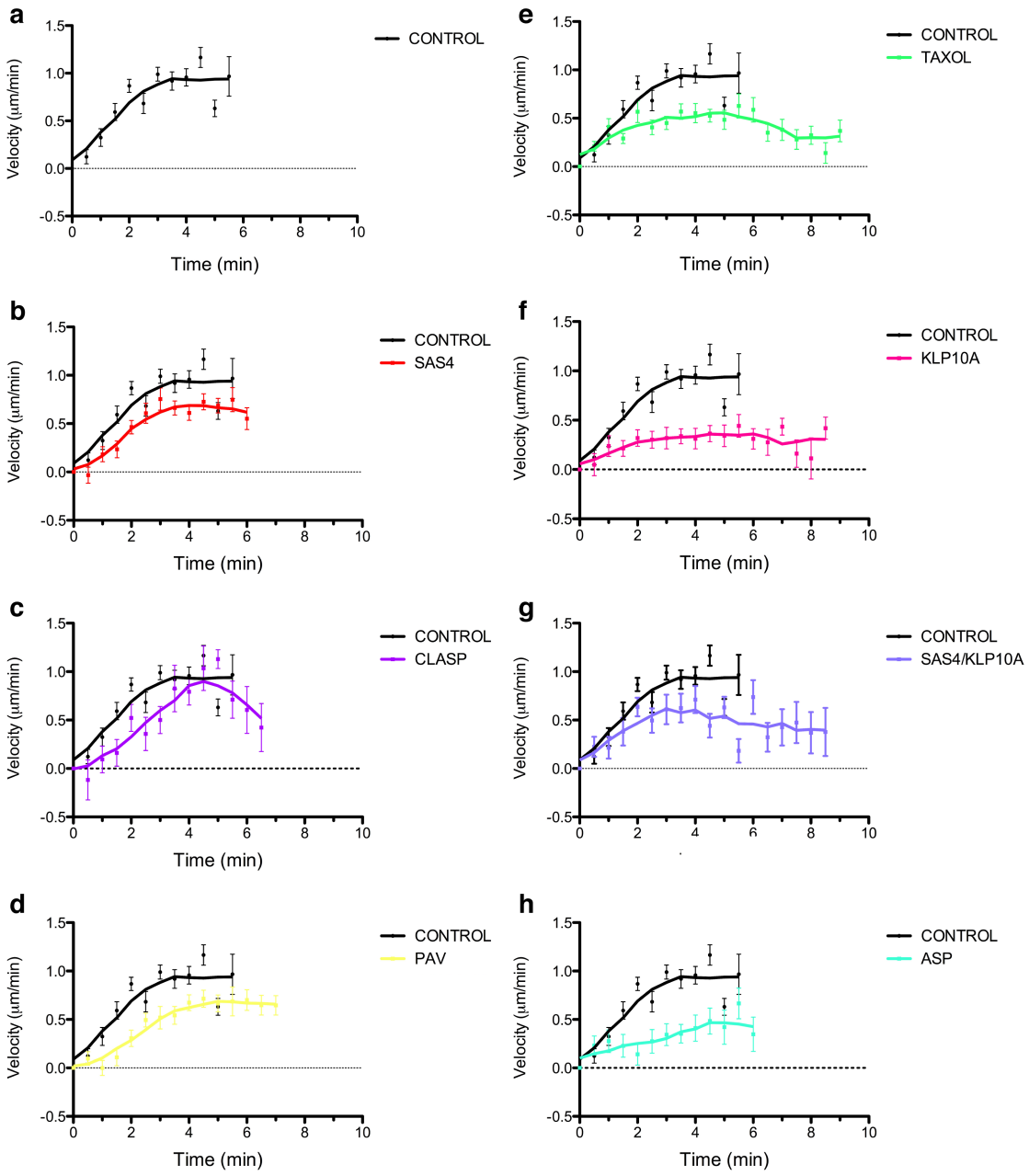


Figure 3 - Characterization of Spindle Elongation in *Drosophila* S2 Cells. Normalized pole-to-pole distance was plotted against time during an 11 minutes period (from 1 minute before the anaphase onset, until 10 minutes after). From the control graph analysis we defined 3 stages: slow (red), fast (green) and plateau (blue).

To have a better understanding on the spindle elongation kinetics we quantified half-spindle elongation instant velocities (herein referred as spindle elongation instant velocity), for each 30sec instant recorded after anaphase onset (Fig. 4, a-l). From the graph analysis we can clearly distinguish 3 patterns of velocity different from the control.



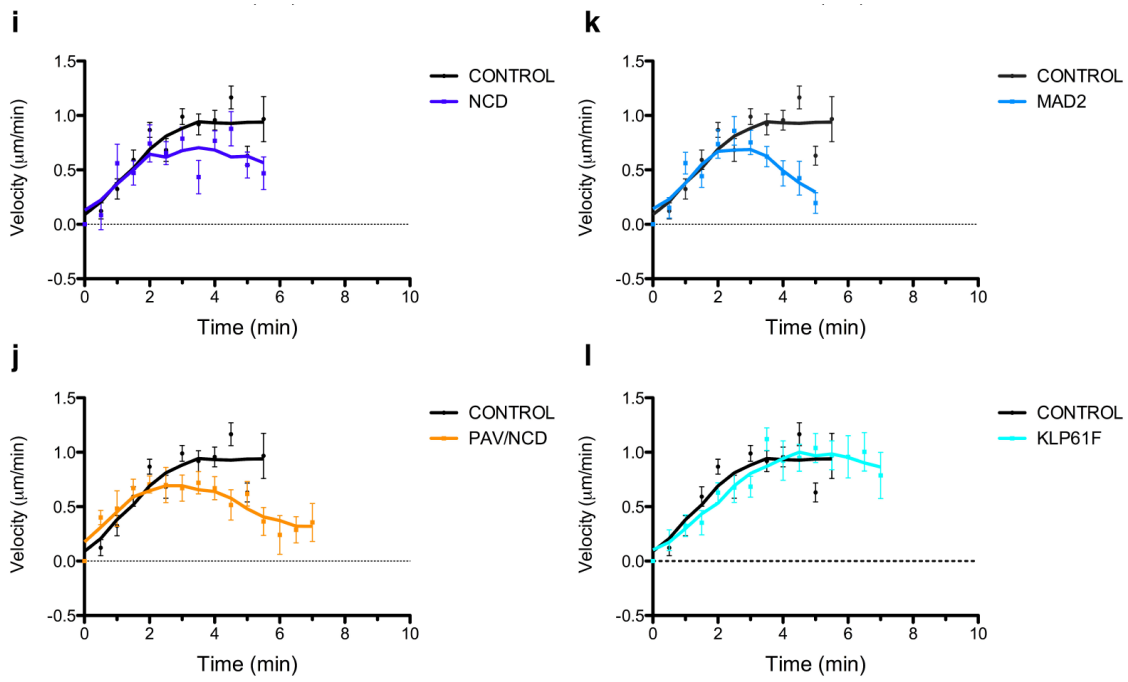


Figure 4 - Spindle elongation instant velocities (a-l) Instant velocities were plot against time. Each dot represents the mean value of instant velocity calculated between two instants starting from anaphase onset. The last point depicted corresponds to the median value of anaphase duration for each treatment. Error bars represent SEM. Dash line is a guide line where Y=0. Black or colored line represents the guide smoothing curves, obtained by averaging 2 neighboring points. The negative velocities observed in Sas4 and CLASP represent the noise resultant from errors inherent to the measurements.

The first pattern observed resulted from Sas4 depletion (Fig. 4, b) and CLASP perturbation (Fig. 4, c), and is characterized by an initial reduced velocity although a similar acceleration may be inferred from the similarity of slopes observed for the first 3-4 minutes of the smoothing curves. As CLASP phenotype is characterized by a short spindle (Fig. 1, see also Fig. 5), astral-MTs may not be long enough to reach the cortex and hence astral forces cannot contribute to the initial spindle elongation kinetics. This pattern of velocity was also observed after the kinesin-6 Pavarotti depletion (Fig. 4, d), and might indicate that this plus-end directed motor facilitates spindle elongation in response to cortical forces.

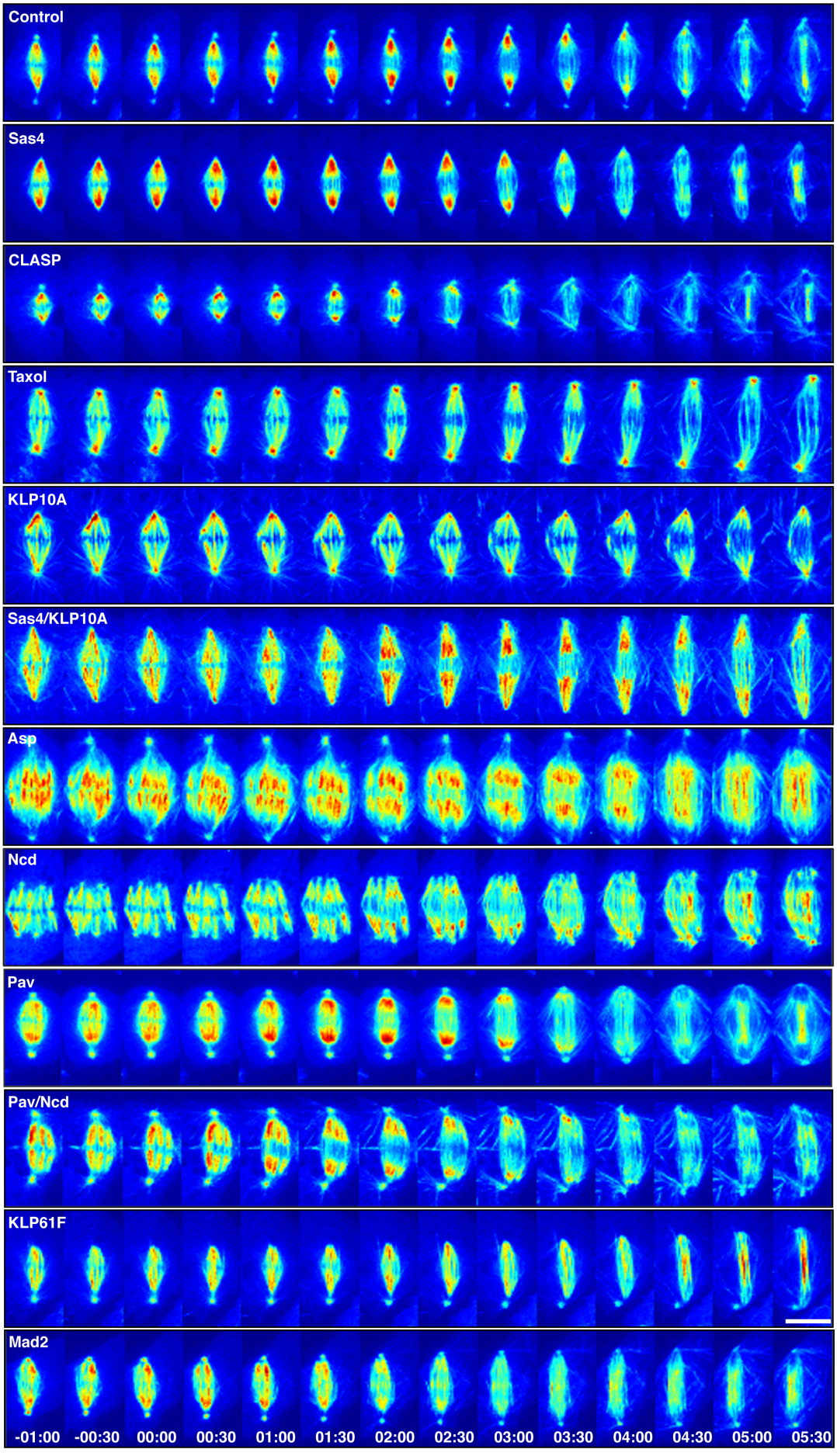
The second pattern identified was observed after MT dynamics perturbation with 10nM Taxol treatment (Fig. 4, e) and KLP10A depletion (Fig. 4, f). Here, both instant velocity and initial acceleration were slower than control since the anaphase onset. These results suggest that although MTs become more stable after the anaphase onset (Higuchi

and Uhlmann 2005), a certain level of dynamics may be important to assure spindle elongation. The reduced instant velocities observed after KLP10A RNAi, could also be a consequence of the large and stable asters. Those may exert pushing/compression forces on the spindle that resist the outward movement of spindle elongation. Indeed, when both Sas4 and KLP10A were co-depleted there was a recovery observed in the velocities (Fig. 4, g), although the movement was still slower than the control and with the same pattern of velocity as KLP10A individual depletion. Moreover, a similar pattern of instant velocities was observed after Asp RNAi (Fig. 4, h).

The last pattern identified was observed after Ncd (Fig. 4, i) and double Pav/Ncd depletion (Fig. 4, j). Here the initial acceleration was similar to control, however, after the first 2 minutes, spindles reached the maximum velocity and hence the plateau. This may indicate that Ncd is not required at the very beginning of anaphase, but is necessary after the 2 initial minutes. Also, it was observed that the double depletion of Pav/Ncd reverted the initial slow movement and acceleration observed after Pavarotti single depletion (Fig. 4, d). This might indicate that in the absence of Ncd, Pavarotti is no longer required to facilitate spindle elongation, having both motors contra-balanced functions. A similar pattern was observed after Mad2 RNAi (Fig. 4, k) although in a reduced time window. This suggests that full maturation of the spindle is needed for the complete action of molecular motors, and thus spindle elongation.

Finally it is important to refer that partial depletion of KLP61F didn't result in any specific pattern different from the control (Fig. 4, l), indicating that although some protein down-regulation is occurring (due to the observable phenotype – bipolar monoastral spindles), the kinesin-5 molecules that are present are sufficient to guarantee an efficient spindle elongation. This is in accordance with previous computational modeling whose simulations predicted that even when severe partial inhibitions of kinesin-5 are performed, anaphase B should not be affected (Wollman *et al.* 2008).

Figure 5 - Spindle Elongation velocity and duration in *Drosophila* S2 cells. Aligned kymographs showing the fast moment of spindle elongation for the different treatments tested. Pseudo color is related to GFP-α-tubulin signal intensity where progression from blue to red represents less to high intensity. Time zero is the point established as anaphase onset. Bar, 10μm.


Control
Sas4
CLASP
Taxol
KLP10A
Sas4/KLP10A
Asp
Ncd
Pav
Pav/Ncd
KLP61F
Mad2
-01:00
-00:30
00:00
00:30
01:00
01:30
02:00
02:30
03:00
03:30
04:00
04:30
05:00
05:30

3.3. Reduction of spindle elongation velocity is balanced by an increase in anaphase duration

As described in the previous chapter spindle elongation velocity is contributing to chromosome segregation as much as the kMT shortening, which guarantees that segregation still happens even if anaphase A is reduced or severely impaired.

Spindle elongation occurs as a consequence of the outward movement of the two half-spindles that can be a result of an active or passive mechanism, depending whether is driven by sliding motors acting on antiparallel MTs, or if it is a result of cortical spindle forces. In order to compare the average half-spindle elongation velocity (hereafter referred to as spindle elongation velocity) between all different conditions (Table 4), we defined a time window where the fastest velocity was observed for controls, and all treatments tested were compared for the same period of time. From the spindle elongation pattern obtained for control cells (Fig. 3) we established this interval from 2 to 4.5 minutes after the anaphase onset. During this interval all treatments, apart from KLP61F partial depletion, showed a statistically significant reduction in the spindle elongation velocity (Table 4, Fig. 6, a and Fig. 7, a-k).

Regarding the contribution of centrosomes and astral MTs to spindle elongation velocity, we noticed a reduction of ~25% after centrosome depletion through Sas4 RNAi. This suggests that although spindle elongation may be driven by an active sliding mechanism (Brust-Mascher *et al.* 2004), astral/cortical forces are still important as suggested by Sharp *et al*, (2000a). Accordingly, CLASP short spindles (Fig. 5) also showed the same reduction. Perturbation of MT dynamics through KLP10A, Sas4/KLP10A RNAi and Taxol treatment led also to significant reductions (38%-60%; all $p \leq 0.0003$), as well as perturbation of the opposing motors Ncd, Pav and Ncd/Pav (22%-33%, all $p \leq 0.005$). Interestingly perturbation of the kinesin-6 Pavarotti led also to a reduction in the spindle elongation velocity (33% $p < 0.0001$) although less severe than that described for fission yeast (Fu *et al.* 2009). Furthermore, Asp depletion led to a 50% reduction in the spindle elongation velocity indicating that the crosslink activity is essential during chromosome segregation in *Drosophila* S2 cells (Table 4, Fig. 6, a and Fig. 7, a-k).

Table 4 - Average spindle elongation velocities

Treatment	Normality	No	Mean	SD	SEM	Median	25th Q	75th Q	P
Control	Y	27	0.91	0.21	0.04	0.85	0.80	1.03	
Sas4 RNAi	Y	29	0.69	0.24	0.04	0.68	0.56	0.83	0.0003
CLASP RNAi	Y	8	0.70	0.37	0.13	0.81	0.42	1.03	0.0445
Taxol10nM	Y	19	0.51	0.17	0.04	0.54	0.39	0.65	<0.0001
KLP10A RNAi	Y	22	0.38	0.22	0.05	0.38	0.17	0.52	<0.0001
Sas4/KLP10A RNAi	Y	13	0.57	0.24	0.07	0.53	0.34	0.78	<0.0001
Asp RNAi	Y	32	0.45	0.22	0.04	0.42	0.26	0.62	<0.0001
Ncd RNAi	Y	15	0.71	0.20	0.05	0.65	0.55	0.84	0.0032
Pav RNAi	Y	27	0.61	0.29	0.06	0.61	0.36	0.81	<0.0001
Pav/Ncd RNAi	Y	10	0.67	0.24	0.07	0.68	0.51	0.82	0.0043
KLP61F RNAi	N	15	0.88	0.29	0.07	0.79	0.63	1.19	Ns
Mad2 RNAi	Y	17	0.65	0.21	0.05	0.66	0.55	0.75	0.0002

Detailed analysis of independent experiments where cells were treated with Taxol, or with the different dsRNA depicted. The results are compared with Control untreated cells. All units are μm/min except No that refers to the number of spindles analyzed. P value is represented for either unpaired t test or Mann-Whitney test depending if the population follows (Y), or not (N), a Gaussian distribution. Normality was tested using the Kolmogorov-Smirnov. Ns refers to not significant.

Table 5 – Anaphase duration

Treatment	Normality	No	Mean	SD	SEM	Median	25th Q	75th Q	P
Control	N	27	5.63	1.41	0.27	5.5	5	6	
Sas4 RNAi	N	29	6.79	2.41	0.45	6	5.5	7.75	0.0144
CLASP RNAi	Y	8	7.5	3.29	1.16	6.25	5.63	8.38	0.036
Taxol10nM	N	19	10.53	3.44	0.79	9	8	12.5	<0.0001
KLP10A RNAi	Y	22	9.27	2.72	0.58	9	7.25	10.5	<0.0001
Sas4/KLP10A RNAi	Y	12	9.21	3.18	0.92	8.5	6.5	11.25	<0.0001
Asp RNAi	Y	32	6.64	2.47	0.44	6	4.63	7.88	Ns
Ncd RNAi	N	15	5.97	1.49	0.39	5.5	5	6.5	Ns
Pav RNAi	Y	27	7.33	2.43	0.47	7	5	8.5	0.0055
Pav/Ncd RNAi	Y	10	6.95	1.46	0.47	6.75	5.88	7.75	0.0045
KLP61F RNAi	Y	15	7.17	1.05	0.27	7.5	6.5	8	0.0001
Mad2 RNAi	Y	17	5.24	1.03	0.25	5	4.75	5.75	Ns

Detailed analysis of independent experiments where cells were treated with Taxol, or with the different dsRNA depicted. The results are compared with Control untreated cells. All units are μm/min except No that refers to the number of spindles analyzed. P value is represented for either unpaired t test or Mann-Whitney test depending if the population follows (Y), or not (N), a Gaussian distribution. Normality was tested using the Kolmogorov-Smirnov. Ns refers to not significant.

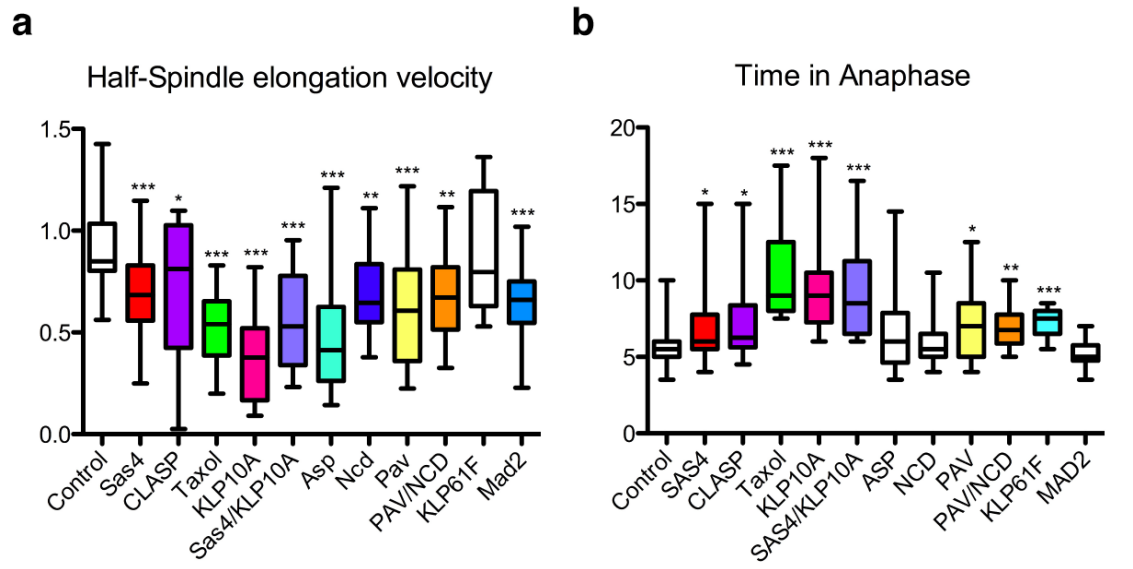
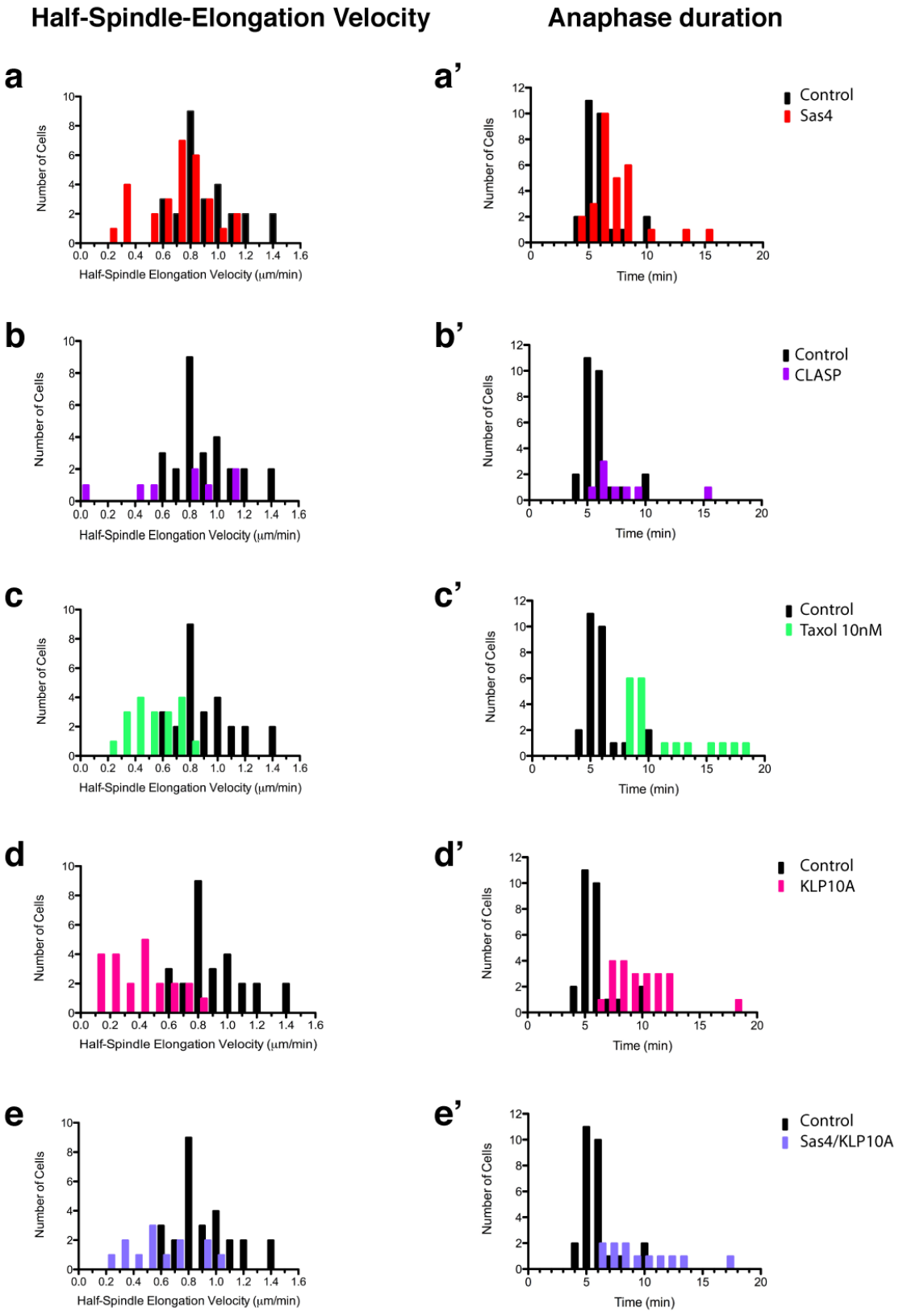
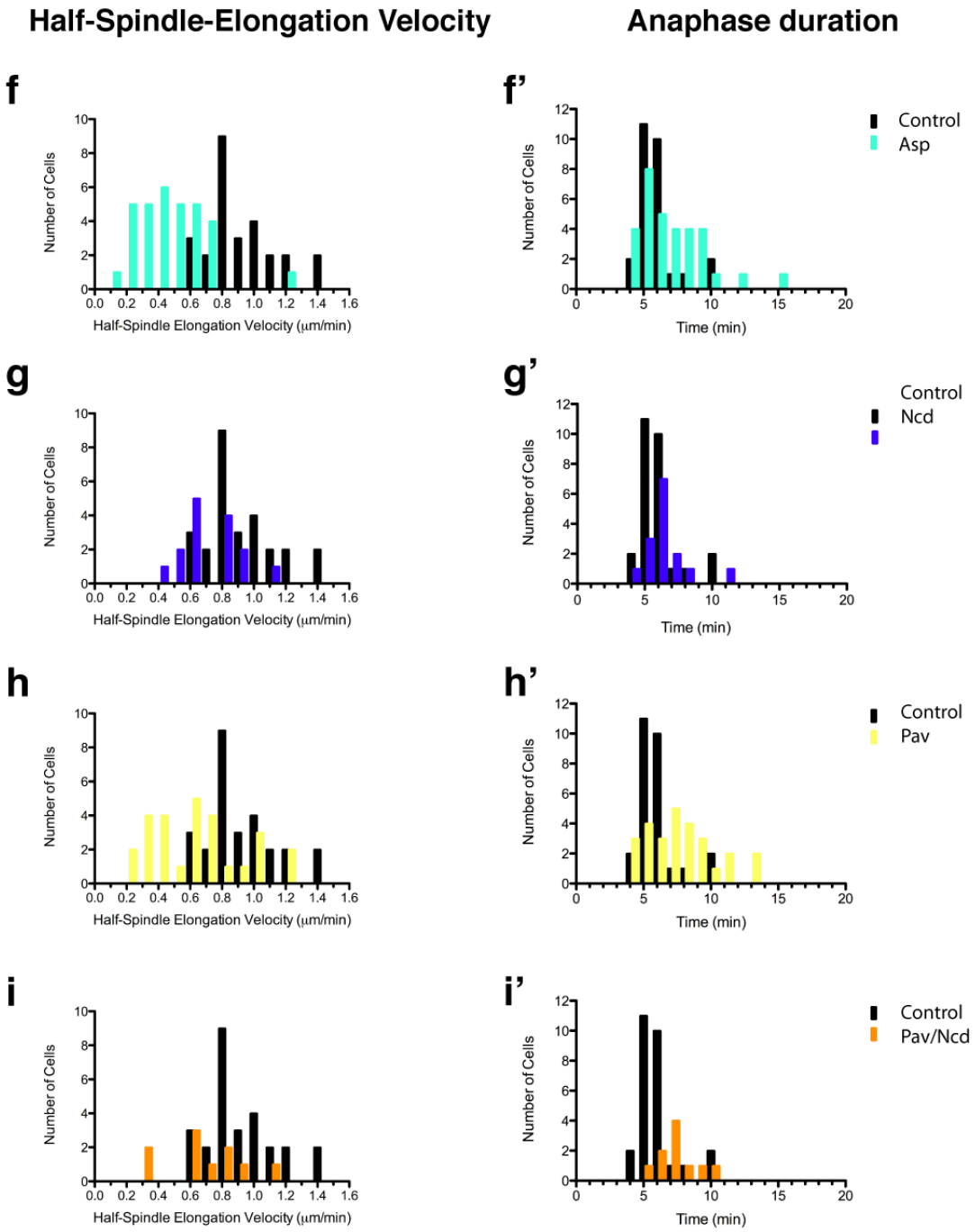


Figure 6 – Corresponding variations of half-spindle elongation velocities and anaphase duration. **(a)** Distribution of spindle elongation velocity and **(b)** anaphase duration measured as the time lagging from the anaphase onset until nuclear envelope reformation inferred by the GFP-α-tubulin signal exclusion in the newly formed nuclei. The box plots define the inter-quartile range and the line inside the box represents the median value of the distribution. The whiskers determine de maximum and minimum value of the distribution. Significant differences are depicted as colored plots. Asterisks refer to the statistic difference as described in the materials and methods section (*** $p<0.001$; ** $0.001<p<0.01$; *$0.01<p<0.05$; ns $p>0.05$).

Curiously, the reduction observed in spindle elongation velocity (Table 4, Fig. 6, a) was accompanied by an increase in anaphase duration (Table 5, Fig. 6, b). This observation, although not verified for Mad2, Asp and Ncd, raises the possibility for the existence of a quality control mechanism that compensates a slower velocity with more time until the nuclear membrane reforms. From the histogram distributions (Fig. 7 a-e, h, i; Fig. 7 a'-e', h', i') it is possible to observe that in comparison to controls, whenever spindle elongation curves as shifted to the left, anaphase duration curves are shifted to the right. This suggests that cells "need" to elongate to a specific distance. Accordingly, by measuring the extent of elongation (elongation spindle length – metaphase length) we observed a tendency that spindles have to separate both half-spindles to a minimum of ~7 µm (Table 6). Curiously, we still observed that the reduced extent for KLP10A depletion was recovered after concomitant depletion of Sas4 (Fig. 8). This is another evidence that the strong astral MTs after this kinesin-13 depletion work as barriers that compress the spindle, impairing the movement of spindle elongation.


Half-Spindle-Elongation Velocity
Anaphase duration
a
a'
Control
Sas4
b
b'
Control
CLASP
c
c'
Control
Taxol 10nM
d
d'
Control
KLP10A
e
e'
Control
Sas4/KLP10A
Number of Cells
Half-Spindle Elongation Velocity (μm/min)
Time (min)


Half-Spindle-Elongation Velocity
Anaphase duration
f
f'
g
g'
h
h'
i
i'
Number of Cells
Half-Spindle Elongation Velocity (μm/min)
Time (min)
Control
Asp
Ncd
Pav
Pav/Ncd

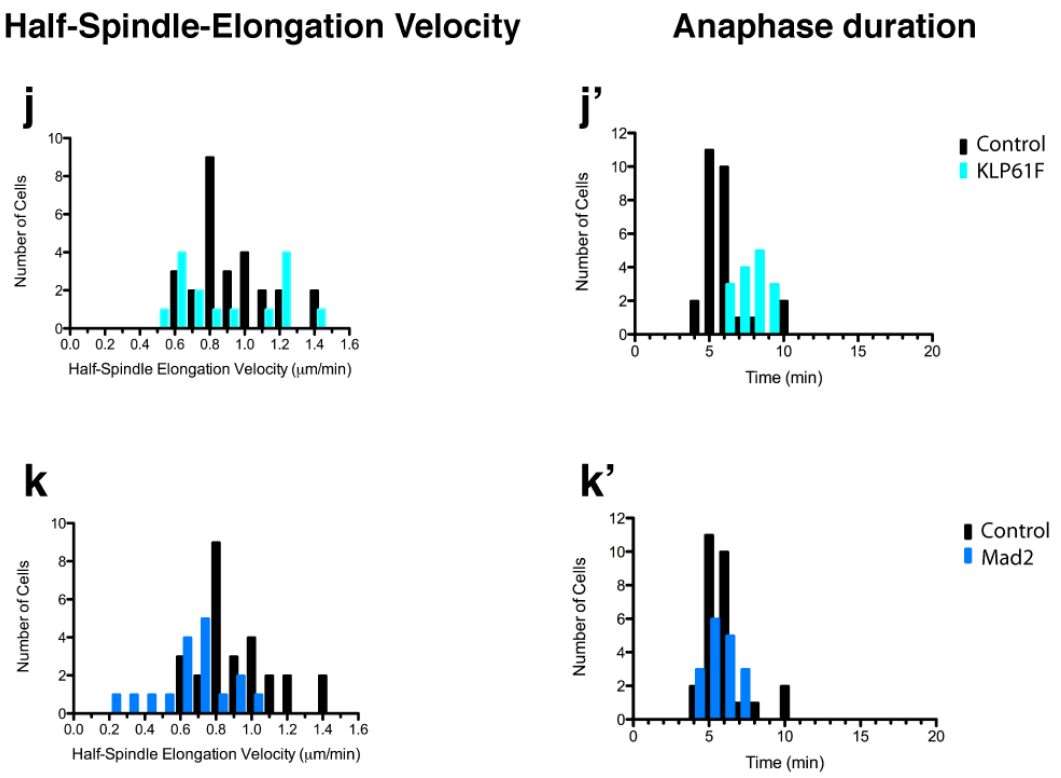


Figure 7 - Spindle Elongation velocity and duration in *Drosophila* S2 cells. (a-k) Distribution of spindle elongation velocity. To prevent data overlap, the represented colored data set was moved 0.04 μm/min within de X axis. (a'-k'). To prevent data overlap, the represented colored data set was moved 0.4 min within de X axis.

Table 6 - Extent

Treatment	Normality	No	Mean	SD	SEM	Median	25th Q	75th Q	P
Control	Y	27	7.92	1.85	0.36	7.93	6.36	9.30	
Sas4 RNAi	Y	29	6.99	2.29	0.43	6.85	5.75	8.09	ns
CLASP RNAi	Y	8	8.30	3.26	1.15	7.64	5.85	9.80	ns
Taxol10nM	Y	19	8.10	1.55	0.36	8.03	7.15	9.18	ns
KLP10A RNAi	Y	22	5.73	3.05	0.65	4.91	3.42	7.33	0.0033
Sas4/KLP10A RNAi	Y	13	8.09	2.02	0.56	8.18	6.68	9.64	ns
Asp RNAi	Y	32	4.87	2.17	0.38	5.04	3.20	5.71	<0.0001
Ncd RNAi	Y	15	6.72	1.10	0.28	6.88	5.87	7.62	0.0278
Pav RNAi	Y	27	6.95	1.33	0.26	6.90	5.89	7.47	0.0310
Pav/Ncd RNAi	Y	10	7.56	2.20	0.69	7.77	6.44	9.06	ns
KLP61F RNAi	Y	15	10.67	1.99	0.51	10.95	9.21	11.91	<0.0001
Mad2 RNAi	Y	17	5.80	1.94	0.47	5.56	5.10	6.55	<0.0001

Detailed analysis of independent experiments where cells were treated with Taxol, or with the different dsRNA depicted. The results are compared with Control untreated cells. All units are μm/min except No that refers to the number of spindles analyzed. P value is represented for either unpaired t test or Mann-Whitney test depending if the population follows (Y), or not (N), a Gaussian distribution. Normality was tested using the Kolmogorov-Smirnov. Ns refers to not significant.

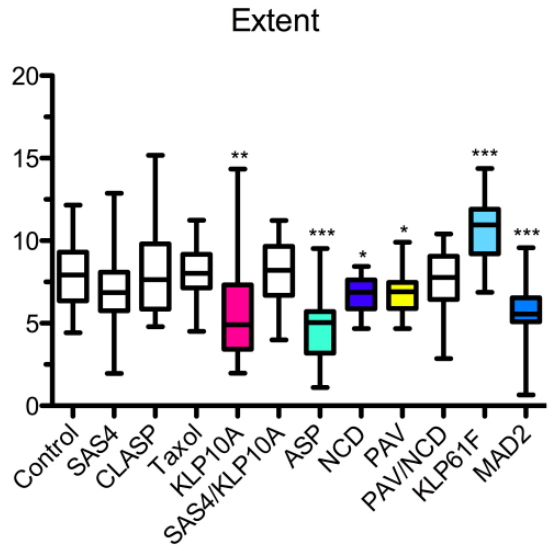


Figure 8 - Extent of Spindle Elongation Extent of spindle elongation is the difference between elongated spindle length and metaphase length. The box plot defines the inter-quartile range and the line inside the box represents the median value of the distribution. The whiskers determine de maximum and minimum value of the distribution. Significant differences are depicted as colored plots. Asterisks refer to the statistic difference as described in the materials and methods section (*** $p<0.001$; ** $0.001<p<0.01$; * $0.01<p<0.05$; ns $p>0.05$).

4. DISCUSSION

With this study we aimed to clarify the importance of different spindle properties to the regulation and kinetics of spindle elongation. Presence of centrosomes, pole focusing, crosslinking activity, MT dynamics and spindle maturation, were the properties investigated. Our strategy focused on the perturbation of already known key players of spindle regulation and maintenance, and consequent analysis of the kinetics of the elongation movement.

4.1. Regulation of metaphase spindle length

Accordingly to what was previously described we observed that metaphase spindle length is sensitive to perturbations on MT dynamics (Rogers *et al.* 2004; Goshima *et al.* 2005b; Maiato *et al.* 2005) and spindle pole integrity (Morales-Mulia and Scholey 2005). Our first interesting observation occurred after centrosome depletion with the lengthening of the spindle. This may be a consequence of an imbalance between outward *vs* inward forces that could occur, for instance, due to loss of cortical pushing forces (Grill and Hyman 2005). Reducing inward compressing forces, that may occur as a result of tubulin incorporation at the plus ends of astral MTs, may lead to a relaxation of the spindle in the opposite direction due to the prevalence of outward forces, and hence an increase in spindle length. In fission yeast this mechanism is responsible for spindle positioning, however there is little evidence that it exists outside this system (Tran *et al.* 2001; Tolic-Norrelykke *et al.* 2004; Grill and Hyman 2005; Tolic-Norrelykke 2008). Another explanation could be that in the absence of astral MTs, spindles do not have a mechanical barrier and expand until they reach an optimum steady-state length. What regulates this optimum length remains unknown. As expected, when KLP10A was co-depleted with Sas4, spindles expanded more than in Sas4 or KlP10A individual depletions. In the absence of centrosomes, the long asters that impair the continuous growth of kinesin-13 depleted spindles are no longer present. Taxol treatment led also to an increase in spindle length. At 10 nM concentration, MTs' plus-ends are biased to subunit incorporation and dynamics is perturbed (Jordan and Wilson 1998). Finally, depletion of Asp led also to an increase in spindle length and this is in accordance with what was previously reported by Morales-Mulia and Scholey, 2005. Spindle lengthening may be a consequence of spindle relaxation due to the loss of crosslink activity at the poles that in turn, lead to a displacement of centrosome and to the loosening of cortical forces. Spindle relaxation can also result from

the displacement of the minus-end direct motors dynein and/or Ncd. Both motors besides contributing to pole focusing (Goshima *et al.* 2005a), are inward force promoters whose action is crucial to balance outward forces (Braun *et al.* 2009; Ferenz *et al.* 2009; Fink *et al.* 2009). In future experiments presence of both motors should be addressed after depletion of Asp. According to what was described by Goshima *et al*., 2005b, depletion of Ncd didn't lead to a significant lengthening of the spindle and the slight increase observed can be explained by a relaxation of the spindle due to reduction of inward sliding forces (Fink *et al.* 2009).

4.2. Spindle elongation capacity: a factor of 2

To better understand how spindle elongation is regulated in *Drosophila* S2 cells and if there is any dependency between cell length and the elongated spindle length, we measured and correlated both variables. Although a sub-linear correlation was observed when all results were pooled together, this correlation was not maintained for control and for other individual correlations. This observation is consistent with the idea that whatever regulates the final length of the spindle does not depend on what defines the cell size. Indeed, when we correlate elongated spindle length with the metaphase spindle length we observe a dependency (both lengths increase together). The linear regression observed reflects the existent correlation between individual results, meaning that longer metaphase spindles will be longer in the end of anaphase. Here some caution should be used as this does not mean that "bigger" spindles elongate more. In fact, after normalization to metaphase length it is possible to observe that are the shorter spindles those that elongate more. Another interesting observation was that in the end of spindle elongation, spindles seem to have a tendency to double its metaphase size within their characteristic anaphase duration. In order to guarantee this relation ipMTs either have the length of the spindle during metaphase or they continuously polymerize during anaphase (Shelden and Wadsworth 1990; Cheerambathur *et al.* 2007). CLASP and KLP61F mild phenotypes had spindles that elongated more than twice their metaphase size. This is an indication that incorporation of MT subunits at plus ends is still occurring. Different questions may arise from this seemingly simple observation: what is the maximum length that a spindle can reach and what are the mechanisms that impair an indefinite elongation? During evolution it seems that elongation of the spindle is loosing significance in anaphase events. Fission yeast spindles are capable of elongating six/seven times their initial length (Fu *et al.* 2009), whereas budding yeast elongates four/five times (Straight *et al.* 1997; Khmelinskii *et al.* 2009). In contrast mammalian cells just elongate the spindle

after chromosomes have started moving to the poles and only 1.4 times their metaphase length (Brennan *et al.* 2007). The same reduced capacity is verified for higher plants (Hayashi *et al.* 2007). Taken this all one can ask: is spindle elongation a *vestigial mechanism* that ultimately guarantees that chromosomes pass the spindle central region?

4.3. Spindle elongation: a synergistic mechanism

Then we wanted to unveil how these identified factors contribute to spindle elongation and interestingly we observed that this is a synergistic movement and a consequence of different mechanisms working together during a certain period of time. Plotting spindle elongation instant velocities as a function of time, led us to understand that different proteins are needed at different moments during spindle elongation. Astral MTs seem to have an important role as soon as anaphase starts, as a delayed acceleration was observed after Sas4 RNAi. Also, we observed that in cells without centrosomes spindle elongation velocity was reduced in 25%. This observation is still corroborated by CLASP mild phenotype where short spindles experienced the same acceleration delay at beginning of anaphase and a reduction of 25% in the spindle elongation velocity. Astral MTs on those short spindles just reach the cortex during late anaphase. These results may be a consequence of loss of cortical pulling forces driven by motors such as dynein (Carminati and Stearns 1997; Sharp *et al.* 2000a). This hypothesis could be tested by cutting the central region of the spindle using laser microsurgery (Pereira *et al.* 2009) during anaphase in different depleted backgrounds, as previously done in other systems (Aist and Berns 1981; Kronebusch and Borisy 1982; Grill *et al.* 2001; Khodjakov *et al.* 2004). Secondly, we addressed the contribution of MT crosslinking properties and we observed a reduction of 50% in the spindle elongation velocity, when Asp was knocked down. This reflects the slow instant velocities measured since the anaphase onset and may be a consequence of loss of spindle coupling due to the lack of MT crosslinking activity. Similarly to what happens with NuMA in vertebrate systems (Compton *et al.* 1992; Gaglio *et al.* 1995; Merdes *et al.* 1996), Asp is important to guarantee spindle pole integrity and organization (do Carmo Avides and Glover 1999; Wakefield *et al.* 2001; Morales-Mulia and Scholey 2005). Consequently, a coupled spindle pole region may be important to facilitate the work of different motors that promote movement through MT outward sliding. Although less severe than Asp, Ncd depletion lead to a 22% reduction in spindle elongation velocity. This minus end directed kinesin-14 was shown to be important to slide and cluster free MTs at the poles and to crosslink MTs within the spindle (Oladipo *et al.* 2007; Braun *et al.* 2009; Fink *et al.* 2009). These results support a model where

bundling and crosslink activity are essential for spindle architecture stabilization and to maintain the MT platform where molecular motors can act. Accordingly, it was recently demonstrated that in budding yeast, the MT crosslinking protein, Ase1, is necessary to recruit the kinesin-5 motor to the spindle midzone. After anaphase onset, Ase1 is dephosphorylated and cin8 is recruited to slide ipMTs apart (Khmelinskii *et al.* 2009). Furthermore, Fu *et al* (2009) demonstrated that in fission yeast Ase1 is necessary to form a complex with a kinesin-6 plus-end directed motor to promote spindle elongation. Based on these observations we tested the kinesin-6 Pavarotti and we observed a reduction of ~33%, meaning that this protein is actively contributing to spindle elongation. Furthermore, from the instant velocities pattern we observe that this motor is contributing to spindle elongation since anaphase onset. Finally, we tested the contribution of time, through depletion of Mad2. As previously reported, impairment of this checkpoint protein leads to a reduction of 30% in spindle elongation velocity, and this seems to be related to a lack of proper spindle MT maturation (Lince-Faria *et al.* 2009). Also, the perturbation of MT dynamics after Taxol and Sas4/KLP10A treatment led to a reduction in spindle elongation velocity since the beginning of anaphase. Here it is important to note that although MTs become more stable after anaphase onset (Higuchi and Uhlmann 2005), this stability may represent less stable MTs than those resultant from Sas4/KLP10A or 10 nM Taxol treatment. This may indicate that efficiency of spindle elongation promoters depends on the dynamic state of MTs.

4.4. Anaphase duration: is there a surveillance mechanism?

The most remarkable observation comes from 10 nM Taxol treatment where a slower spindle elongation velocity was somehow balanced with prolonged anaphase duration. This observation, although not evident for all perturbations tested, let us to raise the question: Is there any mechanism that monitors chromosome positioning during anaphase? We can speculate the existence of two types of quality control mechanisms, one based on time (clock), and another based on spatial positioning (ruler).

As previously described, Cyclin B degradation starts early in metaphase (Sullivan and Morgan 2007) being almost complete in the metaphase/anaphase transition. By that time CDK1 targets must be readily phosphorylated, being the regulation mechanism for anaphase and later mitotic events dependent on their dephosphorylation and destruction (Morgan 2007; Sullivan and Morgan 2007). If this regulation has a characteristic duration, it is reasonable to think that the time for nuclear envelope reformation is "pre-determined" and may start as soon as Cyclin B degradation starts. Accordingly, Wheatley

et al (1997) showed that the injection of non-degradable cyclin B inhibited nuclear envelope reformation. Also, we didn't observe any difference in the anaphase duration in Mad2 depleted cells. Recently, Buffin *et al* (2007) showed that in cells devoid of Mad2, cyclin B degradation was anticipated, however the kinetics and duration of degradation was not different from control situation. This observation leads to another question: if the clock exists can it be delayed in order to guarantee that all chromosomes passed the middle region of the spindle when the elongation velocity is slowed down? From our results the major anaphase delay was observed after Taxol treatment, and in fact, it was previously shown that nanomolar doses of this drug were enough to affected nuclear reformation (Theodoropoulos *et al.* 1999). Accordingly, it is known that during nuclear pore disassembly there are proteins that are targeted to the spindle that in turn will be needed to the nuclear reformation (Hetzer *et al.* 2005). The targeting of these proteins may be compromised in the absence of MT dynamics indicating that the molecular mechanisms that control MT dynamics are likely capable of delaying nuclear envelope reformation. Another hypothesis is that the cell has a mechanical sensing system that triggers nuclear envelope reformation only after sister chromatids reached a certain position within the spindle. However, this does not seem to be the case as recent findings described the existence of a NoCut checkpoint mediated by Aurora B, where the presence of chromatin bridges in the middle of the spindle impairs the formation of the ingression furrow but does not prevent nuclei reformation. Indeed, these bridges are surrounded by nuclear membrane as soon as nuclear membrane is reformed around the decondensed chromatin (Steigemann *et al.* 2009).

Therefore, it is still intriguing that the extent of spindle elongation measured for the great part of treated and untreated spindles tends to the same value. Further experiments will be necessary to dissect this putative *surveillance* mechanism that can also be a concerted action of both hypotheses.

In conclusion, we demonstrated that in *Drosophila melanogaster* S2 cells each spindle has the capacity to elongate twice its size. Those relations seem to be robust to most of the perturbations exerted on spindle architecture and dynamics. Moreover, we propose that proper spindle elongation depends on a concerted and synergistic action of centrosomes, MT dynamics, crosslinkers and sliding motors. We also demonstrated that centrosomes have a reduced contribution to the force needed to slide half-spindles apart. Finally, we propose the existence of a surveillance mechanism that guarantees the reformation of nuclear envelope when all chromosomes are correctly positioned in the daughter cells.

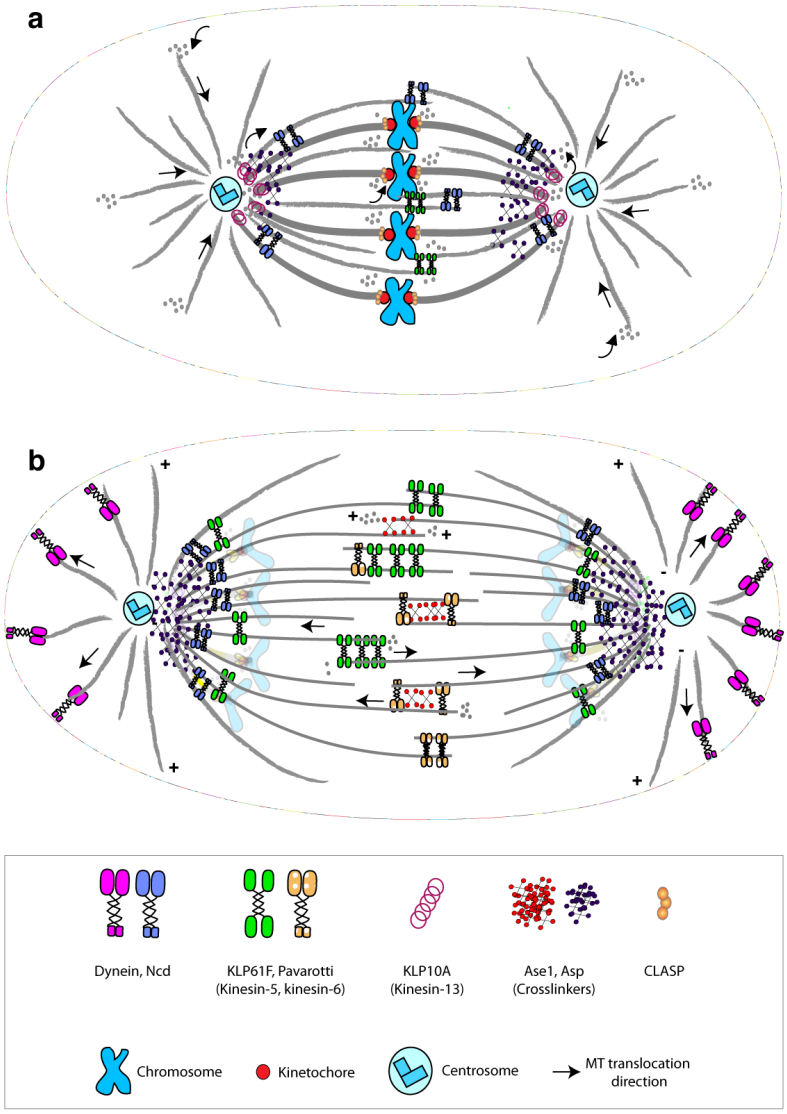


Figure 9 – Integrative model for anaphase B in *Drosophila* S2 cells. (a) During metaphase inward forces driven by Ncd and outward forces driven by KLP61F are counter-balanced. KLP10A destabilizes MTs at the poles in response to outward forces. The steady-length is maintained due to the consequence MT polymerization at the plus-ends facilitated by CLASP. Asp and Ncd guarantee the pole focusing. Pushing forces exerted at the plus-ends of astral-MT are important to position the spindle. **(B)** Spindle elongation starts upon anaphase onset. KLP10A function is down-regulated at the poles and ipMT outward sliding driven by KLP61F and Pavarotti will push half-spindles apart. The role of Ase1 crosslinker (feo in *Drosophila*) may be necessary to target Pavarotti to the spindle midzone. Ncd and Asp maintain the spindle focused and coupled until the end of anaphase. Pulling forces are exerted on astral-MT by motors such as Dynein contribute to spindle elongation.

III. CONCLUSIONS

CONCLUSIONS

The work presented in this thesis provides further insight into the mechanisms of chromosome segregation as well as on the mechanisms that assure its stability and quality control.

Firstly we characterized the mechanism of MT poleward flux in *Drosophila melanogaster* S2 cells and we found that this mechanism is down-regulated upon anaphase transition, being its velocity reduced by ~70%. The higher velocity during metaphase suggests that it has a more important contribution during this period. In fact we observed that when flux was perturbed, the forces that guarantee the inter-kinetochore tension were unevenly distributed. Although a delay from metaphase to anaphase was not observed, the pattern of chromosome segregation was severely affected. Consequently, we proposed a model where the poleward translocation events associated with flux reflect relaxation of the kinetochore–microtubule interface which accounts for the equalization of tensions during the typical metaphase duration. When flux is perturbed the most dramatic outcome is an asynchronous anaphase. Further work should be performed in order to understand how the forces are transmitted between different spindle microtubules and how the mechanics can be translated into biochemical signals that ultimately assure that all chromosomes start to segregate at the same time with the same velocity.

Secondly we investigated the contributions of different mechanisms proposed to drive chromosome segregation, integrating them in one single system. Accordingly we found that in *Drosophila* cells, anaphase A and anaphase B onsets are concomitant and both equally account for the mechanism of chromosome segregation. Moreover, we found that anaphase A can be driven by the Pac-Man mechanism with an equal contribution from MT minus-end depolymerization. Furthermore, we observed that when anaphase B was down-regulated by the acceleration of mitotic progression, anaphase A was faster, suggesting a compensatory mechanism.

Finally we analyzed and characterized the mechanism of anaphase B and noticed that spindle elongation in S2 cells occurs as a synergistic movement mostly driven by the sliding of interpolar MTs and astral-mediated cortical forces. Importantly, not only microtubule motors and crosslinkers were shown to be important, but also microtubule dynamics. We also noticed that the mechanism that guarantees that chromosomes are wrapped inside the new nuclei within a certain time after the anaphase onset can be delayed when the velocity of spindle elongation is reduced. Whether this is due to a

surveillance mechanism or a consequence of loss of MT dynamics remains to be further investigated.

Taken together these results and observations constitute a valuable tool for the understanding of the mechanisms that drive and guarantee accurate chromosome segregation.

IV. SUPPLEMENTARY MATERIAL

1. ABBREVIATIONS

APC/C: Anaphase promoting complex/cyclosome

ATP: Adenosin triphosphate

CDK: Cyclin-dependent kinase

DAPI: 4', 6-diamidino-2'-phenylindole dihydrochloride

dsRNA: Double strand RNA

ECL: Enhanced Chemiluminescence

FBS: Fetal Bovine Serum

FSM: Fluorescent speckle microscopy

GDP: Guanosin diphosphate

GFP: Green fluorescent protein

GTP: Guanosin triphosphate

h: hours

IpMT: interpolar microtubules

IQR: Inter-quartile range

KMT: Kinetochore microtubule

Min: Minutes

MT: Microtubule

MTOC: Microtubule organizing center

NEB: Nuclear envelope breakdown

Pav: Pavarotti

PCR: Polymerase chain reaction

PCM: Pericentriolar material

RNAi: RNA-mediated interference

SAC: Spindle assembly checkpoint

Sec: second

SEM: Standard error of the mean

SD: Standard deviation

2. SUPPLEMENTARY TABLES

Table S1. List of oligonucleotides used and respective sequences.

Primer	Sequence (5'-3')
Asp T7 F	TAATACGACTCACTATAGGGTGTTATCTGCCTGCAACAGC
Asp T7 R	TAATACGACTCACTATAGGGTTTTCAGCTGGGCGTAACTCT
DSas-4 T7 F	TAATACGACTCACTATAGGGAGATCTCGCGGCGCTTAGTCGTT
DSas-4 T7 R	TAATACGACTCACTATAGGGAGAGGCGCAGGATTGGGAGGTG
Ncd T7 F	TAATACGACTCACTATAGGGATTGTTGAGGTCCCTTGAGAGG
Ncd T7 R	TAATACGACTCACTATAGGGCTGATTGACAAACTGGAAGTGG
Mast T7 F	TAATACGACTCACTATAGGGCGAAGGACGAATAGACATT
Mast T7 R	TAATACGACTCACTATAGGGTCCTGTTTGACCTGGTCG
KLP10A T7 F	TAATACGACTCACTATAGGGATGATTACGGTGGGGCA
KLP10A T7 R	TAATACGACTCACTATAGGGGGACATCGATCTCCTTGCG
Mad2 T7 F	TAATACGACTCACTATAGGGAATAGCGGCAATTTAGC
Mad2 T7 R	TAATACGACTCACTATAGGGAGAAGCGCAGCTGGA
Pav T7 F	TAATACGACTCACTATAGGGAAATCCGTAACGAAACTAACCG
Pav T7 R	TAATACGACTCACTATAGGGACAACTGCTCTTGGCAGATACC

Table S2. List of antibodies used and respective dilutions

Target	Antibody	Serum	Dilution (purpose)
	Primary		
α-tubulin	Clone B512, Sigma	Mouse	1:2000 (IF)
α-tubulin	DM1A, Abcam	Mouse	1:10000 (WB)
γ-tubulin	R62	Rabbit	1:500 (IF)
Asp	Asp	Rabbit	1:1000 (WB)
Aurora B	963-1	Rabbit	1:500 (IF)
BubR1	BubR1	Rabbit	1:2500 (IF)
CLASP	CLASP	Rabbit	1:600 (WB)
CID	CID	Chicken	1:300 (IF)
CID	CID	Rat	1:2000 (IF)
EB1	154	Rabbit	1:500 (IF)
KLP10A	KLP10A	Rabbit	1:1500 (WB)
KLP61F	KLP61F	Rabbit	1:250 (IF)
Mad2	Mad2	Rabbit	1:3000 (WB)
Ncd	Ncd	Rabbit	1:5000 (WB)
Pav	Pav/KLP GM2	Rabbit	1:10000 (WB)
	Secondary		
	HRP-anti-Mouse	Sheep	1:5000 (WB)
	HRP-anti-Rabbit	Goat	1:5000 (WB)

Table S3. Cell Size

Treatment	Normality	No	Mean	SD	SEM	Median	25th Q	75th Q	P
CONTROL	Y	27	23.31	5.494	1.057	22.27	19.69	27.68	
TAXOL 10nM	Y	19	20.25	5.418	1.243	21.08	15.47	24.42	ns
MAD2 RNAi	Y	17	24.26	6.653	1.614	23.86	19.13	28.07	ns
SAS4 RNAi	Y	29	24.33	4.087	0.7589	25.79	20.23	27.04	ns
SAS4/KLP10A RNAi	Y	13	29.35	6.134	1.701	28.64	26.41	34.12	0.0033
ASP RNAi	Y	32	26.82	5.559	0.9828	26.6	23.4	30.00	0.0184
NCD RNAi	N	15	24.92	3.624	0.9358	25.8	20.44	28.03	ns
PAV RNAi	N	27	26.92	8.641	1.663	23.35	19.73	34.26	ns
PAV/NCD RNAi	Y	10	27.03	6.293	1.99	27.45	23.1	31.61	ns
KLP61F RNAi	Y	15	26.67	8.601	2.221	25.33	20.5	32.27	ns
CLASP RNAi	Y	8	21.58	5.873	2.076	22.74	14.99	26.28	ns
SCC1 RNAi	N	14	31.32	6.876	1.838	31.79	25.55	32.7	0.0008

Detailed analysis of independent experiments where cells were treated with Taxol, or with the different dsRNA depicted. The results are compared with Control untreated cells. All units are μm/min except No that refers to the number of spindles analyzed. P value is represented for either unpaired t test or Mann-Whitney test depending if the population follows (Y), or not (N), a Gaussian distribution. Normality was tested using the Kolmogorov-Smirnov. Ns refers to not significant.

3. SUPPLEMENTARY FIGURES

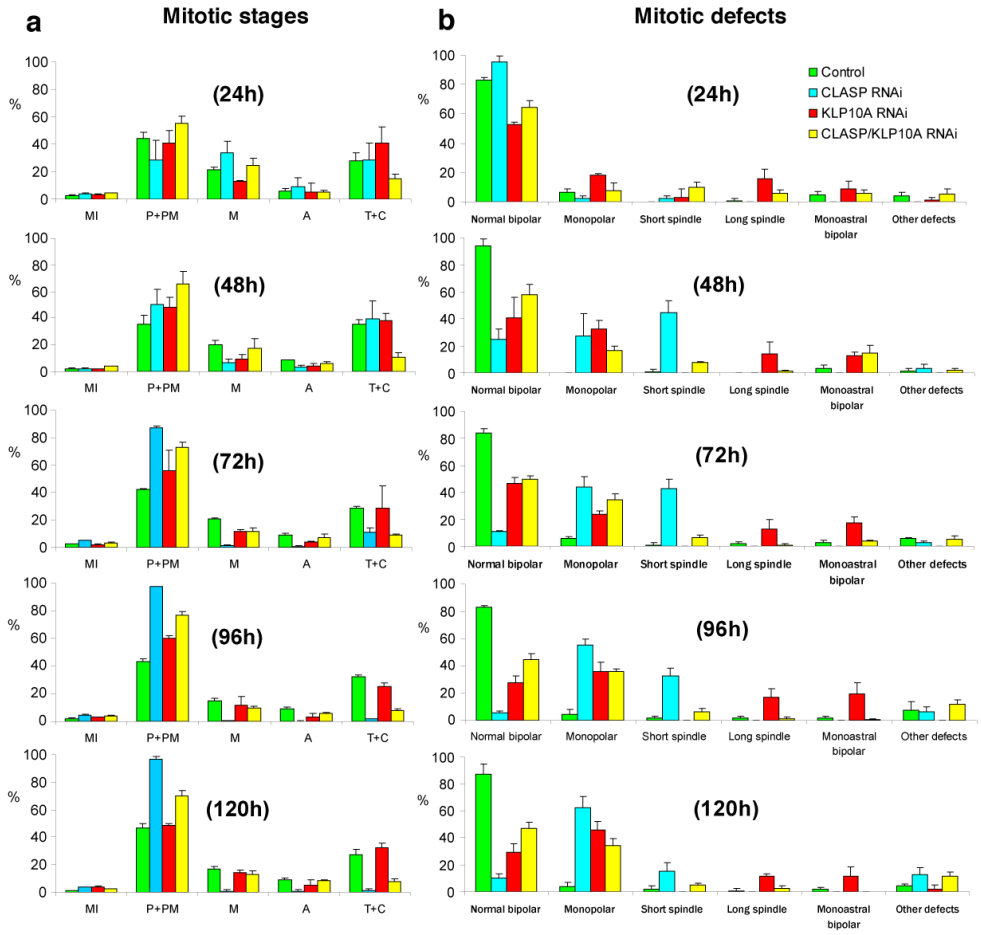


Figure S1 – Time-course analysis of CLASP, KLP10A and CLASP/KLP10A RNAi phenotypes in *Drosophila S2* cells. (a) Mitotic stages were scored every 24 h over a period of 120 h. From 72-120 h a clear phenotype could be observed with an increase in the percentage of prophase and prometaphase cells in the CLASP RNAi with a simultaneous decrease in the number of metaphase and anaphase cells. Co-depletion of CLASP and KLP10A rescues the frequency of metaphase and anaphase cells observed after CLASP RNAi to control levels. **(b)** Quantification of mitotic defects in the different RNAi experiments. Note that the decrease in normal spindle bipolarity after CLASP RNAi correlates with an increase of monopolar and short prometaphase spindles; we also observe an increase of monopolar, monoastral bipolar and long spindles after KLP10A RNAi. From 72-120 h, simultaneous depletion of CLASP and KLP10A restored normal spindle bipolarity in 40-50% of the cells. This correlates well with the fact that at the same time points in the double RNAi, cells were able to establish a metaphase plate and progress through anaphase, suggesting that spindles were functional. Therefore, all our live-cell studies were concentrated between the 96-120 h after RNAi. MI, mitotic index; P+PM, prophase and prometaphase; M, metaphase; A, anaphase; T+C telophase and cytokinesis. Plotted values represent the mean from 3 experiments and error bars represent the respective standard deviations.

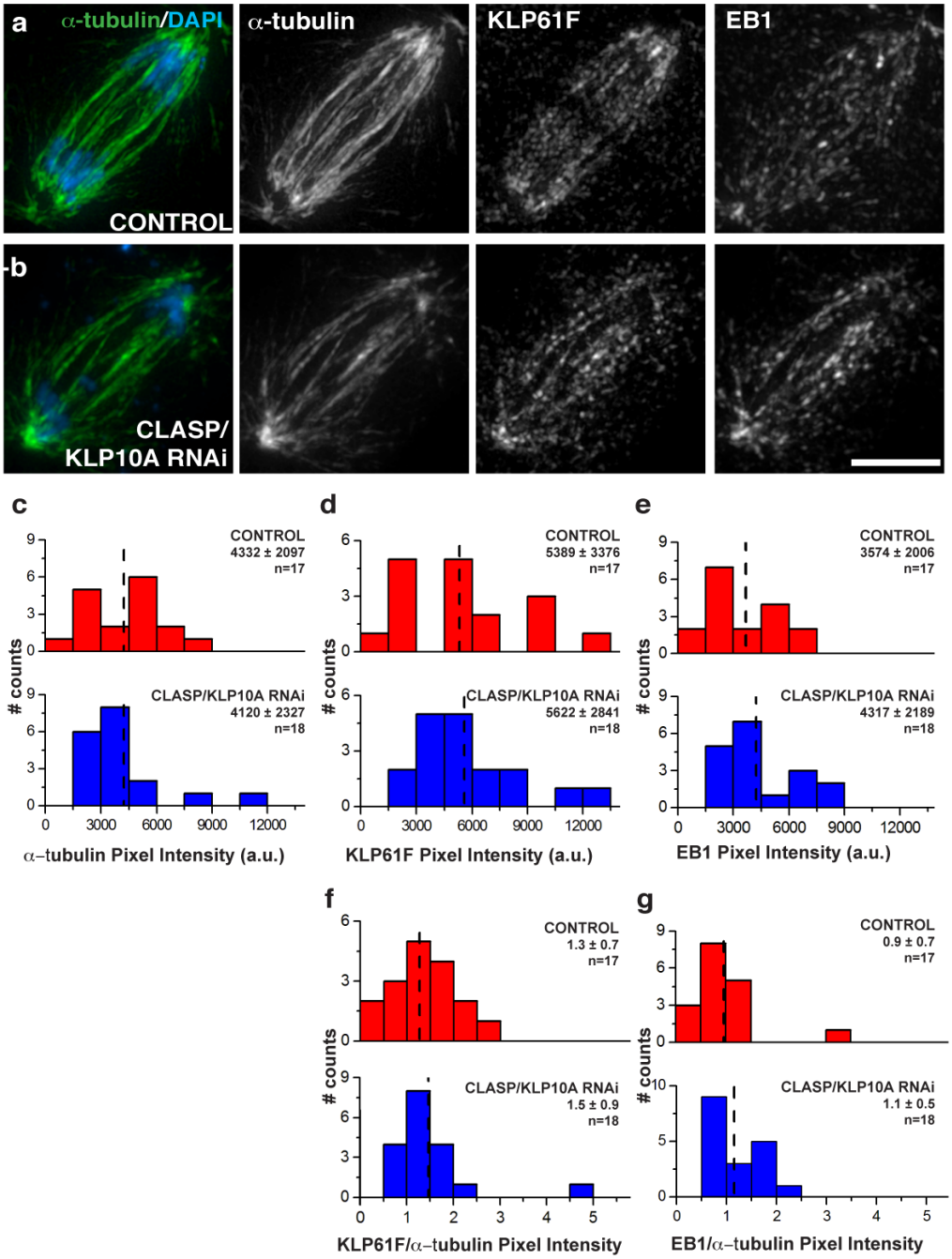


Figure S2 Quantitative analysis of spindle midzone formation by KLP61F and EB1 immunolocalization. **(a)** Control and **(b)** CLASP/KLP10A RNAi mitotic spindles were revealed by α-tubulin immunostaining (green), as well as the localization of KLP61F and EB1 in anaphase; DNA was counterstained with DAPI (blue). **(c)** Distribution of α-tubulin, **(d)** KLP61F and **(e)** EB1 pixel intensity measured in Control and CLASP RNAi treated cells. Distribution of **(f)** KLP61F/α-tubulin intensity and **(g)** EB1/α-tubulin shows no difference in KLP61F and EB1 localization in Control and CLASP/KLP10A RNAi treated cells. The mean ± SD is given for each distribution and the mean position is marked as a dashed vertical line; n represents the number of anaphase cells analysed. Scale bar, 5 µm.

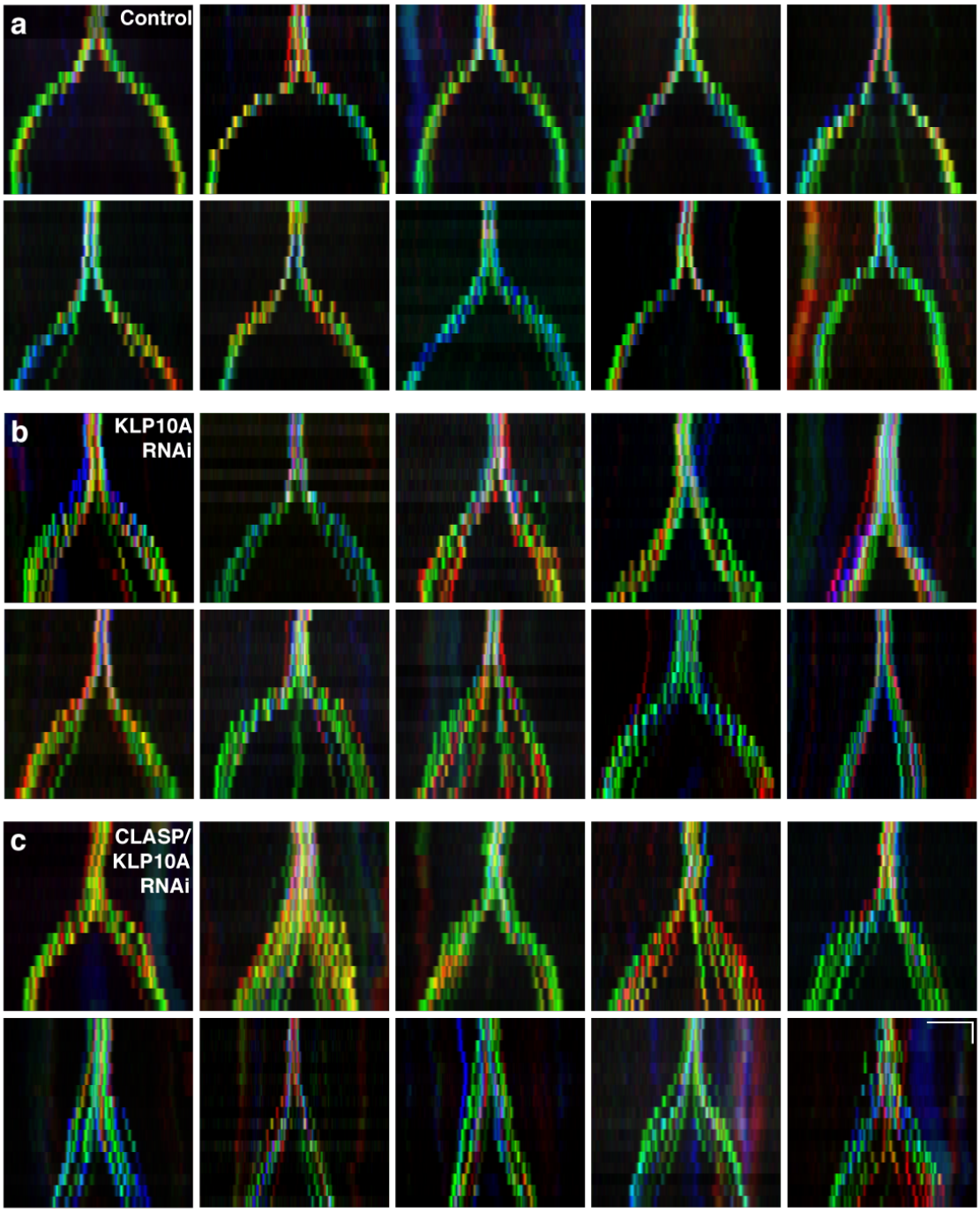


Figure S3 - Cells stably expressing CID-mCherry and GFP-α-tubulin (not depicted). (a-c) Tracking of kinetochores through entire spindle volumes at the metaphase-anaphase transition in control, KLP10A and CLASP/KLP10A RNAi cells, respectively. Ten cells are shown for each experimental condition. In most control cells it is difficult to distinguish individual kinetochore tracks and most kinetochores segregate as a synchronous population. However, after KLP10A and CLASP/KLP10A RNAi several distinct kinetochore tracks are typically observed indicating asynchronous chromosome segregation, despite the formation of apparently normal metaphase plates. Horizontal scale bar, 5 μm; Vertical scale bar , 1 min.

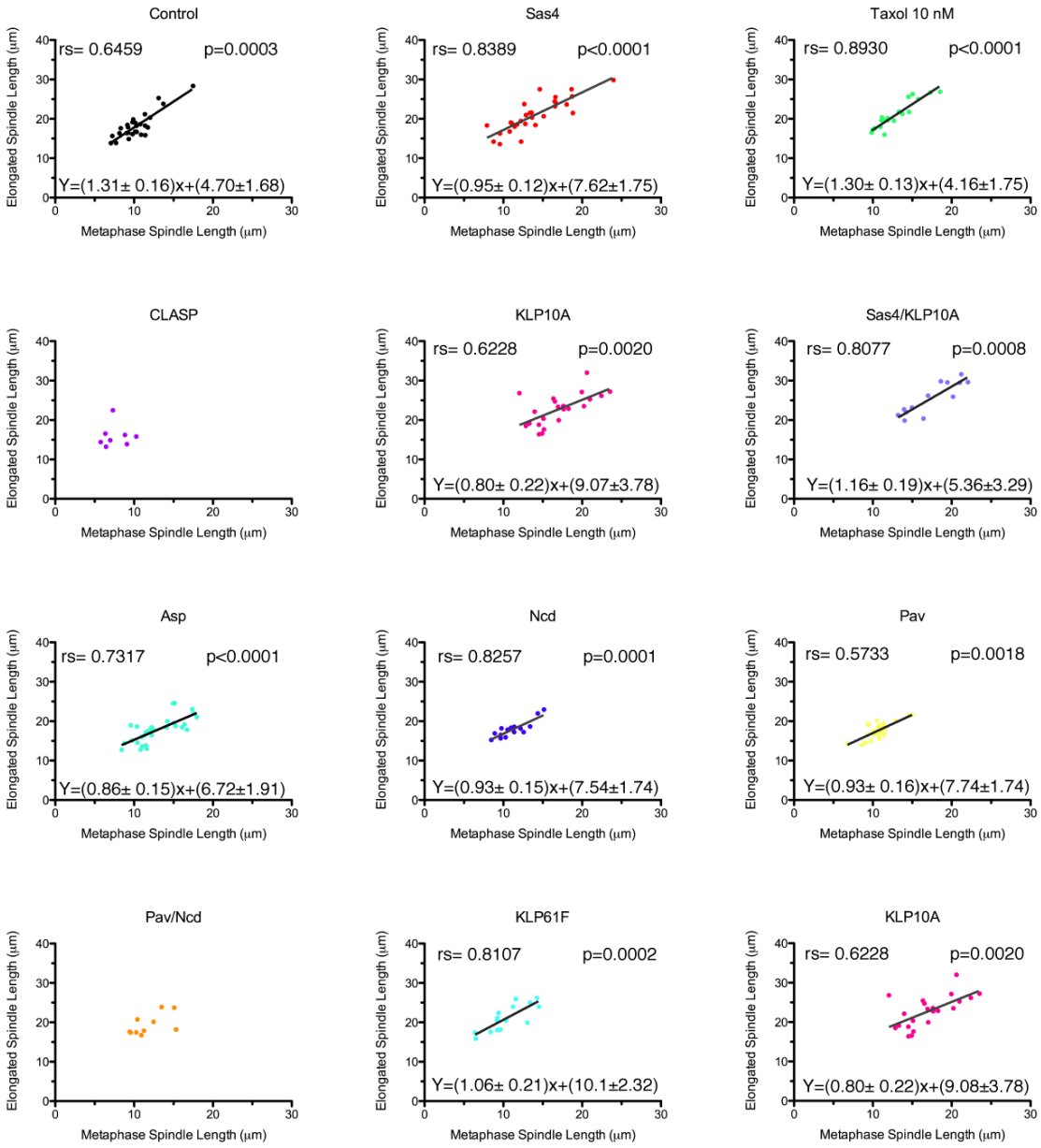


Figure S4 – Correlation between elongated spindle length and metaphase spindle length. Individual correlations are represented. The regression line is shown when a statistical significant correlation ($p<0.05$) is observed (±standart errors of the mean, SEM). Each dot represent the measures obtained for one spindle. r_s refers to the nonparametric Spearmen correlation coefficient. For statistic details see section 2.4, Materials and Methods, Chapter III).

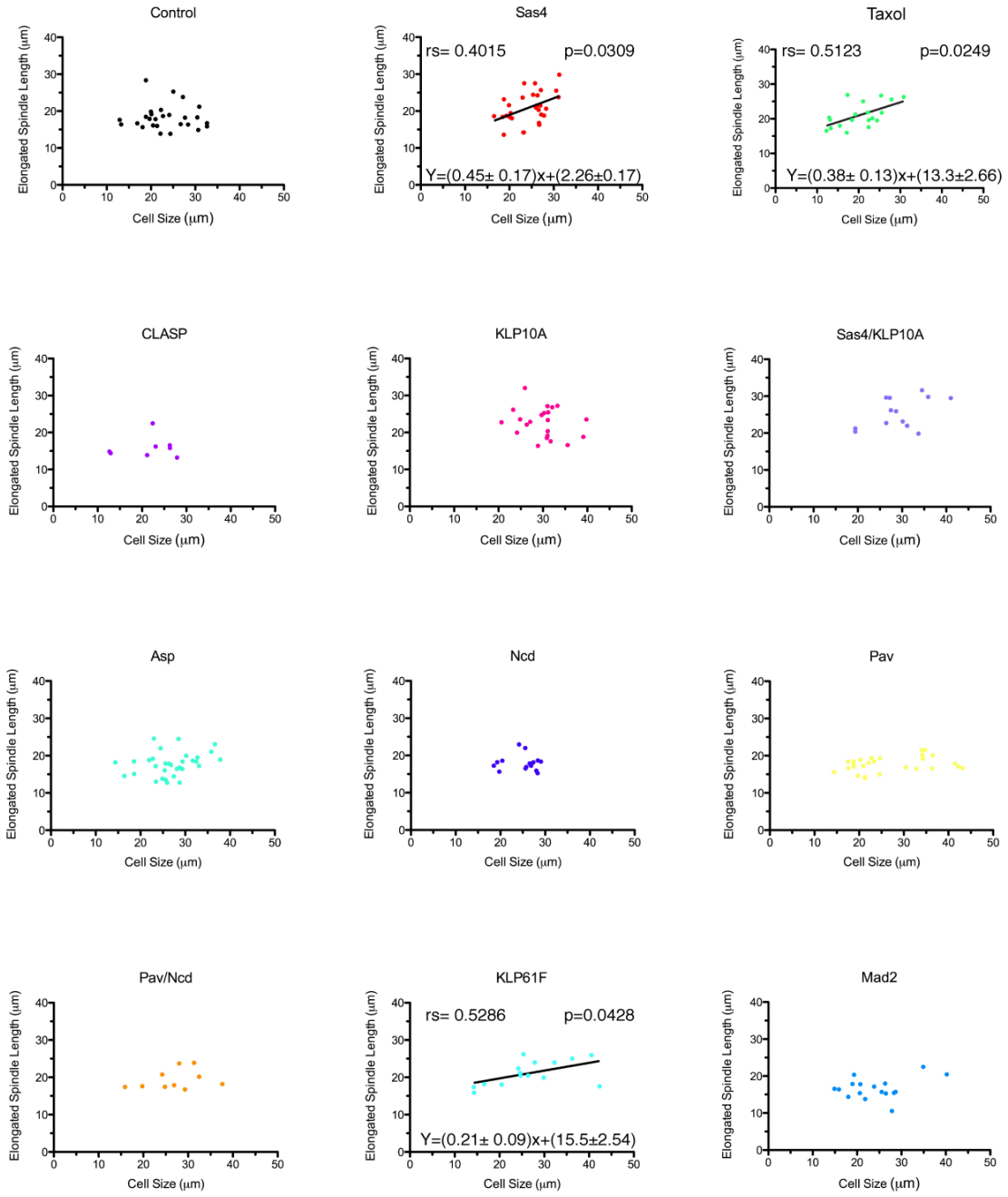


Figure S5 – Correlation between elongated spindle length and cell size. Individual correlations are represented. The regression line is shown when a statistical significant correlation ($p<0.05$) is observed (±standart errors of the mean, SEM). Each dot represent the measures obtained for one spindle. r_s refers to the nonparametric Spearmen correlation coefficient. For statistic details see section 2.4, Materials and Methods, Chapter III).

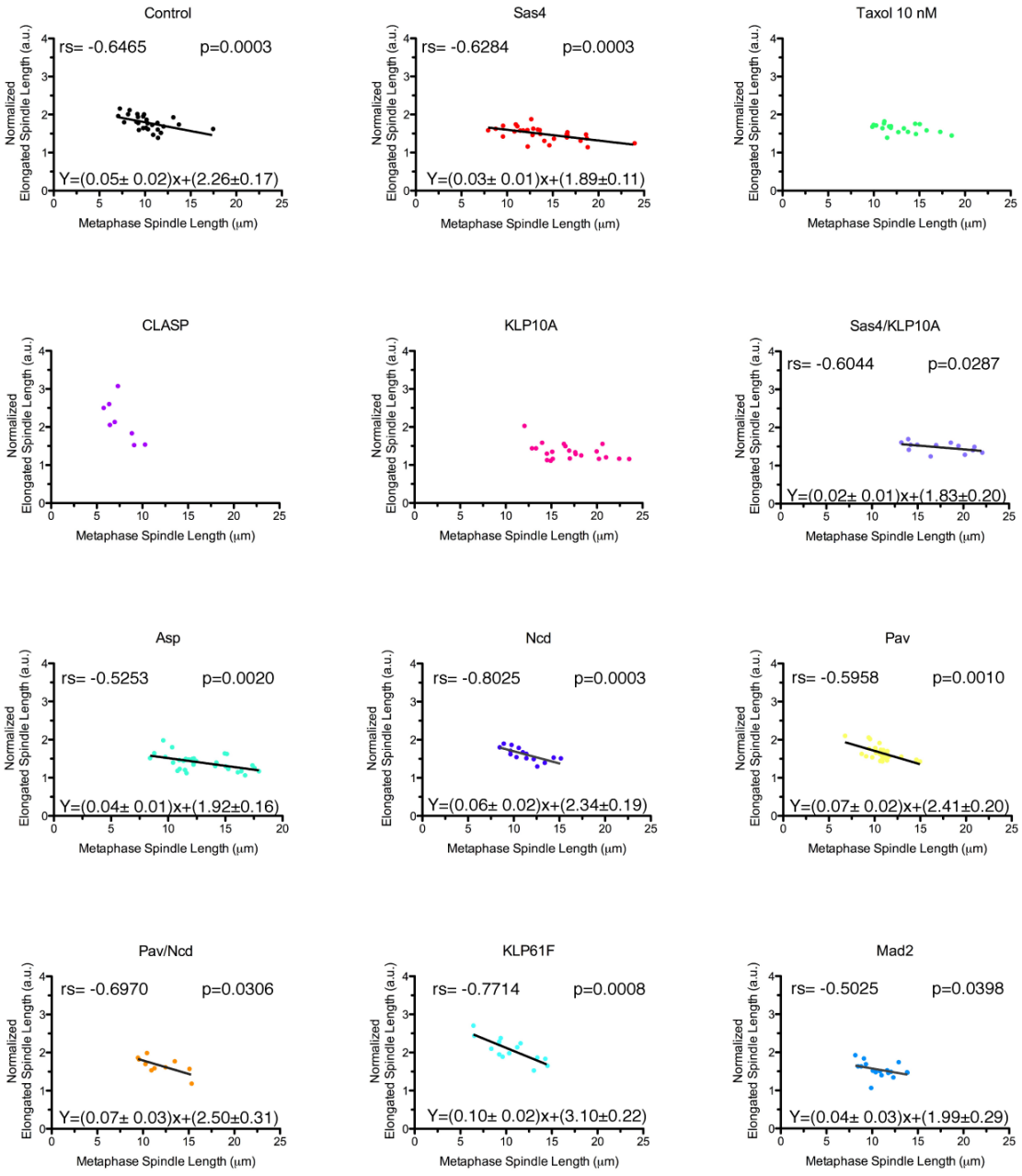


Figure S6 – Correlation between normalized elongated spindle length and metaphase spindle length. Individual correlations are represented. The regression line is shown when a statistical significant correlation ($p<0.05$) is observed (±standart errors of the mean, SEM). Each dot represent the measures obtained for one spindle. r_s refers to the nonparametric Spearmen correlation coefficient. For statistic details see section 2.4, Materials and Methods, Chapter III).

V. REFERENCES

REFERENCES

Adams, M. D.*, et al.* 2000. The genome sequence of Drosophila melanogaster. Science 287:2185-2195.

Aist, J. R., and Berns, M. W. 1981. Mechanics of chromosome separation during mitosis in Fusarium (Fungi imperfecti): new evidence from ultrastructural and laser microbeam experiments. J Cell Biol 91:446-458.

Akhmanova, A., and Steinmetz, M. O. 2008. Tracking the ends: a dynamic protein network controls the fate of microtubule tips. Nat Rev Mol Cell Biol 9:309-322.

Alberts, B. 2002. Molecular biology of the cell. Garland Science, New York.

Alexander, S. P., and Rieder, C. L. 1991. Chromosome motion during attachment to the vertebrate spindle: initial saltatory-like behavior of chromosomes and quantitative analysis of force production by nascent kinetochore fibers. J Cell Biol 113:805-815.

Antonio, C., Ferby, I., Wilhelm, H., Jones, M., Karsenti, E., Nebreda, A. R., and Vernos, I. 2000. Xkid, a chromokinesin required for chromosome alignment on the metaphase plate. Cell 102:425-435.

Bakhoum, S. F., Genovese, G., and Compton, D. A. 2009a. Deviant kinetochore microtubule dynamics underlie chromosomal instability. Curr Biol 19:1937-1942.

Bakhoum, S. F., Thompson, S. L., Manning, A. L., and Compton, D. A. 2009b. Genome stability is ensured by temporal control of kinetochore-microtubule dynamics. Nat Cell Biol 11:27-35.

Basto, R., Lau, J., Vinogradova, T., Gardiol, A., Woods, C. G., Khodjakov, A., and Raff, J. W. 2006. Flies without centrioles. Cell 125:1375-1386.

Belar, K. 1929. Beitrage zur Kausalanalyse der Mitosis II. Arch.Entwicklungsmech. Organ. 118:359-480.

Bettencourt-Dias, M., and Glover, D. M. 2007. Centrosome biogenesis and function: centrosomics brings new understanding. Nat Rev Mol Cell Biol 8:451-463.

Bettencourt-Dias, M., and Goshima, G. 2009. RNAi in Drosophila S2 cells as a tool for studying cell cycle progression. Methods Mol Biol 545:39-62.

Biggins, S., and Murray, A. W. 2001. The budding yeast protein kinase Ipl1/Aurora allows the absence of tension to activate the spindle checkpoint. Genes Dev 15:3118-3129.

Black, B. E., and Bassett, E. A. 2008. The histone variant CENP-A and centromere specification. Curr Opin Cell Biol 20:91-100.

Bloom, J., and Cross, F. R. 2007. Multiple levels of cyclin specificity in cell-cycle control. Nat Rev Mol Cell Biol 8:149-160.

Bloom, K. 2008. Kinetochores and microtubules wed without a ring. Cell 135:211-213.

Bloom, K., and Joglekar, A. 2010. Towards building a chromosome segregation machine. Nature 463:446-456.

Blower, M. D., Sullivan, B. A., and Karpen, G. H. 2002. Conserved organization of centromeric chromatin in flies and humans. Dev Cell 2:319-330.

Boveri, T. 1888. Zellenstudien. II. Fischer. jena.

Brangwynne, C. P., MacKintosh, F. C., Kumar, S., Geisse, N. A., Talbot, J., Mahadevan, L., Parker, K. K., Ingber, D. E., and Weitz, D. A. 2006. Microtubules can bear enhanced compressive loads in living cells because of lateral reinforcement. J Cell Biol 173:733-741.

Braun, M., Drummond, D. R., Cross, R. A., and McAinsh, A. D. 2009. The kinesin-14 Klp2 organizes microtubules into parallel bundles by an ATP-dependent sorting mechanism. Nat Cell Biol 11:724-730.

Brennan, I. M., Peters, U., Kapoor, T. M., and Straight, A. F. 2007. Polo-like kinase controls vertebrate spindle elongation and cytokinesis. PLoS One 2:e409.

Brinkley, B. R., and Stubblefield, E. 1966. The fine structure of the kinetochore of a mammalian cell in vitro. Chromosoma 19:28-43.

Brinkley, B. R., Ouspenski, I., and Zinkowski, R. P. 1992. Structure and molecular organization of the centromere-kinetochore complex. Trends Cell Biol 2:15-21.

Brust-Mascher, I., and Scholey, J. M. 2002. Microtubule flux and sliding in mitotic spindles of Drosophila embryos. Mol Biol Cell 13:3967-3975.

Brust-Mascher, I., Civelekoglu-Scholey, G., Kwon, M., Mogilner, A., and Scholey, J. M. 2004. Model for anaphase B: role of three mitotic motors in a switch from poleward flux to spindle elongation. Proc Natl Acad Sci U S A 101:15938-15943.

Brust-Mascher, I., and Scholey, J. M. 2007. Mitotic spindle dynamics in Drosophila. Int Rev Cytol 259:139-172.

Brust-Mascher, I., Sommi, P., Cheerambathur, D. K., and Scholey, J. M. 2009. Kinesin-5-dependent poleward flux and spindle length control in Drosophila embryo mitosis. Mol Biol Cell 20:1749-1762.

Buffin, E., Emre, D., and Karess, R. E. 2007. Flies without a spindle checkpoint. Nat Cell Biol 9:565-572.

Bullough, W. S., and Johnson, M. 1951. The energy relations of mitotic activity in adult mouse epidermis. Proc R Soc Lond B Biol Sci 138:562-575.

Burbank, K. S., Groen, A. C., Perlman, Z. E., Fisher, D. S., and Mitchison, T. J. 2006. A new method reveals microtubule minus ends throughout the meiotic spindle. J Cell Biol 175:369-375.

Buster, D. W., Zhang, D., and Sharp, D. J. 2007. Poleward tubulin flux in spindles: regulation and function in mitotic cells. Mol Biol Cell 18:3094-3104.

Cai, S., O'Connell, C. B., Khodjakov, A., and Walczak, C. E. 2009. Chromosome congression in the absence of kinetochore fibres. Nat Cell Biol 11:832-838.

Carminati, J. L., and Stearns, T. 1997. Microtubules orient the mitotic spindle in yeast through dynein-dependent interactions with the cell cortex. J Cell Biol 138:629-641.

Carvalho, P., Tirnauer, J. S., and Pellman, D. 2003. Surfing on microtubule ends. Trends Cell Biol 13:229-237.

Cassimeris, L., Inoue, S., and Salmon, E. D. 1988. Microtubule dynamics in the chromosomal spindle fiber: analysis by fluorescence and high-resolution polarization microscopy. Cell Motil Cytoskeleton 10:185-196.

Cassimeris, L. 2002. The oncoprotein 18/stathmin family of microtubule destabilizers. Curr Opin Cell Biol 14:18-24.

Cassimeris, L. U., Walker, R. A., Pryer, N. K., and Salmon, E. D. 1987. Dynamic instability of microtubules. Bioessays 7:149-154.

Chan, J., Jensen, C. G., Jensen, L. C., Bush, M., and Lloyd, C. W. 1999. The 65-kDa carrot microtubule-associated protein forms regularly arranged filamentous cross-bridges between microtubules. Proc Natl Acad Sci U S A 96:14931-14936.

Cheerambathur, D. K., Civelekoglu-Scholey, G., Brust-Mascher, I., Sommi, P., Mogilner, A., and Scholey, J. M. 2007. Quantitative analysis of an anaphase B switch: predicted role for a microtubule catastrophe gradient. J Cell Biol 177:995-1004.

Cheeseman, I. M., Chappie, J. S., Wilson-Kubalek, E. M., and Desai, A. 2006. The conserved KMN network constitutes the core microtubule-binding site of the kinetochore. Cell 127:983-997.

Cheeseman, I. M., and Desai, A. 2008. Molecular architecture of the kinetochore-microtubule interface. Nat Rev Mol Cell Biol 9:33-46.

Cimini, D., Moree, B., Canman, J. C., and Salmon, E. D. 2003. Merotelic kinetochore orientation occurs frequently during early mitosis in mammalian tissue cells and error correction is achieved by two different mechanisms. J Cell Sci 116:4213-4225.

Cimini, D., Cameron, L. A., and Salmon, E. D. 2004. Anaphase spindle mechanics prevent mis-segregation of merotelically oriented chromosomes. Curr Biol 14:2149-2155.

Cimini, D., Wan, X., Hirel, C. B., and Salmon, E. D. 2006. Aurora kinase promotes turnover of kinetochore microtubules to reduce chromosome segregation errors. Curr Biol 16:1711-1718.

Civelekoglu-Scholey, G., and Scholey, J. M. 2007. Mitotic motors: kinesin-5 takes a brake. Curr Biol 17:R544-547.

Civelekoglu-Scholey, G., and Scholey, J. M. 2010. Mitotic force generators and chromosome segregation. Cell. Mol. Life Sci. (in press).

Cleveland, D. W., Mao, Y., and Sullivan, K. F. 2003. Centromeres and kinetochores: from epigenetics to mitotic checkpoint signaling. Cell 112:407-421.

Coelho, P. A., Queiroz-Machado, J., Carmo, A. M., Moutinho-Pereira, S., Maiato, H., and Sunkel, C. E. 2008. Dual role of topoisomerase II in centromere resolution and aurora B activity. PLoS Biol 6:e207.

Compton, D. A., Szilak, I., and Cleveland, D. W. 1992. Primary structure of NuMA, an intranuclear protein that defines a novel pathway for segregation of proteins at mitosis. J Cell Biol 116:1395-1408.

Coue, M., Lombillo, V. A., and McIntosh, J. R. 1991. Microtubule depolymerization promotes particle and chromosome movement in vitro. J Cell Biol 112:1165-1175.

Courtheoux, T., Gay, G., Gachet, Y., and Tournier, S. 2009. Ase1/Prc1-dependent spindle elongation corrects merotely during anaphase in fission yeast. J Cell Biol 187:399-412.

Danuser, G., and Waterman-Storer, C. M. 2006. Quantitative fluorescent speckle microscopy of cytoskeleton dynamics. Annu Rev Biophys Biomol Struct 35:361-387.

DeLuca, J. G., Gall, W. E., Ciferri, C., Cimini, D., Musacchio, A., and Salmon, E. D. 2006. Kinetochore microtubule dynamics and attachment stability are regulated by Hec1. Cell 127:969-982.

Derry, W. B., Wilson, L., and Jordan, M. A. 1995. Substoichiometric binding of taxol suppresses microtubule dynamics. Biochemistry 34:2203-2211.

Desai, A., and Mitchison, T. J. 1997. Microtubule polymerization dynamics. Annu Rev Cell Dev Biol 13:83-117.

Dhonukshe, P., Vischer, N., and Gadella, T. W., Jr. 2006. Contribution of microtubule growth polarity and flux to spindle assembly and functioning in plant cells. J Cell Sci 119:3193-3205.

do Carmo Avides, M., and Glover, D. M. 1999. Abnormal spindle protein, Asp, and the integrity of mitotic centrosomal microtubule organizing centers. Science 283:1733-1735.

Dogterom, M., and Yurke, B. 1997. Measurement of the force-velocity relation for growing microtubules. Science 278:856-860.

Dogterom, M., Kerssemakers, J. W., Romet-Lemonne, G., and Janson, M. E. 2005. Force generation by dynamic microtubules. Curr Opin Cell Biol 17:67-74.

Dong, Y., Vanden Beldt, K. J., Meng, X., Khodjakov, A., and McEwen, B. F. 2007. The outer plate in vertebrate kinetochores is a flexible network with multiple microtubule interactions. Nat Cell Biol 9:516-522.

Doxsey, S. 2001. Re-evaluating centrosome function. Nat Rev Mol Cell Biol 2:688-698.

Earnshaw, W. C., and Rothfield, N. 1985. Identification of a family of human centromere proteins using autoimmune sera from patients with scleroderma. Chromosoma 91:313-321.

Ems-McClung, S. C., and Walczak, C. E. 2010. Kinesin-13s in mitosis: Key players in the spatial and temporal organization of spindle microtubules. Semin Cell Dev Biol.

Erickson, H. P. 2000. Gamma-tubulin nucleation: template or protofilament? Nat Cell Biol 2:E93-96.

Evans, T., Rosenthal, E. T., Youngblom, J., Distel, D., and Hunt, T. 1983. Cyclin: a protein specified by maternal mRNA in sea urchin eggs that is destroyed at each cleavage division. Cell 33:389-396.

Famulski, J. K., and Chan, G. K. 2007. Aurora B kinase-dependent recruitment of hZW10 and hROD to tensionless kinetochores. Curr Biol 17:2143-2149.

Ferenz, N. P., Paul, R., Fagerstrom, C., Mogilner, A., and Wadsworth, P. 2009. Dynein antagonizes eg5 by crosslinking and sliding antiparallel microtubules. Curr Biol 19:1833-1838.

Fink, G., Schuchardt, I., Colombelli, J., Stelzer, E., and Steinberg, G. 2006. Dynein-mediated pulling forces drive rapid mitotic spindle elongation in Ustilago maydis. EMBO J 25:4897-4908.

Fink, G., Hajdo, L., Skowronek, K. J., Reuther, C., Kasprzak, A. A., and Diez, S. 2009. The mitotic kinesin-14 Ncd drives directional microtubule-microtubule sliding. Nat Cell Biol 11:717-723.

Flemming, W. 1882. Zellsubstanz, Kern and Zelltheilung *in* Vogel, ed, Leipzig.

Flemming, W. 1965. Historical Paper. Contributions to the Knowledge of the Cell and Its Vital Processes. J Cell Biol 25:SUPPL:1-69.

Forer, A. 1965. Local Reduction of Spindle Fiber Birefringence in Living Nephrotoma Suturalis (Loew) Spermatocytes Induced by Ultraviolet Microbeam Irradiation. J Cell Biol 25:SUPPL:95-117.

Forer, A. 1988. Do anaphase chromosomes chew their way to the pole or are they pulled by actin? J Cell Sci 91 (Pt 4):449-453.

Forer, A., and Wilson, P. J. 1994. A model for chromosome movement during mitosis. Protoplasma 179:95-105.

Forer, A., and Pickett-Heaps, J. D. 1998. Cytochalasin D and latrunculin affect chromosome behaviour during meiosis in crane-fly spermatocytes. Chromosome Res 6:533-549.

Forer, A., Spurck, T., Pickett-Heaps, J. D., and Wilson, P. J. 2003. Structure of kinetochore fibres in crane-fly spermatocytes after irradiation with an ultraviolet microbeam: neither microtubules nor actin filaments remain in the irradiated region. Cell Motil Cytoskeleton 56:173-192.

Forer, A., Spurck, T., and Pickett-Heaps, J. D. 2007. Actin and myosin inhibitors block elongation of kinetochore fibre stubs in metaphase crane-fly spermatocytes. Protoplasma 232:79-85.

Forer, A., Pickett-Heaps, J. D., and Spurck, T. 2008. What generates flux of tubulin in kinetochore microtubules? Protoplasma.

Fu, C., Ward, J. J., Loiodice, I., Velve-Casquillas, G., Nedelec, F. J., and Tran, P. T. 2009. Phospho-regulated interaction between kinesin-6 Klp9p and microtubule bundler Ase1p promotes spindle elongation. Dev Cell 17:257-267.

Fuller, B. G., and Stukenberg, P. T. 2009. Cell division: righting the check. Curr Biol 19:R550-553.

Fuller, M. T. 1995. Riding the polar winds: chromosomes motor down east. Cell 81:5-8.

Furuno, N., den Elzen, N., and Pines, J. 1999. Human cyclin A is required for mitosis until mid prophase. J Cell Biol 147:295-306.

Gadde, S., and Heald, R. 2004. Mechanisms and molecules of the mitotic spindle. Curr Biol 14:R797-805.

Gaetz, J., and Kapoor, T. M. 2004. Dynein/dynactin regulate metaphase spindle length by targeting depolymerizing activities to spindle poles. J Cell Biol 166:465-471.

Gaglio, T., Saredi, A., and Compton, D. A. 1995. NuMA is required for the organization of microtubules into aster-like mitotic arrays. J Cell Biol 131:693-708.

Ganem, N. J., Upton, K., and Compton, D. A. 2005. Efficient mitosis in human cells lacking poleward microtubule flux. Curr Biol 15:1827-1832.

Ganem, N. J., and Compton, D. A. 2006. Functional roles of poleward microtubule flux during mitosis. Cell Cycle 5:481-485.

Ganem, N. J., Storchova, Z., and Pellman, D. 2007. Tetraploidy, aneuploidy and cancer. Curr Opin Genet Dev 17:157-162.

Gard, D. L., and Kirschner, M. W. 1987. A microtubule-associated protein from Xenopus eggs that specifically promotes assembly at the plus-end. J Cell Biol 105:2203-2215.

Gardner, M. K., and Odde, D. J. 2006. Modeling of chromosome motility during mitosis. Curr Opin Cell Biol 18:639-647.

Glotzer, M. 2009. The 3Ms of central spindle assembly: microtubules, motors and MAPs. Nat Rev Mol Cell Biol 10:9-20.

Gonczy, P., Pichler, S., Kirkham, M., and Hyman, A. A. 1999. Cytoplasmic dynein is required for distinct aspects of MTOC positioning, including centrosome separation, in the one cell stage Caenorhabditis elegans embryo. J Cell Biol 147:135-150.

Gonczy, P. 2002. Mechanisms of spindle positioning: focus on flies and worms. Trends Cell Biol 12:332-339.

Gong, D., Pomerening, J. R., Myers, J. W., Gustavsson, C., Jones, J. T., Hahn, A. T., Meyer, T., and Ferrell, J. E., Jr. 2007. Cyclin A2 regulates nuclear-envelope breakdown and the nuclear accumulation of cyclin B1. Curr Biol 17:85-91.

Gorbsky, G. J., Sammak, P. J., and Borisy, G. G. 1987. Chromosomes move poleward in anaphase along stationary microtubules that coordinately disassemble from their kinetochore ends. J Cell Biol 104:9-18.

Gorbsky, G. J., Sammak, P. J., and Borisy, G. G. 1988. Microtubule dynamics and chromosome motion visualized in living anaphase cells. J Cell Biol 106:1185-1192.

Gorbsky, G. J., and Borisy, G. G. 1989. Microtubules of the kinetochore fiber turn over in metaphase but not in anaphase. J Cell Biol 109:653-662.

Gorbsky, G. J., Simerly, C., Schatten, G., and Borisy, G. G. 1990. Microtubules in the metaphase-arrested mouse oocyte turn over rapidly. Proc Natl Acad Sci U S A 87:6049-6053.

Gorbsky, G. J., and Ricketts, W. A. 1993. Differential expression of a phosphoepitope at the kinetochores of moving chromosomes. J Cell Biol 122:1311-1321.

Gordon, M. B., Howard, L., and Compton, D. A. 2001. Chromosome movement in mitosis requires microtubule anchorage at spindle poles. J Cell Biol 152:425-434.

Goshima, G., Nedelec, F., and Vale, R. D. 2005a. Mechanisms for focusing mitotic spindle poles by minus end-directed motor proteins. J Cell Biol 171:229-240.

Goshima, G., Wollman, R., Stuurman, N., Scholey, J. M., and Vale, R. D. 2005b. Length control of the metaphase spindle. Curr Biol 15:1979-1988.

Goshima, G., Wollman, R., Goodwin, S. S., Zhang, N., Scholey, J. M., Vale, R. D., and Stuurman, N. 2007. Genes required for mitotic spindle assembly in Drosophila S2 cells. Science 316:417-421.

Grill, S. W., Gonczy, P., Stelzer, E. H., and Hyman, A. A. 2001. Polarity controls forces governing asymmetric spindle positioning in the Caenorhabditis elegans embryo. Nature 409:630-633.

Grill, S. W., and Hyman, A. A. 2005. Spindle positioning by cortical pulling forces. Dev Cell 8:461-465.

Grishchuk, E. L., Molodtsov, M. I., Ataullakhanov, F. I., and McIntosh, J. R. 2005. Force production by disassembling microtubules. Nature 438:384-388.

Grishchuk, E. L., Efremov, A. K., Volkov, V. A., Spiridonov, I. S., Gudimchuk, N., Westermann, S., Drubin, D., Barnes, G., McIntosh, J. R., and Ataullakhanov, F. I. 2008a. The Dam1 ring binds microtubules strongly enough to be a processive as well as energy-efficient coupler for chromosome motion. Proc Natl Acad Sci U S A 105:15423-15428.

Grishchuk, E. L., Spiridonov, I. S., Volkov, V. A., Efremov, A., Westermann, S., Drubin, D., Barnes, G., Ataullakhanov, F. I., and McIntosh, J. R. 2008b. Different assemblies of the DAM1 complex follow shortening microtubules by distinct mechanisms. Proc Natl Acad Sci U S A 105:6918-6923.

Guimaraes, G. J., Dong, Y., McEwen, B. F., and Deluca, J. G. 2008. Kinetochore-microtubule attachment relies on the disordered N-terminal tail domain of Hec1. Curr Biol 18:1778-1784.

Hagting, A., Karlsson, C., Clute, P., Jackman, M., and Pines, J. 1998. MPF localization is controlled by nuclear export. EMBO J 17:4127-4138.

Hamaguchi, Y., Toriyama, M., Sakai, H., and Hiramoto, Y. 1987. Redistribution of fluorescently labeled tubulin in the mitotic apparatus of sand dollar eggs and the effects of taxol. Cell Struct Funct 12:43-52.

Hara, Y., and Kimura, A. 2009. Cell-size-dependent spindle elongation in the Caenorhabditis elegans early embryo. Curr Biol 19:1549-1554.

Harris, P. 1962. Some structural and functional aspects of the mitotic apparatus in sea urchin embryos. J Cell Biol 14:475-487.

Hartwell, L. H., and Weinert, T. A. 1989. Checkpoints: controls that ensure the order of cell cycle events. Science 246:629-634.

Hayashi, T., Sano, T., Kutsuna, N., Kumagai-Sano, F., and Hasezawa, S. 2007. Contribution of anaphase B to chromosome separation in higher plant cells estimated by image processing. Plant Cell Physiol 48:1509-1513.

Heald, R., Tournebize, R., Blank, T., Sandaltzopoulos, R., Becker, P., Hyman, A., and Karsenti, E. 1996. Self-organization of microtubules into bipolar spindles around artificial chromosomes in Xenopus egg extracts. Nature 382:420-425.

Heck, M. M., Pereira, A., Pesavento, P., Yannoni, Y., Spradling, A. C., and Goldstein, L. S. 1993. The kinesin-like protein KLP61F is essential for mitosis in Drosophila. J Cell Biol 123:665-679.

Hetzer, M. W., Walther, T. C., and Mattaj, I. W. 2005. Pushing the envelope: structure, function, and dynamics of the nuclear periphery. Annu Rev Cell Dev Biol 21:347-380.

Higuchi, T., and Uhlmann, F. 2005. Stabilization of microtubule dynamics at anaphase onset promotes chromosome segregation. Nature 433:171-176.

Hill, T. L. 1985. Theoretical problems related to the attachment of microtubules to kinetochores. Proc Natl Acad Sci U S A 82:4404-4408.

Hinchcliffe, E. H., Miller, F. J., Cham, M., Khodjakov, A., and Sluder, G. 2001. Requirement of a centrosomal activity for cell cycle progression through G1 into S phase. Science 291:1547-1550.

Hirokawa, N., Noda, Y., and Okada, Y. 1998. Kinesin and dynein superfamily proteins in organelle transport and cell division. Curr Opin Cell Biol 10:60-73.

Hochegger, H., Takeda, S., and Hunt, T. 2008. Cyclin-dependent kinases and cell-cycle transitions: does one fit all? Nat Rev Mol Cell Biol 9:910-916.

Hoffman, D. B., Pearson, C. G., Yen, T. J., Howell, B. J., and Salmon, E. D. 2001. Microtubule-dependent changes in assembly of microtubule motor proteins and mitotic spindle checkpoint proteins at PtK1 kinetochores. Mol Biol Cell 12:1995-2009.

Holt, L. J., Krutchinsky, A. N., and Morgan, D. O. 2008. Positive feedback sharpens the anaphase switch. Nature 454:353-357.

Holy, T. E., Dogterom, M., Yurke, B., and Leibler, S. 1997. Assembly and positioning of microtubule asters in microfabricated chambers. Proc Natl Acad Sci U S A 94:6228-6231.

Howell, B. J., McEwen, B. F., Canman, J. C., Hoffman, D. B., Farrar, E. M., Rieder, C. L., and Salmon, E. D. 2001. Cytoplasmic dynein/dynactin drives kinetochore protein transport to the spindle poles and has a role in mitotic spindle checkpoint inactivation. J Cell Biol 155:1159-1172.

Hoyt, M. A., Totis, L., and Roberts, B. T. 1991. S. cerevisiae genes required for cell cycle arrest in response to loss of microtubule function. Cell 66:507-517.

Hoyt, M. A., He, L., Loo, K. K., and Saunders, W. S. 1992. Two Saccharomyces cerevisiae kinesin-related gene products required for mitotic spindle assembly. J Cell Biol 118:109-120.

Hsu, J. Y., Sun, Z. W., Li, X., Reuben, M., Tatchell, K., Bishop, D. K., Grushcow, J. M., Brame, C. J., Caldwell, J. A., Hunt, D. F., Lin, R., Smith, M. M., and Allis, C. D. 2000. Mitotic phosphorylation of histone H3 is governed by Ipl1/aurora kinase and Glc7/PP1 phosphatase in budding yeast and nematodes. Cell 102:279-291.

Inoue, S. 1953. [Polarization optical studies of the mitotic spindle. I. The demonstration of spindle fibers in living cells.]. Chromosoma 5:487-500.

Inoue, S., and Bajer, A. 1961. Birefringence in endosperm mitosis. Chromosoma 12:48-63.

Inoue, S. 1964. Organization and function of the mitotic spindle., New York.

Inoue, S., and Sato, H. 1967. Cell motility by labile association of molecules. The nature of mitotic spindle fibers and their role in chromosome movement. J Gen Physiol 50:Suppl:259-292.

Inoue, S. 1981. Cell division and the mitotic spindle. J Cell Biol 91:131s-147s.

Inoue, S. 2008. Microtubule dynamics in cell division: exploring living cells with polarized light microscopy. Annu Rev Cell Dev Biol 24:1-28.

Inoue, Y. H., do Carmo Avides, M., Shiraki, M., Deak, P., Yamaguchi, M., Nishimoto, Y., Matsukage, A., and Glover, D. M. 2000. Orbit, a novel microtubule-associated protein essential for mitosis in Drosophila melanogaster. J Cell Biol 149:153-166.

Janson, M. E., and Dogterom, M. 2004. Scaling of microtubule force-velocity curves obtained at different tubulin concentrations. Phys Rev Lett 92:248101.

Jiang, W., Jimenez, G., Wells, N. J., Hope, T. J., Wahl, G. M., Hunter, T., and Fukunaga, R. 1998. PRC1: a human mitotic spindle-associated CDK substrate protein required for cytokinesis. Mol Cell 2:877-885.

Joglekar, A. P., and Hunt, A. J. 2002. A simple, mechanistic model for directional instability during mitotic chromosome movements. Biophys J 83:42-58.

Joglekar, A. P., Bloom, K., and Salmon, E. D. 2009. In vivo protein architecture of the eukaryotic kinetochore with nanometer scale accuracy. Curr Biol 19:694-699.

Jordan, M. A., and Wilson, L. 1998. Use of drugs to study role of microtubule assembly dynamics in living cells. Methods Enzymol 298:252-276.

Kahana, J. A., Schnapp, B. J., and Silver, P. A. 1995. Kinetics of spindle pole body separation in budding yeast. Proc Natl Acad Sci U S A 92:9707-9711.

Kalab, P., Weis, K., and Heald, R. 2002. Visualization of a Ran-GTP gradient in interphase and mitotic Xenopus egg extracts. Science 295:2452-2456.

Kapitein, L. C., Peterman, E. J., Kwok, B. H., Kim, J. H., Kapoor, T. M., and Schmidt, C. F. 2005. The bipolar mitotic kinesin Eg5 moves on both microtubules that it crosslinks. Nature 435:114-118.

Kapoor, T. M., Lampson, M. A., Hergert, P., Cameron, L., Cimini, D., Salmon, E. D., McEwen, B. F., and Khodjakov, A. 2006. Chromosomes can congress to the metaphase plate before biorientation. Science 311:388-391.

Karsenti, E., and Vernos, I. 2001. The mitotic spindle: a self-made machine. Science 294:543-547.

Khmelinskii, A., Roostalu, J., Roque, H., Antony, C., and Schiebel, E. 2009. Phosphorylation-dependent protein interactions at the spindle midzone mediate cell cycle regulation of spindle elongation. Dev Cell 17:244-256.

Khodjakov, A., Cole, R. W., Oakley, B. R., and Rieder, C. L. 2000. Centrosome-independent mitotic spindle formation in vertebrates. Curr Biol 10:59-67.

Khodjakov, A., and Rieder, C. L. 2001. Centrosomes enhance the fidelity of cytokinesis in vertebrates and are required for cell cycle progression. J Cell Biol 153:237-242.

Khodjakov, A., Copenagle, L., Gordon, M. B., Compton, D. A., and Kapoor, T. M. 2003. Minus-end capture of preformed kinetochore fibers contributes to spindle morphogenesis. J Cell Biol 160:671-683.

Khodjakov, A., La Terra, S., and Chang, F. 2004. Laser microsurgery in fission yeast; role of the mitotic spindle midzone in anaphase B. Curr Biol 14:1330-1340.

Khodjakov, A., and Rieder, C. L. 2009a. The nature of cell-cycle checkpoints: facts and fallacies. J Biol 8:88.

Khodjakov, A., and Rieder, C. L. 2009b. Mitosis: too much of a good thing (can be bad). Curr Biol 19:R1032-1034.

King, J. M., and Nicklas, R. B. 2000. Tension on chromosomes increases the number of kinetochore microtubules but only within limits. J Cell Sci 113 Pt 21:3815-3823.

Kinoshita, K., Arnal, I., Desai, A., Drechsel, D. N., and Hyman, A. A. 2001. Reconstitution of physiological microtubule dynamics using purified components. Science 294:1340-1343.

Kinoshita, K., Habermann, B., and Hyman, A. A. 2002. XMAP215: a key component of the dynamic microtubule cytoskeleton. Trends Cell Biol 12:267-273.

Kirschner, M., and Mitchison, T. 1986. Beyond self-assembly: from microtubules to morphogenesis. Cell 45:329-342.

Kline-Smith, S. L., and Walczak, C. E. 2004. Mitotic spindle assembly and chromosome segregation: refocusing on microtubule dynamics. Mol Cell 15:317-327.

Knowlton, A. L., Lan, W., and Stukenberg, P. T. 2006. Aurora B is enriched at merotelic attachment sites, where it regulates MCAK. Curr Biol 16:1705-1710.

Koshland, D. E., Mitchison, T. J., and Kirschner, M. W. 1988. Polewards chromosome movement driven by microtubule depolymerization in vitro. Nature 331:499-504.

Kozlowski, C., Srayko, M., and Nedelec, F. 2007. Cortical microtubule contacts position the spindle in C. elegans embryos. Cell 129:499-510.

Kronebusch, P. J., and Borisy, G. G. 1982. Mechanics of Anaphase B. In *Biological Functions of Microtubules and Related Structures* (ed. H. Sakai, H. Mohri and G. G. Borisy). Academic Press, Tokyo.

Kumagai, A., and Dunphy, W. G. 1996. Purification and molecular cloning of Plx1, a Cdc25-regulatory kinase from Xenopus egg extracts. Science 273:1377-1380.

Kwok, B. H., and Kapoor, T. M. 2007. Microtubule flux: drivers wanted. Curr Opin Cell Biol 19:36-42.

Kwon, M., Morales-Mulia, S., Brust-Mascher, I., Rogers, G. C., Sharp, D. J., and Scholey, J. M. 2004. The chromokinesin, KLP3A, dives mitotic spindle pole separation during prometaphase and anaphase and facilitates chromatid motility. Mol Biol Cell 15:219-233.

Labbe, J. C., McCarthy, E. K., and Goldstein, B. 2004. The forces that position a mitotic spindle asymmetrically are tethered until after the time of spindle assembly. J Cell Biol 167:245-256.

LaFountain, J. R., Jr., Cohan, C. S., Siegel, A. J., and LaFountain, D. J. 2004. Direct visualization of microtubule flux during metaphase and anaphase in crane-fly spermatocytes. Mol Biol Cell 15:5724-5732.

Lan, W., Zhang, X., Kline-Smith, S. L., Rosasco, S. E., Barrett-Wilt, G. A., Shabanowitz, J., Hunt, D. F., Walczak, C. E., and Stukenberg, P. T. 2004. Aurora B phosphorylates centromeric MCAK and regulates its localization and microtubule depolymerization activity. Curr Biol 14:273-286.

Lane, H. A., and Nigg, E. A. 1996. Antibody microinjection reveals an essential role for human polo-like kinase 1 (Plk1) in the functional maturation of mitotic centrosomes. J Cell Biol 135:1701-1713.

Laycock, J. E., Savoian, M. S., and Glover, D. M. 2006. Antagonistic activities of Klp10A and Orbit regulate spindle length, bipolarity and function in vivo. J Cell Sci 119:2354-2361.

Ledbetter, M. C., and Porter, K. R. 1963. A "Microtubule" in Plant Cell Fine Structure. J Cell Biol 19:239-250.

Lemos, C. L., Sampaio, P., Maiato, H., Costa, M., Omel'yanchuk, L. V., Liberal, V., and Sunkel, C. E. 2000. Mast, a conserved microtubule-associated protein required for bipolar mitotic spindle organization. EMBO J 19:3668-3682.

Leslie, R. J., and Pickett-Heaps, J. D. 1983. Ultraviolet microbeam irradiations of mitotic diatoms: investigation of spindle elongation. J Cell Biol 96:548-561.

Li, R., and Murray, A. W. 1991. Feedback control of mitosis in budding yeast. Cell 66:519-531.

Li, X., and Nicklas, R. B. 1995. Mitotic forces control a cell-cycle checkpoint. Nature 373:630-632.

Lince-Faria, M., Maffini, S., Orr, B., Ding, Y., Claudia, F., Sunkel, C. E., Tavares, A., Johansen, J., Johansen, K. M., and Maiato, H. 2009. Spatiotemporal control of mitosis by the conserved spindle matrix protein Megator. J Cell Biol 184:647-657.

Lindqvist, A., Rodriguez-Bravo, V., and Medema, R. H. 2009. The decision to enter mitosis: feedback and redundancy in the mitotic entry network. J Cell Biol 185:193-202.

Liu, D., Vader, G., Vromans, M. J., Lampson, M. A., and Lens, S. M. 2009. Sensing Chromosome Bi-Orientation by Spatial Separation of Aurora B Kinase from Kinetochore Substrates. Science.

Logarinho, E., Bousbaa, H., Dias, J. M., Lopes, C., Amorim, I., Antunes-Martins, A., and Sunkel, C. E. 2004. Different spindle checkpoint proteins monitor microtubule attachment and tension at kinetochores in Drosophila cells. J Cell Sci 117:1757-1771.

Lohka, M. J., Hayes, M. K., and Maller, J. L. 1988. Purification of maturation-promoting factor, an intracellular regulator of early mitotic events. Proc Natl Acad Sci U S A 85:3009-3013.

Loiodice, I., Staub, J., Setty, T. G., Nguyen, N. P., Paoletti, A., and Tran, P. T. 2005. Ase1p organizes antiparallel microtubule arrays during interphase and mitosis in fission yeast. Mol Biol Cell 16:1756-1768.

Lombillo, V. A., Stewart, R. J., and McIntosh, J. R. 1995. Minus-end-directed motion of kinesin-coated microspheres driven by microtubule depolymerization. Nature 373:161-164.

Maddox, P., Desai, A., Oegema, K., Mitchison, T. J., and Salmon, E. D. 2002. Poleward microtubule flux is a major component of spindle dynamics and anaphase a in mitotic Drosophila embryos. Curr Biol 12:1670-1674.

Maddox, P., Straight, A., Coughlin, P., Mitchison, T. J., and Salmon, E. D. 2003. Direct observation of microtubule dynamics at kinetochores in Xenopus extract spindles: implications for spindle mechanics. J Cell Biol 162:377-382.

Maddox, P. S., Bloom, K. S., and Salmon, E. D. 2000. The polarity and dynamics of microtubule assembly in the budding yeast Saccharomyces cerevisiae. Nat Cell Biol 2:36-41.

Maffini, S., Maia, A. R., Manning, A. L., Maliga, Z., Pereira, A. L., Junqueira, M., Shevchenko, A., Hyman, A., Yates, J. R., 3rd, Galjart, N., Compton, D. A., and Maiato, H. 2009. Motor-independent targeting of CLASPs to kinetochores by CENP-E promotes microtubule turnover and poleward flux. Curr Biol 19:1566-1572.

Mahoney, N. M., Goshima, G., Douglass, A. D., and Vale, R. D. 2006. Making microtubules and mitotic spindles in cells without functional centrosomes. Current Biology: CB 16:564-569.

Maiato, H., Sampaio, P., Lemos, C. L., Findlay, J., Carmena, M., Earnshaw, W. C., and Sunkel, C. E. 2002. MAST/Orbit has a role in microtubule-kinetochore attachment and is essential for chromosome alignment and maintenance of spindle bipolarity. J Cell Biol 157:749-760.

Maiato, H., Fairley, E. A., Rieder, C. L., Swedlow, J. R., Sunkel, C. E., and Earnshaw, W. C. 2003a. Human CLASP1 is an outer kinetochore component that regulates spindle microtubule dynamics. Cell 113:891-904.

Maiato, H., Sunkel, C. E., and Earnshaw, W. C. 2003b. Dissecting mitosis by RNAi in Drosophila tissue culture cells. Biol Proced Online 5:153-161.

Maiato, H., DeLuca, J., Salmon, E. D., and Earnshaw, W. C. 2004a. The dynamic kinetochore-microtubule interface. J Cell Sci 117:5461-5477.

Maiato, H., Rieder, C. L., and Khodjakov, A. 2004b. Kinetochore-driven formation of kinetochore fibers contributes to spindle assembly during animal mitosis. J Cell Biol 167:831-840.

Maiato, H., Sampaio, P., and Sunkel, C. E. 2004c. Microtubule-associated proteins and their essential roles during mitosis. Int Rev Cytol 241:53-153.

Maiato, H., Khodjakov, A., and Rieder, C. L. 2005. Drosophila CLASP is required for the incorporation of microtubule subunits into fluxing kinetochore fibres. Nat Cell Biol 7:42-47.

Maiato, H., and Lince-Faria, M. 2010. The perpetual movements of anaphase. Cell. Mol. Life Sci. (in press).

Malumbres, M., and Barbacid, M. 2001. To cycle or not to cycle: a critical decision in cancer. Nat Rev Cancer 1:222-231.

Malumbres, M., and Barbacid, M. 2009. Cell cycle, CDKs and cancer: a changing paradigm. Nat Rev Cancer 9:153-166.

Malumbres, M., Harlow, E., Hunt, T., Hunter, T., Lahti, J. M., Manning, G., Morgan, D. O., Tsai, L. H., and Wolgemuth, D. J. 2009. Cyclin-dependent kinases: a family portrait. Nat Cell Biol 11:1275-1276.

Manning, A. L., and Compton, D. A. 2007. Mechanisms of spindle-pole organization are influenced by kinetochore activity in mammalian cells. Curr Biol 17:260-265.

Maresca, T. J., and Salmon, E. D. 2009. Intrakinetochore stretch is associated with changes in kinetochore phosphorylation and spindle assembly checkpoint activity. J Cell Biol.

Maresca, T. J., and Salmon, E. D. 2010. Welcome to a new kind of tension: translating kinetochore mechanics into a wait-anaphase signal. J Cell Sci 123:825-835.

Margolis, R. L., and Wilson, L. 1978. Opposite end assembly and disassembly of microtubules at steady state in vitro. Cell 13:1-8.

Margolis, R. L., Wilson, L., and Keifer, B. I. 1978. Mitotic mechanism based on intrinsic microtubule behaviour. Nature 272:450-452.

Margolis, R. L., and Wilson, L. 1981. Microtubule treadmills--possible molecular machinery. Nature 293:705-711.

Matos, I., Pereira, A. J., Lince-Faria, M., Cameron, L. A., Salmon, E. D., and Maiato, H. 2009. Synchronizing chromosome segregation by flux-dependent force equalization at kinetochores. J Cell Biol 186:11-26.

Mazia, D., and Dan, K. 1952. The Isolation and Biochemical Characterization of the Mitotic Apparatus of Dividing Cells. Proc Natl Acad Sci U S A 38:826-838.

Mazia, D. 1961. Mitosis and the physiology of Cell Division. *In* "the Cell" (J. Brachet and A. E. Mirsky, eds). Academic Press, New York.

Mazia, D. 1984. Centrosomes and mitotic poles. Exp Cell Res 153:1-15.

Mazumdar, M., Sundareshan, S., and Misteli, T. 2004. Human chromokinesin KIF4A functions in chromosome condensation and segregation. J Cell Biol 166:613-620.

McIntosh, J. R., Cande, W. Z., and Snyder, J. A. 1975. Structure and physiology of the mammalian mitotic spindle. Pp. 31-76 *in* S. Inoue, and R. E. Stephens, eds. Molecules and Cell Movement. Raven Press, New York.

McIntosh, J. R., Grishchuk, E. L., Morphew, M. K., Efremov, A. K., Zhudenkov, K., Volkov, V. A., Cheeseman, I. M., Desai, A., Mastronarde, D. N., and Ataullakhanov, F. I. 2008. Fibrils connect microtubule tips with kinetochores: a mechanism to couple tubulin dynamics to chromosome motion. Cell 135:322-333.

McKim, K. S., and Hawley, R. S. 1995. Chromosomal control of meiotic cell division. Science 270:1595-1601.

Meraldi, P., Draviam, V. M., and Sorger, P. K. 2004. Timing and checkpoints in the regulation of mitotic progression. Dev Cell 7:45-60.

Merdes, A., Ramyar, K., Vechio, J. D., and Cleveland, D. W. 1996. A complex of NuMA and cytoplasmic dynein is essential for mitotic spindle assembly. Cell 87:447-458.

Miller, P. M., Folkmann, A. W., Maia, A. R., Efimova, N., Efimov, A., and Kaverina, I. 2009. Golgi-derived CLASP-dependent microtubules control Golgi organization and polarized trafficking in motile cells. Nat Cell Biol 11:1069-1080.

Miller, S. A., Johnson, M. L., and Stukenberg, P. T. 2008. Kinetochore attachments require an interaction between unstructured tails on microtubules and Ndc80(Hec1). Curr Biol 18:1785-1791.

Miranda, J. J., De Wulf, P., Sorger, P. K., and Harrison, S. C. 2005. The yeast DASH complex forms closed rings on microtubules. Nat Struct Mol Biol 12:138-143.

Mitchison, T., and Kirschner, M. 1984a. Microtubule assembly nucleated by isolated centrosomes. Nature 312:232-237.

Mitchison, T., and Kirschner, M. 1984b. Dynamic instability of microtubule growth. Nature 312:237-242.

Mitchison, T., Evans, L., Schulze, E., and Kirschner, M. 1986. Sites of microtubule assembly and disassembly in the mitotic spindle. Cell 45:515-527.

Mitchison, T. J. 1989. Polewards microtubule flux in the mitotic spindle: evidence from photoactivation of fluorescence. J Cell Biol 109:637-652.

Mitchison, T. J., and Salmon, E. D. 1992. Poleward kinetochore fiber movement occurs during both metaphase and anaphase-A in newt lung cell mitosis. J Cell Biol 119:569-582.

Mitchison, T. J., and Salmon, E. D. 2001. Mitosis: a history of division. Nat Cell Biol 3:E17-21.

Mitchison, T. J. 2005. Mechanism and function of poleward flux in Xenopus extract meiotic spindles. Philos Trans R Soc Lond B Biol Sci 360:623-629.

Miyamoto, D. T., Perlman, Z. E., Burbank, K. S., Groen, A. C., and Mitchison, T. J. 2004. The kinesin Eg5 drives poleward microtubule flux in Xenopus laevis egg extract spindles. J Cell Biol 167:813-818.

Moores, C. A., and Milligan, R. A. 2006. Lucky 13-microtubule depolymerisation by kinesin-13 motors. J Cell Sci 119:3905-3913.

Morales-Mulia, S., and Scholey, J. M. 2005. Spindle pole organization in Drosophila S2 cells by dynein, abnormal spindle protein (Asp), and KLP10A. Mol Biol Cell 16:3176-3186.

Morgan, D. O. 1997. Cyclin-dependent kinases: engines, clocks, and microprocessors. Annu Rev Cell Dev Biol 13:261-291.

Morgan, D. O. 2007. The cell cycle : principles of control. New Science Press; Sinauer Associates, London, Sunderland, MA.

Moritz, M., Braunfeld, M. B., Guenebaut, V., Heuser, J., and Agard, D. A. 2000. Structure of the gamma-tubulin ring complex: a template for microtubule nucleation. Nat Cell Biol 2:365-370.

Mota, M. 1957. A new hypothesis of the anaphase movement. In Proceedings of the International Genetics Symposia (1956). Cytologia, Supplement:pp. 113-116.

Moutinho-Pereira, S., Debec, A., and Maiato, H. 2009. Microtubule cytoskeleton remodeling by acentriolar microtubule-organizing centers at the entry and exit from mitosis in Drosophila somatic cells. Mol Biol Cell 20:2796-2808.

Moutinho-Pereira, S., Matos, I., and Maiato, H. 2010. Drosophila S2 cells as a model system to investigate mitotic spindle dynamics, architecture and function. Methods in Cell Biology (in press).

Mulder, A. M., Glavis-Bloom, A., Moores, C. A., Wagenbach, M., Carragher, B., Wordeman, L., and Milligan, R. A. 2009. A new model for binding of kinesin 13 to curved microtubule protofilaments. J Cell Biol 185:51-57.

Murata, T., Sonobe, S., Baskin, T. I., Hyodo, S., Hasezawa, S., Nagata, T., Horio, T., and Hasebe, M. 2005. Microtubule-dependent microtubule nucleation based on recruitment of gamma-tubulin in higher plants. Nat Cell Biol 7:961-968.

Musacchio, A., and Salmon, E. D. 2007. The spindle-assembly checkpoint in space and time. Nat Rev Mol Cell Biol 8:379-393.

Nasmyth, K., Peters, J. M., and Uhlmann, F. 2000. Splitting the chromosome: cutting the ties that bind sister chromatids. Science 288:1379-1385.

Nicklas, R. B., and Koch, C. A. 1969. Chromosome micromanipulation. 3. Spindle fiber tension and the reorientation of mal-oriented chromosomes. J Cell Biol 43:40-50.

Nicklas, R. B. 1988. The forces that move chromosomes in mitosis. Annu Rev Biophys Biophys Chem 17:431-449.

Nicklas, R. B. 1989. The motor for poleward chromosome movement in anaphase is in or near the kinetochore. J Cell Biol 109:2245-2255.

Nicklas, R. B., and Ward, S. C. 1994. Elements of error correction in mitosis: microtubule capture, release, and tension. J Cell Biol 126:1241-1253.

Nicklas, R. B., Ward, S. C., and Gorbsky, G. J. 1995. Kinetochore chemistry is sensitive to tension and may link mitotic forces to a cell cycle checkpoint. J Cell Biol 130:929-939.

Nigg, E. A., and Raff, J. W. 2009. Centrioles, centrosomes, and cilia in health and disease. Cell 139:663-678.

Nurse, P. 1975. Genetic control of cell size at cell division in yeast. Nature 256:547-551.

Nurse, P. 1990. Universal control mechanism regulating onset of M-phase. Nature 344:503-508.

Nurse, P. 2000. A long twentieth century of the cell cycle and beyond. Cell 100:71-78.

O'Connell, C. B., Loncarek, J., Hergert, P., Kourtidis, A., Conklin, D. S., and Khodjakov, A. 2008. The spindle assembly checkpoint is satisfied in the absence of interkinetochore tension during mitosis with unreplicated genomes. J Cell Biol 183:29-36.

Oegema, K., and Hyman, A. A. 2006. Cell division. WormBook:1-40.

Oladipo, A., Cowan, A., and Rodionov, V. 2007. Microtubule motor Ncd induces sliding of microtubules in vivo. Mol Biol Cell 18:3601-3606.

Orr, B., Bousbaa, H., and Sunkel, C. E. 2007. Mad2-independent spindle assembly checkpoint activation and controlled metaphase-anaphase transition in Drosophila S2 cells. Mol Biol Cell 18:850-863.

Ostergren, G. 1951. The mechanism of co-orientation in bivalents and multivalents. The theory of orientation by pulling. Hereditas 37:85-156.

Ostergren, G., Mole-Bajer, J., and Bajer, A. 1960. An interpretation of transport phenomena at mitosis. Ann N Y Acad Sci 90:381-408.

Paschal, B. M., Shpetner, H. S., and Vallee, R. B. 1987. MAP 1C is a microtubule-activated ATPase which translocates microtubules in vitro and has dynein-like properties. J Cell Biol 105:1273-1282.

Paweletz, N. 2001. Walther Flemming: pioneer of mitosis research. Nat Rev Mol Cell Biol 2:72-75.

Pellman, D., Bagget, M., Tu, Y. H., Fink, G. R., and Tu, H. 1995. Two microtubule-associated proteins required for anaphase spindle movement in Saccharomyces cerevisiae. J Cell Biol 130:1373-1385.

Pereira, A. J., Matos, I., Lince-Faria, M., and Maiato, H. 2009. Dissecting mitosis with laser microsurgery and RNAi in Drosophila cells. Methods Mol Biol 545:145-164.

Pereira, A. J., and Maiato, H. 2010. Improved kymography tools and its applications to mitosis. Methods.

Pereira, A. L., Pereira, A. J., Maia, A. R., Drabek, K., Sayas, C. L., Hergert, P. J., Lince-Faria, M., Matos, I., Duque, C., Stepanova, T., Rieder, C. L., Earnshaw, W. C., Galjart, N., and Maiato, H. 2006. Mammalian CLASP1 and CLASP2 cooperate to ensure mitotic fidelity by regulating spindle and kinetochore function. Mol Biol Cell 17:4526-4542.

Peterman, E. J., and Scholey, J. M. 2009. Mitotic microtubule crosslinkers: insights from mechanistic studies. Curr Biol 19:R1089-1094.

Peters, J. M. 2006. The anaphase promoting complex/cyclosome: a machine designed to destroy. Nat Rev Mol Cell Biol 7:644-656.

Pfarr, C. M., Coue, M., Grissom, P. M., Hays, T. S., Porter, M. E., and McIntosh, J. R. 1990. Cytoplasmic dynein is localized to kinetochores during mitosis. Nature 345:263-265.

Pickett-Heaps, J., and Forer, A. 2009. Mitosis: spindle evolution and the matrix model. Protoplasma 235:91-99.

Pickett-Heaps, J. D., Forer, A., and Spurck, T. 1996. Rethinking anaphase: where "Pac-Man" fails and why a role for the spindle matrix is likely. Protoplasma 192:1-10.

Pickett-Heaps, J. D., Forer, A., and Spurck, T. 1997. Traction fibre: toward a "tensegral" model of the spindle. Cell Motil Cytoskeleton 37:1-6.

Pickett-Heaps, J. D., and Forer, A. 2001. Pac-Man does not resolve the enduring problem of anaphase chromosome movement. Protoplasma 215:16-20.

Piel, M., Nordberg, J., Euteneuer, U., and Bornens, M. 2001. Centrosome-dependent exit of cytokinesis in animal cells. Science 291:1550-1553.

Piel, M., and Tran, P. T. 2009. Cell shape and cell division in fission yeast. Curr Biol 19:R823-827.

Pines, J., and Rieder, C. L. 2001. Re-staging mitosis: a contemporary view of mitotic progression. Nat Cell Biol 3:E3-6.

Pinsky, B. A., and Biggins, S. 2005. The spindle checkpoint: tension versus attachment. Trends Cell Biol 15:486-493.

Pinsky, B. A., Kung, C., Shokat, K. M., and Biggins, S. 2006. The Ipl1-Aurora protein kinase activates the spindle checkpoint by creating unattached kinetochores. Nat Cell Biol 8:78-83.

Powers, A. F., Franck, A. D., Gestaut, D. R., Cooper, J., Gracyzk, B., Wei, R. R., Wordeman, L., Davis, T. N., and Asbury, C. L. 2009. The Ndc80 kinetochore complex forms load-bearing attachments to dynamic microtubule tips via biased diffusion. Cell 136:865-875.

Rath, U., Rogers, G. C., Tan, D., Gomez-Ferreria, M. A., Buster, D. W., Sosa, H. J., and Sharp, D. J. 2009. The Drosophila kinesin-13, KLP59D, impacts Pacman- and Flux-based chromosome movement. Mol Biol Cell 20:4696-4705.

Reis, R., Feijao, T., Gouveia, S., Pereira, A. J., Matos, I., Sampaio, P., Maiato, H., and Sunkel, C. E. 2009. Dynein and mast/orbit/CLASP have antagonistic roles in regulating kinetochore-microtubule plus-end dynamics. J Cell Sci 122:2543-2553.

Rieder, C. L., and Salmon, E. D. 1994. Motile kinetochores and polar ejection forces dictate chromosome position on the vertebrate mitotic spindle. J Cell Biol 124:223-233.

Rieder, C. L., Cole, R. W., Khodjakov, A., and Sluder, G. 1995. The checkpoint delaying anaphase in response to chromosome monoorientation is mediated by an inhibitory signal produced by unattached kinetochores. J Cell Biol 130:941-948.

Rieder, C. L., and Cole, R. W. 1998. Entry into mitosis in vertebrate somatic cells is guarded by a chromosome damage checkpoint that reverses the cell cycle when triggered during early but not late prophase. J Cell Biol 142:1013-1022.

Rodionov, V. I., and Borisy, G. G. 1997. Microtubule treadmilling in vivo. Science 275:215-218.

Rodrigues-Martins, A., Riparbelli, M., Callaini, G., Glover, D. M., and Bettencourt-Dias, M. 2007. Revisiting the role of the mother centriole in centriole biogenesis. Science 316:1046-1050.

Rogers, G. C., Rogers, S. L., Schwimmer, T. A., Ems-McClung, S. C., Walczak, C. E., Vale, R. D., Scholey, J. M., and Sharp, D. J. 2004. Two mitotic kinesins cooperate to drive sister chromatid separation during anaphase. Nature 427:364-370.

Rogers, G. C., Rogers, S. L., and Sharp, D. J. 2005. Spindle microtubules in flux. J Cell Sci 118:1105-1116.

Roychowdhury, S., Panda, D., Wilson, L., and Rasenick, M. M. 1999. G protein alpha subunits activate tubulin GTPase and modulate microtubule polymerization dynamics. J Biol Chem 274:13485-13490.

Sabatini, D. D., Bensch, K., and Barrnett, R. J. 1963. Cytochemistry and electron microscopy. The preservation of cellular ultrastructure and enzymatic activity by aldehyde fixation. J Cell Biol 17:19-58.

Salmon, E. D., Leslie, R. J., Saxton, W. M., Karow, M. L., and McIntosh, J. R. 1984. Spindle microtubule dynamics in sea urchin embryos: analysis using a fluorescein-labeled tubulin and measurements of fluorescence redistribution after laser photobleaching. J Cell Biol 99:2165-2174.

Santaguida, S., and Musacchio, A. 2009. The life and miracles of kinetochores. EMBO J 28:2511-2531.

Saunders, A. M., Powers, J., Strome, S., and Saxton, W. M. 2007. Kinesin-5 acts as a brake in anaphase spindle elongation. Curr Biol 17:R453-454.

Saunders, W. S., Koshland, D., Eshel, D., Gibbons, I. R., and Hoyt, M. A. 1995. Saccharomyces cerevisiae kinesin- and dynein-related proteins required for anaphase chromosome segregation. J Cell Biol 128:617-624.

Sawin, K. E., and Mitchison, T. J. 1991. Poleward microtubule flux mitotic spindles assembled in vitro. J Cell Biol 112:941-954.

Saxton, W. M., Stemple, D. L., Leslie, R. J., Salmon, E. D., Zavortink, M., and McIntosh, J. R. 1984. Tubulin dynamics in cultured mammalian cells. J Cell Biol 99:2175-2186.

Saxton, W. M., and McIntosh, J. R. 1987. Interzone microtubule behavior in late anaphase and telophase spindles. J Cell Biol 105:875-886.

Schliwa, M., and Woehlke, G. 2003. Molecular motors. Nature 422:759-765.

Schmit, A. C., and Lambert, A. M. 1990. Microinjected fluorescent phalloidin in vivo reveals the F-actin dynamics and assembly in higher plant mitotic cells. Plant Cell 2:129-138.

Schmit, A. C. 2002. Acentrosomal microtubule nucleation in higher plants. Int Rev Cytol 220:257-289.

Scholey, J. M., and Mogilner, A. 2003. Mitotic Spindle Motors: In Molecular motors (ed. Schliwa, M.). Wiley-VCH, Weinheim [Great Britain].

Schrader, F. 1944. Mitosis, the movements of chromosomes in cell division. Columbia University Press, New York.

Schuh, M., and Ellenberg, J. 2007. Self-organization of MTOCs replaces centrosome function during acentrosomal spindle assembly in live mouse oocytes. Cell 130:484-498.

Sharp, D. J., Yu, K. R., Sisson, J. C., Sullivan, W., and Scholey, J. M. 1999. Antagonistic microtubule-sliding motors position mitotic centrosomes in Drosophila early embryos. Nat Cell Biol 1:51-54.

Sharp, D. J., Brown, H. M., Kwon, M., Rogers, G. C., Holland, G., and Scholey, J. M. 2000a. Functional coordination of three mitotic motors in Drosophila embryos. Mol Biol Cell 11:241-253.

Sharp, D. J., Rogers, G. C., and Scholey, J. M. 2000b. Microtubule motors in mitosis. Nature 407:41-47.

Sharp, D. J., Rogers, G. C., and Scholey, J. M. 2000c. Cytoplasmic dynein is required for poleward chromosome movement during mitosis in Drosophila embryos. Nat Cell Biol 2:922-930.

Shelden, E., and Wadsworth, P. 1990. Interzonal microtubules are dynamic during spindle elongation. J Cell Sci 97 (Pt 2):273-281.

Shirasu-Hiza, M., Perlman, Z. E., Wittmann, T., Karsenti, E., and Mitchison, T. J. 2004. Eg5 causes elongation of meiotic spindles when flux-associated microtubule depolymerization is blocked. Curr Biol 14:1941-1945.

Silk, A. D., Holland, A. J., and Cleveland, D. W. 2009. Requirements for NuMA in maintenance and establishment of mammalian spindle poles. J Cell Biol 184:677-690.

Simon, J. R., Parsons, S. F., and Salmon, E. D. 1992. Buffer conditions and non-tubulin factors critically affect the microtubule dynamic instability of sea urchin egg tubulin. Cell Motil Cytoskeleton 21:1-14.

Skoufias, D. A., Andreassen, P. R., Lacroix, F. B., Wilson, L., and Margolis, R. L. 2001. Mammalian mad2 and bub1/bubR1 recognize distinct spindle-attachment and kinetochore-tension checkpoints. Proc Natl Acad Sci U S A 98:4492-4497.

Snyder, J. A., and McIntosh, J. R. 1975. Initiation and growth of microtubules from mitotic centers in lysed mammalian cells. J Cell Biol 67:744-760.

Steigemann, P., Wurzenberger, C., Schmitz, M. H., Held, M., Guizetti, J., Maar, S., and Gerlich, D. W. 2009. Aurora B-mediated abscission checkpoint protects against tetraploidization. Cell 136:473-484.

Steuer, E. R., Wordeman, L., Schroer, T. A., and Sheetz, M. P. 1990. Localization of cytoplasmic dynein to mitotic spindles and kinetochores. Nature 345:266-268.

Straight, A. F., Marshall, W. F., Sedat, J. W., and Murray, A. W. 1997. Mitosis in living budding yeast: anaphase A but no metaphase plate. Science 277:574-578.

Straight, A. F., Sedat, J. W., and Murray, A. W. 1998. Time-lapse microscopy reveals unique roles for kinesins during anaphase in budding yeast. J Cell Biol 143:687-694.

Sullivan, M., and Morgan, D. O. 2007. Finishing mitosis, one step at a time. Nat Rev Mol Cell Biol 8:894-903.

Tan, D., Asenjo, A. B., Mennella, V., Sharp, D. J., and Sosa, H. 2006. Kinesin-13s form rings around microtubules. J Cell Biol 175:25-31.

Theodoropoulos, P. A., Polioudaki, H., Kostaki, O., Derdas, S. P., Georgoulias, V., Dargemont, C., and Georgatos, S. D. 1999. Taxol affects nuclear lamina and pore complex organization and inhibits import of karyophilic proteins into the cell nucleus. Cancer Res 59:4625-4633.

Tokai, N., Fujimoto-Nishiyama, A., Toyoshima, Y., Yonemura, S., Tsukita, S., Inoue, J., and Yamamota, T. 1996. Kid, a novel kinesin-like DNA binding protein, is localized to chromosomes and the mitotic spindle. EMBO J 15:457-467.

Tolic-Norrelykke, I. M., Sacconi, L., Thon, G., and Pavone, F. S. 2004. Positioning and elongation of the fission yeast spindle by microtubule-based pushing. Curr Biol 14:1181-1186.

Tolic-Norrelykke, I. M. 2008. Push-me-pull-you: how microtubules organize the cell interior. Eur Biophys J 37:1271-1278.

Toyoshima-Morimoto, F., Taniguchi, E., Shinya, N., Iwamatsu, A., and Nishida, E. 2001. Polo-like kinase 1 phosphorylates cyclin B1 and targets it to the nucleus during prophase. Nature 410:215-220.

Trammell, M. A., Mahoney, N. M., Agard, D. A., and Vale, R. D. 2008. Mob4 plays a role in spindle focusing in Drosophila S2 cells. J Cell Sci 121:1284-1292.

Tran, P. T., Marsh, L., Doye, V., Inoue, S., and Chang, F. 2001. A mechanism for nuclear positioning in fission yeast based on microtubule pushing. J Cell Biol 153:397-411.

Tucker, J. D., and Preston, R. J. 1996. Chromosome aberrations, micronuclei, aneuploidy, sister chromatid exchanges, and cancer risk assessment. Mutat Res 365:147-159.

Tulu, U. S., Rusan, N. M., and Wadsworth, P. 2003. Peripheral, non-centrosome-associated microtubules contribute to spindle formation in centrosome-containing cells. Curr Biol 13:1894-1899.

Tulu, U. S., Fagerstrom, C., Ferenz, N. P., and Wadsworth, P. 2006. Molecular requirements for kinetochore-associated microtubule formation in mammalian cells. Curr Biol 16:536-541.

Uchida, K. S., Takagaki, K., Kumada, K., Hirayama, Y., Noda, T., and Hirota, T. 2009. Kinetochore stretching inactivates the spindle assembly checkpoint. J Cell Biol.

Uhlmann, F., and Nasmyth, K. 1998. Cohesion between sister chromatids must be established during DNA replication. Curr Biol 8:1095-1101.

Urbani, L., and Stearns, T. 1999. The centrosome. Curr Biol 9:R315-317.

Vale, R. D., Reese, T. S., and Sheetz, M. P. 1985. Identification of a novel force-generating protein, kinesin, involved in microtubule-based motility. Cell 42:39-50.

Van Beneden, E. 1883. Recherches sur la maturation de l'oeuf et la fécondation. Arch. Biol. 4:265-640.

Wakefield, J. G., Bonaccorsi, S., and Gatti, M. 2001. The drosophila protein asp is involved in microtubule organization during spindle formation and cytokinesis. J Cell Biol 153:637-648.

Walczak, C. E., and Heald, R. 2008. Mechanisms of mitotic spindle assembly and function. Int Rev Cytol 265:111-158.

Walczak, C. E., Cai, S., and Khodjakov, A. 2010. Mechanisms of chromosome behaviour during mitosis. Nat Rev Mol Cell Biol 11:91-102.

Walker, R. A., O'Brien, E. T., Pryer, N. K., Soboeiro, M. F., Voter, W. A., Erickson, H. P., and Salmon, E. D. 1988. Dynamic instability of individual microtubules analyzed by video light microscopy: rate constants and transition frequencies. J Cell Biol 107:1437-1448.

Wan, X., O'Quinn, R. P., Pierce, H. L., Joglekar, A. P., Gall, W. E., DeLuca, J. G., Carroll, C. W., Liu, S. T., Yen, T. J., McEwen, B. F., Stukenberg, P. T., Desai, A., and Salmon, E. D. 2009. Protein architecture of the human kinetochore microtubule attachment site. Cell 137:672-684.

Waterman-Storer, C. M., Desai, A., Bulinski, J. C., and Salmon, E. D. 1998. Fluorescent speckle microscopy, a method to visualize the dynamics of protein assemblies in living cells. Curr Biol 8:1227-1230.

Waters, J. C., Cole, R. W., and Rieder, C. L. 1993. The force-producing mechanism for centrosome separation during spindle formation in vertebrates is intrinsic to each aster. J Cell Biol 122:361-372.

Waters, J. C., Mitchison, T. J., Rieder, C. L., and Salmon, E. D. 1996. The kinetochore microtubule minus-end disassembly associated with poleward flux produces a force that can do work. Mol Biol Cell 7:1547-1558.

Waters, J. C., Chen, R. H., Murray, A. W., and Salmon, E. D. 1998. Localization of Mad2 to kinetochores depends on microtubule attachment, not tension. J Cell Biol 141:1181-1191.

Welburn, J. P., and Cheeseman, I. M. 2008. Toward a molecular structure of the eukaryotic kinetochore. Dev Cell 15:645-655.

Wells, W. A. 1996. The spindle-assembly checkpoint: aiming for a perfect mitosis, every time. Trends Cell Biol 6:228-234.

Westermann, S., Avila-Sakar, A., Wang, H. W., Niederstrasser, H., Wong, J., Drubin, D. G., Nogales, E., and Barnes, G. 2005. Formation of a dynamic kinetochore- microtubule interface through assembly of the Dam1 ring complex. Mol Cell 17:277-290.

Westermann, S., Wang, H. W., Avila-Sakar, A., Drubin, D. G., Nogales, E., and Barnes, G. 2006. The Dam1 kinetochore ring complex moves processively on depolymerizing microtubule ends. Nature 440:565-569.

Wheatley, S. P., Hinchcliffe, E. H., Glotzer, M., Hyman, A. A., Sluder, G., and Wang, Y. 1997. CDK1 inactivation regulates anaphase spindle dynamics and cytokinesis in vivo. J Cell Biol 138:385-393.

Whyte, J., Bader, J. R., Tauhata, S. B., Raycroft, M., Hornick, J., Pfister, K. K., Lane, W. S., Chan, G. K., Hinchcliffe, E. H., Vaughan, P. S., and Vaughan, K. T. 2008. Phosphorylation regulates targeting of cytoplasmic dynein to kinetochores during mitosis. J Cell Biol 183:819-834.

Wilson, E. B. 1925. The cell in development and heredity. Macmillan, New York.

Wittmann, T., Wilm, M., Karsenti, E., and Vernos, I. 2000. TPX2, A novel xenopus MAP involved in spindle pole organization. J Cell Biol 149:1405-1418.

Wittmann, T., Hyman, A., and Desai, A. 2001. The spindle: a dynamic assembly of microtubules and motors. Nat Cell Biol 3:E28-34.

Wojcik, E., Basto, R., Serr, M., Scaerou, F., Karess, R., and Hays, T. 2001. Kinetochore dynein: its dynamics and role in the transport of the Rough deal checkpoint protein. Nat Cell Biol 3:1001-1007.

Wollman, R., Cytrynbaum, E. N., Jones, J. T., Meyer, T., Scholey, J. M., and Mogilner, A. 2005. Efficient chromosome capture requires a bias in the 'search-and-capture' process during mitotic-spindle assembly. Curr Biol 15:828-832.

Wollman, R., Civelekoglu-Scholey, G., Scholey, J. M., and Mogilner, A. 2008. Reverse engineering of force integration during mitosis in the Drosophila embryo. Mol Syst Biol 4:195.

Wordeman, L., Wagenbach, M., and von Dassow, G. 2007. MCAK facilitates chromosome movement by promoting kinetochore microtubule turnover. J Cell Biol 179:869-879.

Yanagida, M. 2009. Clearing the way for mitosis: is cohesin a target? Nat Rev Mol Cell Biol 10:489-496.

Yang, J., Bardes, E. S., Moore, J. D., Brennan, J., Powers, M. A., and Kornbluth, S. 1998. Control of cyclin B1 localization through regulated binding of the nuclear export factor CRM1. Genes Dev 12:2131-2143.

Yang, Z., Tulu, U. S., Wadsworth, P., and Rieder, C. L. 2007. Kinetochore dynein is required for chromosome motion and congression independent of the spindle checkpoint. Curr Biol 17:973-980.

Zhai, Y., Kronebusch, P. J., and Borisy, G. G. 1995. Kinetochore microtubule dynamics and the metaphase-anaphase transition. J Cell Biol 131:721-734.

Zhang, D., Rogers, G. C., Buster, D. W., and Sharp, D. J. 2007a. Three microtubule severing enzymes contribute to the "Pacman-flux" machinery that moves chromosomes. J Cell Biol 177:231-242.

Zhang, X., Lan, W., Ems-McClung, S. C., Stukenberg, P. T., and Walczak, C. E. 2007b. Aurora B phosphorylates multiple sites on mitotic centromere-associated kinesin to spatially and temporally regulate its function. Mol Biol Cell 18:3264-3276.

Zinkowski, R. P., Meyne, J., and Brinkley, B. R. 1991. The centromere-kinetochore complex: a repeat subunit model. J Cell Biol 113:1091-1110.

VI. ORIGINAL ARTICLES

ORIGINAL ARTICLES

De acordo com o artigo 8º do Decreto Lei nº 388/70, fazem parte integrante desta dissertação os seguintes trabalhos publicados (apenas o primeiro está na secção *original articles*):

I. **Matos, I*.**, Pereira, A. J.*, Lince-Faria, M., Cameron, L. A., Salmon, E. D., and Maiato, H. 2009. Synchronizing chromosome segregation by flux-dependent force equalization at kinetochores. J Cell Biol 186:11-26.

II. Moutinho-Pereira, S*., **Matos, I.***, and Maiato, H. 2010. *Drosophila* S2 cells as a model system to investigate mitotic spindle dynamics, architecture and function. Methods in Cell Biology (in press).

III. Pereira, A. J., **Matos**, **I.**, Lince-Faria, M., and Maiato, H. 2009. Dissecting mitosis with laser microsurgery and RNAi in Drosophila cells. Methods Mol Biol 545:145-164.

* os autores tiveram igual contributo para a realização do trabalho

O seguinte artigo não é parte integrante desta tese, mas nele é usada uma linha celular gerada no correr deste trabalho:

IV. Reis, R., Feijao,T., Gouveia, S., Pereira, A. J., **Matos, I.**, Sampaio, P., Maiato, H., and Sunkel, C. E. 2009. Dynein and mast/orbit/CLASP have antagonistic roles in regulating kinetochore-microtubule plus-end dynamics. J Cell Sci 122:2543-2553.

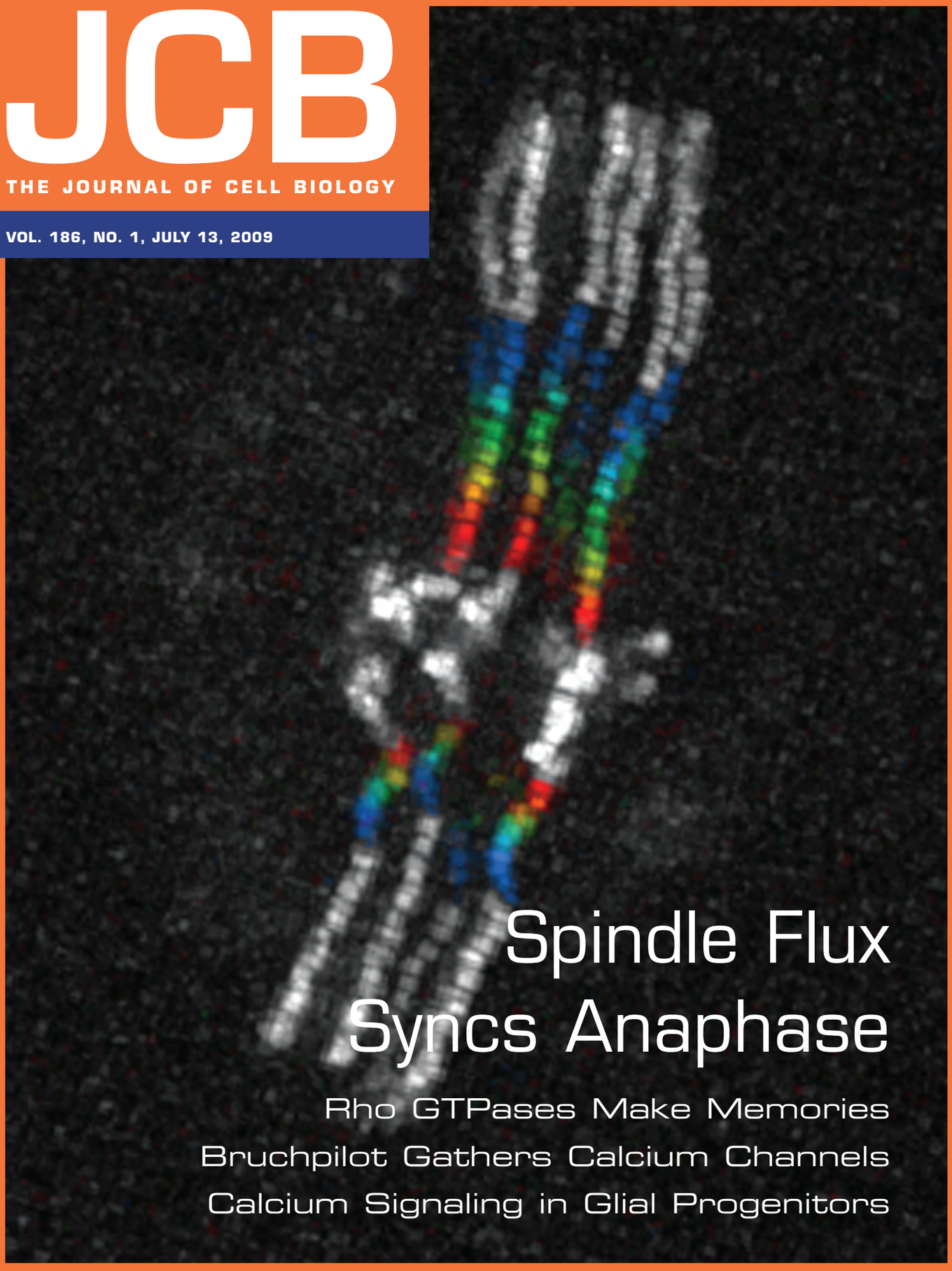
Em cumprimento do disposto no referido Decreto-Lei, declara que participou activamente na recolha e análise de dados e escreveu o artigo I e II com a colaboração dos co-autores. Declara ainda que participou activamente na recolha e análise de dados e colaborou na redação dos artigos III e IV.

Synchronizing chromosome segregation by flux-dependent force equalization at kinetochores.

Matos, I*., Pereira, A. J.*, Lince-Faria, M., Cameron, L. A., Salmon, E. D., and Maiato, H.

J Cell Biol 186:11-26. (2009)

JCB
THE JOURNAL OF CELL BIOLOGY
VOL. 186, NO. 1, JULY 13, 2009



Spindle Flux Syncs Anaphase

Rho GTPases Make Memories

Bruchpilot Gathers Calcium Channels

Calcium Signaling in Glial Progenitors

www.jcb.org

Published July 13, 2009

This article has original data in the JCB Data Viewer
http://jcb-dataviewer.rupress.org/jcb/browse/1402

Synchronizing chromosome segregation by flux-dependent force equalization at kinetochores

Irina Matos,[1] António J. Pereira,[1] Mariana Lince-Faria,[1] Lisa A. Cameron,[2] Edward D. Salmon,[2] and Helder Maiato[1,3]

[1]Instituto de Biologia Molecular e Celular, Universidade do Porto, 4150-180 Porto, Portugal
[2]Department of Biology, University of North Carolina, Chapel Hill, NC 27599
[3]Laboratory of Cell and Molecular Biology, Faculdade de Medicina, Universidade do Porto, 4200-319 Porto, Portugal

The synchronous movement of chromosomes during anaphase ensures their correct inheritance in every cell division. This reflects the uniformity of spindle forces acting on chromosomes and their simultaneous entry into anaphase. Although anaphase onset is controlled by the spindle assembly checkpoint, it remains unknown how spindle forces are uniformly distributed among different chromosomes. In this paper, we show that tension uniformity at metaphase kinetochores and subsequent anaphase synchrony in *Drosophila* S2 cells are promoted by spindle microtubule flux. These results can be explained by a mechanical model of the spindle where microtubule poleward translocation events associated with flux reflect relaxation of the kinetochore–microtubule interface, which accounts for the redistribution and convergence of kinetochore tensions in a timescale comparable to typical metaphase duration. As predicted by the model, experimental acceleration of mitosis precludes tension equalization and anaphase synchrony. We propose that flux-dependent equalization of kinetochore tensions ensures a timely and uniform maturation of kinetochore–microtubule interfaces necessary for error-free and coordinated segregation of chromosomes in anaphase.

Introduction

The sense and purpose of mitosis is revealed in its climax during anaphase, when sister chromatids migrate synchronously toward opposite poles. This critical task is accomplished by a highly dynamic microtubule (MT)-based apparatus: the mitotic spindle, which interacts with specialized structures at the centromere of each chromosome termed kinetochores (Maiato et al., 2004a). Anaphase synchrony prevents the occurrence of lagging chromosomes that could lead to the formation of micronuclei after nuclear envelope restoration or reversion of cleavage furrow ingression during cytokinesis. These cytological features may lead to aneuploidy or polyploidy, and have been associated with elevated risk of cancer in mammalian models and humans (Tucker and Preston, 1996; Ganem et al., 2007). In higher eukaryotic cells, anaphase synchrony is ensured by the strategic positioning of all chromosomes at the cell equator during metaphase and the strict coordination of sister chromatid separation. Although anaphase onset is regulated by the spindle assembly checkpoint (SAC), which ensures that all kinetochores are properly attached to the spindle before loss of sister chromatid cohesion (Musacchio and Salmon, 2007), the mechanism responsible for the uniform action of spindle forces at kinetochores remains to be elucidated.

During metaphase, many animal and plant spindles are characterized by a conspicuous "flux" activity due to continuous MT poleward translocation, while maintaining steady-state length (Mitchison, 1989; Rogers et al., 2005). Spatio-temporal scales of flux dictate that spindle MTs are fully recycled before anaphase, which results from continuous incorporation of tubulin subunits at kinetochores (Maiato et al., 2005) balanced by MT depolymerization at the poles (Rogers et al., 2004). In addition, sister kinetochores on metaphase chromosomes are pulled toward opposite poles by spindle forces that stretch the interconnecting centromeric chromatin. This tension is thought to control the maturation (King and Nicklas, 2000) and correction (Nicklas and Ward, 1994) of kinetochore–MT attachments before cells enter anaphase.

I. Matos and A.J. Pereira contributed equally to this paper.

Correspondence to Helder Maiato: maiato@ibmc.up.pt

Abbreviations used in this paper: CID, centromere identifier; CLASP, cytoplasmic linker associated protein; FSM, fluorescent speckle microscopy; ipMT, interpolar MT; kMT, kinetochore MT; MT, microtubule; ROI, region of interest; SAC, spindle assembly checkpoint.

© 2009 Matos et al. This article is distributed under the terms of an Attribution–Noncommercial–Share Alike–No Mirror Sites license for the first six months after the publication date (see http://www.jcb.org/misc/terms.shtml). After six months it is available under a Creative Commons License (Attribution–Noncommercial–Share Alike 3.0 Unported license, as described at http://creativecommons.org/licenses/by-nc-sa/3.0/).

Supplemental Material can be found at:
http://jcb.rupress.org/content/suppl/2009/07/06/jcb.200904153.DC1.html
Original image data can be found at:
http://jcb-dataviewer.rupress.org/jcb/browse/1402

The Rockefeller University Press $30.00
J. Cell Biol. Vol. 186 No. 1 11–26
www.jcb.org/cgi/doi/10.1083/jcb.200904153

THE JOURNAL OF CELL BIOLOGY

Downloaded from jcb.rupress.org on June 13, 2010

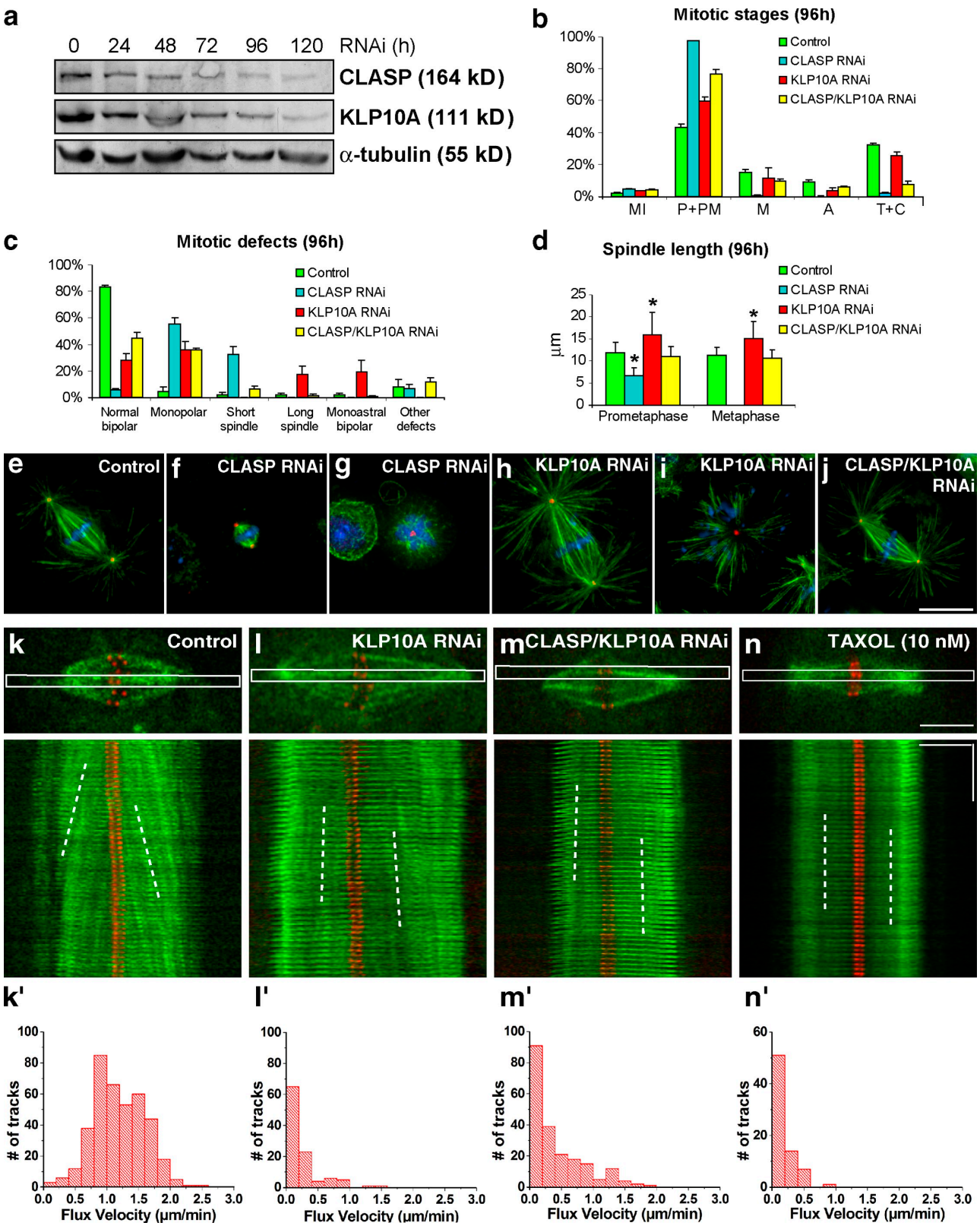


Figure 1. **Phenotypic analyses of CLASP, KLP10A, and CLASP/KLP10A RNAi in *Drosophila S2* cells.** (a) Western blot analysis after CLASP and KLP10A RNAi at different time points revealed a 70–90% reduction in protein levels after 96 h of RNAi treatment. α-tubulin was used as loading control. (b) Quantification of mitotic parameters reveals a significant rescue of the CLASP phenotype by simultaneous depletion of KLP10A. Note that metaphases and anaphases were restored in the double RNAi experiments. (c and d) Quantification of mitotic defects in controls and after CLASP, KLP10A, and CLASP/KLP10A RNAi show that simultaneous depletion of CLASP and KLP10A significantly restored spindle bipolarity and length. Plotted values in panels b–d represent the mean from three experiments, and error bars represent the respective standard deviations. Asterisks in panel d indicate statistically significant differences when compared with controls ($P < 0.001$; Mann-Whitney test). (e–j) Immunofluorescence analysis of mitotic spindles from control, CLASP, KLP10A, and CLASP/KLP10A RNAi. MTs (green) and centrosomes (red) were, respectively, revealed with anti–α- and γ-tubulin antibodies, whereas DNA

Simultaneity of tension and MT translocation/flux relative to the kinetochore suggests that the flux-driving force is not generated at the kinetochore–MT interface. Indeed, any mechanical event at this interface that hypothetically pushes kinetochore MTs (kMTs) poleward (e.g., a kinesin power stroke) would react against the kinetochore structure, leading to centromere compression, not stretching. MT poleward flux may be driven by active MT minus-end depolymerization at the poles (Waters et al., 1996; Rogers et al., 2004; Ganem et al., 2005) or by motors acting along the length of kMTs (Mitchison, 2005; Forer et al., 2008). Growing emphasis in several cell types is being given to kinesin-5 motors, which slide apart antiparallel interpolar MTs (ipMTs), as the main flux-driving force (Miyamoto et al., 2004; Goshima et al., 2005; Brust-Mascher et al., 2009). Polymerization and depolymerization at MT plus and minus ends, respectively, are viewed as downstream responses to MT poleward translocation that regulate spindle length (Gaetz and Kapoor, 2004; Maiato et al., 2005). In this framework, kinesin-5 motors may drive kMT flux by directly cross-linking kMTs to ipMTs of opposite polarity (Mitchison, 2005) or, indirectly, by laterally transmitting the force generated by sliding ipMTs to kMTs within the same half spindle (Brust-Mascher et al., 2009). The key ingredient in both models is that ipMT sliding may prompt kMT poleward translocation through force transmission via a mechanical coupler, which in a more general view may consist of proteins with MT cross-linking activity (Manning and Compton, 2007) or a viscoelastic network (Brangwynne et al., 2006). The existence of such mechanical coupler may be heuristically inferred by the fact that spindles rotate and translate as a unified structure, which ultimately means that all chromosomes are mechanically connected.

The conservation and energetic cost of flux during metaphase, together with its dispensability for chromosome segregation in systems where it is normally present (Ganem et al., 2005; Buster et al., 2007), poses obvious questions regarding its functional roles. Besides, MT poleward translocation relative to the kinetochore (i.e., kMT flux) reflects the relaxation of the kinetochore–MT interface (implying a certain loss of tension), which may be seen as an apparent disadvantage to the cell. Here, we used *Drosophila* S2 cells to test whether the existence of flux represents a way to redistribute excess tensions on metaphase chromosomes, thereby contributing to the equalization of forces acting at kinetochores and anaphase "quality."

Results

Experimental attenuation of kMT flux in *Drosophila* S2 cells

The poleward flux of kMTs requires a corresponding rate of MT polymerization and slippage at the kinetochore. To test whether flux-associated slippage at the kinetochore–MT interface contributes to a uniform distribution of forces acting on kinetochores, we started by experimentally reducing kMT flux on bipolar spindles. In *Drosophila* S2 cells, kMT flux requires cytoplasmic linker associated protein (CLASP)-mediated incorporation of tubulin subunits at kinetochores (Maiato et al., 2005) balanced by KLP10A-dependent MT depolymerization at the poles (Rogers et al., 2004; Buster et al., 2007). Although CLASP RNAi causes kMT shortening and a strong accumulation of prometaphase cells with monopolar or short spindles (Fig. 1, a–g; Maiato et al., 2005), KLP10A RNAi increases spindle length without precluding bipolar spindle formation and function (Fig. 1, a–e, h, and i; Goshima et al., 2005; Buster et al., 2007). Simultaneous knockdown of CLASP and KLP10A significantly restores normal spindle bipolarity, length, and morphology (Fig. 1, a–e, and j; Laycock et al., 2006). To verify that bipolar spindles after KLP10A or CLASP/KLP10A RNAi undergo slower kMT flux, we used S2 cells stably expressing GFP–α-tubulin under the control of an inducible promoter and the kinetochore marker mCherry–centromere identifier (CID)-mCherry. The leaky expression of GFP–α-tubulin can be used to measure kMT flux by fluorescent speckle microscopy (FSM; Goshima et al., 2005; Danuser and Waterman-Storer, 2006). KMT flux in control metaphase cells is 1.2 µm/min (median) at 25°C, with only 2% of the speckles moving slower than 0.2 µm/min relative to kinetochores (Fig. 1, k and k′; Table I). After KLP10A or CLASP/KLP10A RNAi, kMT flux drops to 0.2 µm/min (Fig. 1, l–m′; Table I), which is comparable to the velocity of kMT flux observed after MT stabilization with 10 nM taxol (Fig. 1, n and n′; Table I). Although flux velocity is slow, these slowly fluxing spindles satisfy the SAC, enter anaphase, and segregate chromosomes. We conclude that KLP10A or CLASP/KLP10A RNAi represent valid strategies to reduce kMT flux, while allowing the formation of functional bipolar spindles in S2 cells.

Flux-associated kMT minus-end depolymerization is down-regulated at anaphase onset and has a minor role in anaphase chromosome-to-pole motility in *Drosophila* S2 cells

We next used dual-wavelength spinning-disk confocal microscopy to investigate the impact of reduced kMT flux on chromosome segregation. Anaphase poleward velocity of sister chromatids after KLP10A or CLASP/KLP10A RNAi was reduced by ∼0.5 µm/min relative to controls. This reduction was essentially caused by a KLP10A-dependent decrease in the velocity of spindle elongation and not reduced kMT shortening velocity (Fig. 2, a–f; Table I). Because KLP10A is apparently not required for the formation of the spindle midzone or recruitment of kinesin-5 motors to this location (unpublished data), we reasoned that the slower spindle elongation could be caused by increased resistance due to cortical interactions with the abnormally

(blue) was counterstained with DAPI. S2 cells stably expressing low levels of GFP-α-tubulin (green) and CID-mCherry (red) were used to analyze kMT poleward flux by FSM. Bar, 10 µm. (k–n) Control (k), KLP10A RNAi (l), CLASP/KLP10A RNAi (m), and Taxol-treated cells (n). Speckle poleward velocity was determined by measuring the slopes obtained from the kymographs (white broken lines). (k′–n′) Distribution of flux velocity in control, KLP10A RNAi, CLASP/KLP10A RNAi, and Taxol-treated cells, respectively. Horizontal bar, 5 µm; vertical bar, 1 min. All treatments were statistically different from controls ($P < 0.05$; Dunn's test).

Published July 13, 2009

Table I. **Summary of measured mitotic parameters**

Experiment	Metaphase flux velocity	Anaphase kMT minus-end depolymerization velocity	Inter-KT distance measured from fixed cells	Pixel intensity BubR1/CID	Inter-KT distance measured from live imaging	Chromosome poleward velocity [V_{ch}]	Half-spindle elongation velocity [V_{pole}]	KMT shortening velocity [V_{ch}-V_{pole}]
	μm/min	*μm/min*	*μm*		*μm*	*μm/min*	*μm/min*	*μm/min*
Control								
M	1.2[a]	0.4[a]	1.0[a]	1.1	0.9[a]	1.7	0.9	0.8
SD	0.4	0.4	0.2	0.6	0.1	0.5	0.2	0.4
IQR	0.6	0.5	0.2	0.8	0.2	0.7	0.2	0.6
n	392 tracks; 23 cells	43 tracks; 8 cells	207 tracks; 34 cells	59 tracks; 9 cells	198 tracks; 21 cells	88 tracks; 30 cells	30 cells	88 tracks; 30 cells
Control + colchicine								
M			0.7					
SD			0.1					
IQR			0.2					
n			56 tracks; 8 cells					
Control + MG132								
M			1.1[a]	1.2				
SD			0.2	0.6				
IQR			0.4	0.7				
n			125 tracks; 20 cells	57 tracks; 9 cells				
Control (Prophase)								
M					0.4[a]			
SD					0.1			
IQR					0.2			
n					*n* = 102; 3 cells			
KLP10A RNAi								
M	0.2[a]		0.9[a]	1.6	0.8[a]	1.3	0.4	0.9[a]
SD	0.3		0.2	0.9	0.1	0.6	0.2	0.6
IQR	0.2		0.2	1.2	0.2	0.9	0.3	0.9
n	105 tracks; 6 cells		137 tracks; 16 cells	50 tracks; 8 cells	267 tracks; 25 cells	186 tracks; 32 cells	32 cells	186 tracks; 32 cells
KLP10A RNAi + MG132								
M			0.9					
SD			0.2					
IQR			0.2					
n			50 tracks; 7 cells					
KLP10A RNAi + (Prophase)								
M					0.4[a]			
SD					0.1			
IQR					0.1			
n					*n* = 79; 3 cells			
CLASP/KLP10A RNAi								
M	0.2[a]	0.2[a]	1.0	1.7[a]	0.8[a]	1.1	0.4	0.7[a]
SD	0.4	0.4	0.2	1.7	0.2	0.4	0.2	0.4
IQR	0.6	0.4	0.2	1.4	0.2	0.6	0.2	0.6
n	208 tracks; 13 cells	51 tracks; 10 cells	159 tracks; 23 cells	51 tracks; 9 cells	241 tracks; 25 cells	219 tracks; 33 cells	33 cells	219 tracks; 33 cells
CLASP/KLP10A RNAi + MG132								
M			1.1[a]	1.4[a]				
SD			0.2	0.7				
IQR			0.2	1.0				
n			129 tracks; 20 cells	44 tracks; 8 cells				

Downloaded from jcb.rupress.org on June 13, 2010

Table I. **Summary of measured mitotic parameters** *(Continued)*

Experiment	Metaphase flux velocity	Anaphase kMT minus-end depolymerization velocity	Inter-KT distance measured from fixed cells	Pixel intensity BubR1/CID	Inter-KT distance measured from live imaging	Chromosome poleward velocity [V_{ch}]	Half-spindle elongation velocity [V_{pole}]	KMT shortening velocity [V_{ch}-V_{pole}]
CLASP/KLP10A RNAi (Prophase)								
M					0.4[a]			
SD					0.1			
IQR					0.1			
n					22 tracks; 2 cells			
Mad2 RNAi								
M					0.8[a]			
SD					0.2			
IQR					0.2			
n					122 tracks; 12 cels			
Mad2 RNAi (Prophase)								
M					0.4[a]			
SD					0.1			
IQR					0.1			
n					54 tracks; 3 cells			
KLP10A/SAS4 RNAi								
M						1.6	0.7	0.9
SD						0.6	0.2	0.5
IQR						0.6	0.2	0.7
n						84 tracks; 14 cells	14 cells	84 tracks; 14 cells
Taxol								
M	0.1[a]		0.7	3.3[a]				
SD	0.2		0.1	2.0				
IQR	0.2		0.1	3.4				
n	73 tracks; 5 cells		44 tracks; 7 cells	42 tracks; 7 cells				

Blank cells indicate that the value was not determined. KT, kinetochore; M, represents the mean, except for the distributions that do not follow a normal distribution; IQR, interquartile range; *n*, the number of measurements (in the prophase situation, *n* represents the number of interkinetochore distances measured before nuclear envelope breakdown).
[a]Distrubutions that do not follow a normal distribution, where median is represented.

long astral MTs observed after perturbation of KLP10A (Fig. 1, h and j). Indeed, codepletion of KLP10A with Sas4, a protein required for the formation of functional centrosomes and astral MTs (Basto et al., 2006), restores normal spindle elongation velocity (Table I and Fig. S1, a–d).

Our results show that a substantial decrease in metaphase flux velocity does not significantly affect the mean velocity of kMT shortening in anaphase. This finding is surprising in light of the recent proposal that MT minus-end depolymerization associated with flux is the main force driving chromosome-to-pole movement during anaphase in S2 cells (Buster et al., 2007). One important difference between this previous report and our study was our inclusion of a kinetochore marker and collection of z stacks through the entire volume of the cell, which allowed us to directly measure kMT shortening velocities for the full chromosome set. To investigate this further, we performed FSM in control anaphase cells and found that kMT translocation velocity is equivalent to that observed in metaphase, as revealed by the constant slope of speckle tracks on kMTs (Fig. 3 a and Table I). Because spindles elongate immediately after anaphase onset at ∼0.9 µm/min in S2 cells, this indicates that MT minus-end depolymerization must be attenuated by an equivalent rate. Indeed, we found that >50% of the speckles move slower than 0.4 µm/min relative to spindle MT minus ends (Fig. 3, a and c; and Table I), which is consistent with a model where the extent of down-regulation of MT minus-end depolymerization governs the rate of spindle elongation during anaphase (Brust-Mascher et al., 2004). Finally, the rate of speckle movement relative to kMT minus ends in anaphase is only marginally affected after RNAi depletion of CLASP/KLP10A, which suggests that their flux-associated activities during metaphase in untreated cells are significantly down-regulated at anaphase onset (Fig. 3, b and c; and Table I). These results support the finding that, as in human cells (Gorbsky et al., 1987; Ganem et al., 2005), kinetochore motility coupled to MT plus-end depolymerization ("Pac-Man" activity) is the main driver of anaphase chromosome-to-pole movement in *Drosophila* S2 cells (Fig. 3 a).

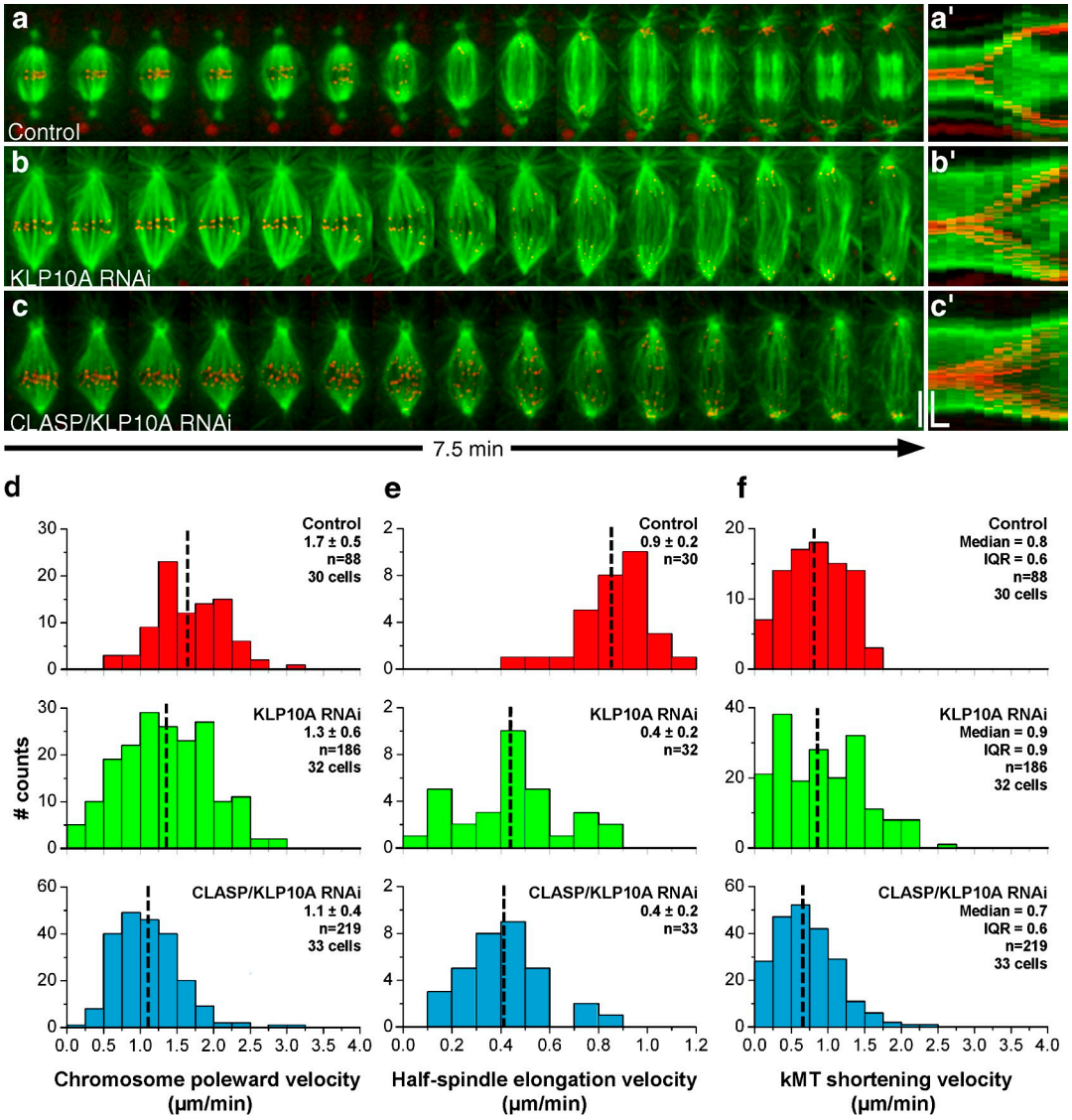


Figure 2. **Analysis of chromosome and spindle dynamics during anaphase.** (a–c) S2 cells stably expressing GFP–α-tubulin (green) and CID-mCherry (red) were used to track kinetochore movement and spindle elongation during anaphase. Control (a), KLP10A RNAi (b), and CLASP/KLP10A RNAi cells (c). Bar, 5 μm. (a′–c′) Corresponding collapsed kymograph analysis. Horizontal bar, 60 s; vertical bar, 5 μm. (d) Distribution of chromosome poleward velocity in control, KLP10A, and CLASP/KLP10A RNAi. All RNAi treatments are statistically different from control ($P < 0.05$; Dunn's test). (e) Distribution of spindle elongation velocity. All RNAi treatments were statistically different from controls ($P < 0.001$; Student-Newman-Keuls test). (f) Distribution of kMT shortening velocity in control, KLP10A, and CLASP/KLP10A RNAi. The differences were not statistically significant. The mean ± SD or median and interquartile range are indicated for each distribution. The mean or median values are marked with a broken vertical line.

KMT flux ensures anaphase synchrony in *Drosophila* S2 cells

Although experimental attenuation of flux has only a minor effect on mean kinetochore-to-pole velocity, we discovered that it significantly impaired anaphase synchrony (Fig. 2, a–c′). To measure the uniformity of chromosome segregation after attenuation of flux, we developed a chromo-kymograph algorithm to show the movements of multiple kinetochores as a function of time through the metaphase–anaphase transition. In control cells, we generally observed 2 main kinetochore tracks during anaphase, which indicated synchronous segregation of chromosomes (Fig. 3, d and d′; $n = 30$ cells). After KLP10A or CLASP/KLP10A RNAi, we typically found 3–12 kinetochore tracks per cell (Fig. 3, e, e′, f, and f′; $n = 31$ cells for each RNAi), despite the formation of normal metaphase plates. Closer inspection of the chromo-kymographs revealed marked asynchrony in the entry and/or poleward migration during anaphase (Fig. 3, d–f′′). One plausible explanation for the observed asynchrony during anaphase could be the presence of kinetochores with merotelic attachments (Cimini et al., 2004). Indeed, members of the kinesin-13 family were implicated in correcting kinetochore–MT attachments in human cells (Ganem et al., 2005; Bakhoum et al., 2009). Therefore, it is possible that KLP10A, which localizes to centromeres in addition to spindle poles (Rogers et al., 2004), is also involved in this process. Analysis of KLP10A RNAi spindles revealed the persistence of cold-resistant kMTs that were indistinguishable from controls, which suggests normal kinetochore function (Fig. S1, e–g). Because the correction of merotelic

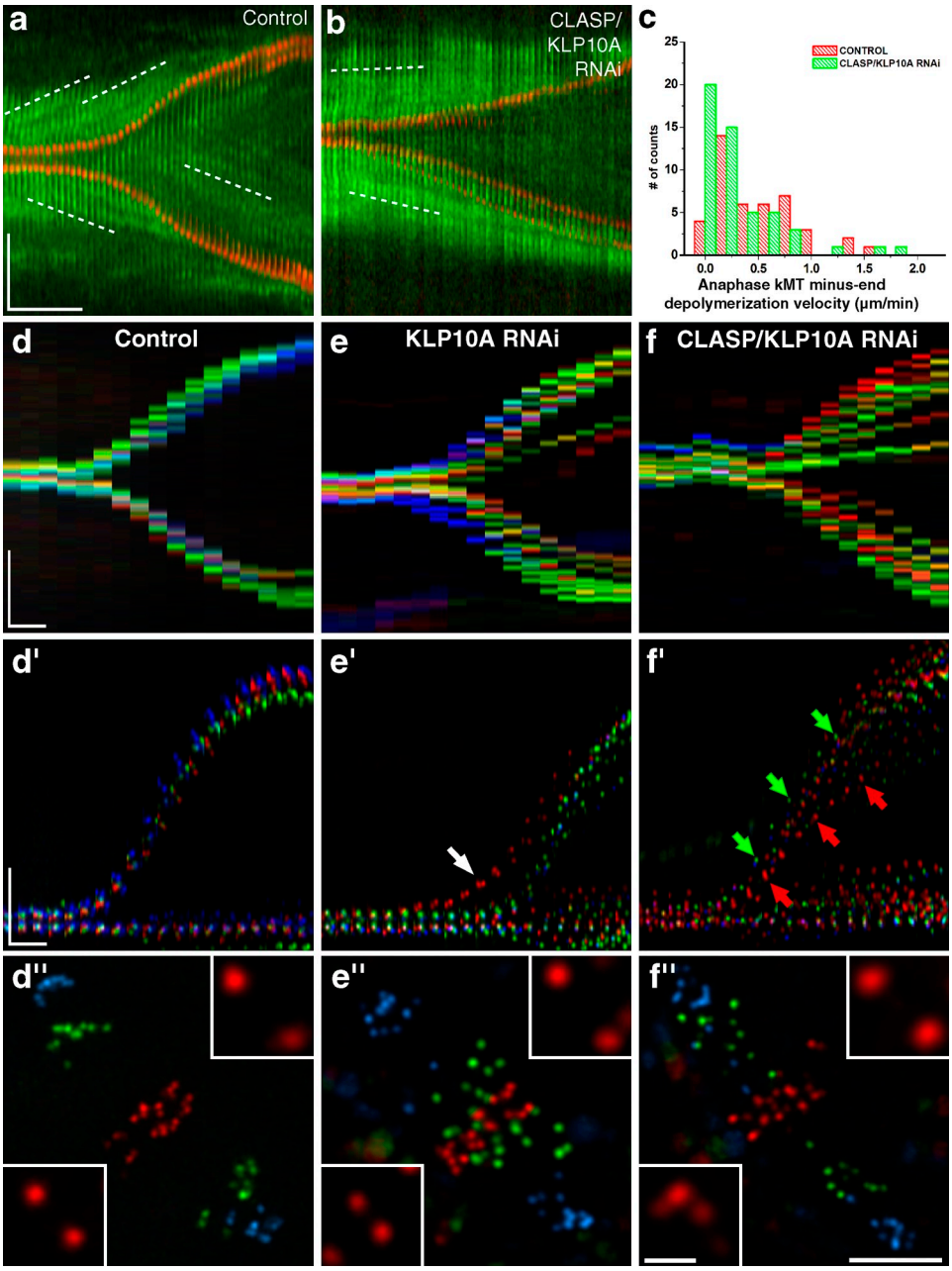


Figure 3. **Analysis of chromosome segregation during anaphase.** (a and b) S2 cells stably expressing low levels of GFP–α-tubulin (green) and CID-mCherry (red) were used to track tubulin speckle movement (white broken lines) relative to spindle MT minus ends by FSM. (a) Control cell. (b) CLASP/KLP10A RNAi cell. Note that in both cases, kinetochores approach the speckles. (c) Distribution of kMT minus end depolymerization velocity in control and CLASP/KLP10A RNAi cells. The differences are statistically significant ($P < 0.05$; Mann-Whitney test). (d–f) Chromo-kymograph analysis of kinetochores in control, KLP10A RNAi, and CLASP/KLP10A RNAi cells at the metaphase–anaphase transition. (d′–f′) Overlay of guided kymographs showing three kinetochore pairs color coded red/green/blue. Arrows indicate precocious entry of anaphase (white) or differential poleward migration (green/red). (d′′–f′′) Respective projections of three different time frames. Red/green/blue frames correspond to 1, 3.5, and 7 min after anaphase onset. Insets highlight the kinetochore pairs where interkinetochore distances were maximum and minimum. Bars: (space) 5 μm; (time) 1 min; (inset) 1 μm.

attachments involves mechanisms acting before and during anaphase (Cimini et al., 2003), we quantified merotelic attachments after KLP10A RNAi using two criteria: accumulation of Aurora B at the inner centromere during metaphase (Knowlton et al., 2006) and stretching of the merotelic kinetochore during anaphase (Cimini et al., 2004). We were unable to detect a significant enrichment of Aurora B on metaphase plates after knocking down KLP10A (Fig. S1, h–j). In contrast, our live-cell analysis of anaphase did reveal a two-to-three–fold increase in the percentage of KLP10A ($n = 31$)- and CLASP/KLP10A ($n = 29$)-depleted cells with merotelic attachments in anaphase (13% and 10%, respectively, as opposed to 4% of control cells [$n = 25$]). However, we never found more than one chromosome or chromatid with merotelic-attached kinetochores per depleted cell, which is too infrequent to account for the observed level of asynchrony in anaphase cells depleted of KLP10A or CLASP/KLP10A.

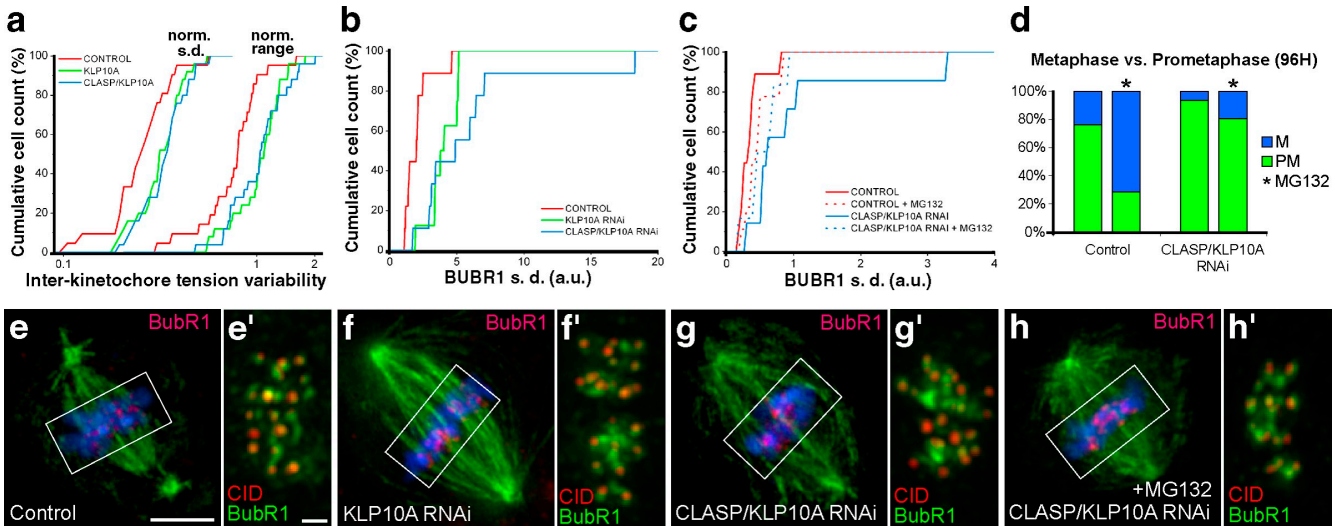


Figure 4. **Experimental analysis of tension uniformity during metaphase.** (a) Cumulative histogram for the normalized standard deviation (left) and range (right) of intracellular interkinetochore distances along a metaphase plate for control (n = 21), KLP10A RNAi (n = 25), and CLASP/KLP10A RNAi (n = 25), where n is the number of cells. CLASP/KLP10A RNAi is statistically different from control but not KLP10A RNAi ($P < 0.05$; Dunn's test). (b) Cumulative histograms for the standard deviation of BubR1 fluorescence intensity for control (n = 10), KLP10A RNAi (n = 7), and CLASP/KLP10A RNAi (n = 7) cells. Both treatments cause a statistically significant variability relative to controls ($P < 0.05$; Dunn's test). (c) Cumulative histograms for the standard deviation of BubR1 fluorescence intensity on metaphase kinetochores in control and CLASP/KLP10A RNAi before and after incubation with MG132 for 2 h. Note the approximation of the control and CLASP/KLP10A RNAi distributions after MG132 treatment. Only CLASP/KLP10A RNAi is statistically different from controls ($P < 0.05$; Dunn's test). (d) Quantification of prometaphase and metaphase figures in fixed cells before and after MG132 treatment. Note that CLASP/KLP10A RNAi-treated cells have problems aligning chromosomes at the metaphase plate, which is slightly attenuated if additional time is provided by incubation with MG132. The asterisks indicate the presence of MG132. (e–h) Mitotic spindles from control, KLP10A RNAi, CLASP/KLP10A RNAi, and CLASP/KLP10A RNAi after MG132 treatment, respectively. α-tubulin is shown in green, BubR1 in red, and DNA in blue. Bar, 5 µm. (e′–h′) Insets of the respective metaphase plates indicated in e–h, where CID is shown in red and BubR1 in green. Only cells with aligned chromosomes after CLASP/KLP10A RNAi were used for all quantitative analyses of metaphase. Bar, 1 µm.

Still, it remains possible that these numbers represent an underestimate of the full complement of merotelic attachments, especially more subtle cases, which cannot be resolved by the abovementioned methods. We conclude that molecular players involved in kMT flux may be implicated in correcting erroneous kinetochore–MT attachments invisible to the SAC and somehow help in ensuring the coordinated movement of chromosomes during anaphase.

Anaphase synchrony reflects the uniformity of forces acting on metaphase kinetochores

Flux players may promote anaphase synchrony by mediating the equalization of forces acting at kinetochores of metaphase chromosomes. Indeed, measurement of interkinetochore distances as a readout of centromere tension in living metaphase cells revealed that tension was highly variable between sister kinetochore pairs after KLP10A or CLASP/KLP10A RNAi (Fig. 4 a). In agreement, live-cell imaging of the tension-sensitive protein BubR1 in KLP10A or CLASP/KLP10A-depleted cells revealed that several kinetochores retain abnormal high levels of BubR1, which correlated with a delayed initiation of poleward migration and local degradation of the cohesin subunit Scc1 (Fig. S2). Quantitatively, we confirmed that flux reduction by these methods causes an increase in the variability of BubR1 at metaphase kinetochores, which is attenuated if cells are allowed to stay in metaphase for 2 h by incubation with the proteasome inhibitor MG132 (Fig. 4, b–h′).

Force equalization by flux can be explained by an MT-coupling model

In an attempt to explain how kMT flux contributes to the uniformity of forces on metaphase kinetochores, we developed a minimal mathematical model for the metaphase spindle, which assumes that kMT flux is driven by forces that are laterally transmitted through a mechanical coupler cross-linking kMTs with sliding ipMTs. In this context, antiparallel ipMT sliding may be driven either by plus end–directed bipolar motors (Brust-Mascher et al., 2009; Goshima et al., 2005) or by active depolymerases at ipMT minus ends (Rogers et al., 2004). We support the finding that forces are laterally transmitted to kMTs based on the uninterrupted poleward translocation at near flux rates of laser-severed kMTs (Fig. 5, a–d; kMT growth = 0.9 ± 0.2 µm/min, n = 17; Table I), which don't reach near the poles and whose minus ends are not depolymerizing (Maiato et al., 2004b), suggesting that kMT minus-end depolymerization by itself is not a major flux-driving force.

We next simulated the mechanical behavior of the proposed fluxing metaphase spindle model (Fig. 6 a; see Materials and methods for details), where ipMTs translocate poleward driven by a force P (a generalization for non-ipMT forces is discussed in Materials and methods). In this context, motor force decreases with sliding velocity (Valentine et al., 2006), a dependence that is assumed to be linear. ipMT sliding is not free; instead, it is resisted by MT cross-linking or coupling, here modeled as a serial linkage of viscous and elastic elements. This viscoelastic coupler cross-links spindle MTs, and

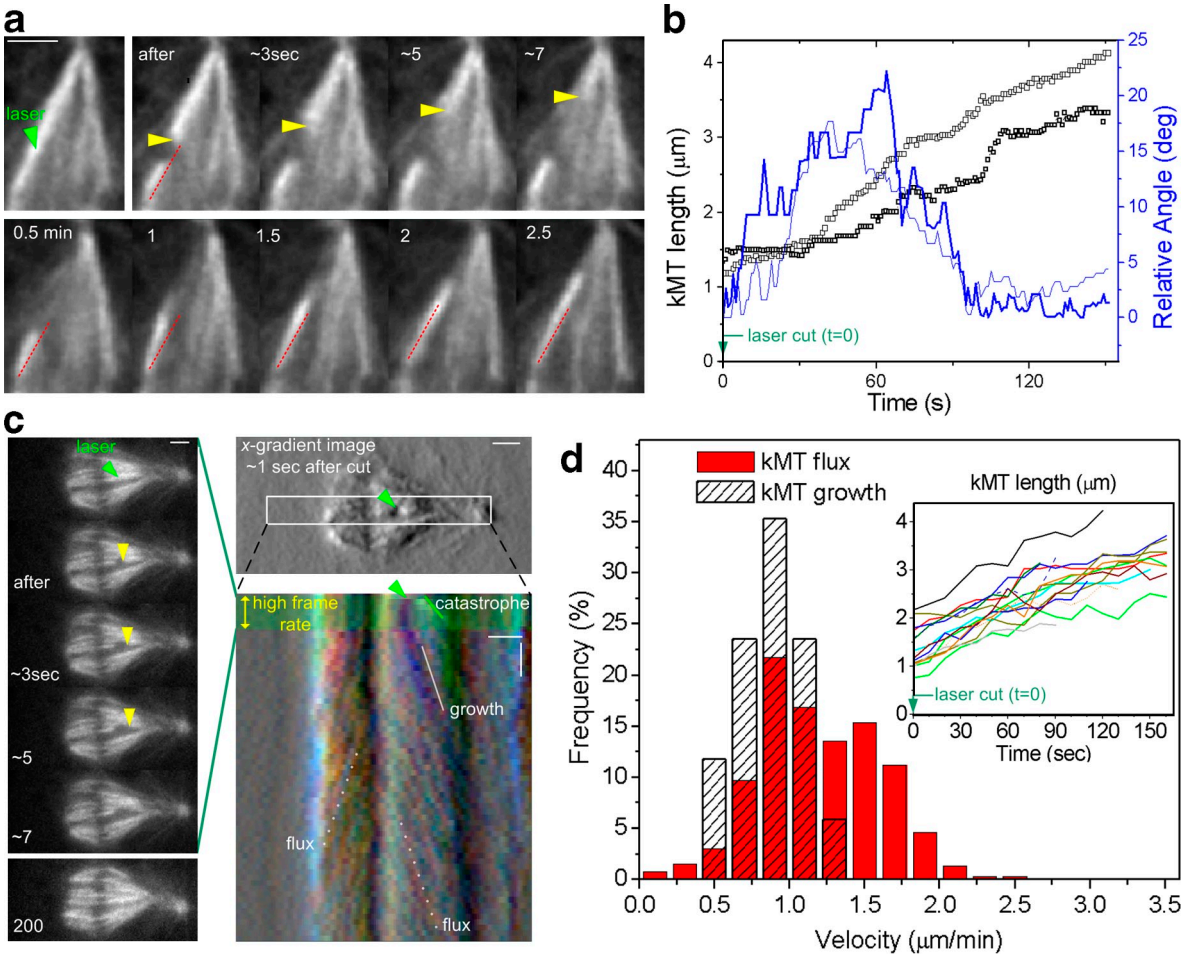


Figure 5. **KMT fiber regrowth after laser microsurgery at near-flux velocity.** (a) Selected frames of a laser microsurgery experiment on a kMT fiber during metaphase. The readouts for a successful laser cut are (1) a catastrophe of newly created kMT plus ends (~20 μm/min) and (2) reorientation of the kinetochore-associated MT fiber after a laser cut (red lines have equal length and slope). (b) kMT fiber length and orientation over time after microsurgery. Data points correspond to two high-speed acquisitions (light and dark lines) in kMT fibers associated with chromosomes positioned at the periphery of the metaphase plate. The relative angle corresponds to the fiber deviation from the initial (presurgery) orientation. (c) FSM during metaphase after laser microsurgery on a kMT fiber. A first high-speed acquisition phase (~1 s interval) is used to confirm the catastrophe of newly created kMT plus ends (left). After the catastrophe, images are acquired at a 10-s interval to observe kinetochore-associated MT fiber growth and intact kMT fiber flux, as revealed by the chromo-kymograph. The kymograph is based on intensity-gradient images along the horizontal direction, which helped observation of the minus ends of a growing kMT fiber. Green arrowheads in a and c indicate the location of the laser cut. Yellow arrowheads indicate the catastrophe of newly created kMT plus ends after surgery. (d) Velocity distributions of growing kMT fibers after laser microsurgery and of poleward flux, i.e., translocating intact kMT fibers. The elongation of kMT fibers was tracked and is shown in the inset. Bars: (space) 2 μm; (time) 1 min.

therefore acts as a mechanical mediator that allows force transference between ipMTs and kMTs. As a result, kMTs are pulled poleward, exhibiting flux, which is primarily resisted by friction at the kinetochore–MT interface. We represent this friction as a viscous interaction, $T(t) = \varepsilon_k V_+(t)$, where T is the centromeric tension, ε_k is the friction drag coefficient associated with kinetochore-MT affinity, and V_+ is the slippage/flux velocity of the MT relative to the kinetochore. Finally, the centromere is assumed to be linearly elastic, with tension given by $T(t) = k_k E_k(t)$, where k_k is the elastic constant characterizing centromere stiffness and E_k is the interkinetochore elongation resulting from an applied tension T. In parallel, all n chromosomes are described by equivalent interdependent equations. The mechanical coupling between adjacent MTs integrates the system, which will react globally to local events on individual chromosomes. For simplicity, this model disregards position and velocity-dependent forces driving chromosome oscillation. It is plausible, however, that it applies to systems where chromosomes do oscillate, given that MT poleward translocation is independent of the directional state (poleward or antipoleward) of metaphase chromosomes (Cameron et al., 2006).

Analytical solution of the model shows that two characteristic time scales fully describe the system dynamics (Fig. 6 b; and Materials and methods). First, mean interkinetochore tension at the metaphase plate tends exponentially to an equilibrium tension. Second, individual tensions converge exponentially to the evolving mean tension within the timescale

$$\tau^{\Delta} = \frac{k_c^{-1} + k_k^{-1}}{\varepsilon_c^{-1} + \varepsilon_k^{-1}} \sim \frac{\lambda}{f}, \quad (1)$$

hereafter referred to as the equalization time, which in the high coupling regime ($\varepsilon_c = \infty$ and $k_c = \infty$) is simply ε_k/k_c. Importantly, τ^{Δ} is

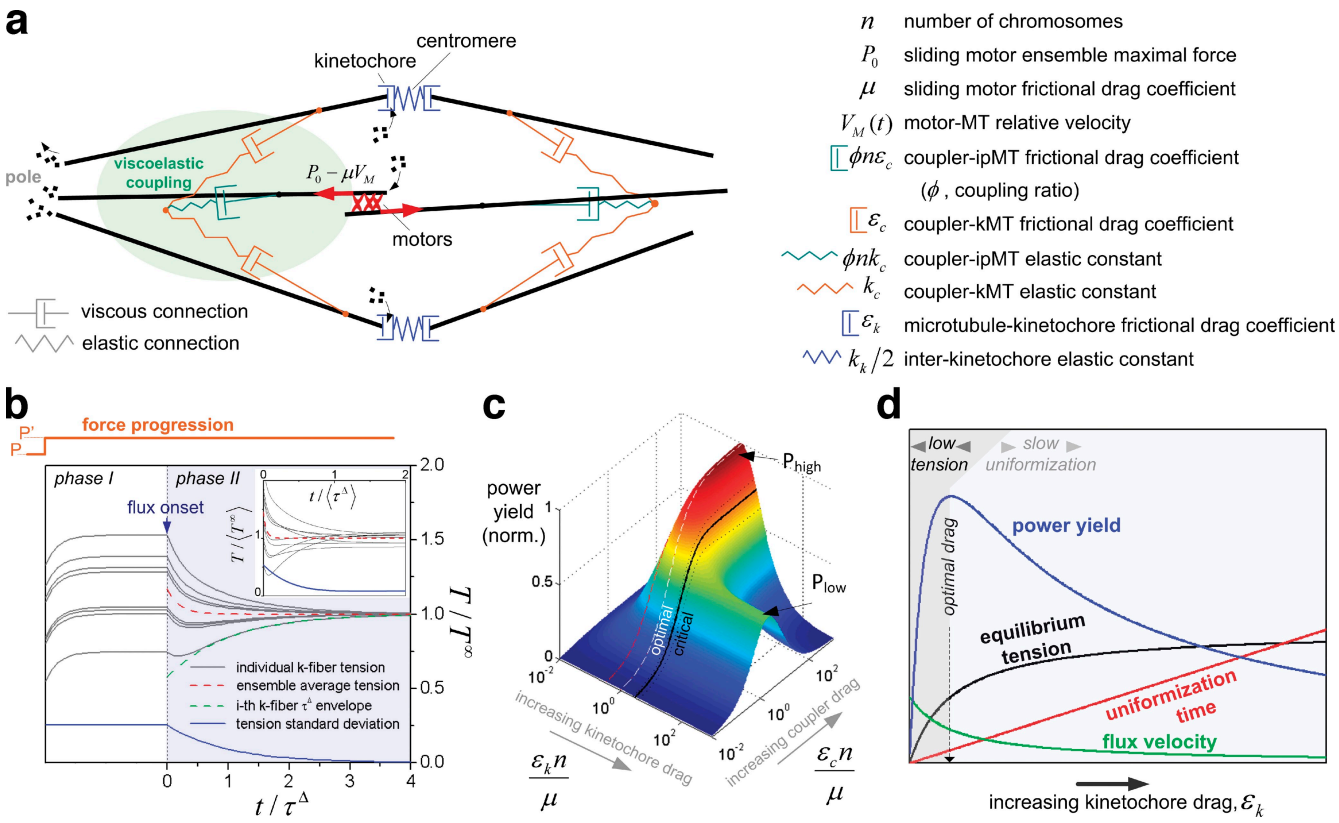


Figure 6. **MT coupling leads to tension uniformity in the presence of flux.** (a) Spring-dashpot (elastic-viscous) functional representation of the coupled spindle. Viscous and elastic elements describe both coupler–MT and MT–chromosome interactions. (b) Normalized centromeric tensions as a function of normalized time without flux (*phase I*) and with flux (*phase II*). A force *P* generates initial (random) tension values. A step-increased force (P′) is applied to the system (see "force progression" above the graph). First, to simulate a nonfluxing spindle, *phase I* shows the system dynamics when no slippage is allowed at the viscous connections, i.e., totally rigid kinetochore–MT and coupler–MT attachments. The system reaches a static (stretched) state when elastic force balances the applied force. Tension heterogeneity (as measured by the standard deviation, blue line) does not decrease because slippage-mediated tension redistribution does not occur. At t = 0, viscous drag coefficients drop to a finite value, allowing slippage to begin (*phase II*). Throughout *phase II*, tensions converge with timescale τ^Δ to the mean tension, which itself decreases (red broken line) to a new asymptotic level T^∞. The inset shows the system behavior when kinetochore–MT attachment drags are variable among chromosomes on the same metaphase plate, following a normal distribution with full width equal to 10% of the mean. (c) Power yield of the mechanical system as a function of normalized MT–coupler drag and normalized kinetochore–MT drag. The system reaches a plateau of highest efficiency (P_{high}) when kMTs are tightly coupled to ipMTs (high coupler drag) but only partially coupled to kinetochores (intermediate kinetochore drag). A secondary plateau (P_{low}) is found if kinetochore drag is higher than a critical value (black line; sub- and supracritical black broken lines are also shown), a condition in which it is beneficial to have a finite coupler drag and infinite kinetochore drag (no kMT flux). Critical kinetochore drag represents an unbiased estimate of the maximal drag expectable for fluxing spindles; i.e., the minimum flux. The critical point-associated power may be used to define the low end of expected drag (red broken line). (d) Summary of the system behavior as a function of kinetochore–MT drag in the high-coupling regime. High kinetochore drag maximizes tension at equilibrium, but it comes at the expense of a long equalization time. The reverse happens for low kinetochore drag, suggesting optimal behavior in an intermediate situation (maximal power yield), where flux velocity is not zero and not as high as it could be if generated by free ipMT motors.

also the characteristic decay time of the tension standard deviation on the entire chromosome set, and therefore represents a global measure of the tension equalization time in the spindle. λ and *f* are, respectively, typical elastic deformation and flux velocity scales of the metaphase spindle. The magnitude for λ lies between interkinetochore stretch (typically around 0.5 µm; Waters et al., 1996; Maddox et al., 2003; Meraldi et al., 2004; Maiato et al., 2006) and MT–coupler stretch, which should be less than one half the spindle length (typically 5–15 µm; Waters et al., 1996; Gaetz and Kapoor, 2004; Goshima et al., 2005; Bird and Hyman, 2008). Using *f* of ~1 µm/min we get from Eq. 1, $\tau^\Delta = 0.5$–15 min. This estimate is in agreement with metaphase duration in several systems (Rieder et al., 1994; Meraldi et al., 2004; Maiato et al., 2005; Brust-Mascher et al., 2009), regardless of the different number of chromosomes (note the independence of *n*), and is not affected by the introduction of a tension-assisting force (e.g., due to dynein; Yang et al., 2007) at the kinetochore–MT interface (see Materials and methods).

Using dimensional analysis, a trade-off between low kinetochore–MT affinity (resulting in low tension) and high kinetochore–MT affinity (leading to high tension but slow equalization) may be found in the form of a centromeric power yield, reflecting the fact that centromeric elastic energy should maximally and uniformly accumulate in the metaphase plate in the shortest possible time (Fig. 6, c and d; and Materials and methods). An optimal flux regime is found for high coupling and when kinetochore–MT attachments are strong/weak enough to allow metaphase flux at a velocity between one and three eighths of the unloaded velocity of motors that slide ipMTs (note that these figures are strongly dependent on the shape of the force–velocity relation characterizing motor activity). Finally, the model predicts that ipMT flux is faster than kMT flux

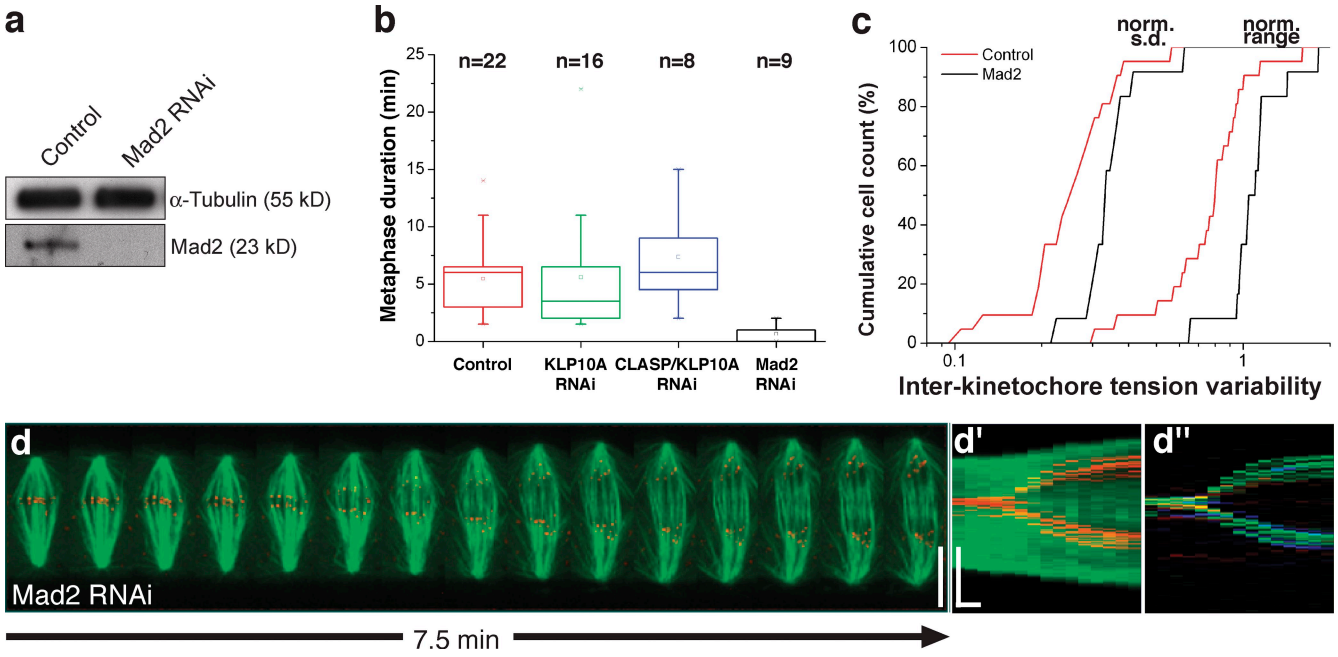


Figure 7. **Tension uniformity and synchrony analysis after acceleration of mitosis.** (a) Western blot showing Mad2 depletion 96 h after RNAi. α-tubulin was used as loading control. (b) Cumulative histogram for the normalized standard deviation (left) and range (right) of intracellular interkinetochore distances along a metaphase plate for control (n = 21) and Mad2 RNAi (n = 12), where n is the number of cells. Mad2 RNAi is statistically different from controls ($P < 0.05$, Student t test). (c) Metaphase duration in control, KLP10A RNAi, CLASP/KLP10A RNAi, and Mad2 RNAi cells, where n represents the number of cells capable of forming a metaphase plate. The box plot determines the interquartile range, the line inside the box represents the median, the point inside the box represents the mean, and the whiskers determine the limits of the distribution disregarding outliers. Mad2 RNAi is the only treatment that is statistically different from controls ($P < 0.001$, Mann-Whitney test). (d–d′′) Kymograph (d), collapsed kymograph (d′), and cromo-kymograph (d′′) analysis of a representative Mad2-depleted cell. Vertical scale bar, 10 µm; horizontal time bar, 1 min.

as a result of imperfect force transmission, a feature indeed observed in several systems (Maddox et al., 2003; LaFountain et al., 2004; Yang et al., 2008; see Materials and methods).

The SAC extends the duration of mitosis to allow the uniform distribution of forces acting on metaphase kinetochores

If cells require time for a uniform distribution of tension on metaphase chromosomes, one would predict that acceleration of mitosis prevents this equalization. Mad2 is a key signaling component of the SAC that extends the duration of mitosis until all kinetochores are attached to the spindle (Meraldi et al., 2004). Indeed, RNAi depletion of Mad2 in S2 cells (Fig. 7 a) significantly accelerated mitosis so that cells entered anaphase prematurely (Fig. 7 b; see Orr et al., 2007). Additionally, Mad2-depleted cells that were able to form a metaphase plate showed increased interkinetochore tension variability (Fig. 7 c) and underwent asynchronous chromosome segregation during anaphase (Fig. 7 d–d′′). These results support our theoretical prediction that cells require time for a uniform distribution of forces acting on kinetochores.

Discussion

In this paper, we propose that flux-associated slippage of MTs at kinetochores allows spindle forces to become evenly distributed along the metaphase plate. The rationale behind this model is that MT slippage at a given kinetochore interface reflects a mechanical relaxation event that allows ipMT sliding motors to do further work, thus providing extra tension to other chromosomes. Sustained slippage events occurring along the metaphase plate eventually drive the spindle to an equilibrium state characterized by homogeneous tension. An analogy to this tension redistribution mechanism is illustrated in Fig. 8. Tension equalization during metaphase ensures that any mechanism relying on tension, such as the maturation and correction of kinetochore–MT attachments (Nicklas and Ward, 1994; King and Nicklas, 2000; Liu et al., 2009), recruitment of SAC proteins (Pinsky and Biggins, 2005; Musacchio and Salmon, 2007), or even the coordination of cohesin degradation between sister chromatids (this study) operates uniformly along the metaphase plate.

The close match found between equalization time and metaphase duration is, in our opinion, the strongest support for a flux-dependent mechanism for tension equalization. However, such correlation poses a delicate question regarding the relationship between equalization time and the SAC. One possibility is that SAC silencing requires that all chromosomes overcome a given tension threshold. In fact, a uniform distribution of tension maximizes the probability of globally surpassing any threshold. Alternatively, SAC satisfaction may rely only on MT occupancy at kinetochores. A cell with a satisfied SAC in the absence of such tension equalization mechanism would be expected to segregate its chromosomes at distinct times and/or with distinct velocities. Because metaphase duration is not significantly affected after experimental perturbation of flux, and acceleration of mitosis precludes tension equalization, a plausible explanation for the observed asynchronous chromosome segregation is the reduced

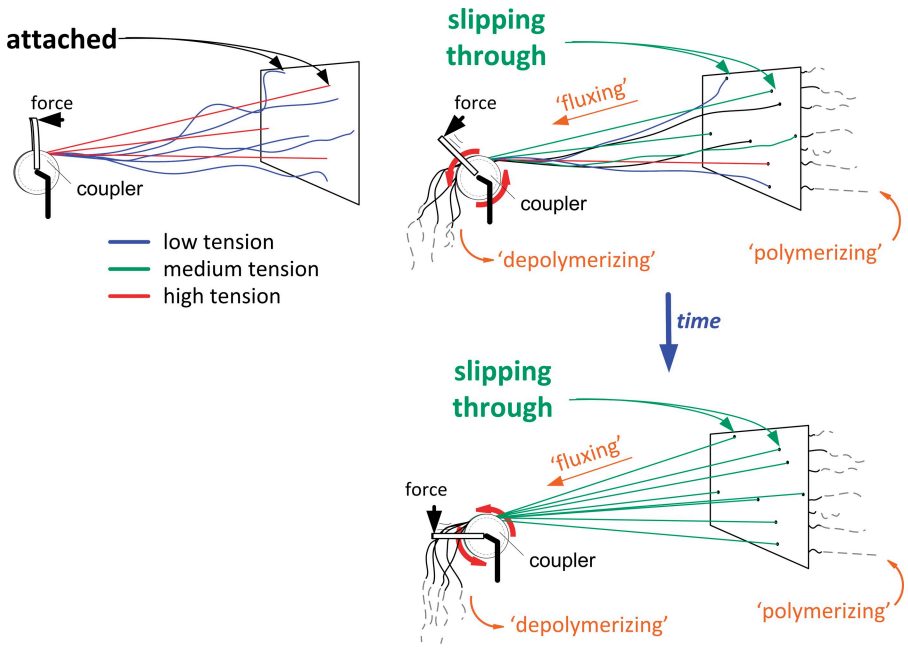


Figure 8. **Schematic representation of the flux-dependent tension redistribution principle.** Several cables (representing kMTs) with random lengths are firmly attached to the wall (representing chromosomes at the metaphase plate). Cables are connected to a coupler, which is subjected to a "rotating force" (torque). In the "no flux" condition (left), the coupler will only rotate up to the point where the first cables become under tension, a point in which they resist further rotation: the system reaches a static equilibrium characterized by large tension heterogeneity. In the strict analogy of inextensible cables, a maximum of three cables experience tension. The "flux" condition (right) is characterized by a single modification: instead of being firmly attached, cables are now passing through tight holes in the wall and thereby slip, although not freely, in response to the applied force. Cable "growth" by slippage allows the coupler to keep rotating, eventually leading to stretching (i.e., development of tension) in previously relaxed cables. The system eventually reaches a dynamic equilibrium, characterized by tension homogeneity, although at the expense of diminished mean tension. For clarity, we represent a point-coupler instead of an extended structure. Rotation of the motorized coupler emulates the linear "hand-over-hand" dynamics that characterize permanent attachment/detachment dynamics of system motors/cross-linkers, which allows maintenance of the coupler "position."

capacity to evenly mature and correct kinetochore–MT attachments that nevertheless satisfy the SAC. Recent works support the finding that interkinetochore tension is dispensable in satisfying the SAC (O'Connell et al., 2008; Maresca and Salmon, 2009; Uchida et al., 2009). However, tension may provide an important readout to allow the detection and correction of potential errors before anaphase onset (Pinsky and Biggins, 2005). Indeed, application of tension to kinetochores is known to promote its saturation with MTs (King and Nicklas, 2000), possibly by increasing MT stability due to spatial separation of kinetochore substrates from Aurora B at centromeres (Liu et al., 2009). However, maximizing tension by firmly grabbing MTs at their kinetochore attachment sites would not only prevent the release of erroneous attachments, but also hinder kMT flux/slippage, which could lead to chromosome segregation defects (Ganem and Compton, 2006; Bakhoum et al., 2009). Therefore, at the expense of some local loss of tension, MT affinity at kinetochores must be regulated to allow MTs to slip and possibly detach. According to our MT-coupling model, the system will respond globally to equilibrate tensions, and, consequently, all tension-dependent processes, precluding the need for tight spatial regulation of force distribution.

Our experimental perturbation of kMT flux involved down-regulation of CLASP and KLP10A, which appeared not to be implicated in force production but rather on how the spindle responds to it. Localization of CLASP at the kinetochore and its requirement for kMT flux away from the kinetochore (Maiato et al., 2005) suggest that its main function is to regulate the affinity of kMT attachments by decreasing the frictional drag (ε_k). In support of this conclusion, preventing Hec1 phosphorylation by Aurora B increases the affinity of the Ndc80 complex to MTs, which impairs kMT flux and turnover, while causing a 50% reduction of CLASP levels at kinetochores in Ptk1 cells (DeLuca et al., 2006). It is interesting to note that, although in this cell type the described perturbation leads to hyperstretching of the centromere without affecting spindle bipolarity, CLASP RNAi in S2 cells leads to spindle collapse without any obvious increase in interkinetochore tension (Maiato et al., 2005). These different responses might reflect mechanical peculiarities associated with each cell type. KLP10A depletion likely prevents MT depolymerization at the poles, leading to increased resistance to kMT poleward translocation and consequent flux reduction (see Materials and methods). Similar to polymerization at the kinetochore, depolymerization at the pole seems essentially a reactive mechanism that regulates kMT length upon translocation. Additionally, localization of KLP10A at the centromeres may account for the observed role in the correction of erroneous attachments described in this paper, which may be intrinsically coupled to its role in flux.

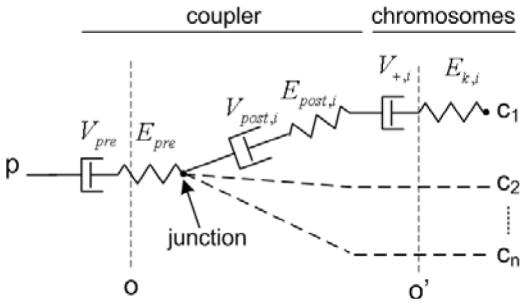
One important outcome of asynchronous chromosome segregation is the increased risk of aneuploidy. Recent work in budding yeast, which lack any detectable flux (Maddox et al., 2000), provided a molecular explanation for the abrupt degradation of cohesins at anaphase onset (Holt et al., 2008). It is noteworthy that budding yeast do not align their chromosomes at the cell equator and rely heavily on spindle elongation for accurate chromosome segregation (Straight et al., 1997). In contrast, animal and plant cells establish a metaphase plate, a high-order state that is only justified if the subsequent synchronous migration of sister chromatids is ensured, where a mechanism involved in force equalization may be essential. The emergence of

flux in higher eukaryotes and its contribution to anaphase "quality" may play particularly important roles in the prevention of chromosomal abnormalities observed in cancers or in several human syndromes, many of which result from defects in chromosome segregation during meiosis, where flux is indeed maintained at high rates.

Materials and methods

Model description

We supported in the main text the finding that poleward translocation of spindle MTs allows the spindle to relax by passively redistributing excess tensions, thereby smoothening initial deviations from average tension. The underlying model is defined by the mechanical circuit in Fig. 6 a in the main text and in the scheme below, which represents a "half-spindle,"



where V_{pre} is the pre-junction coupler dashpot slippage velocity, $V_{post,i}$ is the post-junction coupler dashpot slippage velocity (chromosome-indexed), E_{pre} is the pre-junction spring strain, $E_{post,i}$ is the post-junction spring strain (chromosome-indexed), $V_{+,i}$ is microtubule-kinetochore relative velocity (chromosome-indexed), and $E_{k,i}$ is the interkinetochore strain (chromosome-indexed). To represent the system mathematically, we first use the homogeneous stress condition, i.e., the sum of forces along *o* is equal to that along *o'* or along any other parallel plane. Assuming linearity of the motor force–velocity (F-V) relation and of all elastic and viscous responses in the spindle we get

$$P_0 - \mu V_M(t) = \phi n \varepsilon_c V_{pre}(t) = \phi n k_c E_{pre}(t) = \\ = \sum_{i=1,n} k_c E_{post,i}(t) = \sum_{i=1,n} \varepsilon_c V_{post,i}(t) = \sum_{i=1,n} \varepsilon_k V_{+,i}(t) = \sum_{i=1,n} k_k E_{k,i}(t), \quad (2)$$

where $T_i \equiv k_k E_{k,i}$ is the centromeric tension at the *i*-th chromosome. Second, using the additive strain condition along a path connecting *p* to the i-th chromosome c_i,

$$V_M(t) = V_{pre}(t) + \dot{E}_{pre}(t) + \dot{E}_{post,i}(t) + V_{post,i}(t) + V_{+,i}(t) + \dot{E}_{k,i}(t). \quad (3)$$

Using Eq. 2 to substitute the terms in Eq. 3, we get the ordinary differential equation (ODE) that governs the system dynamics. The *j*-th centromere tension is given by

$$\frac{1}{\phi n k_c}\sum_{i=1}^{n}\dot{T}_i(t) + \left(\frac{1}{k_c}+\frac{1}{k_k}\right)\dot{T}_j(t) + \left(\frac{1}{\mu}+\frac{1}{\phi n \varepsilon_c}\right)\sum_{i=1}^{n}T_i(t) + \left(\frac{1}{\varepsilon_c}+\frac{1}{\varepsilon_k}\right)T_j(t) = \frac{P_0}{\mu}. \quad (4)$$

To gather an intuitive understanding of the system behavior, we separate the problem in two parts. First we follow the evolution of the ensemble-averaged centromeric tension and then focus on how individual centromere tension levels approach the evolving mean tension. For the first step we simply need to calculate $\sum_{i=1}^{n}(\text{Eq. 4})$, giving

$$\left(\frac{1+\phi^{-1}}{k_c}+\frac{1}{k_k}\right)\sum_{i=1}^{n}\dot{T}_i(t) + \left(\frac{n}{\mu}+\frac{1+\phi^{-1}}{\varepsilon_c}+\frac{1}{\varepsilon_k}\right)\sum_{i=1}^{n}T_i(t) = \frac{nP_0}{\mu},$$

a first-order ODE with a solution given by a single exponential that decays in a characteristic time

$$\tau^{\infty} = \frac{\left(1+\phi^{-1}\right)k_c^{-1}+k_k^{-1}}{n\mu^{-1}+\left(1+\phi^{-1}\right)\varepsilon_c^{-1}+\varepsilon_k^{-1}},$$

to the equilibrium tension

$$T^{\infty} = \left\langle T_i\ (t \gg \tau^{\infty})\right\rangle = \frac{P_0}{n+\mu\left(\frac{1}{\varepsilon_k}+\frac{1+\phi^{-1}}{\varepsilon_c}\right)} = \frac{P_0}{n+\frac{\mu}{\varepsilon^*}}, \quad (5)$$

where ε^* is defined as the friction drag coefficient coupling ipMTs to kinetochores. At equilibrium, kMT fiber slippage velocity (or flux velocity) is $V_+^{\infty} = T^{\infty}/\varepsilon_k$. As ε^* increases, T^{∞} tends to its maximum value P_0/n, a condition in which flux velocity would drop to zero. If ε^* decreases, kMT flux velocity tends asymptotically to $V_0/2$, where V_0 is the free motor velocity.

For the second step, we study how any individual centromere tension T_i approaches the evolving mean tension $\langle T\rangle_E$, where the subscript denotes that averaging is done along the chromosome ensemble. The timescale of the decay of $T_i - \langle T\rangle_E$ is equal to that of $\Delta T_{ij} \equiv T_i - T_j$, where *i* and *j* are any distinct chromosomes. We calculate ΔT_{ij} using Eq. 4, where the summation terms vanish, yielding

$$\left(k_c^{-1}+k_k^{-1}\right)\Delta\dot{T}_{ij}(t) + \left(\varepsilon_c^{-1}+\varepsilon_k^{-1}\right)\Delta T_{ij}(t) = 0.$$

Thus, individual tension levels redistribute by approaching each other (and the mean tension) in the timescale defined by

$$\tau^{\Delta} = \frac{k_c^{-1}+k_k^{-1}}{\varepsilon_c^{-1}+\varepsilon_k^{-1}},$$

the equalization time.

We assumed throughout that the system's viscous and elastic properties may be characterized by bulk magnitudes for both MT–kinetochore and MT–coupler interactions. Regarding coupling, the model assumes that all kMT fiber pairs are (1) equally coupled to each other and (2) equally coupled to the ipMTs. However, we let the coupling efficiencies 1 and 2 be different, which is reflected by the coupling ratio parameter ϕ. This factor allows variation of ipMT number or its substitution by other (non–MT dependent) motorized structures. For example: $\phi = 1$ represents a spindle in which ipMT-coupler total drag is equivalent to kMT-coupler total drag; $\phi = \infty$ may represent a situation in which the number of ipMTs is very large, with its connections to the coupler being dominant relative to kMT connections to the coupler, or the case of a non-ipMT–based force generation mechanism, which is tightly bound to the coupler.

Ratio between ipMT and kMT poleward translocation velocities

At equilibrium, the ratio between the translocation/flux velocity of ipMTs and kMTs, *R*, is given by

$$R \equiv \frac{V_M^{\infty}}{V_+^{\infty}} = \frac{\varepsilon_k}{\varepsilon^*} = 1+\left(1+\phi^{-1}\right)\frac{\varepsilon_k}{\varepsilon_c},$$

where we used Eq. 5 along with the relations $P_0 - \mu V_M^{\infty} = nT^{\infty}$ and $\varepsilon_k V_+^{\infty} = T^{\infty}$. In general $R > 1$ unless the perfect-coupling regime strictly holds ($\varepsilon_c = \infty$). We did not determine this factor experimentally because of the low number of fluxing ipMTs that we were able to measure, but it has been consistently shown in several systems, including *Drosophila* S2 cells, that $R > 1$ (Maddox et al., 2003; LaFountain et al., 2004; Goshima et al., 2005).

Optimal performance of the model mechanical system

We now study the trade-off between loose and tight attachment at the microtubule–kinetochore interface. In search of a compromise, we maximize tension and minimize redistribution time by defining a dimensionally meaningful parameter to be maximized, $\Omega \propto T^{\infty 2}/\left(k_k\tau^{\Delta}\right)$ (Fig. 6 c), which is a measure of centromeric power. Power maximization reflects the fact that the physical system is tuned to allow the largest fraction of the available energy in the spindle to be uniformly accumulated in the form of elastic energy at the metaphase plate within the shortest possible

time. The optimal regime is found to occur for high coupling ($\varepsilon_c = \infty$) but with intermediate ε_k (see Fig. 6 c). Optimal ε_k is independent of ϕ and given by $\varepsilon_k^{optimal} = \mu n^{-1}$, which leads to an equilibrium tension equal to half its maximum value $T^\infty = P_0/(2n)$, or a flux velocity equal to $V_0/4$. A critical value of

$$\varepsilon_k^{critical} = \mu n^{-1}\left(1+2\phi^{-1}\right),$$

which corresponds to a flux velocity of $V_0/[4(1 + \phi^{-1})]$, may be found above which $\varepsilon_k = \infty$ always maximizes Ω, a condition in which equalization is achieved solely by slippage at the coupler–MTs interface but at the expense of a reduced power yield: $\Omega_{max,high\text{-}coupling}/\Omega_{max,high\text{-}attachment} = 1 + \phi^{-1}$.

In summary, the mechanical system in Fig. 6 a will behave most efficiently if kMTs are strongly coupled to the poleward force-generating structures (and therefore between them), whereas their attachment to kinetochores allows kMT flux velocity between one and three eighths of the maximal motor velocity when ipMTs and kMTs have comparable attachments to the coupler (ϕ of $\sim$1). This range is broadly consistent with the observed magnitude of flux velocities in different systems if it is assumed that motors with $\sim$5 µm/min free velocity are responsible for ipMT sliding. We stress that nonlinearities in the motor F-V relation will shift this optimal regime.

Effect of polar resistance to microtubule poleward translocation

We have presented a model for the "wild-type" spindle. To study the possible effect of KLP10A depletion on metaphase spindle tension and dynamics, we introduced a set of polar viscous elements antagonizing microtubule sliding. We assume these dashpots to be anchored (e.g., by astral MTs at the cortex). Adding such viscous term $\varepsilon_p V_{-,i}$, where $V_{-,i} = V_{+,i} + E_{k,i}$, is the depolymerization velocity, to Eqs. 2 and 3 yields a second-order ODE with overdamped solutions that tend to an equilibrium tension given by

$$T^\infty = \frac{P_o}{\mu\left[\left(1+\frac{\varepsilon_p}{\varepsilon_k}\right)\left(\frac{1+\phi^{-1}}{\varepsilon_c}+\frac{n}{\mu}\right)+\frac{1}{\varepsilon_k}\right]},$$

where ε_p is the viscous drag at the poles. As expected, an increase in ε_p leads to decreased centromeric tension, which, however, may be recovered by an increase in ε_k. This is in broad agreement with mean tension recovery (as measured by interkinetochore distance) in KLP10A RNAi followed by codepletion of CLASP (Table I). However, flux velocity at equilibrium, given by $V_+^\infty = T^\infty/\varepsilon_k$, will drop upon increased ε_p or ε_k. Polar resistance will in general lead to an increased equalization time, which for stiff coupling ($k_c \to \infty$) is given by

$$\tau^\Delta = \frac{\frac{1}{k_k}}{\frac{1}{\varepsilon_c+\varepsilon_p}+\frac{1}{\varepsilon_k}}.$$

Effect of an active tension-generating mechanism at the kinetochore

An offset force component, F_k, may be introduced in the model to account for kinetochore-based tension generation, possibly by minus end–directed motors like dynein (Howell et al., 2001; Yang et al., 2007). Tension is then given by $T_i(t) = \varepsilon_k V_{+,i}(t) + F_k$. For clarity, we describe F_k as a fraction f of the maximum tension deliverable by an equilibrated spindle, $F_k = f\,P_o/n$. Only the constant term in Eq. 4 is modified, with the RHS becoming $P_0\left(\mu^{-1} + fn^{-1}\varepsilon_k^{-1}\right)$, which naturally doesn't change the timescales that describe the system, τ^Δ or τ^∞. However, equilibrium tension is now increased to

$$T^\infty = \frac{P_o\left(1+f\frac{\mu}{n\varepsilon_k}\right)}{n+\mu\left(\frac{1}{\varepsilon_c}\left(1+\frac{1}{\phi}\right)+\frac{1}{\varepsilon_k}\right)}.$$

To first order in f, optimal behavior (see "Optimal performance of the model mechanical system") occurs for $\mu\varepsilon_{k,optimal}^{-1} \approx n(1+4f)$, valid for $f \ll 1$, with $\varepsilon_c = \infty$. This means that introduction of an active tension-assisting component at the kinetochore shifts the optimal behavior to the slightly increased flux velocity $V_0(1 + f)/4$.

RNAi

RNAi depletion of *Drosophila* CLASP, KLP10A, and Mad2 in S2 cells was performed as described previously (Rogers et al., 2004; Maiato et al., 2005; Orr et al., 2007). Phenotypes were quantified by light microscopy every 24 h over 7 d. Protein knockdown was monitored by Western blotting using the following antibodies and dilutions: rabbit anti-CLASP and anti-Mad2 (gifts from C. Sunkel, Instituto de Biologia Molecular e Cellular, University of Porto, Portugal) 1:600 and 1:3,000, respectively; rabbit anti-KLP10A (gift from J. Scholey, University of California, Davis, Davis, CA) 1:1500; and mouse anti–α-tubulin clone B512 (Sigma-Aldrich) 1:10,000. Secondary antibodies were visualized using the ECL system (GE Healthcare).

Drug treatments

To suppress MT dynamics in S2 cells, we used 10 nM taxol for 10 min before time-lapse recording or immunofluorescence processing. Whenever indicated, the proteasome inhibitor MG132 was used at 20 µM for 2 h. To determine the interkinetochore rest length, we treated S2 cells with 30 µM colchicine for 2 h to induce MT depolymerization.

Immunofluorescence microscopy

S2 cells were grown on 0.5 mg/ml concanavalin A (Sigma-Aldrich)-coated coverslips and processed for immunofluorescence as described previously (Maiato et al., 2004b). Primary antibodies were rabbit anti–γ-tubulin (1:500; gift from A. Debec, Institut Jacques Monod, Paris, France); mouse anti–α-tubulin clone B512 (1:1500; Sigma-Aldrich); rabbit anti-BubR1 and anti-Scc1 (1:2,000 and 1:500, respectively; gifts from C. Sunkel); chicken anti-CID (1:300; gift from G. Karpen, University of California, Berkeley, Berkeley, CA); rabbit anti-Aurora B (1:500; a gift from M. Carmena and B. Earnshaw, University of Edinburgh, Edinburgh, Scotland, UK). All fluorescent-conjugated secondary antibodies were from the Alexa Fluor series (Invitrogen). Quantitative 3D datasets were collected using a wide-field microscope (Imager.Z1; Carl Zeiss, Inc.) equipped with a charge-coupled device (CCD; Axiocam MRm) and using a 100×, 1.4 NA oil immersion objective lens at 0.25 µm z steps, using Axiovision software. For an imaging medium, we used 89.5% glycerol, 10% 1 M Tris-HCl, pH 8.5, and 0.5% *N*-propyl-gallate. Images were subsequently blind deconvolved with AutoDeblur X2 software (Media Cybernetics) and processed for publication using Photoshop CS3 (Adobe).

Time-lapse microscopy

S2 cells stably expressing GFP–α-tubulin (a gift from R. Vale, University of California, San Francisco, San Francisco, CA) and CID-mCherry (the mCherry cDNA was provided by R. Tsien, University of California, San Diego, La Jolla, CA) or mRFP-BubR1 (mRFP-BubR1 construct was modified from a vector provided by R. Karess, Institut Jacques Monod, Paris, France) were grown on concanavalin A–coated coverslips and mounted in modified Rose chambers with Schneider´s medium (Sigma-Aldrich) containing 10% FBS. 4D datasets covering the entire cell volume were collected every 30 s with 1-µm z steps with a 100× 1.4 NA Plan-Apochromatic objective at 25°C with a Revolution Spinning Disk confocal system (Andor) equipped with an electron multiplying CCD (EMCCD) iXon^{EM}+ camera, two laser lines (488 and 561 nm), and a Yokogawa CSU-22 unit based on an inverted microscope (IX81; Olympus) and driven by Andor IQ.

Fluorescent speckle microscopy

To measure flux rates, we used S2 cells stably expressing GFP–α-tubulin under the control of a leaky inducible metallothionein promoter (a gift from R. Vale) and CID-mCherry. Without induction, low levels of GFP–α-tubulin are expressed. Time-lapse images were collected every 5 s at 25°C with an inverted microscope (TE2000U; Nikon) equipped with a CoolSNAP HQ2 CCD camera (Photometrics) using a 100× 1.4 NA Plan-Apochromatic objective, and driven by NIS elements (Nikon). Images were subsequently blind-deconvolved with AutoDeblur X2 (Media Cybernetics).

Guided kymography

In order to either kymograph the entire spindle or to prepare the data for local kymograph analysis, we used a custom routine written in Matlab (The MathWorks, Inc.) to compensate for spindle rotation and translation described by the following steps: (1) 2D tracking of spindle poles, (2) region-of-interest (ROI) dimensions definition, and (3) thick-kymograph generation with the ROI being automatically translated and rotated every frame according to the 2D coordinates of the two reference objects in step 1. The direct output is a whole-spindle kymograph that can be used to generate a

set of aligned images that are the basis for all subsequent analysis. For a detailed description see Pereira and Maiato, 2009.

Chromo-kymography

Chromo-kymograph generation was implemented using Matlab by assigning different colors to the *n* pixel rows of the $n \times m$ ROI by defining a color-gradient filter along the vertical axis (*n* rows). For the color filter, we used linearly varying red/green/blue components. A sum projection is performed on the $n \times m \times 3$ matrix to obtain an $m \times 3$ output. For each time-lapse image, this transformation generates a 90° "tilted" 2D matrix with dimensions $1 \times m \times 3$, where the three layers are weighed red/green/blue contributions. Final chromo-kymograph dimensions are: (number of time-lapse images) $\times m \times 3$. For a detailed description see Pereira and Maiato, 2009.

Collapsed kymography

Raw kymographs are composed of an image stack at different time points, each with dimensions $n \times m$. Collapsed kymographs are projections of the raw kymograph that result from conversion of each time point image matrix into a vector, according to some weighed combination (e.g., mean or maximum) of the pixels along each column of the ROI. Chromo-kymographs are a generalization of collapsed kymographs on which three different weight functions are applied, each one generating an RGB channel of the output chromo-kymograph.

Laser microsurgery

We use the second harmonic (532 nm) of a Nd:YAG laser to generate quasi-single mode ($M^2 < 1.5$) 8-ns pulses. Pulse energy for kMT surgery is 1–2 µJ. The laser beam was steered onto a microscope (TE2000U; Nikon) with "stage up-kit," which allows the laser beam to overlap the microscope optical axis in the infinite-conjugated section. The laser beam diameter is adjusted to fill the objective back aperture to minimize spot diameter at the sample (<0.5 µm). The details of the optical system have been described previously (Pereira et al., 2009).

Quantifications

Spindle length in fixed material was measured for each bipolar spindle as the distance between opposite poles revealed by γ-tubulin immunostaining.

Flux velocities were measured by kymograph analysis in which a long thin rectangular region covering the entire spindle length is extracted from each image in the time-lapse series and sequentially aligned with reference to the poles. The position of the rectangular region is chosen by the presence of a kinetochore pair and correspondent kMTs. On these collapsed kymographs, slopes corresponding to the movement of bright or dark speckles over time (equivalent to the flux velocity) are directly measured. Results obtained by this method reveal slightly faster kinetochore MT flux velocities than those obtained by other techniques such as photobleaching or photoactivation of spindle MTs (Maiato et al., 2005; Rogers et al., 2005; Buster et al., 2007).

Chromosome poleward velocity relative to the equator was measured after each CID-mCherry track obtained from chromo-kymographs covering the entire cell volume. Velocity was determined measuring the slope of the fastest linear movement after anaphase onset within each half spindle. The distribution shown in the histogram represents each track measured in the total number of cells.

Spindle elongation velocity was measured after spindle MT minus ends. Slopes were determined for the same period of time when chromosome poleward velocity was measured. Each value shown in the histogram is the mean from the slopes of both half spindles per cell.

KMT shortening velocity was measured as the difference between each measurement of poleward chromosome velocity and the corresponding half-spindle elongation velocity. Given the observed asynchrony after perturbation of flux, each value represented in the histogram represents individual kMT shortening measurements.

MT minus-end depolymerization rates in anaphase were quantified by subtracting the MT minus-end slope to the speckle slope. MT minus ends were determined using collapsed kymographs, which gather all MT minus ends converging to a common focus.

Interkinetochore distances measured from fixed samples were obtained after immunofluorescence as the distance between centroids of CID-labeled kinetochore pairs through metaphase z stacks using ImageJ 1.30 software (National Institutes of Health). Interkinetochore distances measured from living cells represent the distance between centroids of opposite CID-mCherry pairs through metaphase z stacks 2 min before anaphase onset. Anaphase onset was inferred as the moment where at least two kinetochore pairs were at a distance higher than 1.2 µm. Intracellular tension variability was quantified upon calculation of the coefficient of variation, $\sigma_T/\langle T \rangle$, which for a linear spring is equal to $\sigma_d/(\langle d \rangle - d_0)$, where d is the interkinetochore distance in metaphase and d_0 is the interkinetochore distance in prophase (rest length).

Quantification of BubR1 fluorescence at kinetochores was performed relative to CID fluorescence as described previously (Hoffman et al., 2001) using ImageJ 1.30 software and a partially automated tool written in Matlab. In brief, an inner and an outer ROI are defined so that the first fully encloses the kinetochore and the second additionally encloses a small peripheral area, which is used to estimate intensity background. If the integrated signal is S_i in an inner ROI with dimensions $i \times j$ and S_o in an outer ROI with dimensions $k \times l$, then the background-subtracted signal is $S = S_i - (S_o - S_i) \times (i \times j)/(k \times l - i \times j)$. For kinetochore quantification, we used 9 × 9 pixel and 13 × 13 pixel ROIs (1 pixel = 65 nm). To measure Aurora B signal in the metaphase plate, we quantified both Aurora B and CID in the entire metaphase plate with a fixed ROI. Background intensity was estimated from an area contiguous to the spindle.

Cold stable kMTs were quantified by immunofluorescence after 10 min at 4°C.

Metaphase duration was defined from the moment of alignment of the last chromosome at the metaphase plate until anaphase onset.

Regrowth of laser-cut kMT fibers was only measured when the newly created kMT plus ends underwent clear catastrophe. The minus ends of the growing kinetochore-associated fibers were manually tracked using a Matlab script. A linear fit was done to the data points of kMT length over time to obtain growth velocity.

Statistical analyses

Statistical analysis was performed using either parametric one-way (ANOVA) or nonparametric analysis of variance (Kruskal-Wallis) for multiple group comparisons according to the normality of the distribution as determined by Kolmogorov-Smirnov test. All pairwise multiple comparisons were subsequently analyzed using either post hoc Student-Newman-Keuls (parametric) or Dunn's (nonparametric) tests. A parametric *t* test or nonparametric Mann-Whitney was used for two group comparisons. We used both standard deviation and interquartile range as measures of the distribution spread. All statistical analysis was performed using SigmaStat 3.5 (Systat Software).

Online supplemental material

Fig. S1 shows analysis of spindle elongation and kinetochore–MT attachments after KLP10A RNAi. Fig. S2 shows analysis of sister chromatid separation in anaphase and BubR1 levels at kinetochores. Online supplemental material is available at http://www.jcb.org/cgi/content/full/jcb.200904153/DC1.

We thank J. Scholey for communicating results before publication and for a gift of antibodies; R. Vale, G. Karpen, R. Tsien, R. Karess, Mar Carmena, Bill Earnshaw, and C. Sunkel for the gift of reagents; M.S. Belsley, F.P. Ferreira, J.V. Gomes, and P.A. Coelho for discussions; and A. Khodjakov and V. Magidson for advice on the set up of our laser microsurgery system.

I. Matos and M. Lince-Faria hold fellowships (SFRD/BD/22020/2005 and SFRH/BPD/26780/2006) from Fundação para a Ciência e a Tecnologia (FCT) of Portugal, and A.J. Pereira was supported by Crioestaminal/Viver a Ciência. Work in the laboratory of H. Maiato is supported by grants PTDC/BIA-BCM/66106/2006 and PTDC/SAU-OBD/66113/2006 from FCT, and the Gulbenkian Programmes for Research Stimulation and Frontiers in the Life Sciences.

Submitted: 28 April 2009
Accepted: 5 June 2009

References

Bakhoum, S.F., S.L. Thompson, A.L. Manning, and D.A. Compton. 2009. Genome stability is ensured by temporal control of kinetochore-microtubule dynamics. *Nat. Cell Biol.* 11:27–35.

Basto, R., J. Lau, T. Vinogradova, A. Gardiol, C.G. Woods, A. Khodjakov, and J.W. Raff. 2006. Flies without centrioles. *Cell.* 125:1375–1386.

Bird, A.W., and A.A. Hyman. 2008. Building a spindle of the correct length in human cells requires the interaction between TPX2 and Aurora A. *J. Cell Biol.* 182:289–300.

Brangwynne, C.P., F.C. MacKintosh, S. Kumar, N.A. Geisse, J. Talbot, L. Mahadevan, K.K. Parker, D.E. Ingber, and D.A. Weitz. 2006. Microtubules

Published July 13, 2009

can bear enhanced compressive loads in living cells because of lateral reinforcement. *J. Cell Biol.* 173:733–741.

Brust-Mascher, I., G. Civelekoglu-Scholey, M. Kwon, A. Mogilner, and J.M. Scholey. 2004. Model for anaphase B: role of three mitotic motors in a switch from poleward flux to spindle elongation. *Proc. Natl. Acad. Sci. USA.* 101:15938–15943.

Brust-Mascher, I., P. Sommi, D.K. Cheerambathur, and J.M. Scholey. 2009. Kinesin-5-dependent poleward flux and spindle length control in *Drosophila* embryo mitosis. *Mol. Biol. Cell.* 20:1749–1762.

Buster, D.W., D. Zhang, and D.J. Sharp. 2007. Poleward tubulin flux in spindles: regulation and function in mitotic cells. *Mol. Biol. Cell.* 18:3094–3104.

Cameron, L.A., G. Yang, D. Cimini, J.C. Canman, O. Kisurina-Evgenieva, A. Khodjakov, G. Danuser, and E.D. Salmon. 2006. Kinesin 5-independent poleward flux of kinetochore microtubules in PtK1 cells. *J. Cell Biol.* 173:173–179.

Cimini, D., B. Moree, J.C. Canman, and E.D. Salmon. 2003. Merotelic kinetochore orientation occurs frequently during early mitosis in mammalian tissue cells and error correction is achieved by two different mechanisms. *J. Cell Sci.* 116:4213–4225.

Cimini, D., L.A. Cameron, and E.D. Salmon. 2004. Anaphase spindle mechanics prevent mis-segregation of merotelically oriented chromosomes. *Curr. Biol.* 14:2149–2155.

Danuser, G., and C.M. Waterman-Storer. 2006. Quantitative fluorescent speckle microscopy of cytoskeleton dynamics. *Annu. Rev. Biophys. Biomol. Struct.* 35:361–387.

DeLuca, J.G., W.E. Gall, C. Ciferri, D. Cimini, A. Musacchio, and E.D. Salmon. 2006. Kinetochore microtubule dynamics and attachment stability are regulated by Hec1. *Cell.* 127:969–982.

Forer, A., J.D. Pickett-Heaps, and T. Spurck. 2008. What generates flux of tubulin in kinetochore microtubules? *Protoplasma.* 232:137–141.

Gaetz, J., and T.M. Kapoor. 2004. Dynein/dynactin regulate metaphase spindle length by targeting depolymerizing activities to spindle poles. *J. Cell Biol.* 166:465–471.

Ganem, N.J., and D.A. Compton. 2006. Functional roles of poleward microtubule flux during mitosis. *Cell Cycle.* 5:481–485.

Ganem, N.J., K. Upton, and D.A. Compton. 2005. Efficient mitosis in human cells lacking poleward microtubule flux. *Curr. Biol.* 15:1827–1832.

Ganem, N.J., Z. Storchova, and D. Pellman. 2007. Tetraploidy, aneuploidy and cancer. *Curr. Opin. Genet. Dev.* 17:157–162.

Gorbsky, G.J., P.J. Sammak, and G.G. Borisy. 1987. Chromosomes move poleward in anaphase along stationary microtubules that coordinately disassemble from their kinetochore ends. *J. Cell Biol.* 104:9–18.

Goshima, G., R. Wollman, N. Stuurman, J.M. Scholey, and R.D. Vale. 2005. Length control of the metaphase spindle. *Curr. Biol.* 15:1979–1988.

Hoffman, D.B., C.G. Pearson, T.J. Yen, B.J. Howell, and E.D. Salmon. 2001. Microtubule-dependent changes in assembly of microtubule motor proteins and mitotic spindle checkpoint proteins at PtK1 kinetochores. *Mol. Biol. Cell.* 12:1995–2009.

Holt, L.J., A.N. Krutchinsky, and D.O. Morgan. 2008. Positive feedback sharpens the anaphase switch. *Nature.* 454:353–357.

Howell, B.J., B.F. McEwen, J.C. Canman, D.B. Hoffman, E.M. Farrar, C.L. Rieder, and E.D. Salmon. 2001. Cytoplasmic dynein/dynactin drives kinetochore protein transport to the spindle poles and has a role in mitotic spindle checkpoint inactivation. *J. Cell Biol.* 155:1159–1172.

King, J.M., and R.B. Nicklas. 2000. Tension on chromosomes increases the number of kinetochore microtubules but only within limits. *J. Cell Sci.* 113:3815–3823.

Knowlton, A.L., W. Lan, and P.T. Stukenberg. 2006. Aurora B is enriched at merotelic attachment sites, where it regulates MCAK. *Curr. Biol.* 16:1705–1710.

LaFountain, J.R. Jr., C.S. Cohan, A.J. Siegel, and D.J. LaFountain. 2004. Direct visualization of microtubule flux during metaphase and anaphase in crane-fly spermatocytes. *Mol. Biol. Cell.* 15:5724–5732.

Laycock, J.E., M.S. Savoian, and D.M. Glover. 2006. Antagonistic activities of Klp10A and Orbit regulate spindle length, bipolarity and function in vivo. *J. Cell Sci.* 119:2354–2361.

Liu, D., G. Vader, M.J. Vromans, M.A. Lampson, and S.M. Lens. 2009. Sensing chromosome bi-orientation by spatial separation of aurora B kinase from kinetochore substrates. *Science.* 323:1350–1353.

Maddox, P., A. Straight, P. Coughlin, T.J. Mitchison, and E.D. Salmon. 2003. Direct observation of microtubule dynamics at kinetochores in *Xenopus* extract spindles: implications for spindle mechanics. *J. Cell Biol.* 162:377–382.

Maddox, P.S., K.S. Bloom, and E.D. Salmon. 2000. The polarity and dynamics of microtubule assembly in the budding yeast *Saccharomyces cerevisiae*. *Nat. Cell Biol.* 2:36–41.

Maiato, H., J. DeLuca, E.D. Salmon, and W.C. Earnshaw. 2004a. The dynamic kinetochore-microtubule interface. *J. Cell Sci.* 117:5461–5477.

Maiato, H., C.L. Rieder, and A. Khodjakov. 2004b. Kinetochore-driven formation of kinetochore fibers contributes to spindle assembly during animal mitosis. *J. Cell Biol.* 167:831–840.

Maiato, H., A. Khodjakov, and C.L. Rieder. 2005. *Drosophila* CLASP is required for the incorporation of microtubule subunits into fluxing kinetochore fibres. *Nat. Cell Biol.* 7:42–47.

Maiato, H., P.J. Hergert, S. Moutinho-Pereira, Y. Dong, K.J. Vandenbeldt, C.L. Rieder, and B.F. McEwen. 2006. The ultrastructure of the kinetochore and kinetochore fiber in *Drosophila* somatic cells. *Chromosoma.* 115:469–480.

Manning, A.L., and D.A. Compton. 2007. Mechanisms of spindle-pole organization are influenced by kinetochore activity in mammalian cells. *Curr. Biol.* 17:260–265.

Maresca, T.J., and E.D. Salmon. 2009. Intrakinetochore stretch is associated with changes in kinetochore phosphorylation and spindle assembly checkpoint activity. *J. Cell Biol.* 184:373–381.

Meraldi, P., V.M. Draviam, and P.K. Sorger. 2004. Timing and checkpoints in the regulation of mitotic progression. *Dev. Cell.* 7:45–60.

Mitchison, T.J. 1989. Polewards microtubule flux in the mitotic spindle: evidence from photoactivation of fluorescence. *J. Cell Biol.* 109:637–652.

Mitchison, T.J. 2005. Mechanism and function of poleward flux in *Xenopus* extract meiotic spindles. *Philos. Trans. R. Soc. Lond. B Biol. Sci.* 360:623–629.

Miyamoto, D.T., Z.E. Perlman, K.S. Burbank, A.C. Groen, and T.J. Mitchison. 2004. The kinesin Eg5 drives poleward microtubule flux in *Xenopus laevis* egg extract spindles. *J. Cell Biol.* 167:813–818.

Musacchio, A., and E.D. Salmon. 2007. The spindle-assembly checkpoint in space and time. *Nat. Rev. Mol. Cell Biol.* 8:379–393.

Nicklas, R.B., and S.C. Ward. 1994. Elements of error correction in mitosis: microtubule capture, release, and tension. *J. Cell Biol.* 126:1241–1253.

O'Connell, C.B., J. Loncarek, P. Hergert, A. Kourtidis, D.S. Conklin, and A. Khodjakov. 2008. The spindle assembly checkpoint is satisfied in the absence of interkinetochore tension during mitosis with unreplicated genomes. *J. Cell Biol.* 183:29–36.

Orr, B., H. Bousbaa, and C.E. Sunkel. 2007. Mad2-independent spindle assembly checkpoint activation and controlled metaphase-anaphase transition in *Drosophila* S2 cells. *Mol. Biol. Cell.* 18:850–863.

Pereira, A.J., and H. Maiato. 2009. Improved kymography tools and its applications to mitosis. *Methods.* In press.

Pereira, A.J., I. Matos, M. Lince-Faria, and H. Maiato. 2009. Dissecting mitosis with laser microsurgery and RNAi in *Drosophila* cells. *Methods Mol. Biol.* 545:145–164.

Pinsky, B.A., and S. Biggins. 2005. The spindle checkpoint: tension versus attachment. *Trends Cell Biol.* 15:486–493.

Rieder, C.L., A. Schultz, R. Cole, and G. Sluder. 1994. Anaphase onset in vertebrate somatic cells is controlled by a checkpoint that monitors sister kinetochore attachment to the spindle. *J. Cell Biol.* 127:1301–1310.

Rogers, G.C., S.L. Rogers, T.A. Schwimmer, S.C. Ems-McClung, C.E. Walczak, R.D. Vale, J.M. Scholey, and D.J. Sharp. 2004. Two mitotic kinesins cooperate to drive sister chromatid separation during anaphase. *Nature.* 427:364–370.

Rogers, G.C., S.L. Rogers, and D.J. Sharp. 2005. Spindle microtubules in flux. *J. Cell Sci.* 118:1105–1116.

Straight, A.F., W.F. Marshall, J.W. Sedat, and A.W. Murray. 1997. Mitosis in living budding yeast: anaphase A but no metaphase plate. *Science.* 277:574–578.

Tucker, J.D., and R.J. Preston. 1996. Chromosome aberrations, micronuclei, aneuploidy, sister chromatid exchanges, and cancer risk assessment. *Mutat. Res.* 365:147–159.

Uchida, K.S., K. Takagaki, K. Kumada, Y. Hirayama, T. Noda, and T. Hirota. 2009. Kinetochore stretching inactivates the spindle assembly checkpoint. *J. Cell Biol.* 184:383–390.

Valentine, M.T., P.M. Fordyce, T.C. Krzysiak, S.P. Gilbert, and S.M. Block. 2006. Individual dimers of the mitotic kinesin motor Eg5 step processively and support substantial loads in vitro. *Nat. Cell Biol.* 8:470–476.

Waters, J.C., T.J. Mitchison, C.L. Rieder, and E.D. Salmon. 1996. The kinetochore microtubule minus-end disassembly associated with poleward flux produces a force that can do work. *Mol. Biol. Cell.* 7:1547–1558.

Yang, G., L.A. Cameron, P.S. Maddox, E.D. Salmon, and G. Danuser. 2008. Regional variation of microtubule flux reveals microtubule organization in the metaphase meiotic spindle. *J. Cell Biol.* 182:631–639.

Yang, Z., U.S. Tulu, P. Wadsworth, and C.L. Rieder. 2007. Kinetochore dynein is required for chromosome motion and congression independent of the spindle checkpoint. *Curr. Biol.* 17:973–980.

Downloaded from jcb.rupress.org on June 13, 2010

Published July 13, 2009

Supplemental material

JCB

Matos et al., http://www.jcb.org/cgi/content/full/jcb.200904153/DC1

THE JOURNAL OF CELL BIOLOGY

Downloaded from jcb.rupress.org on June 13, 2010

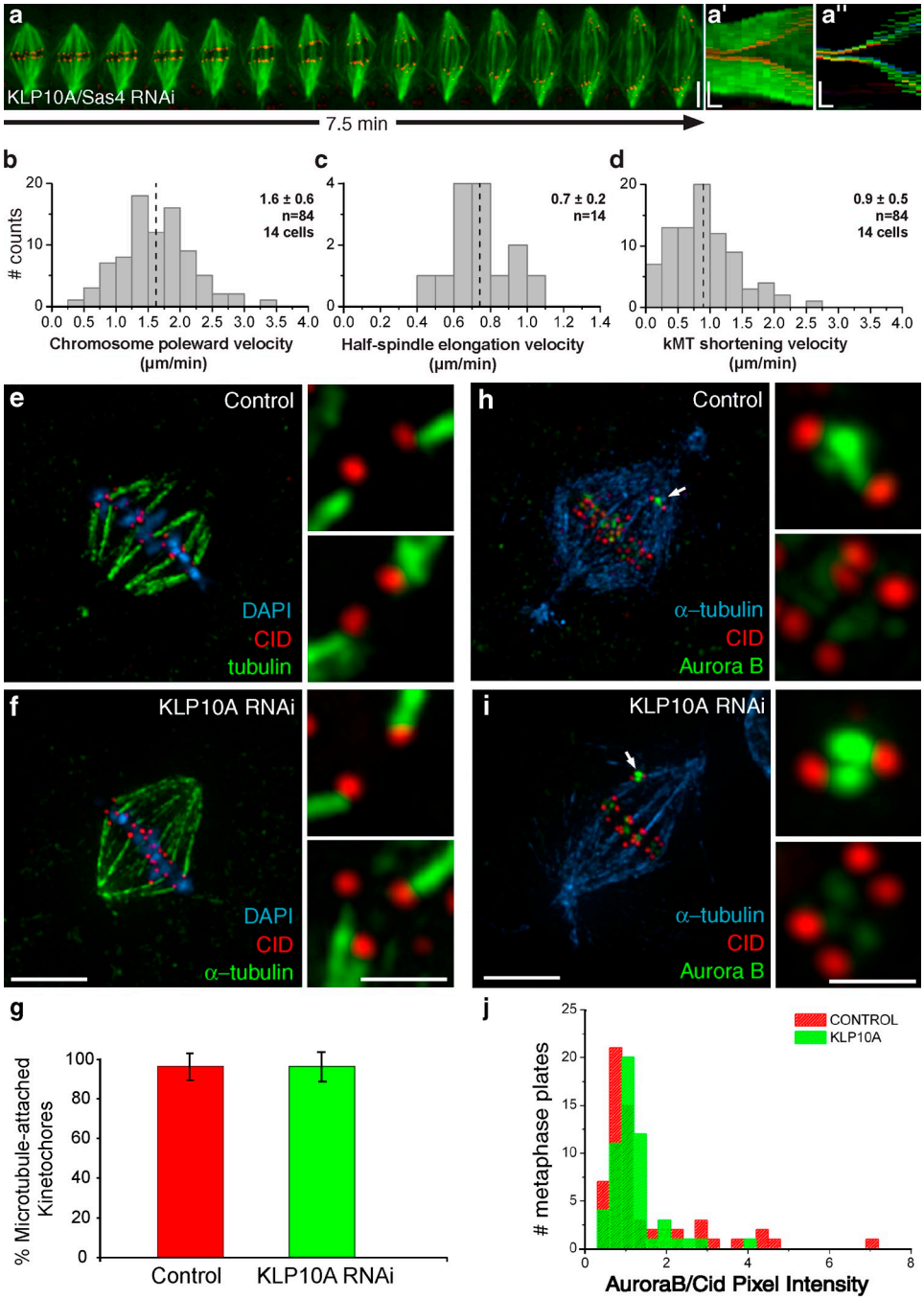


Figure S1. **Analysis of spindle elongation and kinetochore–MT attachments after KLP10A RNAi.** (a–a'') Kymograph (a), collapsed kymograph (a'), and chromo-kymograph (a'') analysis of a KLP10A/Sas4-depleted cell. Note the asynchronous movement of kinetochores toward the pole. Vertical bars, 5 μm; horizontal bars, 60 s. (b–d) Distribution of chromosome poleward velocity (b), half-spindle elongation velocity (c), and kMT shortening velocity (d) for KLP10A/Sas4 RNAi. Chromosome poleward velocity and half-spindle elongation velocities are statistically different from KLP10A RNAi cells ($p = <0.001$; *t* test). The mean ± SD is indicated for each distribution. The mean values are marked as a broken vertical line. (e and f) Formation of stable kMTs after cold treatment in control and KLP10A RNAi cells, respectively. MTs (green) and kinetochores (red) were, respectively, revealed with anti–α-tubulin and anti-CID antibodies, whereas DNA (blue) was counterstained with DAPI. Bars, 5 μm. (insets) Highlight of the kinetochore–MT interactions after cold treatment. Bars, 1 μm. (g) The formation of cold-resistant kMTs after KLP10A RNAi (96.4%, $n = 25$ cells) was not statistically different from control cells (96.2%, $n = 25$ cells; $P = 0.733$, Mann-Whitney test). Median and interquartile range are indicated in the graph. (h–j) Aurora B accumulation (green) during metaphase in control and KLP10A-depleted cells was not statistically different ($P = 0.322$; Mann-Whitney test). MTs (blue), kinetochores (red), and Aurora B (green) were respectively revealed with anti–α-tubulin, anti-CID, and anti–Aurora B antibodies. Insets highlight the higher levels of Aurora B on misaligned chromosomes (arrows) and the lower levels on metaphase chromosomes. Bars, 5 μm; inset bars, 1 μm.

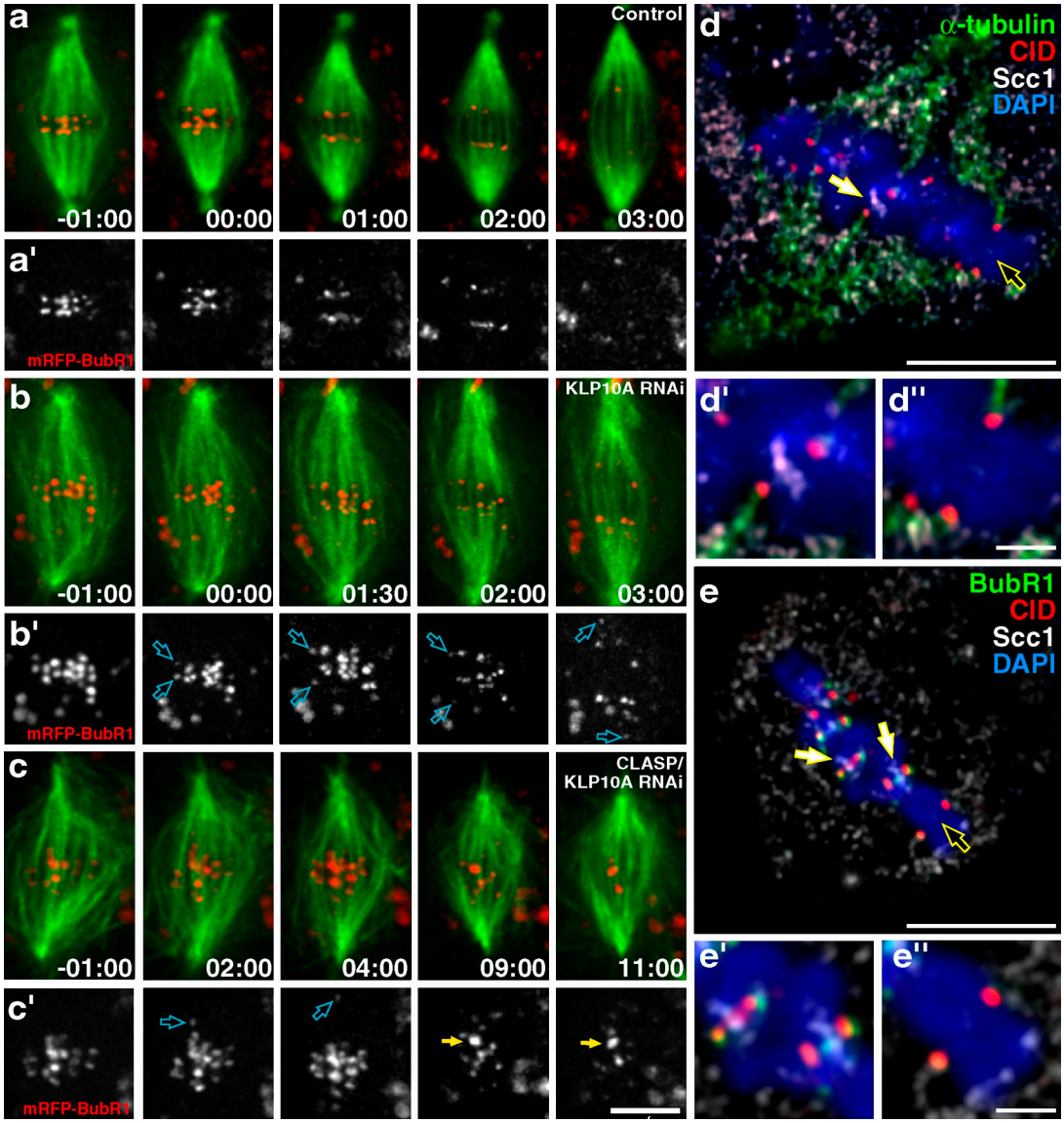


Figure S2. **The timing of sister–chromatid separation in anaphase correlates with BubR1 levels at kinetochores.** (a and a′) Control S2 cell stably expressing mRFP-BubR1 (red) and GFP–α-tubulin (green). Note that mRFP-BubR1 levels at kinetochores homogenously decrease in all chromosomes at anaphase onset. (b–b′ and c–c′) **A** KLP10A- and CLASP/KLP10A-depleted cell showing marked asynchronous sister–chromatid separation with the first kinetochore pair that separated (blue arrows) associated with lower mRFP-BubR1 levels when compared with those that separated last (yellow arrows). (d) Differential degradation of Scc1 (white) at the metaphase–anaphase transition in a KLP10A-depleted cell. MTs are shown in green, the kinetochore marker CID is shown in red, and DNA was counterstained with DAPI (blue). (d′–d′′) Higher magnification views of the chromosomes indicated with arrows in d. (e) A KLP10A-depleted cell showing differential degradation of Scc1 (white), where undetectable Scc1 correlates with lower BubR1 (green) levels at kinetochores. The kinetochore marker CID is shown in red and DNA was counterstained with DAPI (blue). Bars, 5 μm. (e′–e′′) Higher magnification views of the chromosomes indicated with arrows in e. Open and closed arrows in d and e represent undetectable and detectable Scc1, respectively. Bars in d′′ and e′′, 1 μm.